Title

Quantification of and Controls on Soil Carbon and Greenhouse Gas Fluxes from Managed Wetland Ecosystems

Author

Anthony, Tyler L

Publication Date

2021

Peer reviewed|Thesis/dissertation

Quantification and Controls on Soil Carbon and Greenhouse Gas Fluxes from Managed Peatland Ecosystems

by

Tyler Lee Anthony

A dissertation submitted in partial satisfaction of the

requirements for the degree of

Doctor of Philosophy

in

Environmental Science, Policy, and Management

in the

Graduate Division

of the

University of California, Berkeley

Committee in charge:

Professor Whendee L. Silver, Chair
Professor Dennis D. Baldocchi
Professor Todd E. Dawson

Summer 2021

Quantification and Controls on Soil Carbon and Greenhouse Gas Fluxes from Managed Wetland Ecosystems

by Tyler Lee

Anthony

Abstract

Quantification of and Controls on Soil Carbon and Greenhouse Gas Fluxes

from Managed Wetland Ecosystems

by

Tyler Lee Anthony

Doctor of Philosophy in Environmental Science, Policy, and Management

University of California, Berkeley

Professor Whendee L. Silver, Chair

Wetlands and peatlands represent only 3% of the world's soils but account for approximately 21% of the global soil organic carbon (C) stock. Due to their high nutrient availability, more than 10% of wetlands worldwide have been drained for agriculture and further drainage is expected to meet growing agricultural demands. Conversion of wetlands to croplands is likely to contribute to climate change through the loss of soil C and increased the emissions of nitrous oxide (N_2O) emissions from agricultural practices. The magnitude and drivers of C and nitrogen (N) emissions are poorly understood for drained wetland soils. For my dissertation, I first conducted a large-scale sampling campaign across a range of soil C concentrations in drained and restored wetland soils to quantify the importance of soil mineralogy in soil C storage and loss. I found that reactive iron (Fe) was negatively correlated to soil C across soils, suggesting reactive Fe pools may drive additional C losses in drained soils and limit C sequestration in flooded soils. Reactive organo-aluminum (Al) complexes were strongly positively correlated to soil C concentrations in drained soils, suggesting organo-Al complexes facilitate aggregation and anaerobic (micro)sites that may protect residual soil C from oxidation. Using automated chambers and cavity ring-down spectroscopy, I also conducted some of the longest continuous greenhouse gas flux measurements from organic-rich maize and mineral-rich alfalfa ecosystems, two dominant land uses in drained peatland soils. Flux measurements were conducted alongside continuous soil sensor monitoring, weekly soil N sampling, and satellite vegetation imagery to explore the biogeochemical and phenological drivers of CO_2, methane (CH_4), and N_2O emissions.

In the maize ecosystem, I found that soils were significant N_2O sources, contributing to 16-35% of annual CO_2e emissions from these already high emitting ecosystems. Using over 70,000 flux measurements I determined that hot moments of N_2O and CH_4 emissions represented 1.1 ± 0.2 and 1.3 ± 0.2% of measurements, respectively, but contributed to 45 ±

1% of mean annual N_2O fluxes and to 140 ± 9% of mean annual CH_4 fluxes. Soil moisture, soil temperature, and bulk soil oxygen (O_2) concentrations were strongly positively correlated with both soil N_2O and CH_4 emissions and soil nitrate (NO_3^-) concentrations were also correlated with N_2O emissions. To further explore the production and consumption pathways of N_2O and CH_4 I conducted ^{15}N-N_2O and ^{13}C-CH_4 stable isotope pool dilution experiments under contrasting drained and flooded conditions. Gross N_2O production was strongly positively correlated to soil moisture. However, gross N_2O consumption rates were highest in drained subsoils and were increased with increasing NO_3^- concentrations, suggesting N_2O consumption was indirectly controlled by substrate availability for denitrifiers. Combined with a decline in net N_2O fluxes observed under drained conditions, our results suggest organic-Al complexes may facilitate anaerobic hotspots of N_2O consumption. For CH_4, gross consumption was generally greater than gross production. Gross CH_4 production increased with soil depth, likely driven by both increased soil moisture and anaerobic soil conditions. Gross CH_4 consumption was negatively correlated with soil moisture and positively correlated with soil pH, indicating low pH and O_2 availability directly limit CH_4 consumption. Gross CH_4 consumption also accounted for up to 25% of net CO_2 production (mean ± SE: 7% ± 3%) in drained soils. Our results suggest that gross N_2O and CH_4 production were temporally decoupled from gross N_2O and CH_4 consumption and are driven by soil moisture status and its effects on NO_3^- and pH.

Continuous flux measurements from the alfalfa ecosystem showed a smaller consistent source of N_2O and an overall small net CH_4 sink. Using more than 100,000 flux measurements over four years from agricultural alfalfa, I also found that hot moments of N_2O emissions were only 0.2% to 1.1% of annual measurements but were 31.6% to 56.8% of the annual flux. I found that both the magnitude and contribution of hot N_2O moments to overall emissions decreased over time. Normalized difference vegetation index (NDVI), soil temperature, moisture, and oxygen (O_2) were all significantly correlated with soil CO_2, N_2O, and CH_4 fluxes, although associations varied across both soil depth and timescales. Our combined observations suggest that plant productivity regulates background N_2O emissions but soil moisture and soil O_2 availability are the dominant controls on the net greenhouse gas budget of alfalfa agroecosystems. Together, the findings in this dissertation contribute to a better understanding of the biogeochemical pathways of soil CO_2, N_2O, and CH_4 fluxes in managed peatland soils. They also highlight the importance of land management decisions in stimulating soil greenhouse gas emissions and improve our understanding of the processes, controls, and distribution of hot spots and hot moments of greenhouse gas emissions.

TABLE OF CONTENTS

ACKNOWLEDGMENTS

I certainly cannot put into words all the support and mentorship I have received. I am particularly thankful for my PhD advisor, Whendee Silver, who has invested so much in my development as a scientist. She has not only taught me invaluable knowledge in the fields of ecosystem ecology and soil biogeochemistry but also helped me develop the tools to conduct rigorous, policy-relevant scientific research, and become a better mentor than I ever thought possible. Her unwavering commitment to my development is no doubt the hallmark of my success.

The assistance and advice of many Silver Lab members have made my research possible: Allegra Mayer, Yang Lin, Wendy Yang, Kris Daum, and Brian Yudkin. Without Sintana Vergara's mentorship during my year as a lab technician, I likely would have not pursued a PhD. Summer Ahmed's unmatched organization made weekly soil sampling possible and maintained my sanity during countless hours in the lab. Heather Dang suffered through many trips to the field, helping to install and troubleshoot three separate field sites. Most importantly she also answered countless questions, particularly about the mass spectrometer. Tibisay Pérez was my go-to for scientific advice, helping me troubleshoot or repair any lab instrument.

I also must thank the many collaborators who provided me with the tools and knowledge to help me perform my scientific research. Dr. Dennis Baldocchi's help ranged from collecting bulk density measurements in a soil pit together to serving on both my qualifying and dissertation committees, all of which have shaped my approach to science and my understanding of the world around me. Numerous members of the Baldocchi lab, including Joe Verfaillie, Daphne Szutu, Sam Chamberlain, Kyle Hemes, Alex Valach, Kuno Kasak, Elke Eichelmann, and Camilo Rey-Sanchez provided unwavering support with soil sampling, instrumentation troubleshooting, and general scientific advice. From the Dawson Lab, Dr. Todd Dawson, Wenbo Yang, and Kelsey

Crutchfield-Peters provided invaluable advice about stable C and N isotopes and mass spectrometry, with Wenbo also helping measure countless samples on the ICP. I also want to thank Dr. Laura Lammers, Dr. David Sedlak, and Jennifer Mills for solidifying my understanding of redox reactions, critical to the complex biogeochemistry my research explores.

Most importantly, I could not have completed my dissertation without my wife, Rose Fruci-Anthony, by my side. Her unwavering confidence in my ability as a scientist helped get through the worst days. Her love and companionship kept me balanced and grounded when I needed to step away and reset. Her unwavering passion to give back to and uplift her community has continually reminded me why I do research and why any positive contribution makes the world a better place. I would also thank my parents and my brother Conner who have always provided the love and support necessary to pursue my dreams and aspirations as well as the ability to appreciate all the details in the world around me.

I was supported by a Contract by the California Department of Water Resources (award 4600011240) and the California Sea Grant Delta Science Fellowship. This material is based upon work supported by the Delta Stewardship Council Delta Science Program under Grant No. 5298 and California Sea Grant College Program Project R/SF-89. The contents of this material do not necessarily reflect the views and policies of the Delta Stewardship Council or California Sea Grant, nor does mention of trade names or commercial products constitute endorsement or recommendation for use. I thank the California Department of Water Resources and the Metropolitan Water District of Southern California for continuous research site access.

Chapter 1. Introduction

Wetlands represent only 3% of the world's soils, but account for approximately 21% of the global soil organic carbon (C) stock (Scharlemann, Tanner, Hiederer, & Kapos, 2014; Yu, Loisel, Brosseau, Beilman, & Hunt, 2010). Under natural, waterlogged conditions, high plant productivity and slow organic matter decomposition favors the accumulation of soil C, leading to a net CO_2 sink (Dise, 2009; Wilson et al., 2016). However, due to their high nutrient availability, more than 10% of wetlands worldwide have been drained for agriculture (Kramer & Shabman, 1993; Leifeld, 2013; Stephens, Allen, & Chen, 1984) and future increases in drainage is expected to meet growing demands for food production (Verhoeven & Setter, 2010). These land-use related disturbances often result in large soil C losses and significant N_2O emissions, currently contributing to substantial greenhouse gas emissions globally (1.91 Gt CO_2eq/year; Leifeld & Menichetti, 2018; Wilson et al., 2016). Reflooding has been proposed as a restoration approach for disturbed wetlands to reintroduce anaerobic conditions, limiting soil CO_2 and N_2O emissions and enhancing soil C sequestration (Hemes et al., 2019; Negandhi et al., 2019; Pfeifer-Meister, Gayton, Roy, Johnson, & Bridgham, 2018). Eddy-covariance studies suggest that reflooded soils have the potential to become net C sinks (on the order of 4.1 Mg ha^{-1} $year^{-1}$; Hemes et al., 2019), but increased CH_4 emissions from anaerobic soil conditions following reflooding can hinder or delay net C storage (Hatala, Detto, & Baldocchi, 2012; Knox et al., 2015).

When wetland soils are drained for agriculture, extensive losses of organic matter can also lead to the concentration of residual soil minerals. The role of soil minerals in soil C cycling and sequestration has been studied extensively in upland soils (Chen, Hall, Coward, & Thompson, 2020; Hall & Silver, 2015; Markus Kleber et al., 2015; Kögel-Knabner et al., 2008). Reactive iron (Fe) and aluminum (Al) minerals are thought to contribute to soil C accumulation in soils, particularly under aerobic conditions (Chen et al., 2020; W. Huang, Ye, Hockaday, & Hall, 2020; Markus Kleber et al., 2015). In contrast, oxidation-reduction (redox) active Fe minerals can also contribute significantly to C loss via anaerobic respiration of Fe-reducing bacteria and is a significant pathway of C loss in some upland ecosystems. (Baldock & Skjemstad, 2000; Kaiser & Guggenberger, 2000; Peretyazhko & Sposito, 2005; Wagai & Mayer, 2007). Reflooding drained wetlands has been proposed as a pathway to sequester C for climate change mitigation. However, the potential role of reactive Fe and Al minerals in C biogeochemistry is not well studied in drained and restored wetland soils. Understanding the interactions between reactive Fe and Al minerals and soil C pools would contribute to our understanding of the role of water and land management in C sequestration and loss.

In chapter two, I utilized soil samples from both drained and restored mineral-rich wetland soils across a range of soil C concentrations to explore relationships among management, Fe and Al concentrations, and soil C stocks. I hypothesized that the concentration of reactive Fe and Al minerals limit soil C losses in drained soils from increased recalcitrance following the formation of mineral-C associations (Chen et al., 2020; W. Huang et al., 2020; Markus Kleber et al., 2015). I also hypothesized that reactive Fe and Al mineral concentrations would not be related to C storage in reflooded systems where persistent anaerobic conditions would limited soil organic matter decomposition (Dise, 2009; Wilson et al., 2016). I quantified a suite of reactive Fe and Al pools to explore the potential interactions between these reactive

metal species and soil C across drained and reflooded soils. I found that reactive Fe was negatively correlated to soil C across all sites, suggesting reactive Fe pools may drive additional C losses in drained soils and limit C sequestration in reflooded soils. In contrast, reactive organo-Al complexes were strongly correlated to soil C concentrations in drained soils, suggesting organo-Al complexes facilitate aggregation and/or the formation of anaerobic (micro)sites that may protect residual soil C from oxidation and may partially offset C losses.

Nitrous oxide (N_2O), a potent greenhouse gas, can be both produced or consumed in soils under anaerobic conditions. The magnitude and controls on N_2O emissions from managed wetlands remain a key uncertainty in wetland ecosystem greenhouse gas budgets (Liu, Wrage-Mönnig, & Lennartz, 2020). This is largely driven by previous limitations in the ability to conduct continuous, long-term N_2O flux measurements under field conditions (Baldocchi, 2014; Bonn et al., 2014; Frolking et al., 2011; Günther et al., 2020; Levy et al., 2017; Rochette & Eriksen-Hamel, 2008). In chapter three, I conducted a long-term, continuous *in-situ* observations of soil greenhouse gas fluxes from an organic-rich drained peatland soil. I used cavity ring-down spectroscopy and automated soil flux chambers deployed over three complete years to accurately quantify the annual ecosystem fluxes of CO_2, CH_4, and N_2O. Drained agricultural peatlands are known to be significant sources of greenhouse gases, but N_2O emissions are often underestimated in agricultural peatland greenhouse gas budgets due to previous limitations in conducting continuous, long-term N_2O flux measurements (Baldocchi, 2014; Bonn et al., 2014; Frolking et al., 2011; Günther et al., 2020; Levy et al., 2017; Rochette & Eriksen-Hamel, 2008). I found that N_2O alone contributed up to 33% of annual CO_2-equivalent ecosystem emissions, which suggests IPCC benchmarks may underestimate N_2O emissions from drained agricultural peatland soils by 225%. I also quantified the importance of hot moments on annual greenhouse gas fluxes and found that hot moments of N_2O and CH_4 emissions represented only 1.1 ± 0.2 and 1.3 ± 0.2% of measurements but increased annual N_2O fluxes by 45 ± 1% and CH_4 fluxes by 140 ± 9%, respectively. I found that the main drivers of soil N_2O fluxes were elevated nitrate (NO_3^-) concentrations and significant increases in soil moisture, which quickly reduced soil O_2 availability. Soil moisture, soil temperature, and bulk soil O_2 concentrations were also strongly associated with soil CH_4 emissions, but only extended periods of anaerobic conditions produced hot moments of CH_4 flux.

In chapter four, I explored the production and consumption pathways of N_2O and CH_4 in this same organic-rich drained peatland soil. Net flux measurements quantify the balance of production and consumption pathways of soil N_2O and CH_4 but are not adequate to fully infer their controls. A better understanding of the controls on production and consumption pathways is necessary to understand how hot moments of net N_2O and CH_4 emissions from agricultural soils will vary with climate change and land management. I first used continuous net flux measurements from chapter 3 to identify patterns in GHG emissions. I then utilized targeted pool dilution experiments that use the isotopic dilution and loss of ^{15}N-N_2O and ^{13}C-CH_4 to calculate gross rates of production and consumption of both N_2O and CH_4. I used this technique on soil samples across multiple depths during both the growing season and following a winter flooding event to measure gross N_2O and CH_4 fluxes under contrasting soil conditions. I quantified the same reactive Fe and Al pools from chapter two as these reactive minerals may interact with N_2O and CH_4 pathways via several biogeochemical processes. Net soil N_2O fluxes were highest in surface soils shortly after soil saturation and corresponded to higher rates of gross N_2O

production than when soils were drained. Gross N_2O production was strongly correlated to soil moisture across all samples. Gross N_2O consumption rates were highest under drained subsoils (up to 2.2 ± 1.0 μg N g $soil^{-1}$ d^{-1}) and were correlated with NO_3^- concentrations, suggesting N_2O consumption was indirectly controlled by substrate availability for denitrifiers. Combined with a decline in net N_2O fluxes observed under drained soil conditions, this suggests anaerobic hotspots may maintain areas of N_2O consumption sparsely distributed throughout the soil. This ecosystem was a net CH_4 sink during the measurement period. Gross CH_4 consumption (range: 0-5.6 μg C g $soil^{-1}$ d^{-1}) was generally greater than gross CH_4 production (range: 0-2.8 μg C g $soil^{-1}$ d^{-1}). Gross CH_4 production increased with soil depth, likely driven by both increased soil moisture and anaerobic soil conditions. Gross CH_4 consumption was negatively correlated with soil moisture and positively correlated with soil pH in surface soils, indicating both low pH and O_2 availability directly limit CH_4 consumption. Gross CH_4 consumption accounted for up to 24.9% of net CO_2 production (mean ± SE: 6.6% ± 3.4%) in drained soils at depth. Our results suggest that gross N_2O and CH_4 production were temporally decoupled from gross N_2O and CH_4 consumption and are driven by soil moisture status and associated effects on NO_3^- and pH.

In chapter five, I conducted a separate long-term, continuous *in-situ* observations of soil greenhouse gas fluxes from an alfalfa field planted on a mineral-rich drained peatland soil. Using the same cavity ring-down spectroscopy and automated soil flux chamber technology from chapter three, I collected over 108,000 individual flux measurements of CO_2, CH_4, and N_2O fluxes over four years to quantify the annual greenhouse gas budgets of an intensively managed alfalfa ecosystem. Accurate measurements of soil greenhouse gas fluxes from this system are important as alfalfa is the most widely grown perennial forage legume worldwide, and is the largest crop by acreage in the Western United States (Ottman et al., 2013; S. Yang et al., 2008). Additionally, alfalfa has been suggested as a more sustainable feedstock relative to corn given its suggested potential to increase soil C sequestration as a perennial plant and its ability to fix N_2, which can decrease the need for N fertilizer inputs. This ecosystem was a consistent source of N_2O and a small net sink of CH_4. Soil CO_2 fluxes were greater than other alfalfa ecosystem estimates, likely driven by plant productivity and soil temperatures throughout the growing season. Hot moment of N_2O fluxes were 0.2% to 1.1% of annual measurements but contributed to 31.6% to 56.8% of annual N_2O fluxes. I found that both the magnitude and the contribution of N_2O hot moments to annual N_2O emissions decreased over time. Normalized difference vegetation index (NDVI), soil temperature, moisture, and O_2 were all significantly correlated with soil CO_2, N_2O, and CH_4 fluxes, although associations varied across both soil depth and timescales. These data suggest that flood-irrigated alfalfa is a significant source of agricultural N_2O emissions, and plant productivity and soil moisture effects on O_2 availability may modulate the net GHG budget of alfalfa agroecosystems.

References

Baldocchi, D. (2014). Measuring fluxes of trace gases and energy between ecosystems and the atmosphere - the state and future of the eddy covariance method. *Global Change Biology*, *20*(12), 3600–3609. https://doi.org/10.1111/gcb.12649

Baldock, J. A., & Skjemstad, J. O. (2000). Role of the soil matrix and minerals in protecting natural organic materials against biological attack. *Organic*

Geochemistry, *31*, 697–710. https://doi.org/https://doi.org/10.1016/S0146-6380(00)00049-8

Barcellos, D., O'Connell, C., Silver, W., Meile, C., & Thompson, A. (2018). Hot Spots and Hot Moments of Soil Moisture Explain Fluctuations in Iron and Carbon Cycling in a Humid Tropical Forest Soil. *Soil Systems*, *2*(4), 59. https://doi.org/10.3390/soilsystems2040059

Bazilevskaya, E., Archibald, D. D., & Martínez, C. E. (2018). Mineral colloids mediate organic carbon accumulation in a temperate forest Spodosol: depth-wise changes in pore water chemistry. *Biogeochemistry*, *141*(1), 75–94. https://doi.org/10.1007/s10533-018-0504-4

Bhattacharyya, A., Campbell, A. N., Tfaily, M. M., Lin, Y., Silver, W. L., Nico, P. S., & Pett-Ridge, J. (2018). Redox fluctuations control the coupled cycling of iron and carbon in tropical forest soils. *Environmental Science & Technology*, *52*, 14129−14139. https://doi.org/10.1101/312108

Bonn, A., Reed, M. S., Evans, C. D., Joosten, H., Bain, C., Farmer, J., … Birnie, D. (2014). Investing in nature: Developing ecosystem service markets for peatland restoration. *Ecosystem Services*, *9*, 54–65. https://doi.org/10.1016/j.ecoser.2014.06.011

Catallo, W. J. (Ed.). (1999). *Hourly and daily variation of sediment redox potential in tidal wetland sediments*. *Biological Science Report*. Reston, VA. Retrieved from http://pubs.er.usgs.gov/publication/bsr19990001

Chamberlain, S. D., Anthony, T. L., Silver, W. L., Eichelmann, E., Hemes, K. S., Oikawa, P. Y., … Baldocchi, D. D. (2018). Soil properties and sediment accretion modulate methane fluxes from restored wetlands. *Global Change Biology*, *24*(9), 4107–4121. https://doi.org/10.1111/gcb.14124

Chen, C., Hall, S. J., Coward, E., & Thompson, A. (2020). Iron-mediated organic matter decomposition in humid soils can counteract protection. *Nature Communications*, *11*(1), 2255. https://doi.org/10.1038/s41467-020-16071-5

Coby, A. J., Picardal, F., Shelobolina, E., Xu, H., & Roden, E. E. (2011). Repeated anaerobic microbial redox cycling of iron. *Applied and Environmental Microbiology*, *77*(17), 6036–6042. https://doi.org/10.1128/AEM.00276-11

Conrad, R. (1996, December). *Soil microorganisms as controllers of atmospheric trace gases (H2, CO, CH4, OCS, N2O, and NO)*. *Microbiological Reviews*. Retrieved from http://mmbr.asm.org/content/60/4/609.abstract

Coward, E. K., Thompson, A., & Plante, A. F. (2018). Contrasting Fe speciation in two humid forest soils: Insight into organomineral associations in redox-active environments. *Geochimica et Cosmochimica Acta*, *238*, 68–84. https://doi.org/10.1016/j.gca.2018.07.007

Coward, E. K., Thompson, A. T., & Plante, A. F. (2017). Iron-mediated mineralogical control of organic matter accumulation in tropical soils. *Geoderma*, *306*, 206–216. https://doi.org/10.1016/j.geoderma.2017.07.026

De-Campos, A. B., Mamedov, A. I., & Huang, C. (2009). Short-Term Reducing Conditions Decrease Soil Aggregation. *Soil Science Society of America Journal*, *73*(2), 550. https://doi.org/10.2136/sssaj2007.0425

Deverel, S. J., Ingrum, T., & Leighton, D. (2016). Present-day oxidative subsidence of organic soils and mitigation in the Sacramento-San Joaquin Delta, California,

USA. *Hydrogeology Journal*, *24*(3), 569–586. https://doi.org/10.1007/s10040-016-1391-1

Dise, N. B. (2009). Peatland Response to Global Change. *Science*, *326*(5954), 810–811. https://doi.org/10.1126/science.1174268

Drexler, J. Z., Fontaine, C. S., & Deverel, S. J. (2009). The legacy of wetland drainage on the remaining peat in the Sacramento — San Joaquin Delta, California, USA. *Wetlands*, *29*(1), 372–386. https://doi.org/10.1672/08-97.1

Eichelmann, E., Hemes, K. S., Knox, S. H., Oikawa, P. Y., Chamberlain, S. D., Verfaillie, J., & Baldocchi, D. D. (2018). The Effect of Land Cover Type and Structure on Evapotranspiration from Agricultural and Wetland Sites in the Sacramento/San Joaquin River Delta, California. *Agricultural and Forest Meteorology*, *256–257*, 179–195. https://doi.org/https://doi.org/10.1016/j.agrformet.2018.03.007

Emsens, W.-J., Aggenbach, C. J. S., Schoutens, K., Smolders, A. J. P., Zak, D., & van Diggelen, R. (2016). Soil Iron Content as a Predictor of Carbon and Nutrient Mobilization in Rewetted Fens. *PloS One*, *11*(4), 1–17. https://doi.org/10.1371/journal.pone.0153166

Fredrickson, J. K., Zachara, J. M., Kennedy, D. W., Dong, H., Onstott, T. C., Hinman, N. W., & Li, S. M. (1998). Biogenic iron mineralization accompanying the dissimilatory reduction of hydrous ferric oxide by a groundwater bacterium. *Geochimica et Cosmochimica Acta*, *62*(19–20), 3239–3257. https://doi.org/10.1016/S0016-7037(98)00243-9

Frolking, S., Talbot, J., Jones, M. C., Treat, C. C., Kauffman, J. B., Tuittila, E. S., & Roulet, N. (2011). Peatlands in the Earth's 21st century climate system. *Environmental Reviews*, *19*(1), 371–396. https://doi.org/10.1139/a11-014

Günther, A., Barthelmes, A., Huth, V., Joosten, H., Jurasinski, G., Koebsch, F., & Couwenberg, J. (2020). Prompt rewetting of drained peatlands reduces climate warming despite methane emissions. *Nature Communications*, *11*(1), 1–5. https://doi.org/10.1038/s41467-020-15499-z

Hall, S. J., & Silver, W. L. (2013). Iron oxidation stimulates organic matter decomposition in humid tropical forest soils. *Global Change Biology*, 2804–2813. https://doi.org/10.1111/gcb.12229

Hall, S. J., & Silver, W. L. (2015). Reducing conditions, reactive metals, and their interactions can explain spatial patterns of surface soil carbon in a humid tropical forest. *Biogeochemistry*, *125*(2), 149–165. https://doi.org/10.1007/s10533-015-0120-5

Hatala, J. A., Detto, M., & Baldocchi, D. D. (2012). Gross ecosystem photosynthesis causes a diurnal pattern in methane emission from rice. *Geophysical Research Letters*, *39*(6), 1–5. https://doi.org/10.1029/2012GL051303

Hatala, J. A., Detto, M., Sonnentag, O., Deverel, S. J., Verfaillie, J., & Baldocchi, D. D. (2012). Greenhouse gas (CO2, CH4, H2O) fluxes from drained and flooded agricultural peatlands in the Sacramento-San Joaquin Delta. *Agriculture, Ecosystems and Environment*, *150*, 1–18. https://doi.org/10.1016/j.agee.2012.01.009

Hemes, K. S., Chamberlain, S. D., Eichelmann, E., Anthony, T., Valach, A., Kasak, K., … Baldocchi, D. D. (2019). Assessing the carbon and climate benefit of

restoring degraded agricultural peat soils to managed wetlands. *Agricultural and Forest Meteorology*, *268*, 202–214. https://doi.org/10.1016/j.agrformet.2019.01.017

Hemes, K. S., Chamberlain, S. D., Eichelmann, E., Knox, S. H., & Baldocchi, D. D. (2018). A Biogeochemical Compromise: The High Methane Cost of Sequestering Carbon in Restored Wetlands. *Geophysical Research Letters*, *45*(12), 6081–6091. https://doi.org/10.1029/2018GL077747

Holden, J., Chapman, P. J., & Labadz, J. C. (2004). Artificial drainage of peatlands: Hydrological and hydrochemical process and wetland restoration. *Progress in Physical Geography*, *28*(1), 95–123. https://doi.org/10.1191/0309133304pp403ra

Huang, W., & Hall, S. J. (2017). Optimized high-throughput methods for quantifying iron biogeochemical dynamics in soil. *Geoderma*, *306*(November 2016), 67–72. https://doi.org/10.1016/j.geoderma.2017.07.013

Huang, W., Ye, C., Hockaday, W. C., & Hall, S. J. (2020). Trade-offs in soil carbon protection mechanisms under aerobic and anaerobic conditions. *Global Change Biology*, (March), 3726–3737. https://doi.org/10.1111/gcb.15100

Huang, X., Tang, H., Kang, W., Yu, G., Ran, W., Hong, J., & Shen, Q. (2018). Redox interface-associated organo-mineral interactions: A mechanism for C sequestration under a rice-wheat cropping system. *Soil Biology and Biochemistry*, *120*, 12–23. https://doi.org/10.1016/j.soilbio.2018.01.031

IPCC, 2014. (2013). 2013 Supplement to the 2006 IPCC Guidelines for National Greenhouse Gas Inventories: Wetlands, Hiraishi, T., Krug, T., Tanabe, K., Srivastava, N., Baasansuren, J., Fukuda, M. and Troxler, T.G. (eds).

Jansen, B., Nierop, K. G. J., & Verstraten, J. M. (2004). Mobilization of dissolved organic matter, aluminium and iron in podzol eluvial horizons as affected by formation of metal-organic complexes and interactions with solid soil material. *European Journal of Soil Science*, *55*(2), 287–297. https://doi.org/10.1111/j.1365-2389.2004.00598.x

Kaiser, K., Eusterhues, K., Rumpel, C., Guggenberger, G., & Kögel-Knabner, I. (2002). Stabilization of organic matter by soil minerals - Investigations of density and particle-size fractions from two acid forest soils. *Journal of Plant Nutrition and Soil Science*, *165*(4), 451–459. https://doi.org/10.1002/1522-2624(200208)165:4<451::AID-JPLN451>3.0.CO;2-B

Kaiser, K., & Guggenberger, G. (2000). The role of DOM sorption to mineral surfaces in the preservation of organic matter in soils. *Organic Geochemistry*, *31*(7–8), 711–725. https://doi.org/10.1016/S0146-6380(00)00046-2

Kaplan, D. I., Xu, C., Huang, S., Lin, Y., Tolić, N., Roscioli-Johnson, K. M., … Jaffé, P. R. (2016). Unique Organic Matter and Microbial Properties in the Rhizosphere of a Wetland Soil. *Environmental Science and Technology*, *50*(8), 4169–4177. https://doi.org/10.1021/acs.est.5b05165

Keiluweit, M., Nico, P. S., Kleber, M., & Fendorf, S. (2016). Are oxygen limitations under recognized regulators of organic carbon turnover in upland soils? *Biogeochemistry*, *127*(2–3), 157–171. https://doi.org/10.1007/s10533-015-0180-6

Kleber, M., Mikutta, R., Torn, M. S., & Jahn, R. (2005). Poorly crystalline mineral phases protect organic matter in acid subsoil horizons. *European Journal of Soil Science*, *56*(6), 717–725. https://doi.org/10.1111/j.1365-2389.2005.00706.x

Kleber, Markus, Eusterhues, K., Keiluweit, M., Mikutta, C., Mikutta, R., & Nico, P. S. (2015). *Mineral-Organic Associations: Formation, Properties, and Relevance in Soil Environments*. *Advances in Agronomy* (Vol. 130). Elsevier Ltd. https://doi.org/10.1016/bs.agron.2014.10.005

Knox, S. H., Sturtevant, C., Matthes, J. H., Koteen, L., Verfaillie, J., & Baldocchi, D. (2015). Agricultural peatland restoration: Effects of land-use change on greenhouse gas (CO2 and CH4) fluxes in the Sacramento-San Joaquin Delta. *Global Change Biology*, *21*(2), 750–765. https://doi.org/10.1111/gcb.12745

Kögel-Knabner, I., Amelung, W., Cao, Z., Fiedler, S., Frenzel, P., Jahn, R., … Schloter, M. (2010). Biogeochemistry of paddy soils. *Geoderma*, *157*(1–2), 1–14. https://doi.org/10.1016/j.geoderma.2010.03.009

Kögel-Knabner, I., Guggenberger, G., Kleber, M., Kandeler, E., Kalbitz, K., Scheu, S., … Leinweber, P. (2008). Organo-mineral associations in temperate soils: Integrating biology, mineralogy, and organic matter chemistry. *Journal of Plant Nutrition and Soil Science*, *171*(1), 61–82. https://doi.org/10.1002/jpln.200700048

Kramer, R. A., & Shabman, L. (1993). The Effects of Agricultural and Tax Policy Reform on the Economic Return to Wetland Drainage in the Mississippi Delta Region, *69*(3), 249–262.

LaCroix, R., Tfaily, M., McCreight, M., Jones, M. E., Spokas, L., & Keiluweit, M. (2018). Shifting Mineral and Redox Controls on Carbon Cycling in Seasonally Flooded Soils. *Biogeosciences Discussions*, 1–36. https://doi.org/10.5194/bg-2018-432

Lalonde, K., Mucci, A., Ouellet, A., & Gélinas, Y. (2012). Preservation of organic matter in sediments promoted by iron. *Nature*, *483*(7388), 198–200. https://doi.org/10.1038/nature10855

Leifeld, J. (2013). Prologue paper: Soil carbon losses from land-use change and the global agricultural greenhouse gas budget. *Science of the Total Environment*, *465*, 3–6. https://doi.org/10.1016/j.scitotenv.2013.03.050

Leifeld, J., & Menichetti, L. (2018). The underappreciated potential of peatlands in global climate change mitigation strategies. *Nature Communications*, *9*. https://doi.org/10.1038/s41467-018-03406-6

Levy, P. E., Cowan, N., van Oijen, M., Famulari, D., Drewer, J., & Skiba, U. (2017). Estimation of cumulative fluxes of nitrous oxide: uncertainty in temporal upscaling and emission factors. *European Journal of Soil Science*, *68*(4), 400–411. https://doi.org/10.1111/ejss.12432

Liu, H., Wrage-Mönnig, N., & Lennartz, B. (2020). Rewetting strategies to reduce nitrous oxide emissions from European peatlands. *Communications Earth & Environment*, *1*(1), 17. https://doi.org/10.1038/s43247-020-00017-2

Loeppert, R. H., & Inskeep, W. P. (1996). *Methods of Soil Analysis. Part 3. Chemical Methods*.

Lovley, D. R. (1991). Dissimilatory Fe(III) and Mn(IV) reduction. *Microbiological Reviews*, *55*(2), 259–287. Retrieved from https://pubmed.ncbi.nlm.nih.gov/1886521

McLean, E. O. (1982). Soil pH and Lime Requirement. In *Page, A.L., Ed., Methods of Soil Analysis. Part 2. Chemical and Microbiological Properties, American*

Society of Agronomy, Soil Science Society of America, Madison, (pp. 199–224).
Mejia, J., Roden, E. E., & Ginder-Vogel, M. (2016). Influence of Oxygen and Nitrate on Fe (Hydr)oxide Mineral Transformation and Soil Microbial Communities during Redox Cycling. *Environmental Science and Technology*, *50*(7), 3580–3588. https://doi.org/10.1021/acs.est.5b05519
Melton, E. D., Swanner, E. D., Behrens, S., Schmidt, C., & Kappler, A. (2014). The interplay of microbially mediated and abiotic reactions in the biogeochemical Fe cycle. *Nature Reviews. Microbiology*, *12*(12), 797–809. https://doi.org/10.1038/nrmicro3347
Miller, R. L., Fram, M. S., Fujii, R., & Wheeler, G. (2008). Subsidence Reversal in a Re-established Wetland in the Sacramento-San Joaquin Delta, California, USA. *San Francisco Estuary and Watershed Science*, *6*(3), 1–20. https://doi.org/10.5811/westjem.2011.5.6700
Negandhi, K., Edwards, G., Kelleway, J. J., Howard, D., Safari, D., & Saintilan, N. (2019). Blue carbon potential of coastal wetland restoration varies with inundation and rainfall. *Scientific Reports*, *9*(1), 4368. https://doi.org/10.1038/s41598-019-40763-8
Niedermeier, A., & Robinson, J. S. (2007). Hydrological controls on soil redox dynamics in a peat-based, restored wetland. *Geoderma*, *137*(3–4), 318–326. https://doi.org/10.1016/j.geoderma.2006.08.027
Nikolausz, M., Kappelmeyer, U., Székely, A., Rusznyák, A., Márialigeti, K., & Kästner, M. (2008). Diurnal redox fluctuation and microbial activity in the rhizosphere of wetland plants. *European Journal of Soil Biology*, *44*(3), 324–333. https://doi.org/10.1016/j.ejsobi.2008.01.003
Oades, J. M., & Waters, A. G. (1991). Aggregate hierarchy in soils. *Australian Journal of Soil Research*, *29*(6), 815–825. https://doi.org/10.1071/SR9910815
Ottman, M., Putnam, D., Barlow, V., Brummer, J., Bohle, M., Davison, J., … Norberg, S. (2013). Long term trends and the future of the alfalfa and forage industry. *Proceedings, 2013 Western Alfalfa & Forage Symposium, Reno, NV, 11-13, December, 2013. UC Cooperative Extension, Plant Sciences Department, University of California, Davis, CA 95616.*, 11–13. Retrieved from http://www.pnas.org/lookup/doi/10.1073/pnas.1707322114
Peretyazhko, T., & Sposito, G. (2005). Iron(III) reduction and phosphorous solubilization in humid tropical forest soils. *Geochimica et Cosmochimica Acta*, *69*(14), 3643–3652. https://doi.org/10.1016/j.gca.2005.03.045
Pfeifer-Meister, L., Gayton, L. G., Roy, B. A., Johnson, B. R., & Bridgham, S. D. (2018). Greenhouse gas emissions limited by low nitrogen and carbon availability in natural, restored, and agricultural Oregon seasonal wetlands. *PeerJ*, *2018*(8). https://doi.org/10.7717/peerj.5465
Phillips, E. J. P., Lovley, D. R., & Roden, E. E. (1993). Composition of non-microbially reducible Fe(III) in aquatic sediments. *Applied and Environmental Microbiology*, *59*(8), 2727–2729. https://doi.org/10.1128/aem.59.8.2727-2729.1993
Porras, R. C., Hicks Pries, C. E., McFarlane, K. J., Hanson, P. J., & Torn, M. S. (2017). Association with pedogenic iron and aluminum: effects on soil organic carbon storage and stability in four temperate forest soils. *Biogeochemistry*.

https://doi.org/10.1007/s10533-017-0337-6
Rochette, P., & Eriksen-Hamel, N. S. (2008). Chamber Measurements of Soil Nitrous Oxide Flux: Are Absolute Values Reliable? *Soil Science Society of America Journal*, *72*(2), 331–342. https://doi.org/10.2136/sssaj2007.0215
Scharlemann, J. P. W., Tanner, E. V. J., Hiederer, R., & Kapos, V. (2014). Global soil carbon: Understanding and managing the largest terrestrial carbon pool. *Carbon Management*, *5*(1), 81–91. https://doi.org/10.4155/cmt.13.77
Scheel, T., Dörfl, C., & Kalbitz, K. (2007). Precipitation of Dissolved Organic Matter by Aluminum Stabilizes Carbon in Acidic Forest Soils. *Soil Science Society of America Journal*, *71*(1), 64–74. https://doi.org/10.2136/sssaj2006.0111
Silver, W. L., Ryals, R., & Eviner, V. (2010). Soil Carbon Pools in California's Annual Grassland Ecosystems. *Rangeland Ecology & Management*, *63*(1), 128–136. https://doi.org/10.2111/REM-D-09-00106.1
Six, J., & Paustian, K. (2014). Aggregate-associated soil organic matter as an ecosystem property and a measurement tool. *Soil Biology and Biochemistry*, *68*, A4–A9. https://doi.org/10.1016/j.soilbio.2013.06.014
Spivak, A. C., Sanderman, J., Bowen, J. L., Canuel, E. A., & Hopkinson, C. S. (2019). Global-change controls on soil-carbon accumulation and loss in coastal vegetated ecosystems. *Nature Geoscience*, *12*(9), 685–692. https://doi.org/10.1038/s41561-019-0435-2
Stephens, J. C., Allen, L. H., & Chen, E. (1984). Organic Soil Subsidence. *Reviews in Engineering Geology*, *VI*(225). https://doi.org/10.1130/REG6-p107
Stepniewski, W., Gliński, J., & Ball, B. C. (1994). Effects of Compaction on Soil Aeration Properties. *Developments in Agricultural Engineering*, *11*(C), 167–189. https://doi.org/10.1016/B978-0-444-88286-8.50016-7
Takahashi, T., & Dahlgren, R. A. (2016). Nature, properties and function of aluminum-humus complexes in volcanic soils. *Geoderma*, *263*, 110–121. https://doi.org/10.1016/j.geoderma.2015.08.032
Teh, Y. A., Silver, W. L., Sonnentag, O., Detto, M., Kelly, M., & Baldocchi, D. D. (2011). Large Greenhouse Gas Emissions from a Temperate Peatland Pasture. *Ecosystems*, *14*(2), 311–325. https://doi.org/10.1007/s10021-011-9411-4
Thompson, A., Rancourt, D. G., Chadwick, O. A., & Chorover, J. (2011). Iron solid-phase differentiation along a redox gradient in basaltic soils. *Geochimica et Cosmochimica Acta*, *75*(1), 119–133. https://doi.org/10.1016/j.gca.2010.10.005
Todorova, S. G., Siegel, D. I., & Costello, A. M. (2005). Microbial Fe(III) reduction in a minerotrophic wetland - Geochemical controls and involvement in organic matter decomposition. *Applied Geochemistry*, *20*(6), 1120–1130. https://doi.org/10.1016/j.apgeochem.2005.02.005
Torn, M. S., Trumbore, S. E., Chadwick, O. A., Vitousek, P. M., & Hendricks, D. M. (1997). Mineral control of soil organic carbon storage and turnover. *Nature*, *389*(6647), 170–173. https://doi.org/10.1038/38260
Torrent, I. R. J. (1997). Citrate-Ascorbate as a Highly Selective Extractant for Poorly Crystalline Iron Oxides. *Soil Science Society of America Journal*, *61*, 1647–1654. https://doi.org/10.2136/sssaj1997.03615995006100060015x
Totsche, K. U., Amelung, W., Gerzabek, M. H., Guggenberger, G., Klumpp, E., Knief, C., … Kögel-Knabner, I. (2017). Microaggregates in soils. *Journal of Plant*

Nutrition and Soil Science, 104–136. https://doi.org/10.1002/jpln.201600451
Verhoeven, J. T. A., & Setter, T. L. (2010). Agricultural use of wetlands: Opportunities and limitations. *Annals of Botany*, *105*(1), 155–163. https://doi.org/10.1093/aob/mcp172
Verschoor, M. J., & Molot, L. A. (2013). A comparison of three colorimetric methods of ferrous and total reactive iron measurement in freshwaters. *Limnology and Oceanography: Methods*, *11*(MAR), 113–125. https://doi.org/10.4319/lom.2013.11.113
Viollier, E., Inglett, P. W., Hunter, K., Roychoudhury, A. N., & Van Cappellen, P. (2000). The ferrozine method revisited: Fe(II)/Fe(III) determination in natural waters. *Applied Geochemistry*, *15*(6), 785–790. https://doi.org/10.1016/S0883-2927(99)00097-9
Vorenhout, M., van der Geest, H. G., van Marum, D., Wattel, K., & Eijsackers, H. J. P. (2004). Automated and Continuous Redox Potential Measurements in Soil. *Journal of Environment Quality*, *33*(4), 1562. https://doi.org/10.2134/jeq2004.1562
Wagai, R., & Mayer, L. M. (2007). Sorptive stabilization of organic matter in soils by hydrous iron oxides. *Geochimica et Cosmochimica Acta*, *71*, 25–35. https://doi.org/10.1016/j.gca.2006.08.047
Wagai, R., Mayer, L. M., Kitayama, K., & Shirato, Y. (2013). Association of organic matter with iron and aluminum across a range of soils determined via selective dissolution techniques coupled with dissolved nitrogen analysis. *Biogeochemistry*, *112*(1–3), 95–109. https://doi.org/10.1007/s10533-011-9652-5
Wang, H., River, M., & Richardson, C. J. (2019). Does an 'iron gate' carbon preservation mechanism exist in organic–rich wetlands? *Soil Biology and Biochemistry*, *135*, 48–50. https://doi.org/10.1016/j.soilbio.2019.04.011
Warren, S. D., Nevill, M. B., Blackburn, W. H., & Garza, N. E. (1986). Soil Response to Trampling Under Intensive Rotation Grazing. *Soil Science Society of America Journal*, *50*(5), 1336. https://doi.org/10.2136/sssaj1986.03615995005000050050x
Weber, K. A., Achenbach, L. A., & Coates, J. D. (2006). Microorganisms pumping iron: anaerobic microbial iron oxidation and reduction. *Nature Reviews*, *4*(iii), 752–764. https://doi.org/10.1038/nrmicro1490
Wilson, S., Blain, D., Couwenberg, J., Evans, C. D., Murdiyarso, D., Page, S. E., … Tuittila, E.-S. (2016). Greenhouse gas emission factors associated with rewetting of organic soils. *Mires and Peat*, *17*(4), 1–28. https://doi.org/10.19189/MaP.2016.OMB.222
Wiseman, C. L. S., & Püttmann, W. (2006). Interactions between mineral phases in the preservation of soil organic matter. *Geoderma*, *134*(1–2), 109–118. https://doi.org/10.1016/j.geoderma.2005.09.001
Yang, S., Gao, M., Xu, C., Gao, J., Deshpande, S., Lin, S., … Zhu, H. (2008). Alfalfa benefits from Medicago truncatula: The RCT1 gene from M. truncatula confers broad-spectrum resistance to anthracnose in alfalfa. *Proceedings of the National Academy of Sciences of the United States of America*, *105*(34), 12164–12169. https://doi.org/10.1073/pnas.0802518105
Yang, W. H., & Liptzin, D. (2015). High potential for iron reduction in upland soils.

Ecology, *96*(7), 2015–2020. https://doi.org/10.1890/14-2097.1
Yu, Z., Loisel, J., Brosseau, D. P., Beilman, D. W., & Hunt, S. J. (2010). Global peatland dynamics since the Last Glacial Maximum. *Geophysical Research Letters*, *37*(13), 1–5. https://doi.org/10.1029/2010GL043584

Chapter 2. Mineralogical associations with soil carbon in managed wetland soils[1]

2.1 Abstract

Carbon (C) rich wetland soils are often drained for agriculture due to their capacity to support high net primary productivity. Increased drainage is expected this century to meet the agricultural demands of a growing population. Wetland drainage can result in large soil C losses and the concentration of residual soil minerals such as iron (Fe) and aluminum (Al). In upland soils, reactive Fe and Al minerals can contribute to soil C accumulation through sorption to poorly crystalline minerals and precipitation of organo-metal complexes, as well as C loss via anaerobic respiration by Fe-reducing bacteria. The role of these minerals in soil C dynamics is often overlooked in managed wetland soils and may be particularly important in both drained and reflooded systems with elevated mineral concentrations. Reflooding drained soils has been proposed as a means to sequester C for climate change mitigation, yet little is known about how reactive Fe and Al minerals affect C cycling in restored wetlands. We explored the interactions among soil C and reactive Fe and Al minerals in drained and reflooded wetland soils. In reflooded soils, soil C was negatively associated with reactive Fe and reduced Fe(II), a proxy for anaerobic conditions (reactive Fe: R^2=0.54-0.79; Fe(II): R^2=0.59-0.89). In drained soils, organo-Al complexes were positively associated with soil C and Fe(II) (Al R^2 =0.91; Fe(II): R^2=0.54-0.60). Soil moisture, organo-Al, and reactive Fe explained most of the variation observed in soil C concentrations across all sites ($P<0.01$). Reactive Fe was negatively correlated to soil C concentrations across sites, suggesting these Fe pools may drive additional C losses in drained soils and limit C sequestration with reflooding. In contrast, reactive organo-Al in drained soils facilitates C storage via aggregation and/or formation of anaerobic (micro)sites that protect residual soil C from oxidation and may at least partially offset C losses.

[1]This chapter is reprinted, with permission from Wiley Publishing, from the original journal article: Anthony, T. L., & Silver, W. L. (2020). Mineralogical associations with soil carbon in managed wetland soils. *Global Change Biology*, 1–13. https://doi.org/10.1111/gcb.15309

2.2 Introduction

Wetlands represent only 3% of the world's soils, but account for approximately 21% of the global soil organic carbon (C) stock (Scharlemann et al., 2014; Yu et al., 2010). Under natural, waterlogged conditions, slow decomposition favors the accumulation of soil organic matter, leading to a net C sink (Dise, 2009; Wilson et al., 2016). However, >10% of wetlands worldwide have been drained for agriculture (Kramer & Shabman, 1993; Leifeld, 2013; Stephens et al., 1984), and future increases in drainage are expected this century to meet growing demands for food production (Verhoeven & Setter, 2010). These land use-related disturbances to soil and hydrologic conditions often result in large soil C losses and currently contribute to substantial greenhouse gas emissions globally (1.91 Gt CO_{2eq} yr^{-1}, (Hemes et al., 2019; Leifeld & Menichetti, 2018; Wilson et al., 2016). Following drainage, rapid oxidation enhances soil organic matter decomposition, leading to significant land surface subsidence and carbon dioxide (CO_2) emissions (Deverel, Ingrum, & Leighton, 2016; IPCC, 2013; Teh et al., 2011). Reflooding has been proposed as a restoration approach on drained soils to reintroduce anaerobic conditions, reverse land subsidence, and enhance soil C sequestration. Eddy-covariance studies suggest that reflooded soils have the potential to become net C sinks (on the order of 4.1 Mg ha^{-1} yr^{-1}, (Hemes et al., 2019), but C emissions following flooding can hinder or delay net C storage (Hatala, Detto, Sonnentag, et al., 2012; Hemes, Chamberlain, Eichelmann, Knox, & Baldocchi, 2018; Knox et al., 2015; Miller, Fram, Fujii, & Wheeler, 2008). Given their large soil C stocks, high soil C sequestration potential, and the potential for large greenhouse gas emissions, better understanding of the mechanisms controlling soil C dynamics in both drained and restored reflooded wetlands is needed (Spivak, Sanderman, Bowen, Canuel, & Hopkinson, 2019).

When wetland soils are drained for agriculture, extensive losses of organic matter can lead to the concentration of minerals in soils. The role of soil minerals in soil C sequestration and loss has been studied extensively in upland soils (Hall & Silver, 2015; Markus Kleber et al., 2015; Kögel-Knabner et al., 2008, Chen et al. 2020), but the relationships between soil minerals and C storage in organic-rich soils has not been explored. Reactive iron (Fe) and aluminum (Al) minerals are thought to contribute to soil C accumulation in soils through direct sorption to poorly crystalline minerals and/or precipitation of organo-metal complexes, particularly under aerobic conditions (Chen et al., 2020; W. Huang et al., 2020; Markus Kleber et al., 2015). In contrast, Fe minerals can also contribute significantly to C loss via anaerobic respiration of Fe-reducing bacteria (Baldock & Skjemstad, 2000; Kaiser & Guggenberger, 2000; Peretyazhko & Sposito, 2005; Wagai & Mayer, 2007). In upland tropical forest soils, microbial Fe reduction accounted for up to 44% of organic C oxidation from soils on an annual basis (Dubinsky et al., 2010).

Most research exploring the role of reactive Fe and Al minerals in soil C dynamics has been conducted either in relatively low C soils or natural wetlands (X. Huang et al., 2018; Kaiser, Eusterhues, Rumpel, Guggenberger, & Kögel-Knabner, 2002; LaCroix et al., 2018; Takahashi & Dahlgren, 2016; Wagai, Mayer, Kitayama, & Shirato, 2013). Wetland soils recently drained for agriculture tend to be C-rich and often experience extremes in water table height (Holden, Chapman, & Labadz, 2004), with farmers maintaining an artificially low water table interspersed with periodic flood irrigation. Drainage and periodic flooding events lead to fluctuating oxidation-reduction (redox) conditions (Niedermeier & Robinson, 2007). Some

research has highlighted the effects of fluctuating redox conditions on Fe redox cycling in wetlands (Chamberlain et al., 2018; Niedermeier & Robinson, 2007; Todorova, Siegel, & Costello, 2005), but the importance of Fe and Al biogeochemistry as controls on soil C accumulation or loss in drained or reflooded soils is not well understood.

Redox-active Fe minerals can be readily reduced or oxidized through a number of biogeochemical pathways (Coby, Picardal, Shelobolina, Xu, & Roden, 2011; Mejia, Roden, & Ginder-Vogel, 2016; Melton, Swanner, Behrens, Schmidt, & Kappler, 2014; Weber, Achenbach, & Coates, 2006) and the oxidation states of Fe form a dominant redox couple in many soils (Conrad, 1996; Lovley, 1991). In fact, the concentrations of reactive Fe often exceed concentrations of most other electron acceptors in soils. Fluctuating redox conditions with abundant reactive Fe and high C concentrations essentially create a biogeochemical engine for anaerobic microbial metabolism (Barcellos, O'Connell, Silver, Meile, & Thompson, 2018; Bhattacharyya et al., 2018; Hall & Silver, 2015; Weber et al., 2006). The combination of high concentrations of reactive Fe, abundant C availability, and fluctuating redox could thus drive considerable soil C losses (Dubinsky et al. 2010). However, reactive Fe minerals can also protect soil C from microbial oxidation via sorption or complexation mechanisms (M. Kleber, Mikutta, Torn, & Jahn, 2005; Wagai & Mayer, 2007). While oxidized Fe is generally thought to be important for soil C storage, anoxic conditions can mobilize mineral-bound C that can subsequently be oxidized under fluctuating redox conditions (Chen et al. 2020, Huang et al. 2020).

Aluminum also plays a key role in soil C storage and loss. The decomposition of Al-associated soil C can be inhibited via the direct recalcitrance of ligand exchange (M. Kleber et al., 2005). Reactive Al species have also been shown to lower soil C lability to microbes, and can be positively correlated with soil C concentrations (M. Kleber et al., 2005; Takahashi & Dahlgren, 2016; Torn, Trumbore, Chadwick, Vitousek, & Hendricks, 1997). Aluminum is not redox-active, but can limit the decomposition of Al-associated organic matter under anaerobic conditions (Hall & Silver, 2015). Given the low metal to C ratios (M/C) observed in other studies (Bazilevskaya, Archibald, & Martínez, 2018; Hall & Silver, 2015; Jansen, Nierop, & Verstraten, 2004) the direct recalcitrance of soil C associated with reactive Al species is improbable in C-rich wetland soils. This suggests other mechanisms, such as a bulk soil conditions or soil aggregation may limit the decomposition of Al-associated soil C.

Here, we hypothesized that the concentration of reactive Fe and Al minerals limit soil C losses in drained wetland soils due to the formation of mineral-C associations. We also hypothesized that reactive Fe and Al mineral concentrations would not be related to patterns in C storage in reflooded systems where persistent anaerobic conditions limited decomposition rates. We sampled nine mineral-rich sites encompassing a range of drained and restored conditions in a regional complex of active agricultural land, recently reflooded farmland, and older restored wetlands. Previous research has focused on utilizing wetland restoration to combat climate change by increasing soil C sequestration and regulating further soil C loss by limiting aerobic respiration (Hatala, Detto, Sonnentag, et al., 2012; Hemes et al., 2019; Knox et al., 2015). Understanding the interactions between reactive Fe and Al minerals and soil C in both drained and reflooded soils could highlight potential mechanisms controlling the rates of C accumulation and loss across a range of soil conditions. A better understanding of these pathways can facilitate

wetland restoration efforts that maximize long-term soil C sequestration and minimize future CO_2 emissions.

2.3 Methods

2.3.1. Site descriptions

The study was conducted in the Sacramento-San Joaquin Delta region of California (hereafter referred to as the Delta). The Delta experiences a Mediterranean climate with hot dry summers and cool wet winters. The region's historical mean annual temperature is 15.1° C and has a yearly average rainfall of 326 mm (Hatala, Detto, Sonnentag, et al., 2012). Much of the Delta was drained for agriculture in the mid-19th century, which has led to high rates of peat oxidation and substantial soil subsidence (Drexler, Fontaine, & Deverel, 2009). Given the differences in management practices and time since drainage across the Delta, the region now consists of Fe-rich soils encompassing a large range of soil organic matter contents. In addition to drained sites, wetland restoration projects have been conducted across the Delta in an effort to reverse soil subsidence and promote soil C sequestration. The combination of historical and current water management practices sampled across a small geographical area (~60 km^2) provided a unique template to explore the importance of mineralogical controls on soil C storage across a range of substrate and redox conditions.

2.3.2. Drained and degraded agricultural sites

The drained and degraded agricultural sites were located on Bouldin, Sherman, and Twitchell Islands. Land uses included a continuous corn site (38.11 N, -121.5 W, Ameriflux ID: US-Bi2), two continuously grazed pasture sites (38.04 N, -121.74 W; US-SND and 38.04 N, -121.7 W; US-Snf), and three perennial alfalfa sites (38.10 N, -121.5 W, US-Bi1; 38.12 N, -121.6 W, US-TW3; and 38.11 N, -121.5 W). The continuous corn site was a highly organic Histosol, with a partially oxidized peat layer approximately 2 m deep; the other agricultural sites were predominantly mineral alluvium Mollisols (Eichelmann et al., 2018; Hemes et al., 2019). Although all agricultural sites were drained, they still experienced spud ditch or flood irrigation during the growing season, and possible short-term winter floods associated with storms or water management activities. As these sites were dominantly unflooded, we refer to them as "drained".

2.3.3. Reflooded restored wetland sites

The wetland sites were perennially flooded and are referred to hereafter as "reflooded". Sites were located on Twitchell and Sherman Islands. West Pond wetland (38.11 N, -121.6 W; US-TW1) was reflooded in 1997 and the accreted layer since restoration was largely undecomposed, saturated plant detritus with a Histosol beneath. Before restoration this site was used for agriculture through the 19th century and was primarily a corn field prior to restoration (Miller et al. 2008, Fleck et al. 2004). Mayberry wetland (38.05 N, -121.8 W; US-MYB), previously a pasture, was reflooded in 2010 and was predominantly a Histosol. East End wetland (38.10 N, -121.6 W, US-TW4) was previously a continuous corn field and was reflooded in 2014 on an iron-rich alluvium Mollisol (Chamberlain et al. 2018, Eichelmann et al. 2018).

2.3.4 Soil sampling and analyses

Samples were collected along three 20 m transects per site; soil cores were taken at five locations at 5 m intervals along each transect. Recognizable surface litter was removed prior to sampling. Each soil core was collected to a depth of 30 cm at all sites as separate 0-15 cm and 15-30 cm samples. Additionally, visible differences across depths in reflooded soils were used to operationally define these soils as "accreted" and "residual" soil in an parallel study (Chamberlain et al., 2018). With the exception of air-dried analyses, soils and in-field extractions were transported in an insulated cooler to maintain soil temperatures within the seasonal range. Samples were processed less than 24 hours after sampling and all laboratory analyses were conducted at U.C. Berkeley.

For total soil C and N analyses, subsamples were air-dried, sieved to < 2 mm, and had visible roots removed before being ground to a fine powder. In reflooded soils, large undecomposed organic material and roots were removed before sieving. Samples were then analyzed in duplicate for total C and N on a CE Elantech elemental analyzer (Lakewood, New Jersey). Soil pH was determined by creating a 1:1 soil to water solution, vortexing for 1 minute, then measuring the solution pH after 10 minutes (McLean, 1982). Soil moisture was determined gravimetrically by weighing fresh soil, oven drying for 24 hours at 105 °C, reweighing the dried soil, and calculating the difference as percent soil moisture.

Table 2.1 Description and the interpretations of measured reactive Fe and Al pools

Variable	Description	Interpretation*	Extraction condition
$Fe(III)_{HCl}$	0.5 M HCl extractable Fe(III)	Poorly crystalline, weak acid soluble short-range order and organo-Fe(III) complexes; proxy for a reactive fraction of Fe(III)	Field
$Fe(II)_{HCl}$	0.5 M HCl extractable Fe(II)	Weak acid soluble Fe(II), proxy for anaerobic conditions	Field
Fe_{CA}	Citrate-ascorbate extractable Fe	Poorly crystalline, redox-active short-range order (oxy)hydroxides and organo-Fe complexes; proxy for microbially reducible Fe	Field
Al_{CA}	Citrate-ascorbate extractable Al	Al-substituted in short-range order (oxy)hydroxides and organo-Al complexes; proxy for substitutable Al	Field
Fe_{AO}	Ammonium-oxalate extractable Fe	Organo-Fe complexes, short-range order (oxy)hydroxides; proxy for chelatable Fe	Ground, air-dried
Al_{AO}	Ammonium-oxalate extractable Al	Organo-Al complexes, short-range order (oxy)hydroxides; proxy for chelatable Al	Ground, air-dried

* Interpretations from: Hall & Silver (2015), Loeppert & Inskeep (1996) and Wagai & Mayer (2007); Hyacinthe et al. (2006)

2.3.5 Reactive Fe and Al pools

We utilized separate soil extractions to characterize three operationally defined indices of reactive Fe and Al. These indices have been mechanistically linked to microbial and geochemical interactions between Fe or Al and organic C storage and loss (Table 1, see also Hall & Silver, 2015; Wagai & Mayer, 2007). First, a 0.5 M hydrochloric acid (HCl) extraction was used to measure both weak-acid soluble, reactive short-range order Fe(III) ($Fe(III)_{HCl}$) and soluble Fe(II) ($Fe(II)_{HCl}$) complexes (Fredrickson et al., 1998). $Fe(II)_{HCl}$ concentrations were also used as an index of reducing conditions, while $Fe(III)_{HCl}$ was used as a proxy for a reactive fraction of Fe(III) (Fredrickson et al., 1998; W. Huang & Hall, 2017). Approximately 3 g soil (oven dry equivalent (ODE)) was added to a 30 ml 0.5 M HCl solution in the field within 1 min of sampling to minimize soil oxidation. The low pH of this extraction also inhibits the oxidation of Fe(II) in solution (Hall & Silver, 2015). Determination of expected ODE masses was determined using residual soil parameters known prior to sampling. An estimated soil-to-volume ratio was determined, then a known volume of soil was added to a preweighed, prefilled Falcon tube. Upon return to the lab, the Falcon tube was reweighed to determine the soil mass added, shaken for 1 h, and centrifuged at 4700 relative centrifugal force (rcf) for 15 min. Samples were subsequently measured colorimetrically within 24 h of sampling using a ferrozine assay buffered with 50 mM HEMES (Viollier, Inglett, Hunter, Roychoudhury, & Van Cappellen, 2000). Soil extracts with high colored dissolved organic C (CDOC) concentrations can lead to $Fe(II)_{HCl}$ overestimations up to 10% during ferrozine assays through either autoreduction or direct absorbance (W. Huang & Hall, 2017; Verschoor & Molot, 2013). Additional samples blanks were run using deionized water (H_2O) instead of ferrozine to determine the interference of CDOC. Interferences from CDOC were generally negligible overall, with maximum interferences of 2.5%. To examine the possible overestimation of $Fe(II)_{HCl}$ via autoreduction in the 0.5 M HCl assay (Verschoor and Molot, 2013), we added an Fe(III) spike as FeCl to 5 mL subsamples of extract from sites with > 10% C (n = 10, 5 from each depth), corresponding to an increase of 0.2 mM Fe(III)/L (see Appendix). Samples were rerun with the ferrozine analysis. The recovery rate of the Fe(III) spike was always > 95%, within the error of the method. While this test does not confirm that autoreduction did not occur in our samples, it does highlight that autoreduction was not a significant source of $Fe(II)_{HCl}$ measured. To further test the potential effects of autoreduction, we determined the impacts of decreasing $Fe(II)_{HCl}$ concentrations by 10% in all drained soil samples, as well as simply removing samples with soil C > 10% from the dataset and redoing the trend analyses. These changes did not significantly alter the patterns observed (Supplemental Figure 3a and 3b). We acknowledge the potential for overestimation, particularly via autoreduction, in $Fe(II)_{HCl}$ data, although it does not appear to have affected the results reported here.

A second, separate field extraction was performed utilizing a 0.2 M sodium citrate and 0.05 M ascorbic acid (citrate-ascorbate) with a pH of 6 to provide a separate estimate of reducible (redox-active) short-range order Fe oxides (Fe_{CA}) and substituted Al oxides (Al_{CA}), (Torrent, 1997). These assays are an index of microbially reducible Fe and substitutable Al. Approximately 1.5 g soil (ODE) was added to 45 ml of solution within 1 minute of sampling utilizing the same in-field methods described in the HCl extractions above. Extracts were shaken for 16 h, centrifuged at 1000 rcf for 20 min, and then decanted and refrigerated until analysis. A third, separate index of chelatable Fe (Fe_{AO}) and Al (Al_{AO}) oxides and organo-metal complexes

(organo-Fe and organo-Al complexes) used an ammonium-oxalate extraction consisting of 0.17 M ammonium oxalate and 0.1 M oxalic acid performed in the dark at pH 3 (Loeppert & Inskeep, 1996). Subsamples were air-dried and ground to directly compare with previously published ammonium oxalate extractions (Hall & Silver, 2015; Loeppert & Inskeep, 1996), and because oxalate can extract crystalline Fe in the presence of Fe(II) (Phillips, Lovley, & Roden, 1993), which was elevated in some soils. Approximately 0.5 g was added to 30 ml of solution, shaken for 2 h, centrifuged at 1000 rcf for 20 min, and decanted and refrigerated until analysis. The ammonium-oxalate extraction represents chelatable Fe and Al species, previously defined as organo-Fe or organo-Al complexes and may also represent some redox-active Fe species. The citrate-ascorbate extraction readily solubilizes Fe via reductive dissolution and can be considered both redox-active Fe species and poorly crystalline Fe and Al species. Both citrate-ascorbate and ammonium-oxalate extractions were analyzed for Fe and Al in triplicate via inductively coupled plasma optical emission spectroscopy (ICP-OES; Perkin Elmer Optima 5300 DV). These three separate, non-sequential soil extractions are commonly used to quantify operationally-defined reactive Fe and Al phases (Table 1; Coward et al., 2018; Hall & Silver, 2015; Thompson et al., 2011; Wagai et al., 2013) that interact in different ways with soil C.

2.3.6 Statistical analyses

Statistical analyses were performed using JMP Pro 13 (SAS Institute Inc., Cary, NC). To determine differences across site, land use type (restored or drained), and soil depths, we performed one-way ANOVAs followed by post-hoc Tukey tests using soil C, soil N, pH, soil moisture, Fe_{AO}, Al_{AO}, $\ln(Fe_{CA})$, $\ln(Al_{CA})$, $\ln(Fe(II)_{HCl})$, and $\ln(Fe(III)_{HCl})$ concentrations, nested within depth values and soil conditions. Data were log-transformed when necessary to create a log-normal distribution to meet ANOVA assumptions.

A multiple regression model was used to further test the relationships between soil C concentrations and the other biogeochemical variables measured and the interactions among them. Three sets of separate sample groups were used with one group containing all sites, and the second and third groups were split into drained or reflooded soils. Depth was again included as a blocking factor to account for sampling design and unexplained depth-related variations in soil C concentrations. Generalized pairwise regression analyses were used to explore the relationships between measured biogeochemical variables and soil C concentrations at the scale of individual samples within and across soil type and conditions. Relevant fits for pairwise regression analyses are included in Supplemental Table 1.

2.3.7 Upscaling

To determine the potential impacts of redox-active Fe species on C stocks over time, we used data from a nearby drained Delta wetland site reported in Yang and Liptzin (2015). They measured Fe reduction rates of 1.18 mg Fe g $soil^{-1}$ d^{-1}. Assuming 0.025 mol C oxidized per mol of Fe(III) reduced and a bulk density of 0.25 g cm^{-3} (Deverel et al., 2016), we estimated a microbial respiration rate from Fe reduction of 0.47 g C m^{-2} d^{-1}. We then assumed 5.5-d of Fe(III) reduction (W. H. Yang & Liptzin, 2015) during 7-d or 14-d redox cycles throughout the year. Note that 5.5-d reduction periods would yield only 65% of the reduced Fe concentrations

measured in flooded soils in this study, and thus is likely a conservative estimate. Further explanation, including sample calculations, are located in the Supplemental Material.

2.4 Results

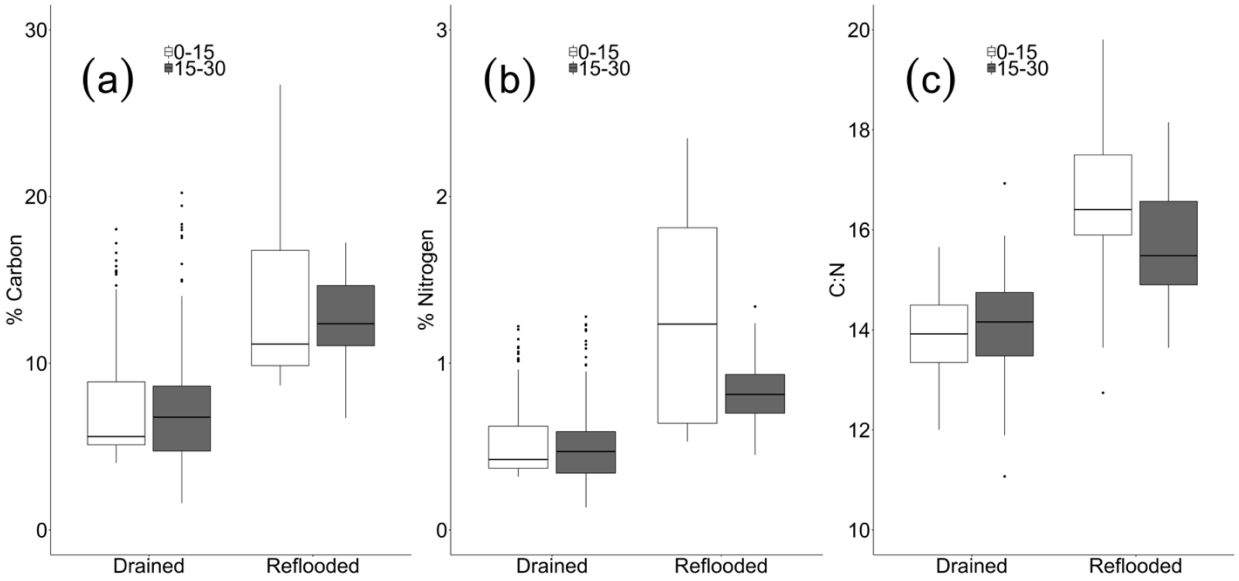

Figure 1 Boxplots of (a) % Carbon, (b) % Nitrogen, and (c) C:N ratios in 0-15 cm and 15-30 cm depths across drained and reflooded soils. Note the difference across y-axes.

2.4.1 Carbon and nitrogen in drained and restored wetland soils

There was a strong gradient in soil C concentrations across sites and depths with values ranging from 3.6 to 44.6% C. Reflooded sites had higher total C and N concentrations than drained soils at both 0-15 cm and 15-30 cm depths ($P < 0.0001$; Figure 1a, Table 1). Soil C concentrations were greatest in the reflooded surface soils (0-15 cm) but varied considerably with a range of 8.7-44.6% C, compared to drained surface soils with a range of 3.6-16.0% C. Reflooded surface soils had significantly higher soil C concentrations than reflooded soils at 15-30 cm depths ($P < 0.0001$), but soil C concentrations in drained surface soils did not differ significantly from drained 15-30 cm depths. Soil N concentrations showed trends similar to C across depths and drainage status. Reflooded soils had significantly higher C:N ratios than drained soils in both 0-15 cm and 15-30 cm depths ($P < 0.0001$). The C:N ratio was significantly higher in the reflooded surface soils than those from the lower depth ($P = 0.01$).

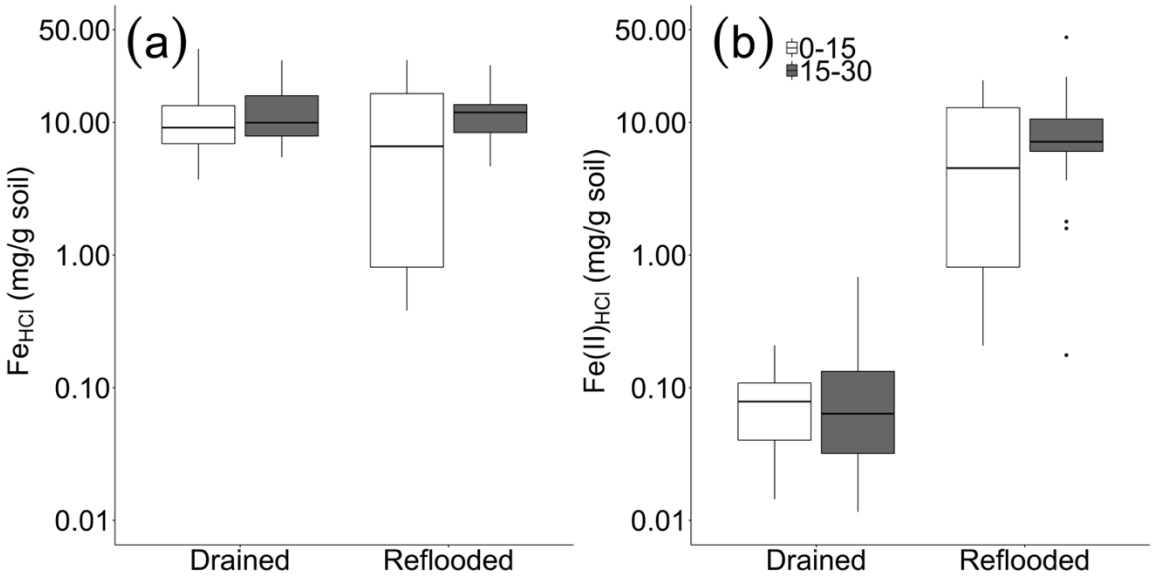

Figure 2 Log-scale boxplots of concentrations of total HCl-extractable Fe (a) and Fe(II) (b) in 0-15 cm and 15-30 cm depths across drained and reflooded soils.

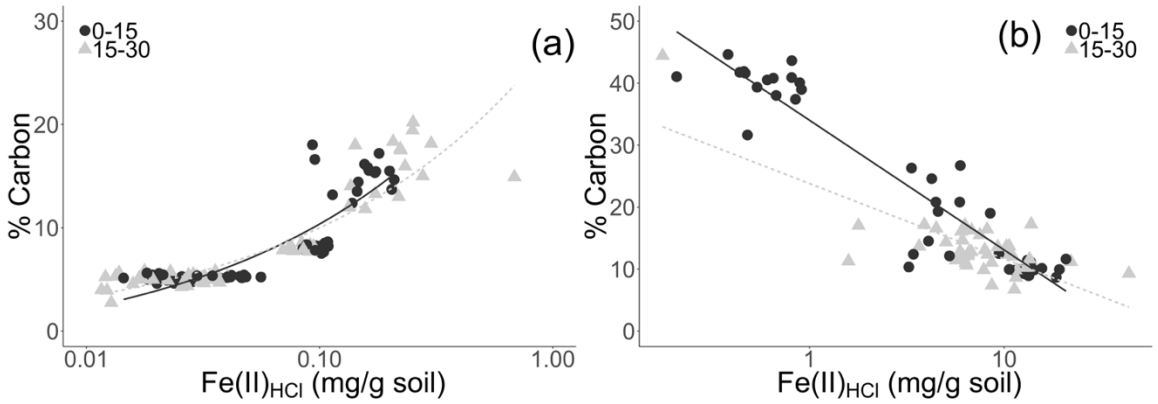

Figure 3 Log-linear relationships between soil carbon and HCl-extractable Fe (II) concentrations at 0-15 cm (black circles) and 15-30 cm (grey triangles) depths across (a) drained soils (0-15 cm $R^2 = 0.49$, $P < 0.0001$; 15-30 cm $R^2 = 0.58$, $P < 0.0001$) and (b) reflooded soils (0-15 cm $R^2 = 0.89$, $P < 0.0001$; 15-30 cm $R^2 = 0.59$, $P < 0.0001$). Note the log scale on the x-axis and the different scales on both axes.

2.4.2 HCl-extractable Fe(II) and Fe(III)

HCl-extractable soil Fe pools tended to accumulate in drained soils. Total concentrations of Fe_{HCl} were elevated at all sites and were significantly greater in drained surface soils ($P < 0.0001$). Concentrations in reflooded surface soils ranged across two orders of magnitude. Expectedly, reduced Fe concentrations ($Fe(II)_{HCl}$), a proxy for the extent of anaerobic conditions, were significantly greater in reflooded soils in comparison to drained soils across both depths ($P < 0.0001$). $Fe(II)_{HCl}$ concentrations were positively correlated with C concentrations in drained soils at both 0-15 and 15-30 cm depths ($R^2 = 0.49$ to 0.58, $P < 0.0001$; Figure 3a). $Fe(II)_{HCl}$

concentrations were roughly an order of magnitude higher in reflooded soils and were negatively correlated with soil C at both 0-15 and 15-30 cm depths (R^2 = 0.59 to 0.89, P < 0.0001; Fig 3b).

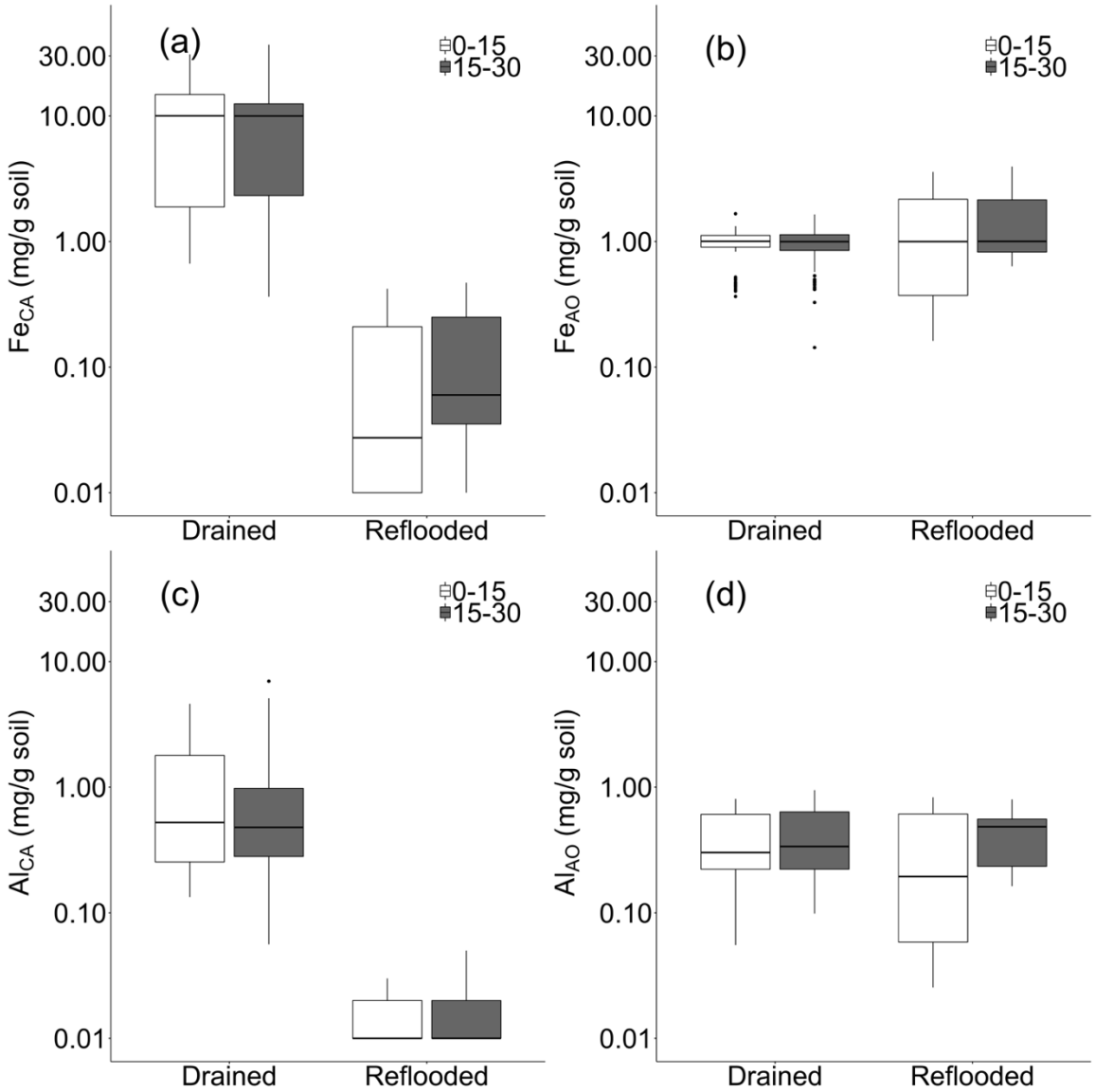

Figure 4 Log-scale boxplots of reactive Fe and Al concentrations in 0-15 cm and 15-30 cm depths separated into drained and reflooded soils: a) citrate-ascorbate extractable Fe; c) citrate-ascorbate extractable Al, b) ammonium-oxalate extractable Fe; d) ammonium-oxalate extractable Al.

2.4.3 Reactive, poorly crystalline and organo-metal complexes of iron and aluminum

Concentrations of both Fe_{CA} and Al_{CA}, representing reactive, poorly crystalline Fe and Al species, were significantly higher in drained soils than reflooded soils at both 0-15 and 15-30 cm

depths ($P < 0.0001$). Extractable Al_{CA} concentrations did not differ across depths in either drained or reflooded soils. Many values were close to the detection limit in reflooded soils (Figure 4c). Extractable Fe_{CA} increased with depth in reflooded systems ($P < 0.05$). Ammonium-oxalate extractable Fe (Fe_{AO}) and Al (Al_{AO}), representative of reactive organo-mineral complexes, were similar in magnitude across drained and reflooded systems, but lower than Fe_{CA} and Al_{CA} in drained systems and greater than Fe_{CA} and Al_{CA} in reflooded systems. Fe_{AO} concentrations were significantly higher in reflooded soils than drained soils at both depths ($P < 0.01$), but Al_{AO} concentrations did not differ across drainage classes.

Concentrations of Fe_{CA} were negatively correlated with C concentrations across soils, regardless of drainage status. There was a strong negative log-linear correlation between mean soil C concentrations and mean Fe_{CA} values in soils at both 0-15 cm ($R^2 = 0.81$, $P < 0.0001$) and 15-30 cm depths ($R^2 = 0.69$, $P < 0.0001$; Figure 5). In reflooded soils, there was a strong negative log-linear correlation between soil C and Fe_{AO} ($R^2 = 0.59$, $P < 0.001$) and Fe_{CA} ($R^2 = 0.54$, $P < 0.001$) in the 0-15 cm depths (Figure 6). This correlation was much weaker at 15-30 cm for both Fe_{AO} ($R^2 = 0.22$, $P < 0.001$) and Fe_{CA} ($R^2 = 0.31$, $P < 0.001$).

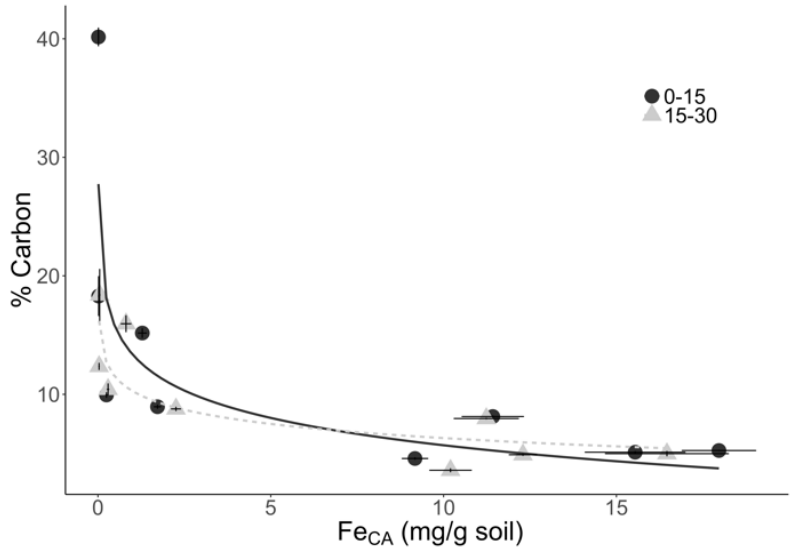

Figure 5. Log-linear relationships between site mean concentrations of soil carbon and reactive poorly crystalline Fe_{CA} (reactive poorly crystalline Fe from the citrate-ascorbate extract) in 0-15 cm (black circles; $R^2 = 0.81$, $P < 0.0001$) and 15-30 cm (grey triangles; $R^2 = 0.69$, $P < 0.0001$) depths across all sites.

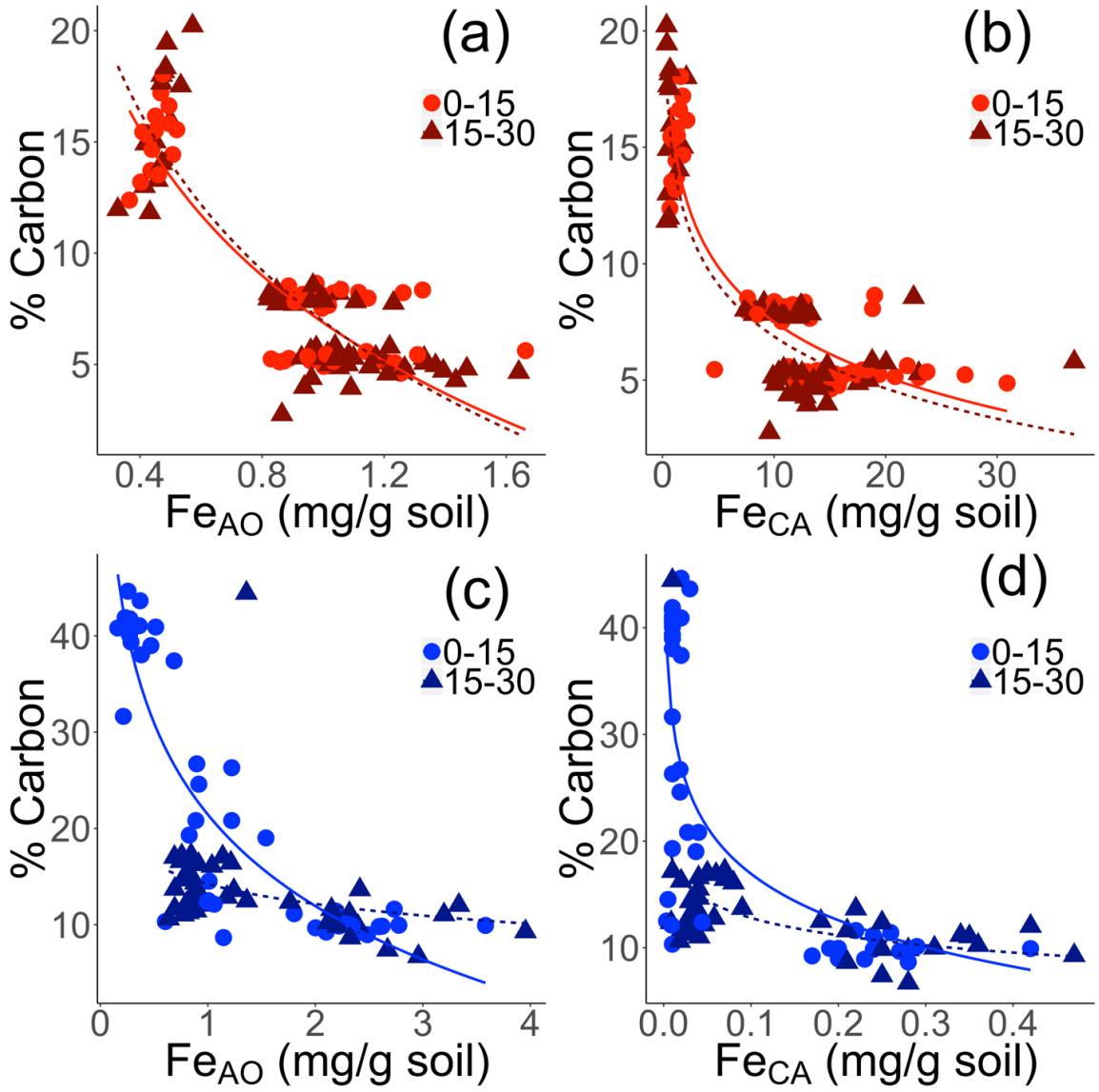

Figure 6. Log-linear relationships between % soil carbon and Fe_{AO} (reactive organo-Fe complexes from the ammonium-oxalate extract); a) drained 0-15 cm depth: $R^2 = 0.59$, $P < 0.001$, 15-30 cm depth: $R^2 = 0.45$, $P < 0.001$; c) reflooded 0-15 cm depth: $R^2 = 0.59$, $P < 0.001$, 15-30 cm: $R^2 = 0.22$, $P < 0.001$); and Fe_{CA} (reactive poorly crystalline Fe from the citrate-ascorbate extract); b) drained 0-15 cm depth: $R^2 = 0.46$, $P < 0.001$,15-30 cm depth: $R^2 = 0.41$, $P < 0.001$; d) reflooded 0-15 cm: $R^2 = 0.54$, $P < 0.001$, 15-30 cm: $R^2 = 0.31$, $P < 0.001$. Drained soils are in red and reflooded soils are in blue. Note differences in scales across axes.

Concentrations of Al_{AO} were strongly correlated with soil C concentrations in drained soils when pasture sites were removed from the dataset (0-15 cm: $R^2 = 0.91$, $P < 0.0001$; 15-30 cm: $R^2 = 0.91$, $P < 0.0001$) (Figure 7, Supplemental Figure 2). Pasture sites were characterized by much higher soil bulk density values in surface soils compared to other drained sites, as continuous grazing practices may have increased surface soil compaction and altered the

mechanism for C-Al interactions (see discussion below; Supplemental Table 3). In reflooded sites, there was a negative log-linear relationship between Al_{AO} and soil C concentrations in surface soils ($R^2 = 0.64$, $P < 0.0001$) but no trend at depth (Supplemental Figure 2b). There was also a strong log-linear correlation between Al_{AO} and increasing $Fe(II)_{HCl}$ concentrations in drained systems across depths (0-15 cm: $R^2 = 0.71$, $P < 0.0001$; 15-30 cm: $R^2 = 0.50$, $P < 0.0001$; Figure 8). On a molar basis, mean total soil C values exceeded mean Al_{AO} values by more than 720 times (M/C ratio < 0.006; C:Al molar ratio 179 ± 9) in all samples.

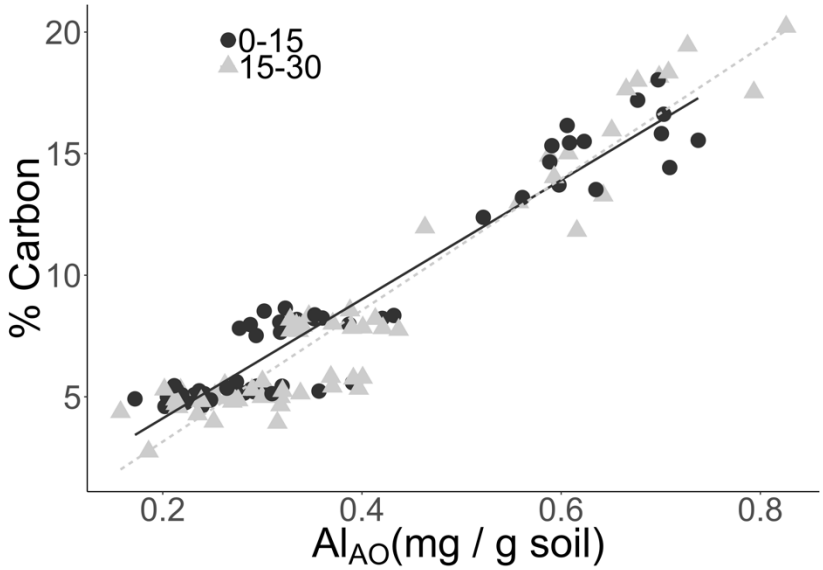

Figure 7. Linear relationships between concentrations of soil carbon and Al_{AO} (reactive organo-Al complexes from the ammonium-oxalate extract) across 0-15 cm (black circles; $R^2 = 0.91$, $P < 0.0001$) and 15-30 cm (grey triangles; $R^2 = 0.91$, $P < 0.0001$) depths in drained soils. Pasture soils were removed from this analysis (see text; Supplemental Figure 2).

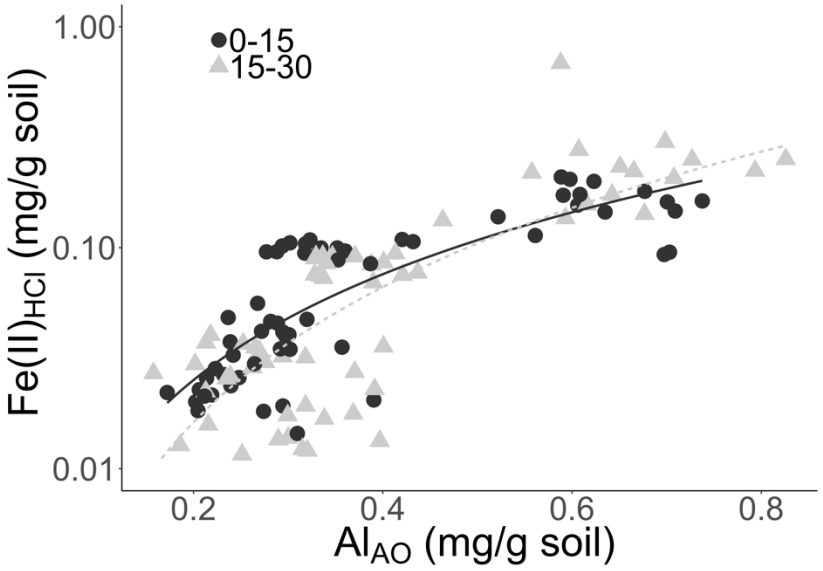

Figure 8. Log-linear relationships between $Fe(II)_{HCl}$ and Al_{AO} (reactive organo-Al complexes from the ammonium-oxalate extract) concentrations across 0-15 cm (black circles; $R^2 = 0.71$, $P < 0.0001$) and 15-30 cm (grey triangles; $R^2 = 0.50$, $P < 0.0001$) depths in drained soils. Pasture soils were removed from this analysis (see text).

2.4.4 Multiple regressions model for predicting soil C concentrations

In the combined dataset, indices of reactive Fe pools were negatively associated with soil C values, while organo-Al complexes were positively associated with soil C values. Across all sites, soil C concentrations declined as the concentrations of reduced and reactive Fe [$ln(Fe(II)_{HCl})$, $ln(Fe_{HCl})$, $ln(Fe_{CA})$, and Fe_{AO}] increased in the 0-15 cm depth ($P \leq 0.02$). A similar negative relationship was also observed for soil C, $ln(Fe_{HCl})$, and $ln(Fe_{CA})$ at 15-30 cm depths ($P \leq 0.01$, Supplemental Table 4). In contrast, soil C concentrations were significantly positively correlated with Al_{AO} in the 0-15 cm depth, and with Al_{AO}, soil moisture, pH in the 15-30 cm depth ($P \leq 0.02$, Supplemental Table 4).

Similar trends between soil C and active Fe and Al pools were observed when datasets were divided into reflooded and drained soils. In reflooded sites, surface soil C concentrations were positively correlated with soil moisture and negatively associated with $ln(Fe(II)_{HCl})$ ($P < 0.10$; Supplemental Table 5). At 15-30 cm in reflooded soils, soil C concentrations were positively correlated with soil moisture, pH, and Al_{AO}, and negatively correlated with $ln(Fe_{HCl})$ ($P \leq 0.05$, Supplemental Table 5).

In drained sites at 0-15 cm, soil C was positively correlated with pH, $ln(Al_{CA})$, and Al_{AO}, and negatively associated with Fe_{AO} concentrations ($P \leq 0.03$, Supplemental Table 6). Soil C concentrations from 15-30 cm depths at drained sites increased with soil moisture, pH, $ln(Al_{CA})$, Al_{AO}, and $ln(Fe(II)_{HCl})$, and decreased with $ln(Fe_{HCl})$ and $ln(Fe_{CA})$ ($p \leq 0.03$, Supplemental Table 6). Generally, soil C concentrations were negatively correlated with Fe species and positively correlated with organo-Al complexes across both depths and drainage status.

2.4.5 Upscaling

Using Fe reduction rates from a nearby drained Delta site (Yang and Liptzin 2015), we estimated that 6.5 mg Fe(II) were produced per g soil during a 14-d oxidation-reduction cycle. If we assume that these 14-d cycles occur throughout the year, Fe reduction would yield approximately 678 kg C ha^{-1} y^{-1}. Using a weekly oxidation-reduction cycle yielded a C flux of 1.4 Mg C ha^{-1} y^{-1} from Fe reduction.

2.5 Discussion

2.5.1 Relationships between reactive Fe pools and soil C in drained and restored wetlands

Reactive Fe species are typically thought to increase C concentrations in soils and sediments, as they can preferentially facilitate soil C accumulation via direct Fe-C associations (Coward, Thompson, & Plante, 2017; Lalonde, Mucci, Ouellet, & Gélinas, 2012; Wagai et al., 2013). However, we observed the opposite trend in both drained and reflooded wetlands. The negative correlation between Fe_{AO} and soil C concentrations in drained soils was surprising, as Fe_{AO} is thought to represent organo-mineral complexes that protect soil C from microbial decomposition (Hall & Silver, 2015; Loeppert & Inskeep, 1996). This soil C protection mechanism has been observed in both dominantly aerobic and anaerobic systems, including sediments, C-rich paddy soils, and upland soils (Kögel-Knabner et al., 2010; Lalonde et al., 2012; Wagai & Mayer, 2007). The negative relationship observed here suggests that reactive organo-Fe complexes are not the predominant mechanism of soil C protection in drained soils (Wang, River, & Richardson, 2019). Alternatively, organo-Fe complexes may also be utilized by microbial Fe reducers in these soils following depletion of other reactive Fe pools (i.e. Fe_{CA}) when soils experience reducing conditions associated with rainfall or irrigation events.

Reactive Fe species (Fe_{CA}, Fe_{AO}) and reduced Fe ($Fe(II)_{HCl}$) concentrations were also associated with lower soil C concentrations in reflooded sites. The negative correlation between $Fe(II)_{HCl}$ and soil C concentrations across reflooded soils suggests an important role for microbial Fe reduction in C oxidation and loss and a limitation on soil C sequestration potential in mineral-rich soils following wetland restoration. The production of Fe(II) via anaerobic microbial respiration coupled to Fe-reduction is known to be a pathway of soil C loss in upland soils and fens (Bhattacharyya et al., 2018; Emsens et al., 2016; Hall & Silver, 2013). Strong negative relationships between soil C and Fe_{CA} and Fe_{AO} values suggest that a residual or recycled redox-active Fe pool is limiting the rate of soil C accumulation in the restored wetlands. Although reduced Fe concentrations were much lower than the soil C concentrations measured in the reflooded systems (up to 30 moles C per mole $Fe(II)_{HCl}$), fluctuating redox conditions as well as dissolved sources of O_2 (Mejia et al., 2016; Weber et al., 2006), can rapidly and repeatedly replenish the reducible Fe so it can be used again and again for anaerobic microbial respiration. Thus, redox fluctuations can facilitate significant soil C oxidation associated with Fe redox cycling. Replenishment of the reducible Fe pool can occur following redox fluctuations driven by a range of processes such as root and rhizome oxygenation of wetland plant rhizospheres (Kaplan et al., 2016; Nikolausz et al., 2008), changes in the water table height (Catallo, 1999), or anaerobic Fe oxidation (Mejia et al., 2016; Weber et al., 2006). Our results

suggest that high concentrations of reactive, reducible Fe species limit soil C accumulation in reflooded soils and increase C loss in drained soils.

As a preliminary upscaling exercise, we used measured Fe reduction rates from a nearby site (W. H. Yang & Liptzin, 2015) and bi-monthly and weekly redox cycling to determine the potential impacts on soil C fluxes. These upscaled C fluxes ranged from 0.7 to 1.4 Mg C ha^{-1} y^{-1}. For comparison, Knox et al (2015) estimated net ecosystem greenhouse gas losses from the drained corn and pasture sites of 5.7 and 3.9 Mg C_{eq} ha^{-1} y^{-1}. Heterotrophic respiration associated with Fe reduction thus accounted for 12 and 17% of these C_{eq} losses, respectively, assuming a 14-d redox cycle. For the reflooded wetlands, a 14-d Fe-redox cycle would oxidize 128% of the C emitted from methane fluxes (0.53 Mg C ha^{-1} y^{-1}) annually (Knox et al., 2015). Previous studies have shown daily redox fluctuations in wetland soils during the growing season (Nikolausz et al., 2008; Vorenhout, van der Geest, van Marum, Wattel, & Eijsackers, 2004). These restored wetlands have long growing seasons of roughly 150 days (Knox et al., 2015), suggesting an important role for reactive Fe in C losses.

While reactive Fe pools were negatively related to soil C concentrations, we observed a positive correlation between Fe(II) concentrations and soil C concentrations in drained soils. In upland soils, $Fe(II)_{HCl}$ may represent a proxy for the extent of soil anaerobic conditions (Hall & Silver, 2015). We posit that the positive relationship between soil C and Fe(II) concentrations in drained soils could be indicative of an increasing number of anaerobic (micro)sites characterized by slower decomposition rates than well-aerated soils. Reduced Fe concentrations in drained soils were roughly an order of magnitude lower than in flooded soils, likely resulting from a generally more oxidized soil volume. The opposite pattern between Fe(II) and soil C concentrations was observed in restored wetlands, with Fe(II) concentrations increasing as soil C concentrations decreased. The much higher concentrations of Fe(II) in the reflooded soils would have resulted in significant C losses from these ecosystems as highlighted above.

2.5.2 Relationships between reactive Al pools and soil C in drained and restored wetlands

As with Fe, Al can react with soil organic matter and facilitate C preservation (Porras, Hicks Pries, McFarlane, Hanson, & Torn, 2017; Scheel, Dörfl, & Kalbitz, 2007). However, unlike Fe, Al is not redox active and thus does not directly drive microbial metabolism. We found that organo-Al complexes were strongly positively correlated with soil C in drained soils, but given the high C:Al molar ratio (179 ± 9), this is probably not an important direct mechanism of C protection in these sites. Rather, we hypothesize that the relationship between soil Al_{AO} and soil C concentrations may be a result of increased aggregation via associations between reactive Al species and larger organic molecules (Oades & Waters, 1991; Totsche et al., 2017; Wiseman & Püttmann, 2006). This soil aggregation mechanism would also explain the strong positive correlation between $Fe(II)_{HCl}$ concentrations, a proxy for anaerobic conditions, and organo-Al complexes in drained soils. Soil aggregation facilitates the development of anaerobic microsites, a mechanism for potential soil C accumulation even in well drained soils (Keiluweit, Nico, Kleber, & Fendorf, 2016; Six & Paustian, 2014). There was no observed trend between $Fe(II)_{HCl}$ and organo-Al complexes in flooded soils (Supplemental Figure 1a). This is also expected as bulk soil anaerobic conditions and decreased soil aggregation limit the importance of anaerobic microsites within aggregates (De-Campos, Mamedov, & Huang, 2009).

The relationship between soil C and organo-Al complexes was not observed in the drained pasture sites we sampled. The continuous grazing at these sites likely led to surface soil compaction (Silver, Ryals, & Eviner, 2010), observed through higher soil bulk density in pasture soils (Supplemental Table 3). Soil compaction would result in a direct loss of aggregation in surface soils (Warren, Nevill, Blackburn, & Garza, 1986), and directly inhibit O_2 diffusion through reduced soil pore space (Stepniewski, Gliński, & Ball, 1994). Soil C concentrations in the pasture sites are thus more likely to be influenced by an increase in anaerobic bulk soil conditions associated with compaction.

2.5.3 Interacting controls on soil C accumulation and loss in drained and restored wetlands

Multiple regression analyses suggested an important role for Fe and Al in patterns in soil C storage with wetland drainage and reestablishment. Soil C was negatively associated with concentrations of reactive and reduced Fe pools under both drained and reflooded conditions, suggesting that Fe reduction coupled to C oxidation may be more important than Fe-C bonding as a driver of C cycling in these soils. Soil C was also positively correlated with soil moisture and organo-Al complexes, particularly in drained soils, again emphasizing the likely importance of anaerobic microsites, facilitated by soil aggregation, for soil C accumulation in these systems. The contrasting trends observed between Al and Fe species and soil C also suggest these relationships are driven by both direct and indirect effects of the concentration of residual soil minerals following wetland drainage.

2.6 Conclusion

Our results suggest that the concentration of mineral material in residual soils following the drainage of wetlands can impact C cycling on drained soils as well as patterns in C concentrations following wetland restoration. In reflooded soils, high concentrations of both reactive Fe and reduced Fe(II) were negatively correlated with soil C concentrations, suggesting that Fe reduction and subsequent organic matter oxidation may at least partially limit soil C sequestration in these ecosystems. Reactive Fe minerals, likely the most abundant alternative electron acceptors under anaerobic conditions across sites, were also associated with decreasing soil C concentrations in drained sites. This suggests that periodic redox fluctuations and reactive, reducible Fe pools may also further increase C emissions from drained wetland soils. However, both soil moisture and a proxy for anaerobic conditions, $Fe(II)_{HCl}$, were positively correlated with soil C concentrations in drained soils, suggesting that reducing conditions may counteract at least some of these C losses. Additionally, we found that reactive organo-Al species were positively correlated with soil C concentrations across drained soils. We hypothesize that these organo-Al species may facilitate soil aggregation or anaerobic (micro)sites that protect residual soil C from oxidation. Our results highlight the potential role of mineral in C cycling, storage and loss with ecosystem management in wetlands. Understanding the underlying mineral composition of soils can help determine if, and how quickly wetland restoration can result in a net C sink for climate change mitigation. Our results also show that the presence of reactive Fe minerals in soils does not necessarily infer increased C sequestration, as redox dynamics can drive microbial C oxidation at potentially high rates in both drained and reflooded ecosystems. Increased understanding of the relationships between Fe and Al biogeochemistry and soil C is

necessary to prioritize wetland restoration projects that balance maximizing soil C sequestration and limiting future soil C losses.

2.7 Acknowledgements

We appreciate field sampling and lab assistance from Heather Dang, Summer Ahmed, Sam Chamberlain, and numerous other members of both the Silver Lab and the Berkeley Biometeorology labs at University of California, Berkeley. We would also like to thank the anonymous reviewers for helping to improve many aspects of this study. This work was supported by the California Department of Water Resources (DWR) through a Contract of the California Department of Water Resources (award 4600011240). We thank the California Department of Water Resources and the Metropolitan Water District of Southern California for access to research sites. T. Anthony was supported by the California Sea Grant Delta Science Fellowship. This material is based upon work supported by the Delta Stewardship Council Delta Science Program under Grant No. 5298 and California Sea Grant College Program Project R/SF-89. The contents of this material do not necessarily reflect the views and policies of the Delta Stewardship Council or California Sea Grant, nor does mention of trade names or commercial products constitute endorsement or recommendation for use. McIntire Stennis grant CA- B-ECO-7673-MS to W. L. Silver partially supported this work. W. L. Silver was also supported by funds from Breakthrough Strategies & Solutions, and the V. Kann Rasmussen, Oak Creek, Jewish Community, Northern Trust, and Trisons Foundations. The authors declare no conflict of interests.

2.8 References

Baldock, J. A., & Skjemstad, J. O. (2000). Role of the soil matrix and minerals in protecting natural organic materials against biological attack. *Organic Geochemistry*, *31*, 697–710. https://doi.org/https://doi.org/10.1016/S0146-6380(00)00049-8

Barcellos, D., O'Connell, C., Silver, W., Meile, C., & Thompson, A. (2018). Hot Spots and Hot Moments of Soil Moisture Explain Fluctuations in Iron and Carbon Cycling in a Humid Tropical Forest Soil. *Soil Systems*, *2*(4), 59. https://doi.org/10.3390/soilsystems2040059

Bazilevskaya, E., Archibald, D. D., & Martínez, C. E. (2018). Mineral colloids mediate organic carbon accumulation in a temperate forest Spodosol: depth-wise changes in pore water chemistry. *Biogeochemistry*, *141*(1), 75–94. https://doi.org/10.1007/s10533-018-0504-4

Bhattacharyya, A., Campbell, A. N., Tfaily, M. M., Lin, Y., Silver, W. L., Nico, P. S., & Pett-Ridge, J. (2018). Redox fluctuations control the coupled cycling of iron and carbon in tropical forest soils. *Environmental Science & Technology*, *52*, 14129−14139. https://doi.org/10.1101/312108

Catallo, W. J. (Ed.). (1999). *Hourly and daily variation of sediment redox potential in tidal wetland sediments*. *Biological Science Report*. Reston, VA. Retrieved from http://pubs.er.usgs.gov/publication/bsr19990001

Chamberlain, S. D., Anthony, T. L., Silver, W. L., Eichelmann, E., Hemes, K. S.,

Oikawa, P. Y., … Baldocchi, D. D. (2018). Soil properties and sediment accretion modulate methane fluxes from restored wetlands. *Global Change Biology*, 1–15. https://doi.org/10.1111/gcb.14124

Chen, C., Hall, S. J., Coward, E., & Thompson, A. (2020). Iron-mediated organic matter decomposition in humid soils can counteract protection. *Nature Communications*, *11*(1), 2255. https://doi.org/10.1038/s41467-020-16071-5

Coby, A. J., Picardal, F., Shelobolina, E., Xu, H., & Roden, E. E. (2011). Repeated anaerobic microbial redox cycling of iron. *Applied and Environmental Microbiology*, *77*(17), 6036–6042. https://doi.org/10.1128/AEM.00276-11

Conrad, R. (1996, December). *Soil microorganisms as controllers of atmospheric trace gases (H2, CO, CH4, OCS, N2O, and NO)*. *Microbiological Reviews*. Retrieved from http://mmbr.asm.org/content/60/4/609.abstract

Coward, E. K., Thompson, A. T., & Plante, A. F. (2017). Iron-mediated mineralogical control of organic matter accumulation in tropical soils. *Geoderma*, *306*, 206–216. https://doi.org/10.1016/j.geoderma.2017.07.026

Coward, E. K., Thompson, A., & Plante, A. F. (2018). Contrasting Fe speciation in two humid forest soils: Insight into organomineral associations in redox-active environments. *Geochimica et Cosmochimica Acta*, *238*, 68–84. https://doi.org/10.1016/j.gca.2018.07.007

De-Campos, A. B., Mamedov, A. I., & Huang, C. (2009). Short-Term Reducing Conditions Decrease Soil Aggregation. *Soil Science Society of America Journal*, *73*(2), 550. https://doi.org/10.2136/sssaj2007.0425

Deverel, S. J., Ingrum, T., & Leighton, D. (2016). Present-day oxidative subsidence of organic soils and mitigation in the Sacramento-San Joaquin Delta, California, USA. *Hydrogeology Journal*, *24*(3), 569–586. https://doi.org/10.1007/s10040-016-1391-1

Dise, N. B. (2009). Peatland Response to Global Change. *Science*, *326*(5954), 810–811. https://doi.org/10.1126/science.1174268

Drexler, J. Z., Fontaine, C. S., & Deverel, S. J. (2009). The legacy of wetland drainage on the remaining peat in the Sacramento — San Joaquin Delta, California, USA. *Wetlands*, *29*(1), 372–386. https://doi.org/10.1672/08-97.1

Dubinsky, E. A., Silver, W. L., & Firestone, M. K. (2010). Tropical forest soil microbial communities couple iron and carbon biogeochemistry. *Ecology*, *91*(9), 2604–2612.

Eichelmann, E., Hemes, K. S., Knox, S. H., Oikawa, P. Y., Chamberlain, S. D., Verfaillie, J., & Baldocchi, D. D. (2018). The Effect of Land Cover Type and Structure on Evapotranspiration from Agricultural and Wetland Sites in the Sacramento/San Joaquin River Delta, California. *Agricultural and Forest Meteorology*, *256–257*, 179–195. https://doi.org/https://doi.org/10.1016/j.agrformet.2018.03.007

Emsens, W.-J., Aggenbach, C. J. S., Schoutens, K., Smolders, A. J. P., Zak, D., & van Diggelen, R. (2016). Soil Iron Content as a Predictor of Carbon and Nutrient Mobilization in Rewetted Fens. *PloS One*, *11*(4), 1–17. https://doi.org/10.1371/journal.pone.0153166

Fredrickson, J. K., Zachara, J. M., Kennedy, D. W., Dong, H., Onstott, T. C., Hinman, N. W., & Li, S. M. (1998). Biogenic iron mineralization accompanying the dissimilatory reduction of hydrous ferric oxide by a groundwater bacterium. *Geochimica et Cosmochimica Acta*, *62*(19–20), 3239–3257. https://doi.org/10.1016/S0016-7037(98)00243-9

Hall, S. J., & Silver, W. L. (2013). Iron oxidation stimulates organic matter decomposition in humid tropical forest soils. *Global Change Biology*, 2804–2813. https://doi.org/10.1111/gcb.12229

Hall, S. J., & Silver, W. L. (2015). Reducing conditions, reactive metals, and their interactions can explain spatial patterns of surface soil carbon in a humid tropical forest. *Biogeochemistry*, *125*(2), 149–165. https://doi.org/10.1007/s10533-015-0120-5

Hatala, J. A., Detto, M., Sonnentag, O., Deverel, S. J., Verfaillie, J., & Baldocchi, D. D. (2012). Greenhouse gas (CO2, CH4, H2O) fluxes from drained and flooded agricultural peatlands in the Sacramento-San Joaquin Delta. *Agriculture, Ecosystems and Environment*, *150*, 1–18. https://doi.org/10.1016/j.agee.2012.01.009

Hemes, K. S., Chamberlain, S. D., Eichelmann, E., Knox, S. H., & Baldocchi, D. D. (2018). A Biogeochemical Compromise: The High Methane Cost of Sequestering Carbon in Restored Wetlands. *Geophysical Research Letters*, *45*(12), 6081–6091. https://doi.org/10.1029/2018GL077747

Hemes, K. S., Chamberlain, S. D., Eichelmann, E., Anthony, T., Valach, A., Kasak, K., … Baldocchi, D. D. (2019). Assessing the carbon and climate benefit of restoring degraded agricultural peat soils to managed wetlands. *Agricultural and Forest Meteorology*, *268*, 202–214. https://doi.org/10.1016/j.agrformet.2019.01.017

Holden, J., Chapman, P. J., & Labadz, J. C. (2004). Artificial drainage of peatlands: Hydrological and hydrochemical process and wetland restoration. *Progress in Physical Geography*, *28*(1), 95–123. https://doi.org/10.1191/0309133304pp403ra

Huang, W., & Hall, S. J. (2017). Optimized high-throughput methods for quantifying iron biogeochemical dynamics in soil. *Geoderma*, *306*(November 2016), 67–72. https://doi.org/10.1016/j.geoderma.2017.07.013

Huang, W., Ye, C., Hockaday, W. C., & Hall, S. J. (2020). Trade-offs in soil carbon protection mechanisms under aerobic and anaerobic conditions. *Global Change Biology*, (March), 3726–3737. https://doi.org/10.1111/gcb.15100

Huang, X., Tang, H., Kang, W., Yu, G., Ran, W., Hong, J., & Shen, Q. (2018). Redox interface-associated organo-mineral interactions: A mechanism for C sequestration under a rice-wheat cropping system. *Soil Biology and Biochemistry*, *120*, 12–23. https://doi.org/10.1016/j.soilbio.2018.01.031

IPCC, 2014. (2013). 2013 Supplement to the 2006 IPCC Guidelines for National Greenhouse Gas Inventories: Wetlands, Hiraishi, T., Krug, T., Tanabe, K., Srivastava, N., Baasansuren, J., Fukuda, M. and Troxler, T.G. (eds).

Jansen, B., Nierop, K. G. J., & Verstraten, J. M. (2004). Mobilization of dissolved organic matter, aluminium and iron in podzol eluvial horizons as affected by

formation of metal-organic complexes and interactions with solid soil material. *European Journal of Soil Science*, *55*(2), 287–297. https://doi.org/10.1111/j.1365-2389.2004.00598.x

Kaiser, K., & Guggenberger, G. (2000). The role of DOM sorption to mineral surfaces in the preservation of organic matter in soils. *Organic Geochemistry*, *31*(7–8), 711–725. https://doi.org/10.1016/S0146-6380(00)00046-2

Kaiser, K., Eusterhues, K., Rumpel, C., Guggenberger, G., & Kögel-Knabner, I. (2002). Stabilization of organic matter by soil minerals - Investigations of density and particle-size fractions from two acid forest soils. *Journal of Plant Nutrition and Soil Science*, *165*(4), 451–459. https://doi.org/10.1002/1522-2624(200208)165:4<451::AID-JPLN451>3.0.CO;2-B

Kaplan, D. I., Xu, C., Huang, S., Lin, Y., Tolić, N., Roscioli-Johnson, K. M., … Jaffé, P. R. (2016). Unique Organic Matter and Microbial Properties in the Rhizosphere of a Wetland Soil. *Environmental Science and Technology*, *50*(8), 4169–4177. https://doi.org/10.1021/acs.est.5b05165

Keiluweit, M., Nico, P. S., Kleber, M., & Fendorf, S. (2016). Are oxygen limitations under recognized regulators of organic carbon turnover in upland soils? *Biogeochemistry*, *127*(2–3), 157–171. https://doi.org/10.1007/s10533-015-0180-6

Kleber, M., Mikutta, R., Torn, M. S., & Jahn, R. (2005). Poorly crystalline mineral phases protect organic matter in acid subsoil horizons. *European Journal of Soil Science*, *56*(6), 717–725. https://doi.org/10.1111/j.1365-2389.2005.00706.x

Kleber, Markus, Eusterhues, K., Keiluweit, M., Mikutta, C., Mikutta, R., & Nico, P. S. (2015). *Mineral-Organic Associations: Formation, Properties, and Relevance in Soil Environments*. *Advances in Agronomy* (Vol. 130). Elsevier Ltd. https://doi.org/10.1016/bs.agron.2014.10.005

Knox, S. H., Sturtevant, C., Matthes, J. H., Koteen, L., Verfaillie, J., & Baldocchi, D. (2015). Agricultural peatland restoration: Effects of land-use change on greenhouse gas (CO2 and CH4) fluxes in the Sacramento-San Joaquin Delta. *Global Change Biology*, *21*(2), 750–765. https://doi.org/10.1111/gcb.12745

Kögel-Knabner, I., Guggenberger, G., Kleber, M., Kandeler, E., Kalbitz, K., Scheu, S., … Leinweber, P. (2008). Organo-mineral associations in temperate soils: Integrating biology, mineralogy, and organic matter chemistry. *Journal of Plant Nutrition and Soil Science*, *171*(1), 61–82. https://doi.org/10.1002/jpln.200700048

Kögel-Knabner, I., Amelung, W., Cao, Z., Fiedler, S., Frenzel, P., Jahn, R., … Schloter, M. (2010). Biogeochemistry of paddy soils. *Geoderma*, *157*(1–2), 1–14. https://doi.org/10.1016/j.geoderma.2010.03.009

Kramer, R. A., & Shabman, L. (1993). The Effects of Agricultural and Tax Policy Reform on the Economic Return to Wetland Drainage in the Mississippi Delta Region, *69*(3), 249–262.

LaCroix, R., Tfaily, M., McCreight, M., Jones, M. E., Spokas, L., & Keiluweit, M. (2018). Shifting Mineral and Redox Controls on Carbon Cycling in Seasonally Flooded Soils. *Biogeosciences Discussions*, 1–36. https://doi.org/10.5194/bg-2018-432

Lalonde, K., Mucci, A., Ouellet, A., & Gélinas, Y. (2012). Preservation of organic matter in sediments promoted by iron. *Nature*, *483*(7388), 198–200. https://doi.org/10.1038/nature10855

Leifeld, J. (2013). Prologue paper: Soil carbon losses from land-use change and the global agricultural greenhouse gas budget. *Science of the Total Environment*, *465*, 3–6. https://doi.org/10.1016/j.scitotenv.2013.03.050

Leifeld, J., & Menichetti, L. (2018). The underappreciated potential of peatlands in global climate change mitigation strategies. *Nature Communications*, *9*. https://doi.org/10.1038/s41467-018-03406-6

Loeppert, R. H., & Inskeep, W. P. (1996). *Methods of Soil Analysis. Part 3. Chemical Methods*.

Lovley, D. R. (1991). Dissimilatory Fe(III) and Mn(IV) reduction. *Microbiological Reviews*, *55*(2), 259–287. Retrieved from https://pubmed.ncbi.nlm.nih.gov/1886521

McLean, E. O. (1982). Soil pH and Lime Requirement. In *Page, A.L., Ed., Methods of Soil Analysis. Part 2. Chemical and Microbiological Properties, American Society of Agronomy, Soil Science Society of America, Madison,* (pp. 199–224).

Mejia, J., Roden, E. E., & Ginder-Vogel, M. (2016). Influence of Oxygen and Nitrate on Fe (Hydr)oxide Mineral Transformation and Soil Microbial Communities during Redox Cycling. *Environmental Science and Technology*, *50*(7), 3580–3588. https://doi.org/10.1021/acs.est.5b05519

Melton, E. D., Swanner, E. D., Behrens, S., Schmidt, C., & Kappler, A. (2014). The interplay of microbially mediated and abiotic reactions in the biogeochemical Fe cycle. *Nature Reviews. Microbiology*, *12*(12), 797–809. https://doi.org/10.1038/nrmicro3347

Miller, R. L., Fram, M. S., Fujii, R., & Wheeler, G. (2008). Subsidence Reversal in a Re-established Wetland in the Sacramento-San Joaquin Delta, California, USA. *San Francisco Estuary and Watershed Science*, *6*(3), 1–20. https://doi.org/10.5811/westjem.2011.5.6700

Niedermeier, A., & Robinson, J. S. (2007). Hydrological controls on soil redox dynamics in a peat-based, restored wetland. *Geoderma*, *137*(3–4), 318–326. https://doi.org/10.1016/j.geoderma.2006.08.027

Nikolausz, M., Kappelmeyer, U., Székely, A., Rusznyák, A., Márialigeti, K., & Kästner, M. (2008). Diurnal redox fluctuation and microbial activity in the rhizosphere of wetland plants. *European Journal of Soil Biology*, *44*(3), 324–333. https://doi.org/10.1016/j.ejsobi.2008.01.003

Oades, J. M., & Waters, A. G. (1991). Aggregate hierarchy in soils. *Australian Journal of Soil Research*, *29*(6), 815–825. https://doi.org/10.1071/SR9910815

Peretyazhko, T., & Sposito, G. (2005). Iron(III) reduction and phosphorous solubilization in humid tropical forest soils. *Geochimica et Cosmochimica Acta*, *69*(14), 3643–3652. https://doi.org/10.1016/j.gca.2005.03.045

Phillips, E. J. P., Lovley, D. R., & Roden, E. E. (1993). Composition of non-microbially reducible Fe(III) in aquatic sediments. *Applied and Environmental Microbiology*, *59*(8), 2727–2729. https://doi.org/10.1128/aem.59.8.2727-

2729.1993
Porras, R. C., Hicks Pries, C. E., McFarlane, K. J., Hanson, P. J., & Torn, M. S. (2017). Association with pedogenic iron and aluminum: effects on soil organic carbon storage and stability in four temperate forest soils. *Biogeochemistry*. https://doi.org/10.1007/s10533-017-0337-6
Scharlemann, J. P. W., Tanner, E. V. J., Hiederer, R., & Kapos, V. (2014). Global soil carbon: Understanding and managing the largest terrestrial carbon pool. *Carbon Management*, *5*(1), 81–91. https://doi.org/10.4155/cmt.13.77
Scheel, T., Dörfl, C., & Kalbitz, K. (2007). Precipitation of Dissolved Organic Matter by Aluminum Stabilizes Carbon in Acidic Forest Soils. *Soil Science Society of America Journal*, *71*(1), 64–74. https://doi.org/10.2136/sssaj2006.0111
Silver, W. L., Ryals, R., & Eviner, V. (2010). Soil Carbon Pools in California's Annual Grassland Ecosystems. *Rangeland Ecology & Management*, *63*(1), 128–136. https://doi.org/10.2111/REM-D-09-00106.1
Six, J., & Paustian, K. (2014). Aggregate-associated soil organic matter as an ecosystem property and a measurement tool. *Soil Biology and Biochemistry*, *68*, A4–A9. https://doi.org/10.1016/j.soilbio.2013.06.014
Spivak, A. C., Sanderman, J., Bowen, J. L., Canuel, E. A., & Hopkinson, C. S. (2019). Global-change controls on soil-carbon accumulation and loss in coastal vegetated ecosystems. *Nature Geoscience*, *12*(9), 685–692. https://doi.org/10.1038/s41561-019-0435-2
Stephens, J. C., Allen, L. H., & Chen, E. (1984). Organic Soil Subsidence. *Reviews in Engineering Geology*, *VI*(225). https://doi.org/10.1130/REG6-p107
Stepniewski, W., Gliński, J., & Ball, B. C. (1994). Effects of Compaction on Soil Aeration Properties. *Developments in Agricultural Engineering*, *11*(C), 167–189. https://doi.org/10.1016/B978-0-444-88286-8.50016-7
Takahashi, T., & Dahlgren, R. A. (2016). Nature, properties and function of aluminum-humus complexes in volcanic soils. *Geoderma*, *263*, 110–121. https://doi.org/10.1016/j.geoderma.2015.08.032
Teh, Y. A., Silver, W. L., Sonnentag, O., Detto, M., Kelly, M., & Baldocchi, D. D. (2011). Large Greenhouse Gas Emissions from a Temperate Peatland Pasture. *Ecosystems*, *14*(2), 311–325. https://doi.org/10.1007/s10021-011-9411-4
Thompson, A., Rancourt, D. G., Chadwick, O. A., & Chorover, J. (2011). Iron solid-phase differentiation along a redox gradient in basaltic soils. *Geochimica et Cosmochimica Acta*, *75*(1), 119–133. https://doi.org/10.1016/j.gca.2010.10.005
Todorova, S. G., Siegel, D. I., & Costello, A. M. (2005). Microbial Fe(III) reduction in a minerotrophic wetland - Geochemical controls and involvement in organic matter decomposition. *Applied Geochemistry*, *20*(6), 1120–1130. https://doi.org/10.1016/j.apgeochem.2005.02.005
Torn, M. S., Trumbore, S. E., Chadwick, O. A., Vitousek, P. M., & Hendricks, D. M. (1997). Mineral control of soil organic carbon storage and turnover. *Nature*, *389*(6647), 170–173. https://doi.org/10.1038/38260
Torrent, I. R. J. (1997). Citrate-Ascorbate as a Highly Selective Extractant for Poorly Crystalline Iron Oxides. *Soil Science Society of America Journal*, *61*, 1647–1654.

https://doi.org/10.2136/sssaj1997.03615995006100060015x
Totsche, K. U., Amelung, W., Gerzabek, M. H., Guggenberger, G., Klumpp, E., Knief, C., … Kögel-Knabner, I. (2017). Microaggregates in soils. *Journal of Plant Nutrition and Soil Science*, 104–136. https://doi.org/10.1002/jpln.201600451
Verhoeven, J. T. A., & Setter, T. L. (2010). Agricultural use of wetlands: Opportunities and limitations. *Annals of Botany*, *105*(1), 155–163. https://doi.org/10.1093/aob/mcp172
Verschoor, M. J., & Molot, L. A. (2013). A comparison of three colorimetric methods of ferrous and total reactive iron measurement in freshwaters. *Limnology and Oceanography: Methods*, *11*(MAR), 113–125. https://doi.org/10.4319/lom.2013.11.113
Viollier, E., Inglett, P. W., Hunter, K., Roychoudhury, A. N., & Van Cappellen, P. (2000). The ferrozine method revisited: Fe(II)/Fe(III) determination in natural waters. *Applied Geochemistry*, *15*(6), 785–790. https://doi.org/10.1016/S0883-2927(99)00097-9
Vorenhout, M., van der Geest, H. G., van Marum, D., Wattel, K., & Eijsackers, H. J. P. (2004). Automated and Continuous Redox Potential Measurements in Soil. *Journal of Environment Quality*, *33*(4), 1562. https://doi.org/10.2134/jeq2004.1562
Wagai, R., & Mayer, L. M. (2007). Sorptive stabilization of organic matter in soils by hydrous iron oxides. *Geochimica et Cosmochimica Acta*, *71*, 25–35. https://doi.org/10.1016/j.gca.2006.08.047
Wagai, R., Mayer, L. M., Kitayama, K., & Shirato, Y. (2013). Association of organic matter with iron and aluminum across a range of soils determined via selective dissolution techniques coupled with dissolved nitrogen analysis. *Biogeochemistry*, *112*(1–3), 95–109. https://doi.org/10.1007/s10533-011-9652-5
Wang, H., River, M., & Richardson, C. J. (2019). Does an ‘iron gate’ carbon preservation mechanism exist in organic–rich wetlands? *Soil Biology and Biochemistry*, *135*, 48–50. https://doi.org/10.1016/j.soilbio.2019.04.011
Warren, S. D., Nevill, M. B., Blackburn, W. H., & Garza, N. E. (1986). Soil Response to Trampling Under Intensive Rotation Grazing. *Soil Science Society of America Journal*, *50*(5), 1336. https://doi.org/10.2136/sssaj1986.03615995005000050050x
Weber, K. A., Achenbach, L. A., & Coates, J. D. (2006). Microorganisms pumping iron: anaerobic microbial iron oxidation and reduction. *Nature Reviews*, *4*(iii), 752–764. https://doi.org/10.1038/nrmicro1490
Wilson, S., Blain, D., Couwenberg, J., Evans, C. D., Murdiyarso, D., Page, S. E., … Tuittila, E.-S. (2016). Greenhouse gas emission factors associated with rewetting of organic soils. *Mires and Peat*, *17*(4), 1–28. https://doi.org/10.19189/MaP.2016.OMB.222
Wiseman, C. L. S., & Püttmann, W. (2006). Interactions between mineral phases in the preservation of soil organic matter. *Geoderma*, *134*(1–2), 109–118. https://doi.org/10.1016/j.geoderma.2005.09.001
Yang, W. H., & Liptzin, D. (2015). High potential for iron reduction in upland soils.

Ecology, *96*(7), 2015–2020. https://doi.org/10.1890/14-2097.1
Yu, Z., Loisel, J., Brosseau, D. P., Beilman, D. W., & Hunt, S. J. (2010). Global peatland dynamics since the Last Glacial Maximum. *Geophysical Research Letters*, *37*(13), 1–5. https://doi.org/10.1029/2010GL043584

2.9 Appendix

2.9.1 Supplemental Methods

Soil bulk density (0–15 cm, 15-30 cm, 30-45 cm, and 45-60 cm depths) was measured at each drained site. This was done by digging pits (one per plot) and carefully sampling soil volumetrically using 9 cm diameter cores along an undisturbed face. Total soil volumes were then weighed, and a subsample was taken to correct for soil moisture. In addition to the analyses in supplemental figures 3a and 3b, we added an Fe(III)-Cl spike to fresh 0.5M HCl soil extracts to quantify potential Fe(III) autoreduction via DOC (only in sites with > 10% C). Five replicate samples were sampled at depths of 0-15 cm and 15-30 cm (n = 10), and approximately 1.5 g soil was added to 30 ml of HCl within one minute of soil sampling. Samples were brought back to the lab and a Fe(III)-Cl spike, prepared in 0.5M HCl, was added to 5 ml subsamples corresponding to an increase of 0.2 mM/L in the sample 0.5M HCl extract. Spiked and non-spiked subsamples were then shaken for one hour and centrifuged at 4700 rcf for 15 min. Samples were decanted and rerun for ferrozine analysis, and the recovery rate of the Fe(III) spike was always > 95%, within the error of the method. While this test does not confirm that no autoreduction occurred in our samples, it does highlight that this was not a significant source of $Fe(II)_{HCl}$ measured.

2.9.2 Estimate of the amount of C oxidized from Fe reduction

Using soils from near our field sites and also in the Sacramento-San Joaquin Delta, Yang and Liptzin (2015) measured an Fe reduction rate of approximately 1180 µg Fe g $soil^{-1}$ d^{-1} using 5.5 d anaerobic laboratory incubations (flooded conditions). This rate of Fe reduction yields 0.47 g C m^{-2} d^{-1}. The total amount of Fe reduced during the redox cycle was 6500 µg Fe g $soil^{-1}$ $cycle^{-1}$ with 2.6 g C m^{-2} $cycle^{-1}$ (W. H. Yang & Liptzin, 2015). We can estimate the amount of C oxidized by Fe using previously published Fe reduction rates above, a soil depth of 30 cm, and a conservative soil bulk density estimate of 0.25 g/cm^3 (Deverel et al., 2016):

$$\frac{6.5\ g\ Fe}{1\ kg\ soil * cycle} * \frac{1\ mol\ Fe}{55.845\ g\ Fe} * \frac{1\ mol\ e-}{1\ mol\ Fe} * \frac{0.025\ mol\ C}{1\ mol\ e-} * \frac{12\ g\ C}{1\ mol\ C} * \frac{1\ kg\ C}{1000\ g\ C} * \frac{1\ kg\ soil}{1000\ g\ soil} * \frac{0.25\ g\ soil}{cm^3\ soil} * 30\ cm * \frac{10^8 cm^2}{1\ ha} = \mathbf{26.1\ kg\ C\ ha^{-1}\ cycle^{-1}}$$

Supplemental Table 1 Fit information for pairwise regression analyses.

Figure	Variable	Status	Depth (cm)	Fit equation	R^2	*P*-value
3a	Soil C (%) and $Fe(II)_{HCl}$	Drained	0-15: 15-30:	y = 3.73*ln(x) + 17.86 y = 3.54*ln(x) + 17.44	0.49 0.58	$P < 0.0001$ $P < 0.0001$
3b	Soil C (%) and $Fe(II)_{HCl}$	Reflooded	0-15: 15-30:	y = -9.09*ln(x) + 34.02 y = -5.28*ln(x) + 23.81	0.89 0.59	$P < 0.0001$ $P < 0.0001$
5	Mean Soil C (%) and Mean Fe_{CA}	All sites	0-15: 15-30:	y = -3.33*ln(x) + 13.37 y = -0.63*ln(x) + 13.48	0.81 0.69	$P < 0.0001$ $P < 0.0001$
6a	Soil C (%) and Fe_{AO}	Drained	0-15: 15-30:	y = -9.02*ln(x) + 6.90 y = -7.18*ln(x) + 6.92	0.59 0.45	$P < 0.0001$ $P < 0.0001$
6b	Soil C (%) and Fe_{CA}	Drained	0-15: 15-30:	y = -2.77*ln(x) + 12.94 y = -3.08*ln(x) + 12.99	0.46 0.41	$P < 0.0001$ $P < 0.0001$
6c	Soil C (%) and Fe_{AO}	Reflooded	0-15: 15-30:	y = -13.69*ln(x) + 21.43 y = -2.97*ln(x) + 14.22	0.59 0.22	$P < 0.0001$ $P < 0.0001$
6d	Soil C (%) and Fe_{CA}	Reflooded	0-15: 15-30:	y = -6.28*ln(x) + 2.48 y = -2.34*ln(x) + 7.41	0.54 0.31	$P < 0.0001$ $P < 0.0001$
7	Soil C (%) and Al_{AO}	Drained	0-15: 15-30:	y = 24.5x - 0.79 y = 27.0x – 2.25	0.91 0.91	$P < 0.0001$ $P < 0.0001$
8	$Fe(II)_{HCl}$ and Al_{AO}	Drained	0-15: 15-30:	Ln(y) = 1.75x - 3.34 Ln(y) = 2.56x - 3.80	0.71 0.51	$P < 0.0001$ $P < 0.0001$
S1a	$Fe(II)_{HCl}$ (%) and Al_{AO}	Reflooded	0-15: 15-30:	y = 20.22x + 0.74 y = 9.00x + 4.80	0.78 0.07	$P < 0.0001$ $P < 0.0001$
S1b	Soil C (%) and soil moisture	Reflooded	0-15: 15-30:	y = -0.59x + 0.81 y = 0.13x + 0.39	0.75 0.04	$P < 0.0001$ $P < 0.0001$
S2a	Soil C (%) and Al_{AO}	Drained	0-15: 15-30:	y = 12.62x + 3.084 y = 12.67x + 2.50	0.59 0.53	$P < 0.0001$ $P < 0.0001$
S2b	Soil C (%) and Al_{AO}	Reflooded	0-15: 15-30:	y = -40.14x + 35.19 y = 6.474x + 10.61	0.64 0.05	$P < 0.0001$ $P < 0.0001$
S3a	Soil C (%) and $Fe(II)_{HCl}$	Drained	0-15: 15-30:	y = 4.43*ln(x) + 20.99 y = 4.16*ln(x) + 20.60	0.64 0.75	$P < 0.0001$ $P < 0.0001$
S3b	Soil C (%) and $Fe(II)_{HCl}$	Drained	0-15: 15-30:	y = 4.5*ln(x) + 12.26 y = 4.37*ln(x) + 12.32	0.79 0.76	$P < 0.0001$ $P < 0.0001$

Supplemental Table 2 Site characteristics. Values are means with standard error in parentheses.

Site	Status	Depth (cm)	% Moisture (SE)	% Soil C (SE)	pH (SE)
Bouldin 1	Drained	0-15	42.34% (0.01)	5.26% (0.02)	4.93 (0.04)
		15-30	42.49% (0.01)	5.00% (0.15)	4.94 (0.04)
Bouldin 2	Drained	0-15	16.90% (0.01)	5.08% (0.04)	5.08 (0.04)
		15-30	22.05% (0.01)	4.89% (0.07)	5.09 (0.03)
Bouldin Corn	Drained	0-15	40.08% (0.01)	15.17% (0.28)	5.89 (0.05)
		15-30	42.44% (0.01)	15.95% (0.49)	6.38 (0.04)
East End	Flooded	0-15	42.80% (0.01)	9.94% (0.16)	5.98 (0.05)
		15-30	35.87% (0.01)	10.42% (0.35)	5.27 (0.10)
Mayberry	Flooded	0-15	66.31% (0.04)	18.9% (1.06)	6.94 (0.12)
		15-30	38.30% (0.01)	12.35% (0.21)	7.09 (0.05)
Sherman Pasture	Drained	0-15	15.13% (0.01)	4.59% (0.07)	6.11 (0.08)
		15-30	14.27% (0.01)	3.59% (0.11)	6.60 (0.05)
Sherman Barn	Drained	0-15	28.67% (0.01)	8.97% (0.10)	5.13 (0.05)
		15-30	30.21% (0.01)	8.77% (0.12)	5.39 (0.10)
Twitchell	Drained	0-15	20.53% (0.01)	8.13% (0.06)	5.82 (0.04)
		15-30	19.87% (0.01)	7.96% (0.05)	5.92 (0.03)
West Pond	Flooded	0-15	82.20% (0.01)	40.15% (0.55)	6.33 (0.06)
		15-30	63.27% (0.02)	21.39% (1.94)	6.19 (0.05)

Supplemental Table 3. Bulk density values (in g cm^{-3}) for drained soils at 0-15, 15-30, 30-45, and 45-60 cm depths.

Depth (cm)	Bouldin 1	Bouldin 2	Bouldin Corn	Twitchell	Sherman Pasture	Sherman Barn
0-15	1.046	1.065	0.587	0.762	1.11	1.088
15-30	0.906	1.049	0.734	0.901	1.237	1.048
30-45	0.948	0.998	0.552	0.819	0.678	0.623
45-60	1.166	1.072	0.576	1.288	0.530	0.671

Supplemental Table 4. Multiple regression models of soil C concentrations incorporating potential predictors with data from all sites, with 0-15 cm and 15-30 cm depths fit separately.

0-15 cm: Term	Estimate	Std Error	P
Intercept	13.941863	9.0290912	0.1341
Soil Moisture	14.195147	4.1179458	0.0008*
pH	-0.154939	1.0734588	0.8862
Fe_{AO}	-2.82124	1.1473142	0.0173*
Al_{AO}	5.8625174	2.1530842	0.0075*
$Ln[Fe(II)_{HCl}]$	-0.85879	0.5468754	0.1227
$Ln[Fe_{HCl}]$	-3.203646	0.5287107	<.0001*
$Ln[Fe_{CA}]$	-1.716782	0.6020297	0.0056*
$Ln[Al_{CA}]$	-0.643101	0.6009931	0.2870

15-30 cm: Term	Estimate	Std Error	P
Intercept	-0.265029	3.5703219	0.9409
Soil Moisture	6.5736351	2.625546	0.0139*
pH	1.761311	0.4028944	<.0001*
Fe_{AO}	-0.715955	0.6105865	0.2435
Al_{AO}	13.066407	1.2849435	<.0001*
$Ln[Fe(II)_{HCl}]$	-0.054744	0.2635995	0.8359
$Ln[Fe_{HCl}]$	-2.50682	0.3515269	<.0001*
$Ln[Fe_{CA}]$	-1.164189	0.3954455	0.0039*
$Ln[Al_{CA}]$	0.4120094	0.3377073	0.2252

Supplemental Table 5. Multiple regressions models of soil C concentrations incorporating potential predictors with data from all reflooded sites, with 0-15 cm and 15-30 cm depths fit separately.

0-15 cm: Term	Estimate	Std Error	P
Intercept	35.877232	15.92593	0.0314*
Soil Moisture	37.036238	12.523854	0.0710
pH	-1.295352	2.2291011	0.5653
Fe_{AO}	0.4935261	3.5253563	0.8899
Al_{AO}	-5.779759	13.975999	0.6993
$Ln[Fe(II)_{HCl}]$	-3.897412	1.9541553	0.0549
$Ln[Fe_{HCl}]$	-2.197612	2.1520412	0.3174
$Ln[Fe_{CA}]$	1.3933055	1.5282266	0.4107
$Ln[Al_{CA}]$	3.3018652	2.4212843	0.1829

15-30 cm: Term	Estimate	Std Error	P
Intercept	-0.051441	6.4774191	0.9937
Soil Moisture	13.036944	3.3447933	0.0005*
pH	1.146068	0.50496	0.0311*
Fe_{AO}	-0.80258	0.7175955	0.2724
Al_{AO}	6.9502803	2.560263	0.0108*
$Ln[Fe(II)_{HCl}]$	1.0747385	0.7702888	0.1744
$Ln[Fe_{HCl}]$	-1.88238	0.9136275	0.0482*
$Ln[Fe_{CA}]$	-0.31011	0.4860623	0.5281
$Ln[Al_{CA}]$	0.0263274	0.7936194	0.9738

Supplemental Table 6. Multiple regressions models of soil C concentrations incorporating potential predictors with data from all drained sites, with 0-15 cm and 15-30 cm depths fit separately.

0-15 cm: Term	Estimate	Std Error	P
Intercept	4.9042537	3.985381	0.2222
Soil Moisture	-3.528904	2.0358239	0.0871
pH	1.6013601	0.4327474	0.0004*
Fe_{AO}	-7.302776	1.1917551	<.0001*
Al_{AO}	10.982192	1.8292768	<.0001*
$Ln[Fe(II)_{HCl}]$	-0.070189	0.3930672	0.8587
$Ln[Fe_{HCl}]$	-0.411782	0.2566941	0.1127
$Ln[Fe_{CA}]$	-0.537457	0.5963818	0.3703
$Ln[Al_{CA}]$	0.7139552	0.309084	0.0237*

15-30 cm: Term	Estimate	Std Error	P
Intercept	11.458986	3.2983062	0.0008*
Soil Moisture	7.553392	2.5128004	0.0035*
pH	0.8104531	0.3688084	0.0309*
Fe_{AO}	-2.037482	1.0398409	0.0536
Al_{AO}	5.000839	1.9449085	0.0120*
$Ln[Fe(II)_{HCl}]$	1.1867613	0.450675	0.0103*
$Ln[Fe_{HCl}]$	-1.428982	0.2865146	<.0001*
$Ln[Fe_{CA}]$	-1.798372	0.6037618	0.0039*
$Ln[Al_{CA}]$	0.8802295	0.3563161	0.0157*

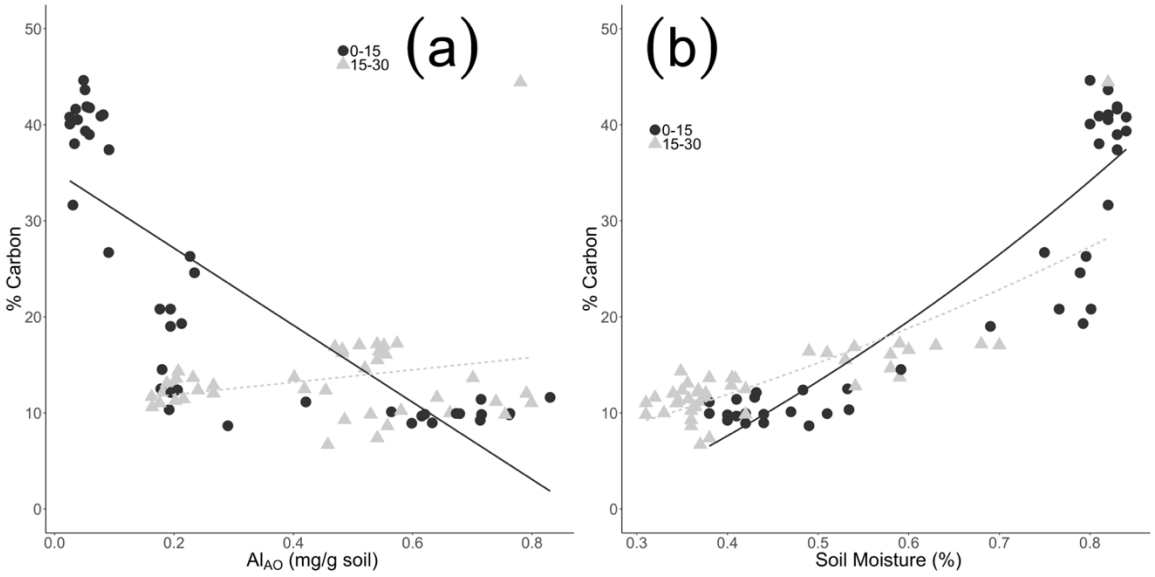

Supplemental Figure 1. Linear relationships between $Fe(II)_{HCl}$ and ammonium-oxalate extractable Al (Al_{AO}) concentrations (a) and % soil carbon and soil moisture, with 0-15 cm (black circles) and 15-30 cm (grey triangles) in reflooded soils.

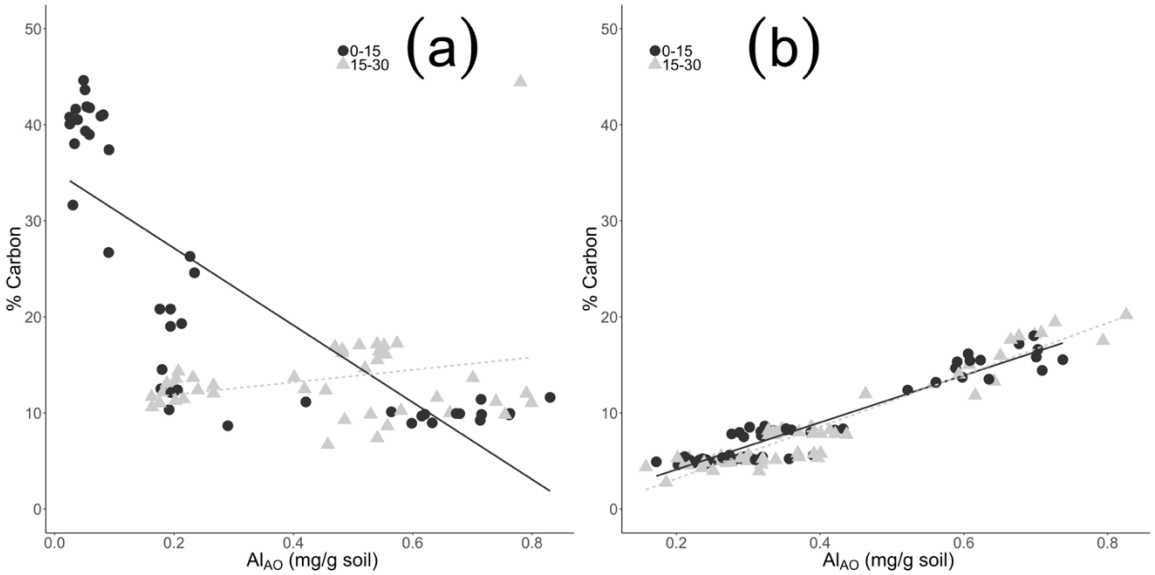

Supplemental Figure 2. Linear relationships between soil carbon and ammonium-oxalate extractable Al (Al_{AO}) concentrations and across 0-15 cm (circles) and 15-30 cm (triangles) depth in drained (a) and reflooded (b) soils with pasture sites included (0-15 cm: $R^2 = 0.59$, 15-30 cm: $R^2 = 0.53$). Note the difference in the y-axis.

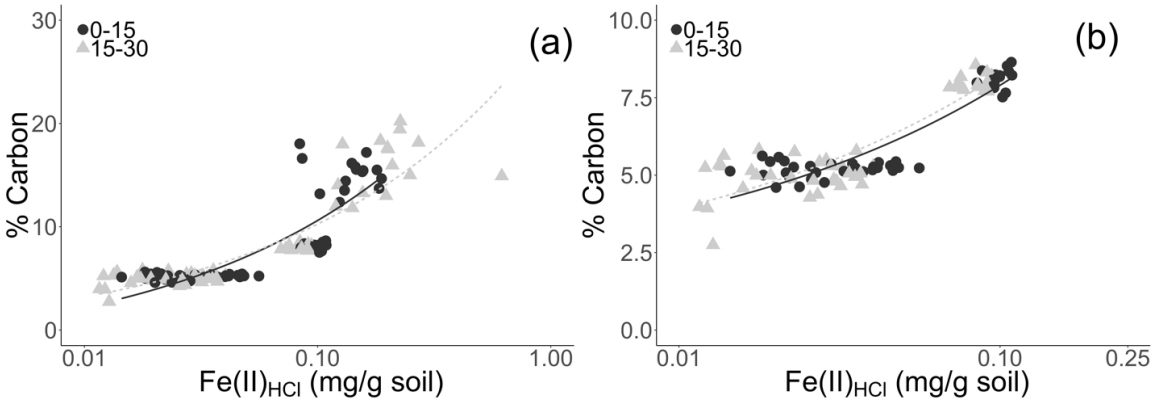

Supplemental Figure 3 (a) Log-linear relationships between soil C and HCl-extractable Fe (II) concentrations in drained soils with Fe(II) concentrations decreased by 10% in samples >10% C at 0-15 (black circles) and 15-30 cm (grey triangles). **(b)** Log-linear relationships between soil carbon and HCl-extractable Fe (II) concentrations with samples >10% C removed at 0-15 (black circles) and 15-30 cm (grey triangles). Note the differences across scales.

In **Chapter 2**, I first quantified the distribution and range of soil carbon (C) content across dominant land uses for both drained and restored wetland soils in the Sacramento-San Joaquin Delta. We found that reactive Fe and Al minerals were important controls on soil C content under both drained and flooded conditions, but soil C alone does not represent the total greenhouse gas budgets of these systems. Using data from **Chapter 2**, in **Chapter 3** I selected an agricultural soil with the highest soil C concentrations to measure long-term emissions of the three major greenhouse gases carbon dioxide (CO_2), methane (CH_4), and nitrous oxide (N_2O) as I aimed to quantify emissions from the highest emitting agricultural peatland soils. I use these long-term greenhouse gas measurements from an organic-rich corn ecosystem to both compare with a mineral-rich alfalfa ecosystem in **Chapter 5** and help further our understanding of the total greenhouse gas emissions from agricultural peatlands in this region. Continuous soil greenhouse gas flux measurements, particularly N_2O, are necessary to better quantify the greenhouse gas emissions reductions via wetland restoration of agricultural peatlands and help select wetland restoration efforts that maximize emissions reductions.

Chapter 3. Hot moments drive extreme nitrous oxide emissions from agricultural peatlands[2]

3.1 Abstract

Agricultural peatlands are estimated to emit approximately one third of global greenhouse gas emissions from croplands, but the temporal dynamics and controls of these emissions are poorly understood, particularly for nitrous oxide (N_2O). We used cavity ringdown spectroscopy and automated chambers in a drained agricultural peatland to measure over 70,000 individual N_2O, methane (CH_4), and carbon dioxide (CO_2) fluxes over 3 years. Our results showed that N_2O fluxes were high, contributing 26% (annual range: 16-35%) of annual CO_2e emissions. Total N_2O fluxes averaged 26 ± 0.5 kg N_2O-N ha^{-1} y^{-1} and exhibited significant inter- and intra-annual variability with a maximum annual flux of 42 ± 1.8 kg N_2O-N ha^{-1} y^{-1}. Hot moments of N_2O and CH_4 emissions represented 1.1 ± 0.2 and 1.3 ± 0.2% of measurements, respectively, but contributed to 45 ± 1% of mean annual N_2O fluxes and to 140 ± 9% of mean annual CH_4 fluxes. Soil moisture, soil temperature, and bulk soil oxygen (O_2) concentrations were strongly correlated with soil N_2O and CH_4 emissions; soil nitrate (NO_3^-) concentrations were also significantly correlated with soil N_2O emissions. These results suggest that IPCC benchmarks underestimate N_2O emissions from these high emitting agricultural peatlands by up to 70%. Scaling to regional agricultural peatlands with similar management suggests these ecosystems could emit up to 1.86 Tg CO_2e y^{-1} (range: 1.58-2.21 Tg CO_2e y^{-1}). Data suggest that these agricultural peatlands are large sources of greenhouse gases, and that short-term hot moments of N_2O and CH_4 are a significant fraction of total greenhouse budgets.

[2] This chapter is reprinted, with permission from Springer Nature, from the original journal article: Anthony, T. L., & Silver, W. L. (2021). Hot moments drive extreme nitrous oxide emissions from agricultural peatlands. *Global Change Biology*, *accepted*.

3.2 Introduction

Drained peatlands occupy only 1% of agricultural land but are estimated to emit 32% of global cropland carbon dioxide (CO_2)-equivalent (CO_2e) emissions (Carlson et al., 2017; Leifeld & Menichetti, 2018). As peatland soils are drained and exposed to the atmosphere, high rates of aerobic decomposition lead to substantial CO_2 respiration rates relative to other ecosystems (Hemes et al., 2019; Tiemeyer et al., 2016; Veber et al., 2017). High rates of peat decomposition along with emissions of other important greenhouse gases (GHG) like methane (CH_4) and nitrous oxide (N_2O) can result in large net GHG emissions from these agricultural ecosystems (Oertel, Matschullat, Zurba, Zimmermann, & Erasmi, 2016; Pärn et al., 2018; Petrescu et al., 2015).

Nitrogen fertilization and flood irrigation are common in peatland agriculture (Kirk, Van Kessel, Horwath, & Linquist, 2015; Pellerin, Anderson, & Bergamaschi, 2014; Verhoeven & Setter, 2010), potentially creating optimal conditions for high denitrification rates and N_2O production. Drained peatlands have been shown to be significant N_2O sources; the IPCC mean estimate for drained agricultural peatlands is 8 kg N_2O-N ha^{-1} y^{-1} (uncertainty range: 2-24 kg N_2O-N ha^{-1} y^{-1}, IPCC, 2019). However, few studies have made continuous multi-year measurements of N_2O emissions, and N_2O fluxes are often absent from long-term agricultural peatland GHG budgets (Bonn et al., 2014; Frolking et al., 2011; Günther et al., 2020; Hemes et al., 2019; Knox et al., 2015). This is partially driven by the technological challenges of conducting continuous, long-term N_2O flux measurements under field conditions (Baldocchi, 2014; Levy et al., 2017; Rochette & Eriksen-Hamel, 2008).

Most N_2O flux measurements are conducted intermittently with sampling frequency often ranging from once per day to once per month using traditional manual static chambers (Grace et al., 2020). This is particularly true in agricultural peatlands (H. Liu, Zak, Rezanezhad, & Lennartz, 2019; Pärn et al., 2018; Tiemeyer et al., 2016). However, CH_4 and N_2O are often characterized by hot spots and hot moments of GHG emissions (Krichels & Yang, 2019; Molodovskaya et al., 2012; Savage, Phillips, & Davidson, 2014), which are difficult to characterize using infrequent manual sampling approaches (Bernhardt et al., 2017; McClain et al., 2003; Sihi, Davidson, Savage, & Liang, 2020). The dynamics of soil oxygen (O_2), temperature, moisture, and nitrate (NO_3) concentrations are likely to contribute to hot moments of soil N_2O flux (Butterbach-Bahl, Baggs, Dannenmann, Kiese, & Zechmeister-Boltenstern, 2013), although the spatial and temporal dynamics of these events are also difficult to predict without high frequency measurement.

Potential hot moments of soil CH_4 fluxes are similarly difficult to capture utilizing manual chamber methods, although CH_4 fluxes from drained agricultural peatlands are assumed to be minimal (Günther et al., 2020; Maljanen et al., 2010; Oktarita, Hergoualc'H, Anwar, & Verchot, 2017). However, management practices such as irrigation can create periods of anaerobic conditions ideal for CH_4 production (Hemes et al., 2019; Teh et al., 2011). Continuous eddy covariance measurements of CH_4 fluxes at the ecosystem-scale have highlighted the influence of soil temperature, water table fluctuations, and plant activity on the exchange of CH_4

across the land-atmosphere interface in restored wetlands (Chamberlain et al., 2019; Oikawa et al., 2017; Sturtevant et al., 2016). In contrast, the spatiotemporal controls on the magnitude and frequency of CH_4 fluxes in irrigated agricultural soils are less well constrained.

The recent development of cavity ringdown spectroscopy and automated chamber measurements has greatly increased the ability to conduct continuous GHG flux measurements. Continuous measurements can increase the chances of capturing hot moments of net GHG fluxes and determining their role in annual GHG budgets. In combination with continuous soil sensor data, spatiotemporally intensive measurements can also be utilized to explore potential drivers of hot moments of soil CH_4 and N_2O emissions (Bernhardt et al., 2017; Groffman et al., 2009; Sihi et al., 2020). We used cavity ringdown spectroscopy and automated chambers to make over 70,000 soil CO_2, CH_4, and N_2O flux measurements over three years from a drained agricultural maize peatland in California, USA. Flux measurements were coupled with continuous soil O_2, temperature, and moisture sensors and a year-long soil N sampling campaign to better constrain the drivers and controls on hot moments of soil CH_4 and N_2O emissions. We utilized multiple statistical approaches, including wavelet coherence analysis and a modified jackknifing technique to further explore the drivers and controls on hot moments of soil CH_4 and N_2O effluxes. We tested the hypothesis that fertilizer application would drive hot moments of N_2O emission through increased substrate availability. We also hypothesized that elevated soil temperatures and soil moisture would stimulate O_2 depletion during the growing season, leading to increased N_2O and CH_4 production within the soil profile and associated hot moments of GHG emissions.

3.3 Methods

3.3.1 Site Information

The study was conducted in the Sacramento-San Joaquin Delta region of California (38.11ºN, 121.5ºW). The field site was farmed continuously for over 10 years for conventional field corn (*Zea mays*). The site was periodically irrigated via spud ditches during the growing season and periodically flooded up to 30 cm above the soil surface in the winter to limit weed growth and provide habitat for migrating waterfowl (Pellerin et al. 2014). Fertilizer application rates were 118 kg N ha^{-1} y^{-1} (*Farmer data).* The climate is Mediterranean with hot dry summers and cool wet winters. The region's historical mean annual temperature was 15.1 ± 6.3 °C and mean annual rainfall averaged 326 ± 4 mm (Hatala et al., 2012). This was also an Ameriflux site (Ameriflux ID: US-Bi2) with continuous eddy covariance measurements of CO_2, CH_4, and water vapor since mid-2017.

Soils are typical of the region and are classified within the Rindge series as Histosols (Soil Survey Staff, 2020). This soil type is frequently drained for agriculture due to its high agricultural productivity (Leinfelder-Miles, 2019). Rindge soils belong to the Euic, thermic Typic Haplosaprists taxonomic class and are characterized by deep, poorly drained marsh soils

formed from decomposed plant organic matter (Soil Survey Staff, 2020). Total soil C values (mean ± standard error) at this site were 15.2 ± 0.4% at 0-15 cm, 15.9 ± 0.7% at 15-30 cm, and 19.5 ± 0.6% at 30-60 cm depth (Anthony & Silver, 2020). Total soil N values were 1.0 ± 0.02% at 0-15 cm, 1.1 ± 0.04% at 15-30 cm, and 1.2 ± 0.03% at 30-60 cm depth (Anthony & Silver, 2020).

3.3.2 Automated chamber flux measurements

Surface soil fluxes of N_2O, CH_4, and CO_2 were measured continuously from June 30, 2017 through June 30, 2020 using an automatic chamber system. This system consisted of nine opaque automated gas flux chambers (eosAC, Eosense, Nova Scotia, Canada) connected to a multiplexer (eosMX, Eosense, Nova Scotia, Canada). The multiplexer allowed for dynamically signaled chamber deployment and routed gases to a cavity ring-down spectrometer (Picarro G2508, Santa Clara, CA, USA). Chambers were measured sequentially over a 10-min sampling period with a 1.5-min flushing period before and after each measurement.

Chambers were deployed in 10 x 10 m grid, with each chamber 5 m apart. Due to periodic flooding events, two sets of extended soil collars were utilized to maintain measurement collection and ensure chambers were not inundated. Chambers were randomly assigned to distinct physical features, beds (n = 4) or furrows (n = 5) during growing seasons and corn stover (n = 4) or bare soil (n = 5) during fallow periods. Throughout most of the year, 15 cm collars were installed with each chamber, offsetting the original chamber height by approximately 10 cm. Due to winter flooding events that raise the water table up to 30 cm above the soil surface, additional 35 cm collars were deployed approximately between November and February. Individual chamber volumes were measured and used to adjust flux calculations (see below). Chambers remained installed in their original positions throughout the field campaigns except during field management activities (plowing, seeding, harvest), which typically lasted less than one week. Two additional periods of chamber removal occurred after delays in initiating corn harvest in site year 1 (18 days) and site year 3 (20 days).

To determine chamber volume, collar heights were measured approximately weekly and values were interpolated over time to account for differences in soil and water table height. Chamber volumes were used to calculate the minimum detectable flux (Courtois et al., 2018) with detection limits of 0.002 nmol N_2O m^{-2} s^{-1}, 0.06 nmol CO_2 m^{-2} s^{-1}, and 0.002 nmol CH_4 m^{-2} s^{-1} for 15 cm collars utilized during non-flooded conditions, and 0.004 nmol N_2O m^{-2} s^{-1}, 0.12 nmol CO_2 m^{-2} s^{-1}, and 0.004 nmol CH_4 m^{-2} s^{-1} for 35 cm collars utilized during flooded conditions. The minimum detectable fluxes reported here are conservative estimates, as the actual chamber volume was always smaller than the maximum theoretical volume used in detection limit calculations.

Flux calculations and fitting were first performed using Eosense eosAnalyze-AC v. 3.7.7 software, then data quality assessment and control were subsequently performed in R (RStudio,

v.1.1.4633, O'Connell, Ruan, & Silver, 2018). Fluxes were removed from the final dataset if they were associated with negative gas concentrations or erroneous spectrometer cavity temperature and pressure readings outside the calibrated operating range, corresponding to instrument malfunction. Fluxes were also removed if the chamber deployment period was less than 9 min or greater than 11 min, indicative of chamber malfunction. This data filtering removed 2.4% of flux measurement periods, generating a final dataset of 71,262, 70,337, and 70,554 individual flux measurements of CO_2, N_2O, and CH_4, respectively. To calculate the impact of soil GHG fluxes on site-level global warming potential (GWP) we utilized net ecosystem exchange (NEE) eddy covariance values at the same site (Camilo, Szutu, Baldocchi, & Hemes, 2021; Hemes et al., 2019). To convert flux measurements to CO_2e, we used the IPCC AR5 100-year GWP values of 28 CO_2e for CH_4 and 298 CO_2e for N_2O (Myhre et al., 2013). Yield-based emission estimates were from derived flux measurements and harvest yield data records that were converted to g dry yield ha^{-1}, assuming corn was harvested at 65% moisture (Hemes et al., 2019).

3.3.3 Quantifying hot moments of CO_2, CH_4, and N_2O

Following data filtering, the importance of very high flux events was determined to identify hot moments and their impact on yearly flux values. We defined hot moments as measurements with values greater than four standard deviations from the mean, as statistically 99.9% of the population should fall within four standard deviations of the mean. Yearly mean flux values were then calculated for only hot moments, the entire flux dataset, and the flux dataset with not moments removed to determine the impact of very high flux events on annual GHG emissions. The term "outlier" is often used to connote values requiring removal or transformation within a dataset to maintain statistical power and limit overinflated estimates from high leverage observations (Lintott & Mathews, 2018). However, systematic elimination or data transformation ignore or underweight important processes such as hot moments of GHG flux (Benhadi-Marín, 2018; Wiggins, 2000). Given our large and continuous dataset, we could also compare mean fluxes with and without hot moments (Benhadi-Marín, 2018) to better quantify the importance of hot moments. We further explored the importance of capturing hot moments by also recalculating mean N_2O and CH_4 flux after excluding fluxes greater than one, two, and three standard deviations from the mean.

A modified statistical jackknifing technique was used to explore the response of mean N_2O and CH_4 flux estimates to changes in sampling interval by repeatedly sampling the dataset at 1-, 2-, 7-, 14-, and 28-day intervals (Barton et al., 2015). As our flux measurements exhibited a standard normal distribution, the importance of sampling frequency was further explored by calculating the minimum number of random flux measurements (n) needed to accurately recalculate the observed mean N_2O and CH_4 flux values with a 95% confidence interval using equation 1:

$$n \geq \left(\frac{z^* \sigma}{MOE}\right)^2 \quad (1)$$

Where n is minimum sample size, z* is z-score, σ is the standard deviation of the dataset, and MOE is a chosen margin of error (MOE). Using a 95% confidence interval (z score = 1.96), we calculated the minimum number of samples needed for a margin of error of 10%, 25%, and 50% for both annual and total (three year) mean flux values of N_2O and CH_4. Minimum sample size calculations were performed in R with the package samplingbook 1.2.4 (Manitz et al. 2020).

3.3.4 Weekly soil measurements

A total of 53 weekly sets of soil samples (n = 10 per week) were collected from the 0-15 cm depth from April 2018 to May 2019. Soil samples were analyzed for gravimetric soil moisture by drying 10 g of field-fresh soil to a constant weight at 105 ˚C, and for soil pH in a slurry of 10 g of field-fresh soil in 10 mL of distilled deionized water (McLean, 1982). Nitrate (NO_3^-) plus nitrite (NO_2^-) and ammonium (NH_4^+) were measured after extraction of 15 g of field-fresh soil in 75 mL of 2M potassium chloride (KCl) solution (Hart, Stark, Davidson, & Firestone, 1994). Soil KCl extracts were analyzed colorimetrically using an AQ300 analyzer (Seal Instruments, Mequon, WI).

3.3.5 Soil sensor measurements

Two sets of soil sensors were installed from September 2018-July 2020 at depths of 10 cm, 30 cm, and 50 cm. Combination SO-110 Oxygen (O_2) and thermistor temperature sensors (Apogee Instruments, Logan, UT) and CS616 moisture sensors (Campbell Scientific, Logan, UT) were connected to CR1000 dataloggers (Campbell Scientific, Logan, UT) that stored data at 15 min intervals. A period of sensor removal occurred in May and June 2019 as multiple agricultural events, including tillage, planting, and discing prevented continuous installation. Sensors were also removed for 3 weeks in September-October 2019 for crop harvest and discing and for 2 weeks the following spring before planting, April to May 2020. Erroneous data corresponding to sensor malfunction were removed from the dataset, which include 0.6% (n = 295) of soil moisture measurements and 0.05% (n = 24) of soil O_2 and temperature measurements. Power loss also contributed to data loss, with a total of 58 days of missing data from agricultural activity or power loss during the sensor measurement period (n = 665 days).

3.3.6 Weekly soil gas samples

To explore the potential distribution of GHG production across the soil profile, two replicate soil gas samples (n = 2 per depth per week) for CO_2, CH_4, and N_2O were also taken in parallel with the soil sensors above at 10 cm, 30 cm, and 50 cm depths weekly during unflooded periods from September 2018 through November 2018, and April through December 2019. Instrument grade stainless steel 1/8” tubing (Restek, Bellefonte, PA) was installed in parallel to the soil sensors above, with approximately 15 cm of tubing installed with multiple sampling holes parallel to the soil surface. Sampling septa (Restek, Bellefonte, PA) were installed in 1/8” Swagelok unions (Swagelok Solon, OH) permanently connected to the stainless-steel tubing.

Septa were changed monthly. Two gas samples were collected with 30 ml BD syringes, discarding the first sample to clear the dead volume in the sampling line. Sampling lines were removed from the field in May and June 2019 for tillage, planting, and discing. The 30 ml gas samples were stored in over-pressurized 20 mL glass vials with thick septa (Geomicrobial Technologies, Oechelata, OK) until manual sample injection analysis on a Shimadzu GC-34 (Shimadzu Corp., Tokyo, Japan).

3.3.6 Statistical analyses

Differences in soil gas concentrations, O_2, moisture, mineral N, and pH across time periods were tested with one-way analysis of variance (ANOVA). Growing season time periods were classified as planting date to harvest date, preceded and followed by fallow periods. Unflooded periods were defined as soil moisture less than 50% at 10 cm depth. For CH_4 fluxes, anaerobic periods were defined as any period of time where daily 10 cm O_2 concentrations were equal to 0. Linear regressions were used to explore relationships between soil atmosphere GHG concentrations and net soil GHG fluxes (Figures S2-S4).

3.3.8 Wavelet coherence analysis

Wavelet coherence analysis was used to identify interactions between GHG fluxes and the soil variables measured (P. C. Liu, 1994; Wood, Detto, & Silver, 2013). Wavelet-coherence analysis measures the cross-correlation between two time series and allowed us to explore relationships between GHG fluxes and potential controls at daily, monthly, and annual timescales. Wavelet coherence is derived from two time series as a function of decomposed frequency (Wave.xy) and the wavelet power spectrum (Power.x, Power.y) of each individual time series (Rösch & Schmidbauer, 2018):

$$Coherence = \frac{|Wave.xy|^2}{Power.x \cdot Power.y} \quad (2)$$

A more detailed description of the approach and calculations can be found in Rösch & Schmidbauer (2018) and Wood et al., (2013). Missing data were replaced with zeroes to compute an unbiased estimator of the wavelet variance for gappy time series (Mondal & Percival, 2010; Wood et al., 2013). Statistical significance (*p*-value) was computed using 1000 Monte Carlo simulations. All wavelet decomposition and coherence calculations were conducted using the WaveletComp 1.1 package (Rösch & Schmidbauer, 2018) in R (RStudio, v.1.1.4633).

3.3.9 Upscaling calculations

We conducted a hypothetical upscaling exercise to estimate the potential impact of agricultural maize peatland emissions in the region. We multiplied our annual GWP values with areal values of 40,000 ha for agricultural maize with similar management practices on peatland soils in the Rindge soil series within the Sacramento-San Joaquin Delta, California, USA

(Deverel, Ingrum, & Leighton, 2016; Soil Survey Staff, 2020). Similar management throughout the region includes conventional maize agricultural practices and winter flooding of fallow maize fields to limit weed growth and provide habitat for migrating waterfowl (Central Valley Joint Venture, 2006; Pellerin et al., 2014).

3.4 Results

3.4.1 Soil CO_2, CH_4, and N_2O emissions

Annual soil GHG emissions averaged 9.20 ± 0.04 CO_2 kg m^{-2} y^{-1}, 4.08 ± 0.10 g N_2O m^{-2} y^{-1} and of 681 ± 157 CH_4 mg m^{-2} y^{-1} (Table 1, Table S1) representing mean annual area- and yield-scaled emissions GWP emissions of 46.7 Mg CO_2e ha^{-1} y^{-1} (range: 39.1-55.5 Mg CO_2e ha^{-1} y^{-1}) and 2.88 kg CO_2e kg dry $yield^{-1}$ y^{-1} (range: 2.41-3.42 kg CO_2e kg dry $yield^{-1}$ y^{-1}), respectively. For N_2O, annual fluxes amount to up to 41.5 ± 1.8 kg N_2O-N ha^{-1} y^{-1} and a mean flux over the three years of 26.0 ± 0.5 kg N_2O-N ha^{-1} y^{-1} or 26% of the GWP (Table 1). We found high intra- and interannual variability in CH_4 fluxes ranging from annual net consumption rates of -111.0 ± 5.0 mg CH_4 m^{-2} y^{-1} to net emissions of 2220.1 ± 519.7 mg CH_4 m^{-2} y^{-1} (Table 1). This corresponded to a maximum annual emission rate of 6.1 ± 1.4 kg CH_4-C ha^{-1} y^{-1}, or 2% of the annual GWP for this ecosystem. Soil respiration was less variable, with annual values ranging from 6.61 ± 0.07 kg CO_2 m^{-2} y^{-1} to 10.72 ± 0.09 kg CO_2 m^{-2} y^{-1} (Figure 1a, Table S1).

3.4.2 Quantifying hot moments of soil CO_2, CH_4, and N_2O emissions

We defined hot moments conservatively as individual flux measurements that were more than four standard deviations from the yearly mean (Table 1). Hot moment fluxes of N_2O represented only 0.64% to 1.50% of annual measurements but increased the mean flux rate by 38.5% to 76.3% (Table 1). For CH_4, hot moment fluxes were only 0.06% to 0.8% of yearly measurements but increased yearly mean fluxes by 132.1% to 486.4% in site years two and three. In site year one, hot moments of CH_4 consumption increased the net CH_4 sink by 249.2%. The substantial hot moment driven changes in CH_4 fluxes were largely due to the majority of CH_4 flux measurements recorded at or near zero (Figure 1b). Hot moments of CO_2 emissions had a significantly lower overall impact on mean CO_2 fluxes, representing only 0.5% of all fluxes (annual range 0.3-0.6%). This increased overall mean fluxes by 5% and annual mean CO_2 fluxes by 2.6 to 9.2% (Table S1).

3.4.3 Drivers of N_2O fluxes

The onset of winter flooding increased soil N_2O emissions exponentially, with daily average fluxes of up to 395.6 ± 87.6 mg N_2O m^{-2} d^{-1} ($p < 0.001$). Irrigation and fertilizer application during the growing season also significantly increased N_2O fluxes (Figure 2a, $p < 0.001$). We used arrays of soil moisture, temperature, and O_2 sensors and weekly soil gas and mineral nitrogen (N) measurements in combination with continuous surface flux measurements

to explore potential controls on GHG fluxes. Daily mean N_2O fluxes increased up to two orders of magnitude shortly after the onset of winter flooding concurrent with a rise in soil moisture and a corresponding reduction in soil O_2 concentrations across soil depths (Figure 2d, $p < 0.001$). Continued inundation led to a decline in soil NO_3^- concentrations (Figure 2b, $p < 0.001$) and a subsequent drop in N_2O fluxes (Figure 2a, $p < 0.001$). Soil gas concentrations were taken at 10 cm, 30 cm, and 50 cm depths during non-flooded periods from September 2018-December 2019. We found that daily mean N_2O fluxes were significantly correlated with soil N_2O concentrations across all depths ($R^2 = 0.45$-0.60, Figure S1), and likely contributed to net fluxes across the soil-atmosphere interface.

Wavelet coherence analysis suggested temporal patterns in soil moisture, soil temperature, and bulk soil O_2 concentrations across all depths were significantly related to patterns in net N_2O fluxes on a daily timescale (Figure S5, $p < 0.05$). Net N_2O fluxes showed significant coherence with soil O_2 concentrations across depths at the seasonal timescale of approximately 100 days, and soil moisture at the yearly scale of approximately 300 days (Figure S5, $p < 0.05$).

3.4.4 Drivers of CH_4 and CO_2 fluxes

Significant CH_4 fluxes were only observed 60 days into an extended period of anoxic conditions lasting a total of 124 days. This period of anoxic conditions was associated with complete soil saturation following winter flooding (Figure 3c) and corresponded to decreased soil O_2 concentrations across depths (Figure 3d). Short periods of elevated NH_4^+ concentrations observed during flooding were also associated with decreases in CH_4 production (Figure 3a and 3b). Shorter periods of sustained anoxic conditions in 2019-2020 (50 total days) did not produce hot moments of CH_4 fluxes. Wavelet coherence analysis of CH_4 fluxes suggested that soil moisture, soil temperature, and bulk soil O_2 concentrations drove patterns in net CH_4 fluxes at a daily time scale (Figure S5, $p < 0.05$). Only soil O_2 concentrations across soil depths had significant coherence with CH_4 fluxes on a weekly timescale (Figure S5, $p < 0.05$), with no significant coherence at longer timescales.

Seasonality explained the high intra-annual variation observed in CO_2 fluxes. Higher soil respiration rates (mean 50.5 ± 1.5 g CO_2 m^{-2} d^{-1}) occurred during the growing season and following harvest (July-September). Fluxes were significantly lower (6.8 ± 0.1 g CO_2 m^{-2} d^{-1}) when soils were saturated (December-March). There was significant coherence with moisture, temperature, and O_2 concentrations across depths at the daily scale (Figure S6, $p < 0.05$). At weekly and seasonal scales, temperature and O_2 concentrations displayed significant ($p < 0.05$) coherence with soil CO_2 fluxes.

We compared chamber fluxes with ecosystem respiration (R_{eco}) measurements conducted via eddy covariance in parallel at this field site (Camilo et al., 2016; Hemes et al., 2019). Similar values were observed for soil CO_2 chamber fluxes (9.20 ± 0.04 kg CO_2 m^{-2} y^{-1}) and R_{eco} eddy-

covariance measurements (9.70 ± 0.01 kg CO_2 m^{-2} y^{-1}) across the study period (Figure S6). Soil CH_4 chamber fluxes (1.2 ± 0.01 g CH_4 m^{-2} y^{-1}) were lower than the eddy-covariance CH_4 fluxes (2.2 ± 0.01 g CH_4 m^{-2} y^{-1}), although eddy covariance also captured similar hot moments of CH_4 emission (Figure S7).

3.4.5 Sampling frequency effects on N_2O and CH_4 flux estimates

Decreasing the measurement sampling interval led to significant under- or overestimates of total N_2O and CH_4 flux. Simulating a 28-day (once monthly) sampling interval underestimated total N_2O flux by a median of -13.0% (Range of 28-day N_2O subsets: -75.1% to +129.2%, Table S2) and CH_4 flux by a median of -17.4% (Range of 28-day CH_4 subsets: -88.6 to + 656%, Table S3). A weekly sampling interval underestimated the total N_2O flux by a median of -2.3% (Range of weekly subsets: -18.3% to +18.8%, Table S2) and total CH_4 flux by a median of +14.1% (Range of 7-day CH_4 subsets: -40.3% to 149% Table S3). A sampling interval of every other day under- or overestimated total N_2O fluxes by ±2.4% but overestimated CH_4 fluxes by +32.9% to +64.4% (Table S2 and 3).

We further explored the importance of missing potential hot moment fluxes by calculating the change in mean N_2O and CH_4 fluxes after removing observations greater than one, two, or three standard deviations from the overall mean flux. Removing all observations more than one standard deviation of the mean underestimated annual N_2O fluxes by 56.6%, while removing observations greater than two and three standard deviations underestimated N_2O fluxes by 42.7% and 34.5%, respectively. Missing N_2O fluxes greater than three standard deviations corresponded to an underestimation of annual N_2O emissions up to 14.3 ± 0.6 kg N-N_2O ha^{-1} yr^{-1}. For CH_4, removing observations greater than one standard deviation underestimated annual CH_4 fluxes by 79%, while removing observations greater than two and three standard deviations underestimated CH_4 fluxes by 69% and 63%, respectively.

Finally, we calculated the minimum number of randomized flux measurements needed to calculate annual and total (3-year) flux values for N_2O and CH_4 with a 95% confidence interval and margins of error of 10%, 25%, and 50% when the occurrence of hot moments are unknown (Table S4). For N_2O, an average of 8,342 (range: 2,700-8,342) individual flux measurements were needed to accurately calculate the annual mean flux within a 10% margin of error. This represents up to 35% (range: 11-35%) of the dataset. Increasing the margin of error to 25% and 50% reduced the number of measurements needed, with a range of 475 to 1,904 and 121 to 507 individual randomized measurements per year, respectively. When analyzing the total N_2O dataset, the minimum number of flux measurements needed was 6,401 with a 10% of margin error, decreasing to 1,108 and 281 for margins of error of 25% and 50%, respectively.

The minimum sample size needed for calculating annual and total mean CH_4 fluxes were greater than N_2O (Table S4). For annual CH_4 fluxes, the minimum sample size needed to recalculate the mean flux within a 10% margin of error was at least 17,133 (range: 17,133-

22,525). Increasing the margin of error to 25% and 50% reduced the minimum annual sample sizes needed to at least 7,562 (range: 7,562-18,284) and 2,525 (range: 2,525-10,770), respectively. The minimum number of flux measurements needed for the total CH_4 dataset was also higher than N_2O with 68,137, 54,419, and 31,656 for margins of error of 10%, 25%, and 50%, respectively.

3.4.5 Upscaling greenhouse gas emissions

We conducted an upscaling exercise to provide a first approximation of the potential impact of peatland maize agriculture on regional GHG emissions. Using the three years of field data, we upscaled these flux measurements using the total regional land area with similar soil series and management practices. We calculated a mean annual GWP of 1.86 Tg CO_2e y^{-1} (range: 1.58-2.21 Tg CO_2e y^{-1}) for agricultural peatlands in the region, with N_2O emissions representing 0.48 Tg CO_2e y^{-1} (range: 0.28-0.77 Tg CO_2e y^{-1}). Assuming the field estimates measured here are representative of local management practices, N_2O fluxes alone could represent 26% (annual range: 18-33%) of agricultural maize peatland CO_2e emissions in this region, a significantly higher percentage than previous estimates (Deverel, Jacobs, Lucero, Dore, & Kelsey, 2017; Hemes et al., 2019). Soil types with similar organic matter content represent over 40,000 ha of agricultural peatlands in the Sacramento-San Joaquin Delta region (Deverel et al., 2016; Soil Survey Staff, 2020) and these soils are dominated by maize production. They are often flooded in the winter for waterfowl habitat (Delta Protection Commission, 2012; Pellerin et al., 2014).

3.5 Discussion

3.5.1 Annual fluxes and hot moments of N_2O emissions

The agricultural peatland soils in this study were extreme N_2O emitters, with mean rates that were 4-27 times greater than other non-peat cropland N_2O emissions (Ferrari Machado et al., 2020; IPCC, 2013; Jin et al., 2014; Johnson, Weyers, Archer, & Barbour, 2012). It is notable that these values for both peatland and non-peatland ecosystems were largely derived from non-continuous data that may not capture all N_2O emission hot moments. The three year average N_2O emissions were greater than the highest IPCC estimates for temperate organic cropland soils, and the peak annual N_2O emissions from this study were five times greater than the average values of 8 kg N_2O-N ha^{-1} y^{-1} (uncertainty range: 2-24 kg N_2O-N ha^{-1} y^{-1}, IPCC, 2019). Estimated mean annual N_2O emissions of 16.8 ± 14.8 kg N_2O-N ha^{-1} y^{-1} have been reported for other drained peatlands with data derived from bulk densities (H. Liu, Wrage-Mönnig, & Lennartz, 2020). Average N_2O emissions observed in this study were similar to or higher than studies of N_2O emissions from agricultural peatlands in the Sacramento-Delta, which ranged from 6.6 ± 3.8 using model estimates (Deverel et al., 2017) to 24 ± 13 kg N_2O-N ha^{-1} y^{-1} using shorter-term periodic manual static chamber measurements (Teh et al., 2011).

Surprisingly winter flooding, not fertilization, was the dominant driver of N_2O emissions. Peak N_2O emissions were observed shortly following winter flooding. The high NO_3^- measured shortly after flooding likely accumulated under oxic, well-drained soil conditions as a result of N mineralization following crop harvest (Kirk et al., 2015), and may have been supplemented by iron coupled anaerobic ammonium oxidation in these iron and C-rich soils (Anthony & Silver, 2020; Golovchenko, Tikhonova, & Zvyagintsev, 2007; Martikainen, Nykänen, Crill, & Silvola, 1993; Yang & Liptzin, 2015; Yang, Weber, & Silver, 2012). Urea-ammonium-nitrate (UAN) fertilizer was applied once per year during planting. This inorganic N fertilizer application also contributed to a short-term increase in N_2O emissions, although this was not the dominant source of annual N_2O emissions.

Denitrification was likely the main pathway of N_2O during hot moments of N_2O flux given elevated NO_3^- concentrations observed immediately prior to peak emissions, as well as the observed increases in soil moisture and decreases in soil O_2 and NO_3^- concentrations during the N_2O hot moments. The NO_3^- was likely consumed during denitrification, with significant amounts of N_2O released as a byproduct of incomplete denitrification in these N-rich soils (Firestone & Davidson, 1989). The strong correlations observed between daily mean N_2O fluxes and soil atmosphere N_2O concentrations also suggest that significant N_2O production was occurring at depth and thus production throughout the profile likely contributed to the large fluxes observed.

3.5.2 Fluxes of CH_4 and CO_2

Prolonged anaerobic conditions coupled with soil temperatures greater than 10º C appeared to drive hot moments of CH_4 fluxes in these systems. Short periods of elevated NH_4^+ concentrations during flooded periods could have limited methanogenesis (Chen, Cheng, & Creamer, 2008) or temporarily shifted the methanogenic pathway (Fotidis, Karakashev, Kotsopoulos, Martzopoulos, & Angelidaki, 2013) and likely contributed to the considerable variability observed. Expectedly, patterns in soil CO_2 fluxes were related to temperature and O_2 concentrations at weekly and seasonal scales. Soil temperature and O_2 availability are important controls on aerobic soil respiration (Kasimir-Klemedtsson et al., 1997), particularly in ecosystems such as drained agricultural peatlands where substrate availability is not likely to be limiting to heterotrophs and nutrient availability to autotrophs is high.

3.5.3 The role of hot moments in N_2O and CH_4 fluxes

The large continuous data set allowed us to explore the importance of hot moments of N_2O and CH_4 emission in total ecosystem GHG budgets. While hot moments represented only 0.63-1.50% and 0.06-0.76% of annual N_2O and CH_4 flux measurements, respectively, they contributed up to 76% of total N_2O emissions and 486% of total CH_4 emissions. This corresponded to N_2O hot moment emissions alone contributing up to 18% of the annual GWP of

these agricultural peatlands. This highlights that missing hot moments may lead to significant underestimates of total ecosystem GHG budgets.

We also explored the effects of sampling interval on N_2O and CH_4 flux quantification. Our results further highlighted the necessity of continuous measurements to accurately estimate total ecosystem N_2O and CH_4 fluxes. Even weekly sampling intervals may underestimate annual N_2O fluxes by up to 20%, a significant fraction of total GWP, even from these high emitting agricultural peatlands. While continuous automated chamber or eddy covariance measurements are ideal to capture hot moments of emissions, long-term continuous measurements are still cost prohibitive in many locations and ecosystems. If hot moments are predictable and well defined, daily flux measurements are likely effective in appropriately quantifying hot moments of N_2O emissions (Ferrari Machado, Wagner-Riddle, MacTavish, Voroney, & Bruulsema, 2019; Reeves, Wang, Salter, & Halpin, 2016). However if the timing and controls on hot moments are unknown or sporadic, less frequent sampling may significantly underestimate N_2O emissions (Grace et al., 2020). Our results suggest that roughly 8,000 randomized individual chamber flux measurements would be needed to accurately estimate annual N_2O budgets from these agricultural peatlands with a 95% confidence interval and 10% margin of error, assuming the drivers of hot moments were not well understood. Approximately 500 individual measurements would yield a 50% margin of error. Given the more sporadic nature of CH_4 hot moments, our results suggest that it is even more difficult to accurately estimate CH_4 fluxes with periodic sampling in these ecosystems. Analyses found that at least 17,000 and 2,500 individual flux measurements would be needed to estimate annual CH_4 budgets within a 10% and 50% margin of error, respectively.

3.5.3 Greenhouse gas budgets and upscaling

The agricultural maize peatland soil studied here was a much larger source of soil GHG emissions than other maize agroecosystems. While agricultural peat soils are highly productive, average annual GHG emissions were 3.6-33.3 times greater on an area-scaled basis and 3-15.6 times greater on a yield-scaled basis relative to other agricultural maize emissions estimates (Table S5, Chai et al., 2019; Jin et al., 2014; Johnson, Weyers, Archer, & Barbour, 2012; Linquist et al., 2012).

We conducted an upscaling exercise as a first approximation of the potential impacts of maize peatland fluxes on regional GHG budgets. Our estimates suggested that maize agriculture on similar peat soils in the region could emit an average of 1.86 Tg CO_2e y^{-1}. Nitrous oxide emissions alone accounted for approximately 26% of the total. This value is significantly higher than previous estimates for the region (Deverel et al., 2017; Hemes et al., 2019) and highlights the importance of including high frequency N_2O measurements to capture hot moments in N_2O fluxes, the disproportionate impact N_2O emissions have on agricultural peatland GHG budgets, and that these agricultural peatlands are significant N_2O sources. We also found that irrigation timing and duration, not fertilization, was the predominant driver of N_2O and CH_4 emissions and a significant source of the total GHG budget. Determining management strategies that reduce

soil N_2O and CH_4 emissions, particularly changes in flood irrigation timing and duration, could have a disproportionate impact on reducing total agricultural peatland GHG emissions (Hemes et al., 2019; Knox et al., 2015; McNicol et al., 2017; Windham-Myers et al., 2018).

3.6 Conclusion

This study presents one of the largest, longest, and most comprehensive soil flux datasets from agricultural peatlands to date. Our results provide evidence that these systems are a significant contributor to agricultural GHG emissions. The continuous dataset allowed us to explore the importance of hot moments of soil CH_4 and N_2O emissions driven by land management changes in soil moisture, soil O_2, and soil N availability. We found that irrigation timing and duration, not fertilization, was the predominant control on soil N_2O and CH_4 emissions from these agricultural peatlands. We also found that N_2O and CH_4 alone contributed up to 37% of the annual GWP of this system. This suggests that land management strategies that limit flooding frequency and duration may significantly reduce total agricultural peatland GHG emissions. We further demonstrate that continuous automated chamber measurements of soil GHG emissions capture hot moments of N_2O and CH_4 production and intensive sampling, particularly during hot moments of emission, are needed to accurately quantify GHG budgets. This is particularly important in high emitting ecosystems such as agricultural peatlands to ensure effective and targeted land management strategies that maximally limit net ecosystem GHG emissions.

3.7 Acknowledgements

We appreciate assistance from Heather Dang, Tibisay Peréz, and numerous other members of both the Silver Lab and the Berkeley Biometeorology Lab at University of California, Berkeley. We thank Christine O'Connell for the initial code development for data filtering. This work was supported by a Contract by the California Department of Water Resources (award 4600011240). We thank the California Department of Water Resources and the Metropolitan Water District of Southern California for research site access. T. L. Anthony was supported by the California Sea Grant Delta Science Fellowship. This material is based upon work supported by the Delta Stewardship Council Delta Science Program under Grant No. 5298 and California Sea Grant College Program Project R/SF-89. The contents of this material do not necessarily reflect the views and policies of the Delta Stewardship Council or California Sea Grant, nor does mention of trade names or commercial products constitute endorsement or recommendation for use. McIntire Stennis grant CA-B-ECO-7673-MS to W. L. Silver partially supported this work. W. L. Silver was also supported by funds from Breakthrough Strategies & Solutions, and the V. Kann Rasmussen, Oak Creek, Jewish Community, Northern Trust, and Trisons Foundations. The authors declare no conflict of interests. The data that support the findings of this study are available from the corresponding author upon reasonable request.

3.8 References

Anthony, T. L., & Silver, W. L. (2020). Mineralogical associations with soil carbon in managed wetland soils. *Global Change Biology*, (March), 1–13. https://doi.org/10.1111/gcb.15309

Baldocchi, D. (2014). Measuring fluxes of trace gases and energy between ecosystems and the atmosphere - the state and future of the eddy covariance method. *Global Change Biology*, *20*(12), 3600–3609. https://doi.org/10.1111/gcb.12649

Barton, L., Wolf, B., Rowlings, D., Scheer, C., Kiese, R., Grace, P., … Butterbach-Bahl, K. (2015). Sampling frequency affects estimates of annual nitrous oxide fluxes. *Scientific Reports*, *5*, 1–9. https://doi.org/10.1038/srep15912

Benhadi-Marín, J. (2018). A conceptual framework to deal with outliers in ecology. *Biodiversity and Conservation*, *27*(12), 3295–3300. https://doi.org/10.1007/s10531-018-1602-2

Bernhardt, E. S., Blaszczak, J. R., Ficken, C. D., Fork, M. L., Kaiser, K. E., & Seybold, E. C. (2017). Control Points in Ecosystems: Moving Beyond the Hot Spot Hot Moment Concept. *Ecosystems*, *20*(4), 665–682. https://doi.org/10.1007/s10021-016-0103-y

Bonn, A., Reed, M. S., Evans, C. D., Joosten, H., Bain, C., Farmer, J., … Birnie, D. (2014). Investing in nature: Developing ecosystem service markets for peatland restoration. *Ecosystem Services*, *9*, 54–65. https://doi.org/10.1016/j.ecoser.2014.06.011

Butterbach-Bahl, K., Baggs, E. M., Dannenmann, M., Kiese, R., & Zechmeister-Boltenstern, S. (2013). Nitrous oxide emissions from soils: how well do we understand the processes and their controls? *Philosophical Transactions of the Royal Society of London. Series B, Biological Sciences*, *368*(1621), 20130122. https://doi.org/10.1098/rstb.2013.0122

Camilo, R.-S., Szutu, D., Baldocchi, D., & Hemes, K. (2016). AmeriFlux US-Bi2 Bouldin Island corn. United States. https://doi.org/10.17190/AMF/1419513

Carlson, K. M., Gerber, J. S., Mueller, N. D., Herrero, M., MacDonald, G. K., Brauman, K. A., … West, P. C. (2017). Greenhouse gas emissions intensity of global croplands. *Nature Climate Change*, *7*(1), 63–68. https://doi.org/10.1038/nclimate3158

Central Valley Joint Venture. (2006). Central Valley Joint Venture Implementation Plan 2006, 1–261.

Chai, R., Ye, X., Ma, C., Wang, Q., Tu, R., Zhang, L., & Gao, H. (2019). Greenhouse gas emissions from synthetic nitrogen manufacture and fertilization for main upland crops in China. *Carbon Balance and Management*, *14*(1), 1–10. https://doi.org/10.1186/s13021-019-0133-9

Chamberlain, S. D., Hemes, K. S., Eichelmann, E., Szutu, D. J., Verfaillie, J. G., & Baldocchi, D. D. (2019). Effect of Drought-Induced Salinization on Wetland Methane Emissions, Gross Ecosystem Productivity, and Their Interactions. *Ecosystems*. https://doi.org/10.1007/s10021-019-00430-5

Chen, Y., Cheng, J. J., & Creamer, K. S. (2008). Inhibition of anaerobic digestion process: A review. *Bioresource Technology*, *99*(10), 4044–4064. https://doi.org/10.1016/j.biortech.2007.01.057

Courtois, E. A., Stahl, C., Burban, B., Van den Berge, J., Berveiller, D., Bréchet, L., … Janssens, I. A. (2018). Automatic high-frequency measurements of full soil greenhouse gas fluxes in a tropical forest. *Biogeosciences Discussions*, 1–21. https://doi.org/10.5194/bg-2018-341

Delta Protection Commission. (2012). Economic Sustainability Plan for the Sacramento-San Joaquin Delta. Retrieved from http://www.delta.ca.gov/res/docs/ESP/ESP_P2_FINAL.pdf

Deverel, S. J., Ingrum, T., & Leighton, D. (2016). Present-day oxidative subsidence of organic soils and mitigation in the Sacramento-San Joaquin Delta, California, USA. *Hydrogeology Journal*, *24*(3), 569–586. https://doi.org/10.1007/s10040-016-1391-1

Deverel, S. J., Jacobs, P., Lucero, C., Dore, S., & Kelsey, T. R. (2017). Implications for Greenhouse Gas Emission reductions and economics of a changing agricultural mosaic in the Sacramento - San Joaquin Delta. *San Francisco Estuary and Watershed Science*, *15*(3). https://doi.org/10.15447/sfews.2017v15iss3art2

Ferrari Machado, P. V., Neufeld, K., Brown, S. E., Voroney, P. R., Bruulsema, T. W., & Wagner-Riddle, C. (2020). High temporal resolution nitrous oxide fluxes from corn (Zea mays L.) in response to the combined use of nitrification and urease inhibitors. *Agriculture, Ecosystems and Environment*, *300*(May), 106996. https://doi.org/10.1016/j.agee.2020.106996

Ferrari Machado, P. V., Wagner-Riddle, C., MacTavish, R., Voroney, P. R., & Bruulsema, T. W. (2019). Diurnal Variation and Sampling Frequency Effects on Nitrous Oxide Emissions Following Nitrogen Fertilization and Spring-Thaw Events. *Soil Science Society of America Journal*, *83*(3), 743–750. https://doi.org/10.2136/sssaj2018.10.0365

Firestone, M. K., & Davidson, E. A. (1989). Microbiologial Basis of NO and N20 production and consumption in soil. *Exchange of Trace Gases between Terrestrial Ecosystems and the Atmosphere*, (January 1989), 7–21.

Fotidis, I. A., Karakashev, D., Kotsopoulos, T. A., Martzopoulos, G. G., & Angelidaki, I. (2013). Effect of ammonium and acetate on methanogenic pathway and methanogenic community composition. *FEMS Microbiology Ecology*, *83*(1), 38–48. https://doi.org/10.1111/j.1574-6941.2012.01456.x

Frolking, S., Talbot, J., Jones, M. C., Treat, C. C., Kauffman, J. B., Tuittila, E. S., & Roulet, N. (2011). Peatlands in the Earth's 21st century climate system. *Environmental Reviews*, *19*(1), 371–396. https://doi.org/10.1139/a11-014

Golovchenko, A. V., Tikhonova, E. Y., & Zvyagintsev, D. G. (2007). Abundance, biomass, structure, and activity of the microbial complexes of minerotrophic and ombrotrophic peatlands. *Microbiology*, *76*(5), 630–637. https://doi.org/10.1134/S0026261707050177

Grace, P. R., van der Weerden, T. J., Rowlings, D. W., Scheer, C., Brunk, C., Kiese, R., … Skiba, U. M. (2020). Global Research Alliance N2O chamber methodology guidelines: Considerations for automated flux measurement. *Journal of Environmental Quality*, *49*(5), 1126–1140. https://doi.org/10.1002/jeq2.20124

Groffman, P. M., Butterbach-Bahl, K., Fulweiler, R. W., Gold, A. J., Morse, J. L., Stander, E. K., … Vidon, P. (2009). Challenges to incorporating spatially and temporally explicit phenomena (hotspots and hot moments) in denitrification models. *Biogeochemistry*, *93*(1–2), 49–77. https://doi.org/10.1007/s10533-008-9277-5

Günther, A., Barthelmes, A., Huth, V., Joosten, H., Jurasinski, G., Koebsch, F., & Couwenberg, J. (2020). Prompt rewetting of drained peatlands reduces climate warming despite methane emissions. *Nature Communications*, *11*(1), 1–5. https://doi.org/10.1038/s41467-020-15499-z

Hart, S. C., Stark, J. M., Davidson, E. A., & Firestone, M. K. (1994). Nitrogen Mineralization, Immobilization, and Nitrification. In R. W. Weaver, J. S. Angle, & P. S. Bottomley (Eds.), *Methods of Soil Analysis, Part 2. Microbial and Biochemical Properties* (pp. 985–1018). Madison, WI: Soil Science Society of America.

Hatala, J. A., Detto, M., Sonnentag, O., Deverel, S. J., Verfaillie, J., & Baldocchi, D. D. (2012). Greenhouse gas (CO2, CH4, H2O) fluxes from drained and flooded agricultural peatlands in the Sacramento-San Joaquin Delta. *Agriculture, Ecosystems and Environment*, *150*, 1–18. https://doi.org/10.1016/j.agee.2012.01.009

Hemes, K. S., Chamberlain, S. D., Eichelmann, E., Anthony, T., Valach, A., Kasak, K., … Baldocchi, D. D. (2019). Assessing the carbon and climate benefit of restoring degraded agricultural peat soils to managed wetlands. *Agricultural and Forest Meteorology*, *268*, 202–214. https://doi.org/10.1016/j.agrformet.2019.01.017

IPCC. (2019). N2O Emissions From Managed Soils, and CO2 Emissions From Lime and Urea Application. *2019 Refinement to the 2006 IPCC Guidelines for National Greenhouse Gas Inventories*, 1–48.

IPCC, 2014. (2013). 2013 Supplement to the 2006 IPCC Guidelines for National Greenhouse Gas Inventories: Wetlands, Hiraishi, T., Krug, T., Tanabe, K., Srivastava, N., Baasansuren, J., Fukuda, M. and Troxler, T.G. (eds).

Jin, V. L., Baker, J. M., Johnson, J. M. F., Karlen, D. L., Lehman, R. M., Osborne, S. L., … Wienhold, B. J. (2014). Soil Greenhouse Gas Emissions in Response to Corn Stover Removal and Tillage Management Across the US Corn Belt. *Bioenergy Research*, *7*(2), 517–527. https://doi.org/10.1007/s12155-014-9421-0

Johnson, J. M. F., Weyers, S. L., Archer, D. W., & Barbour, N. W. (2012). Nitrous Oxide, Methane Emission, and Yield-Scaled Emission from Organically and Conventionally Managed Systems. *Soil Science Society of America Journal*, *76*(4), 1347–1357. https://doi.org/10.2136/sssaj2012.0017

Kasimir-Klemedtsson, Å., Klemedtsson, L., Berglund, K., Martikainen, P., Silvola, J., & Oenema, O. (1997). Greenhouse gas emissions from farmed organic soils: A review. *Soil Use and Management*, *13*(4 SUPPL.), 245–250. https://doi.org/10.1111/j.1475-2743.1997.tb00595.x

Kirk, E. R., Van Kessel, C., Horwath, W. R., & Linquist, B. A. (2015). Estimating annual soil carbon loss in agricultural peatland soils using a nitrogen budget approach. *PLoS ONE*, *10*(3), 1–18. https://doi.org/10.1371/journal.pone.0121432

Knox, S. H., Sturtevant, C., Matthes, J. H., Koteen, L., Verfaillie, J., & Baldocchi, D. (2015). Agricultural peatland restoration: Effects of land-use change on greenhouse gas (CO2 and CH4) fluxes in the Sacramento-San Joaquin Delta. *Global Change Biology*, *21*(2), 750–765. https://doi.org/10.1111/gcb.12745

Krichels, A. H., & Yang, W. H. (2019). Dynamic Controls on Field-Scale Soil Nitrous Oxide Hot Spots and Hot Moments Across a Microtopographic Gradient. *Journal of Geophysical Research: Biogeosciences*, *124*(11), 3618–3634. https://doi.org/10.1029/2019JG005224

Leifeld, J., & Menichetti, L. (2018). The underappreciated potential of peatlands in global climate change mitigation strategies. *Nature Communications*, *9*. https://doi.org/10.1038/s41467-018-03406-6

Leinfelder-Miles, M. (2019). *2019 UCCE Field Corn Variety Trial Results*.

Levy, P. E., Cowan, N., van Oijen, M., Famulari, D., Drewer, J., & Skiba, U. (2017). Estimation of cumulative fluxes of nitrous oxide: uncertainty in temporal upscaling and emission factors. *European Journal of Soil Science*, *68*(4), 400–411. https://doi.org/10.1111/ejss.12432

Linquist, B., Van Groenigen, K. J., Adviento-Borbe, M. A., Pittelkow, C., & Van Kessel, C. (2012). An agronomic assessment of greenhouse gas emissions from major cereal crops. *Global Change Biology*, *18*(1), 194–209. https://doi.org/10.1111/j.1365-2486.2011.02502.x

Lintott, P. R., & Mathews, F. (2018). Basic mathematical errors may make ecological assessments unreliable. *Biodiversity and Conservation*. Springer Netherlands. https://doi.org/10.1007/s10531-017-1418-5

Liu, H., Wrage-Mönnig, N., & Lennartz, B. (2020). Rewetting strategies to reduce nitrous oxide emissions from European peatlands. *Communications Earth & Environment*, *1*(1), 17. https://doi.org/10.1038/s43247-020-00017-2

Liu, H., Zak, D., Rezanezhad, F., & Lennartz, B. (2019). Soil degradation determines release of nitrous oxide and dissolved organic carbon from peatlands. *Environmental Research Letters*, *14*(9), 094009. https://doi.org/10.1088/1748-9326/ab3947

Liu, P. C. (1994). Wavelet Spectrum Analysis and Ocean Wind Waves. In E. Foufoula-Georgiou & P. B. T.-W. A. and I. A. Kumar (Eds.), *Wavelets in Geophysics* (Vol. 4, pp. 151–166). Academic Press. https://doi.org/https://doi.org/10.1016/B978-0-08-052087-2.50012-8

Maljanen, M., Sigurdsson, B. D., Guömundsson, J., Öskarsson, H., Huttunen, J. T., & Martikainen, P. J. (2010). Greenhouse gas balances of managed peatlands in the

Nordic countries present knowledge and gaps. *Biogeosciences*, *7*(9), 2711–2738. https://doi.org/10.5194/bg-7-2711-2010

Martikainen, P. J., Nykänen, H., Crill, P., & Silvola, J. (1993). Effect of a lowered water table on nitrous oxide fluxes from northern peatlands. *Nature*, *366*(6450), 51–53. https://doi.org/10.1038/366051a0

McClain, M. E., Boyer, E. W., Dent, C. L., Gergel, S. E., Grimm, N. B., Groffman, P. M., … Pinay, G. (2003). Biogeochemical Hot Spots and Hot Moments at the Interface of Terrestrial and Aquatic Ecosystems. *Ecosystems*, *6*(4), 301–312. https://doi.org/10.1007/s10021-003-0161-9

McLean, E. O. (1982). Soil pH and Lime Requirement. In *Page, A.L., Ed., Methods of Soil Analysis. Part 2. Chemical and Microbiological Properties, American Society of Agronomy, Soil Science Society of America, Madison,* (pp. 199–224).

McNicol, G., Sturtevant, C. S., Knox, S. H., Dronova, I., Baldocchi, D. D., & Silver, W. L. (2017). Effects of seasonality, transport pathway, and spatial structure on greenhouse gas fluxes in a restored wetland. *Global Change Biology*, *23*(7), 2768–2782. https://doi.org/10.1111/gcb.13580

Molodovskaya, M., Singurindy, O., Richards, B. K., Warland, J., Johnson, M. S., & Steenhuis, T. S. (2012). Temporal Variability of Nitrous Oxide from Fertilized Croplands: Hot Moment Analysis. *Soil Science Society of America Journal*, *76*(5), 1728. https://doi.org/10.2136/sssaj2012.0039

Mondal, D., & Percival, D. B. (2010). Wavelet variance analysis for gappy time series. *Annals of the Institute of Statistical Mathematics*, *62*(5), 943–966. https://doi.org/10.1007/s10463-008-0195-z

Myhre, G., Shindell, D., Bréon, F.-M., Collins, W., Fuglestvedt, J., Huang, J., … Zhang, H. (2013). Anthropogenic and Natural Radiative Forcing. *Climate Change 2013: The Physical Science Basis. Contribution of Working Group I to the Fifth Assessment Report of the Intergovernmental Panel on Climate Change*, 659–740. https://doi.org/10.1017/ CBO9781107415324.018

O'Connell, C. S., Ruan, L., & Silver, W. L. (2018). Drought drives rapid shifts in tropical rainforest soil biogeochemistry and greenhouse gas emissions. *Nature Communications*, *9*(1), 1348. https://doi.org/10.1038/s41467-018-03352-3

Oertel, C., Matschullat, J., Zurba, K., Zimmermann, F., & Erasmi, S. (2016). Greenhouse gas emissions from soils - A review. *Chemie Der Erde - Geochemistry*, *76*(3), 327–352. https://doi.org/10.1016/j.chemer.2016.04.002

Oikawa, P. Y., Jenerette, G. D., Knox, S. H., Sturtevant, C., Verfaillie, J., Dronova, I., … Baldocchi, D. D. (2017). Evaluation of a hierarchy of models reveals importance of substrate limitation for predicting carbon dioxide and methane exchange in restored wetlands. *Journal of Geophysical Research: Biogeosciences*, *122*(1), 145–167. https://doi.org/10.1002/2016JG003438

Oktarita, S., Hergoualc'H, K., Anwar, S., & Verchot, L. V. (2017). Substantial N2O emissions from peat decomposition and N fertilization in an oil palm plantation exacerbated by hotspots. *Environmental Research Letters*, *12*(10). https://doi.org/10.1088/1748-9326/aa80f1

Pärn, J., Verhoeven, J. T. A., Butterbach-Bahl, K., Dise, N. B., Ullah, S., Aasa, A., … Mander, Ü. (2018). Nitrogen-rich organic soils under warm well-drained conditions are global nitrous oxide emission hotspots. *Nature Communications*, *9*(1), 1–8. https://doi.org/10.1038/s41467-018-03540-1

Pellerin, B., Anderson, F. E., & Bergamaschi, B. (2014). *Assessing the role of winter flooding on baseline greenhouse gas fluxes from corn fields in the Sacramento-San Joaquin Bay Delta*. *California Energy Commission*.

Petrescu, A. M. R., Lohila, A., Tuovinen, J.-P., Baldocchi, D. D., Desai, A. R., Roulet, N. T., … Cescatti, A. (2015). The uncertain climate footprint of wetlands under human pressure. *Proceedings of the National Academy of Sciences of the United States of America*, *112*(15), 4594–4599. https://doi.org/10.1073/pnas.1416267112

Reeves, S., Wang, W., Salter, B., & Halpin, N. (2016). Quantifying nitrous oxide emissions from sugarcane cropping systems: Optimum sampling time and frequency. *Atmospheric Environment*, *136*, 123–133. https://doi.org/10.1016/j.atmosenv.2016.04.008

Rochette, P., & Eriksen-Hamel, N. S. (2008). Chamber Measurements of Soil Nitrous Oxide Flux: Are Absolute Values Reliable? *Soil Science Society of America Journal*, *72*(2), 331–342. https://doi.org/10.2136/sssaj2007.0215

Rösch, A., & Schmidbauer, H. (2018). WaveletComp: Computational Wavelet Analysis. R package version 1.1., 1–38. Retrieved from http://www.hs-stat.com/projects/WaveletComp/WaveletComp_guided_tour.pdf%0Ahttps://cran.r-project.org/package=WaveletComp

Savage, K., Phillips, R., & Davidson, E. (2014). High temporal frequency measurements of greenhouse gas emissions from soils. *Biogeosciences*, *11*(10), 2709–2720. https://doi.org/10.5194/bg-11-2709-2014

Sihi, D., Davidson, E. A., Savage, K. E., & Liang, D. (2020). Simultaneous numerical representation of soil microsite production and consumption of carbon dioxide, methane, and nitrous oxide using probability distribution functions. *Global Change Biology*, *26*(1), 200–218. https://doi.org/10.1111/gcb.14855

Soil Survey Staff. (2020). Natural Resources Conservation Service, United States Department of Agriculture. Official Soil Series Descriptions. Available online. Accessed [June/08/2020].

Sturtevant, C., Ruddell, B. L., Knox, S. H., Verfaillie, J., Matthes, J. H., Oikawa, P. Y., & Baldocchi, D. (2016). Identifying scale-emergent, nonlinear, asynchronous processes of wetland methane exchange. *Journal of Geophysical Research: Biogeosciences*, *121*(1), 188–204. https://doi.org/10.1002/2015JG003054

Teh, Y. A., Silver, W. L., Sonnentag, O., Detto, M., Kelly, M., & Baldocchi, D. D. (2011). Large Greenhouse Gas Emissions from a Temperate Peatland Pasture. *Ecosystems*, *14*(2), 311–325. https://doi.org/10.1007/s10021-011-9411-4

Tiemeyer, B., Albiac Borraz, E., Augustin, J., Bechtold, M., Beetz, S., Beyer, C., … Zeitz, J. (2016). High emissions of greenhouse gases from grasslands on peat and other organic soils. *Global Change Biology*, *22*(12), 4134–4149. https://doi.org/10.1111/gcb.13303

Veber, G., Kull, A., Villa, J. A., Maddison, M., Paal, J., Oja, T., … Mander, Ü. (2017). Greenhouse gas emissions in natural and managed peatlands of America: Case studies along a latitudinal gradient. *Ecological Engineering*. https://doi.org/10.1016/j.ecoleng.2017.06.068

Verhoeven, J. T. A., & Setter, T. L. (2010). Agricultural use of wetlands: Opportunities and limitations. *Annals of Botany*, *105*(1), 155–163. https://doi.org/10.1093/aob/mcp172

Wiggins, B. C. (2000). Detecting and Dealing with Outliers in Univariate and Multivariate Contexts. *Annual Meeting of the Mid-South Educational Research Association*.

Windham-Myers, L., Bergamaschi, B., Anderson, F., Knox, S., Miller, R., & Fujii, R. (2018). Potential for negative emissions of greenhouse gases (CO2, CH4 and N2O) through coastal peatland re-establishment: Novel insights from high frequency flux data at meter and kilometer scales. *Environmental Research Letters*, *13*(4). https://doi.org/10.1088/1748-9326/aaae74

Wood, T. E., Detto, M., & Silver, W. L. (2013). Sensitivity of soil respiration to variability in soil moisture and temperature in a humid tropical forest. *PLoS ONE*, *8*(12). https://doi.org/10.1371/journal.pone.0080965

Yang, W. H., & Liptzin, D. (2015). High potential for iron reduction in upland soils. *Ecology*, *96*(7), 2015–2020. https://doi.org/10.1890/14-2097.1

Yang, W. H., Weber, K. A., & Silver, W. L. (2012). Nitrogen loss from soil through anaerobic ammonium oxidation coupled to iron reduction. https://doi.org/10.1038/ngeo1530

3.9 Tables

Table 1. Mean (± standard error) annual N_2O and CH_4 fluxes by site year (July 1 to June 30), number of measurements, number of outlier measurements, outlier mean (± standard error) N_2O and CH_4 fluxes, mean fluxes (± standard error) without outliers included, % of the outlier contribution to total mean flux, and N_2O and CH_4 % of ecosystem GWP. Outliers were calculated separately for each year and in aggregate for the total dataset (All years).

Site Year	Mean ($g\ N_2O\ m^{-2}\ y^{-1}$)	Flux (n)	Hot moment flux (n)	Hot moment mean ($mg\ N_2O\ m^{-2}\ d^{-1}$)	Mean no hot moments ($g\ N_2O\ m^{-2}\ y^{-1}$)	Hot moment % change in mean flux	N_2O % GWP
1 (2017-2018)	3.52 ± 0.11	22,247	294	321.9 ± 8.0	2.00 ± 0.06	+76.3%	26.3%
2 (2018-2019)	6.52 ± 0.25	23,196	147	896.4 ± 65.5	4.44 ± 0.10	+46.0%	35.0%
3 (2019-2020)	2.35 ± 0.04	24,934	374	123.8 ± 2.0	1.69 ± 0.01	+38.5%	15.5%
All years	4.08 ± 0.10	70,377	468	535.5 ± 23.9	2.80 ± 0.04	+45.6%	26.0%

Site Year	Mean ($mg\ CH_4\ m^{-2}\ y^{-1}$)	Flux (n)	Hot moment flux (n)	Hot moment mean ($mg\ CH_4\ m^{-2}\ d^{-1}$)	Mean no hot moments ($mg\ CH_4\ m^{-2}\ y^{-1}$)	Hot moment % change in mean flux	CH_4 % GWP
1 (2017-2018)	-111.0 ± 5.0	22,255	110	-44.4 ± 4.1	-31.8 ± 0.01	-249.2%	-0.13%
2 (2018-2019)	2220.1 ± 519.7	23,358	13	6235.2 ± 1953.3	958.7 ± 0.18	+132.1%	1.9%
3 (2019-2020)	171.6 ± 25.2	24,941	189	78.9 ± 5.7	-44.40 ± 0.02	+486.4%	0.18%
All years	761.4 ± 171.6	70,554	26	3293.8 ± 814.6	319 ± 0.08	+139.7%	0.7%

3.10 Figures

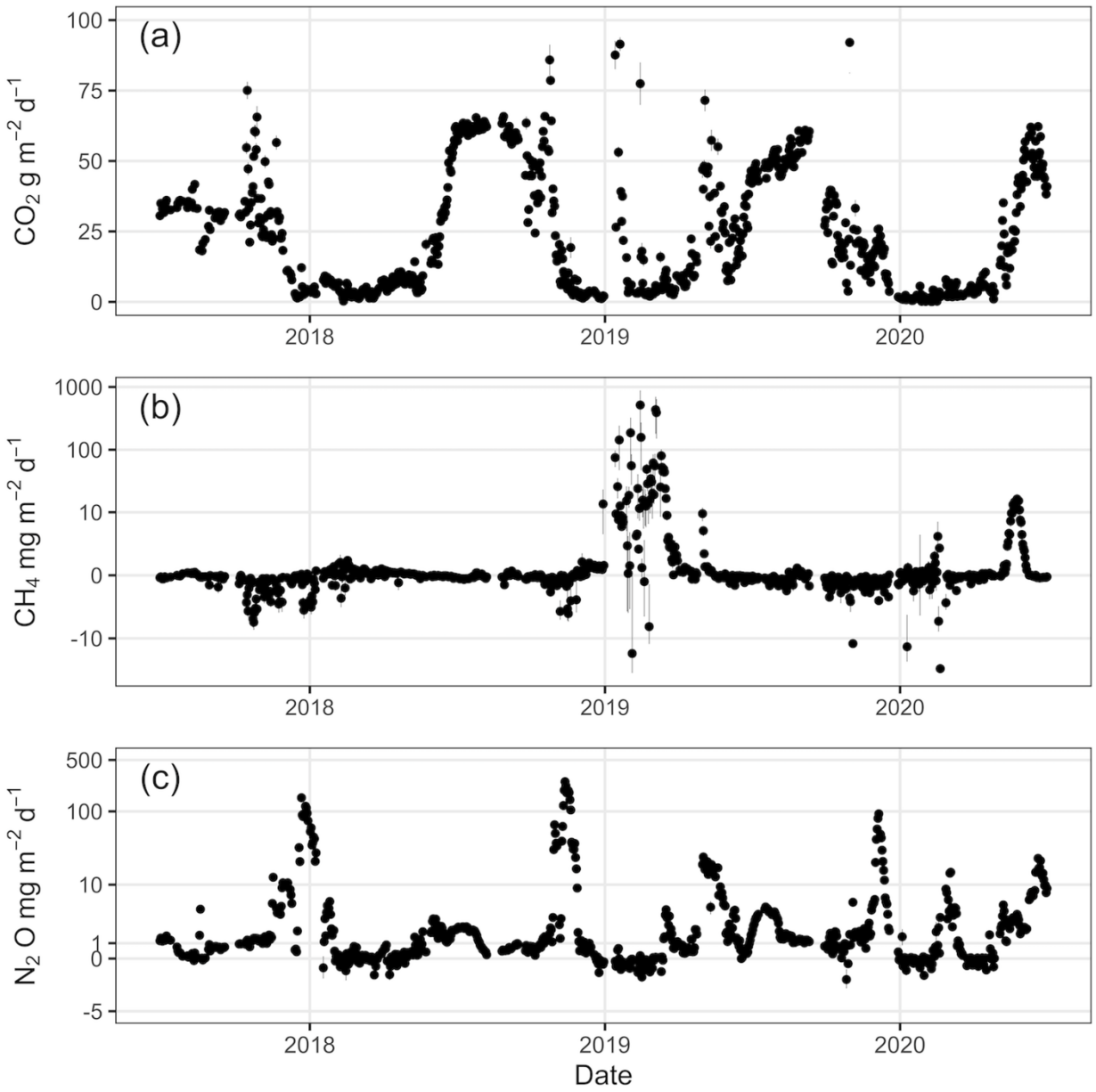

Figure 1. Daily mean greenhouse gas fluxes (± standard error) for (a) CO_2 (g CO_2 m^{-2} d^{-1}), (b) CH_4 (mg CH_4 m^{-2} d^{-1}), and (c) N_2O (mg N_2O m^{-2} d^{-1}). Black circles are daily mean flux measurements (mean n = 81 fluxes per day).

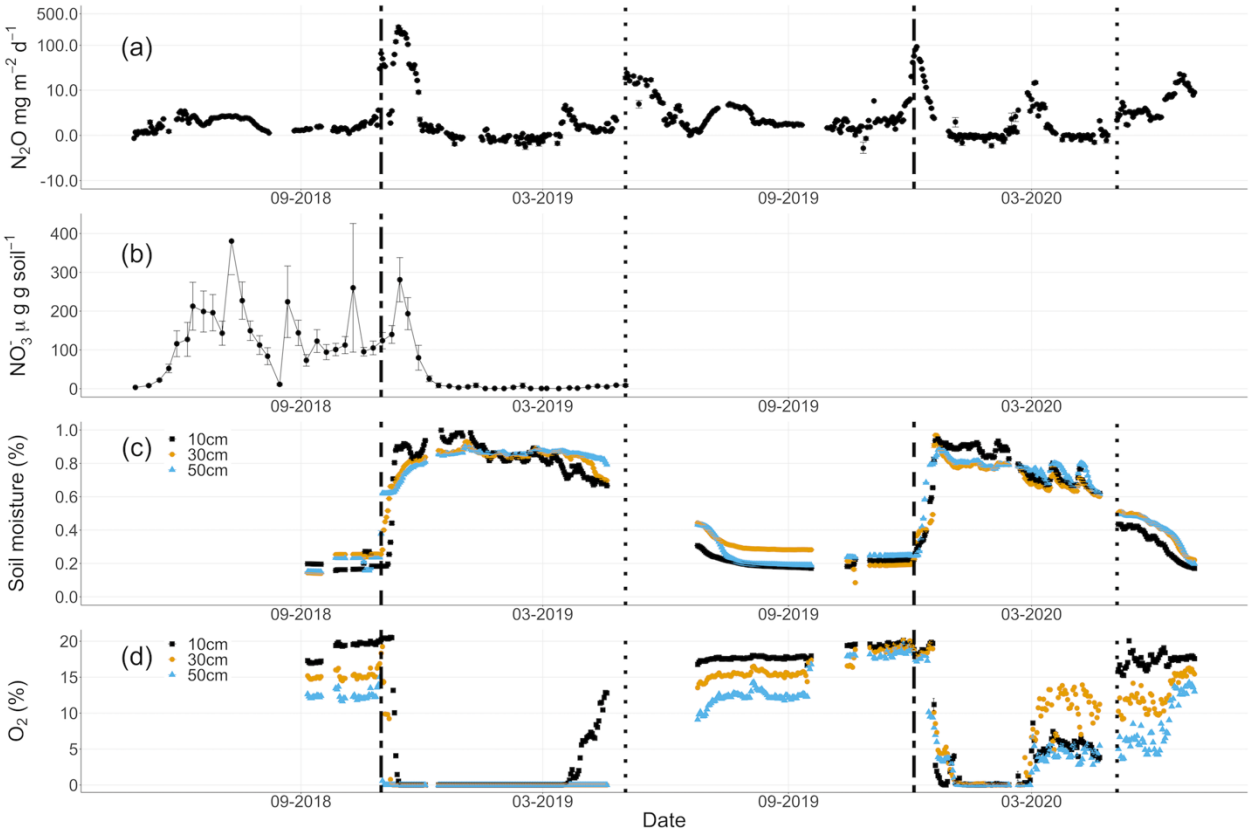

Figure 2. Daily mean (± standard error) (a) N_2O fluxes, (b) soil NO_3^- concentrations, (c) daily mean soil moisture, and (d) daily mean soil O_2 concentrations over the measurement period. Soil NO_3^- measurements (0-10 cm depth) were conducted weekly from May 2018-May 2019. For (c) soil O_2 concentrations and (d) soil moisture, daily average values by soil depth are labeled as squares (10 cm), open circles (30 cm), and triangles (50 cm). Flooding and fertilization events are labeled with dashed and dotted lines, respectively. Gaps represent missing data (see Methods).

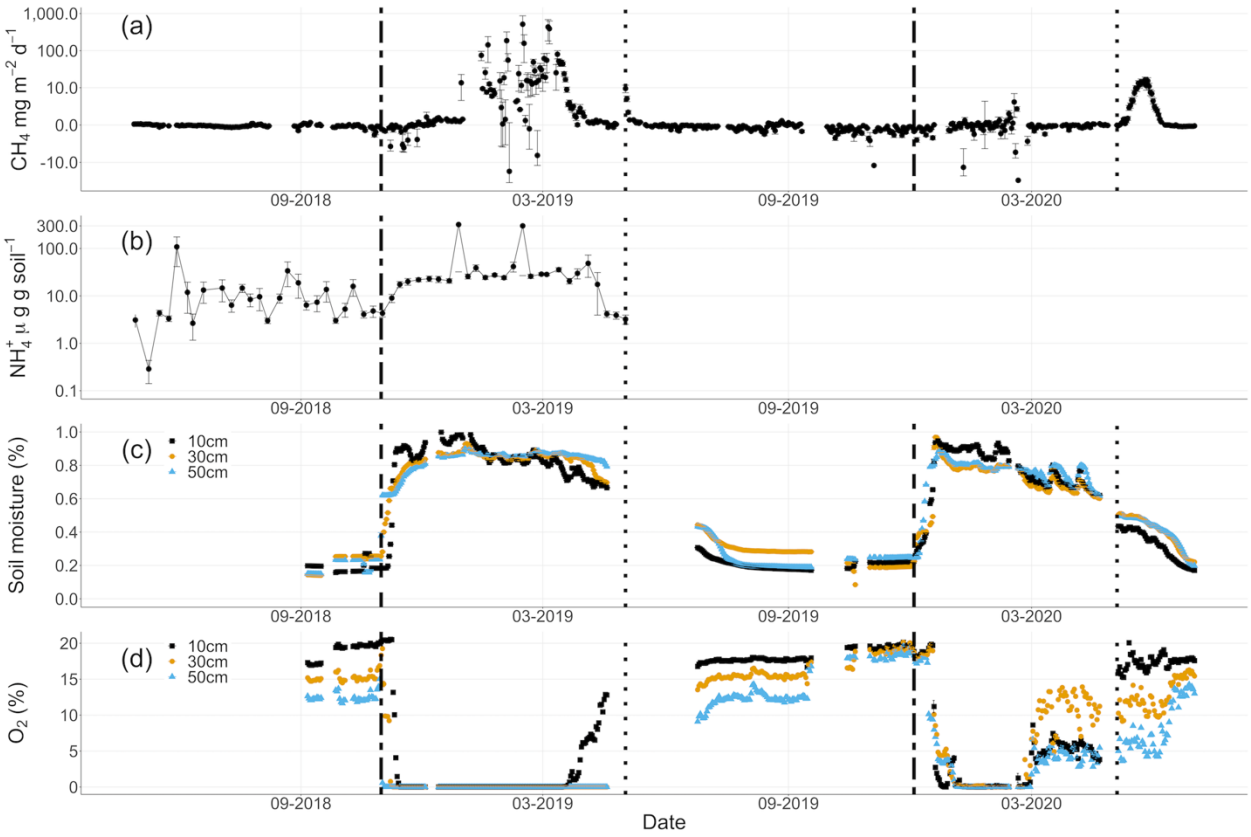

Figure 3. Daily mean (± standard error) values of (a) CH_4 fluxes, (b) soil NH_4^+, (c) soil moisture, and (d) soil O_2 over the measurement period across 10 cm (squares), 30 cm (open circles), and 50 cm (triangles) depths. Soil NH_4^+ measurements were conducted weekly at 0-10 cm depth from May 2018 to May 2019. Flooding and fertilization events are labeled with dashed and dotted lines, respectively. Gaps between data points in (a), (c), and (d) correspond to missing data (see Methods).

3.11 Appendix

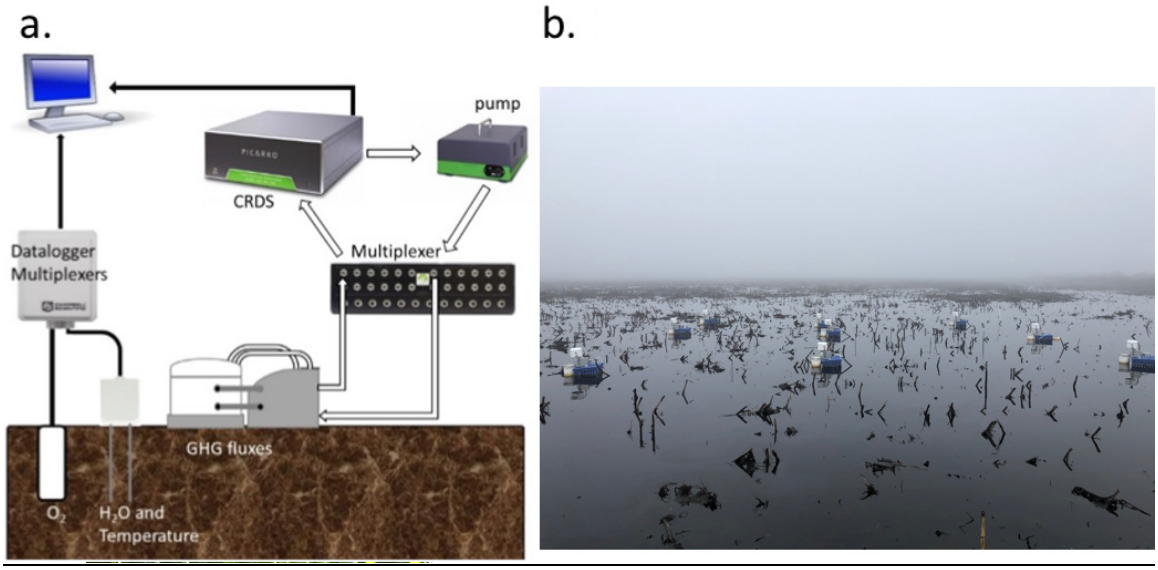

Supplemental Figure 1. a. System design for continuous soil GHG emissions by CRDS and applicable soil moisture, temperature, and oxygen measurements. b. Example deployment of all automated chambers in 10 x 10 m grid.

Supplemental Table 1. Annual mean (± standard error) CO_2 and fluxes by site year (e.g July 1 to June 30), number of measurements and outliers, outlier mean (± standard error) fluxes, mean fluxes (± standard error) without outliers included, and % of the outlier contribution to total mean flux. Outliers were recalculated for each year and for the total dataset.

Site Year	Mean (g CO_2 m^{-2} d^{-1})	Flux (n)	Hot moment flux (n)	Hot moment mean (g CO_2 m^{-2} d^{-1})	Mean no hot moments (g CO_2 m^{-2} d^{-1})	Hot moment % change in mean flux
1 (2017-2018)	18.9 ± 0.2	22,250	150	257.2 ± 12.9	17.3 ± 0.1	+9.2%
2 (2018-2019)	29.9 ± 0.3	23,598	123	316.1 ± 19.0	28.4 ± 0.2	+5.3%
3 (2019-2020)	28.0 ± 0.2	25,414	77	228.8 ± 23.0	27.3 ± 0.1	+2.6%
All years	25.8 ± 0.1	71,262	342	277.1 ± 10.3	24.5 ± 0.1	+5.0%

Supplemental Table 2. Effects of daily sampling interval on mean (± standard error) N_2O flux (g N_2O m^{-2} d^{-1}).

Interval (days)	Median flux (mg N_2O m^{-2} d^{-1})	Change from mean (%)	High estimate (mg N_2O m^{-2} d^{-1})	Change from mean (%)	Low Estimate (mg N_2O m^{-2} d^{-1})	Change from mean (%)
1	10.3 ± 1.3	-	10.3 ± 1.3	-	10.3 ± 1.3	-
2	10.3 ± 1.8	2.4%	10.5 ± 1.8	2.4%	10.0 ±1.8	-2.4%
7	10.1 ± 3.4	-2.3%	12.2 ± 3.9	18.8%	8.4 ± 1.8	-18.3%
14	10.6 ± 6.3	3.4%	13.7 ± 7.0	33.4%	6.3 ± 2.5	-38.5%
28	9.0 ± 9.3	-13.0%	23.6 ± 12.3	129.2%	2.6 ± 0.9	-751%

Supplemental Table 3. Effects of daily sampling interval on mean (± standard error) CH_4 flux (mg CH_4 m^{-2} d^{-1}).

Interval (days)	Median flux (mg CH_4 m^{-2} d^{-1})	Change from mean (%)	High estimate (mg CH_4 m^{-2} d^{-1})	Change from mean (%)	Low Estimate (mg CH_4 m^{-2} d^{-1})	Change from mean (%)
1	1.49 ± 0.56	-	1.49 ± 0.56	-	1.49 ± 0.56	-
2	2.21 ± 0.80	+48.3%	2.45 ± 0.92	+64.4%	1.98 ± 0.68	+32.9%
7	1.70 ± 0.79	+14.1%	3.71 ± 2.42	+149%	0.89 ± 0.31	-40.3%
14	1.48 ± 0.89	-0.7%	6.00 ± 4.00	+302.7	0.58 ± 0.50	-61.3%
28	1.23 ± 2.4	-17.4%	11.26 ± 7.95	+655.7%	0.17 ± 0.15	-88.6%

Supplemental Table 4. Comparison of the minimum sample size needed to calculate annual and total 3-year mean (± standard error) fluxes of N_2O and CH_4 with a 95% confidence interval and 10%, 25%, and 50% margins of error.

N_2O Site Year	Flux measurements (n)	Mean ± SE (g N_2O m^{-2} y^{-1})	Margin of Error (%)	Minimum sample size (n)
1 (2017-2018)	22,568	3.52 ± 0.11	10%	5,959
			25%	1,226
			50%	320
2 (2018-2019)	23,433	6.52 ± 0.25	10%	8,342
			25%	1,904
			50%	507
3 (2019-2020)	25,363	2.35 ± 0.04	10%	2,700
			25%	475
			50%	121
All years	71,634	4.08 ± 0.10	10%	6,401
			25%	1,108
			50%	281
CH_4 Site Year	Flux measurements (n)	Mean ± SE (mg CH_4 m^{-2} y^{-1})	Margin of Error	Minimum sample size (n)
1 (2017-2018)	22,576	-111.0 ± 5.0	10%	17,133
			25%	7,562
			50%	2,525
2 (2018-2019)	23,598	2220.1 ± 519.7	10%	22,525
			25%	18,184
			50%	10,770
3 (2019-2020)	25,370	171.6 ± 25.2	10%	22,012
			25%	12,988
			50%	5,271
All years	71,573	761.4 ± 171.6	10%	68,137
			25%	54,419
			50%	31,656

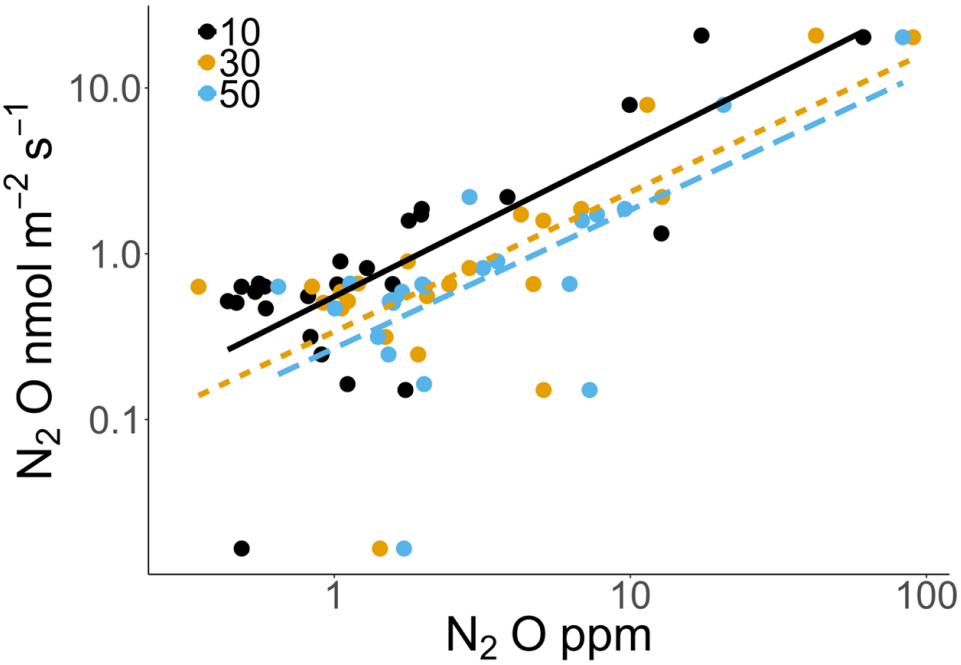

Supplemental Figure 2. Log-scale linear correlations of soil N_2O concentrations (ppmv) across depths (10 cm: black, 30 cm: orange, and 50 cm: blue) with daily mean soil N_2O flux (nmol m^{-2} s^{-1}). At 10 cm depth, $R^2 = 0.60$ ($p < 0.001$, n = 26), at 30 cm depth, $R^2 = 0.53$ ($p < 0.001$, n = 26), and at 50 cm depth, $R^2 = 0.45$ ($p < 0.001$, n = 28).

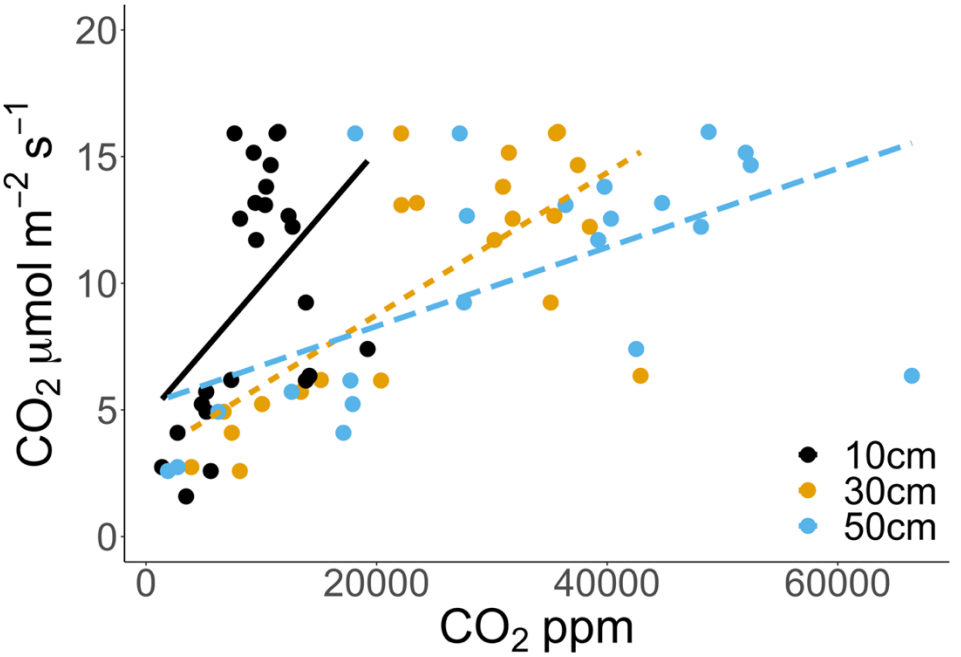

Supplemental Figure 3. Linear correlations of soil CO_2 concentrations (ppmv) across depths (10 cm: black, 30 cm: orange, and 50 cm: blue) with daily mean soil CO_2 flux µmol m^{-2} s^{-1}. At 10 cm depth, $R^2 = 0.20$ ($p = 0.03$, n = 26), at 30 cm depth, $R^2 = 0.50$ ($p < 0.001$, n = 26), and at 50 cm depth, $R^2 = 0.22$ ($p < 0.03$, n = 28).

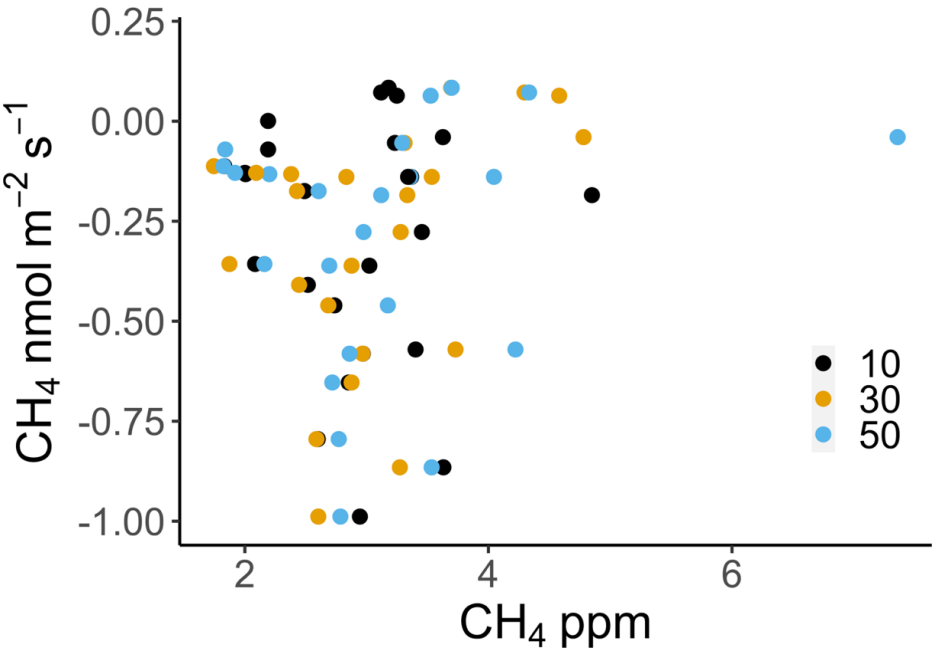

Supplemental Figure 4. Soil CH_4 concentrations (ppmv) plotted against daily mean soil CH_4 flux (nmol m^{-2} s^{-1}) across depths (10 cm: black, 30 cm: orange, and 50 cm: blue). Relationships were not statistically significant.

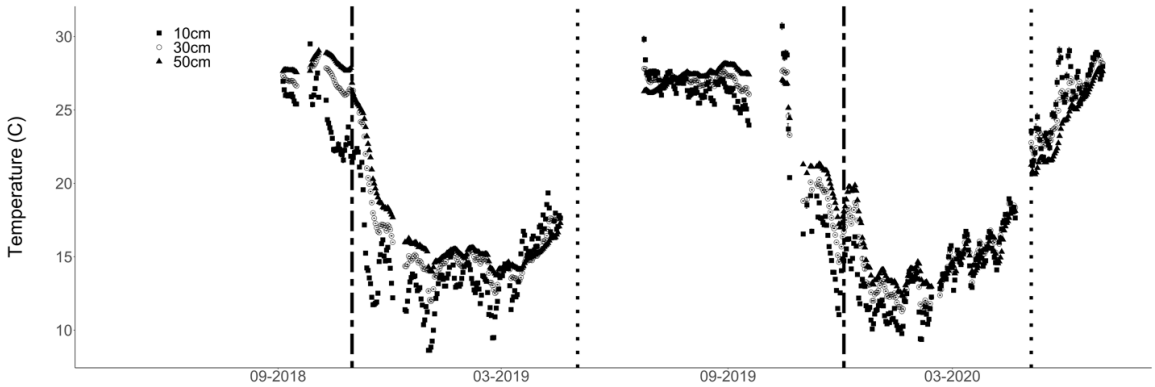

Supplemental Figure 5. Plots of daily mean (± standard error) soil temperature (°C) over the measurement period at 10 cm (squares), 30 cm (open circles), and 50 cm (triangles) depths.

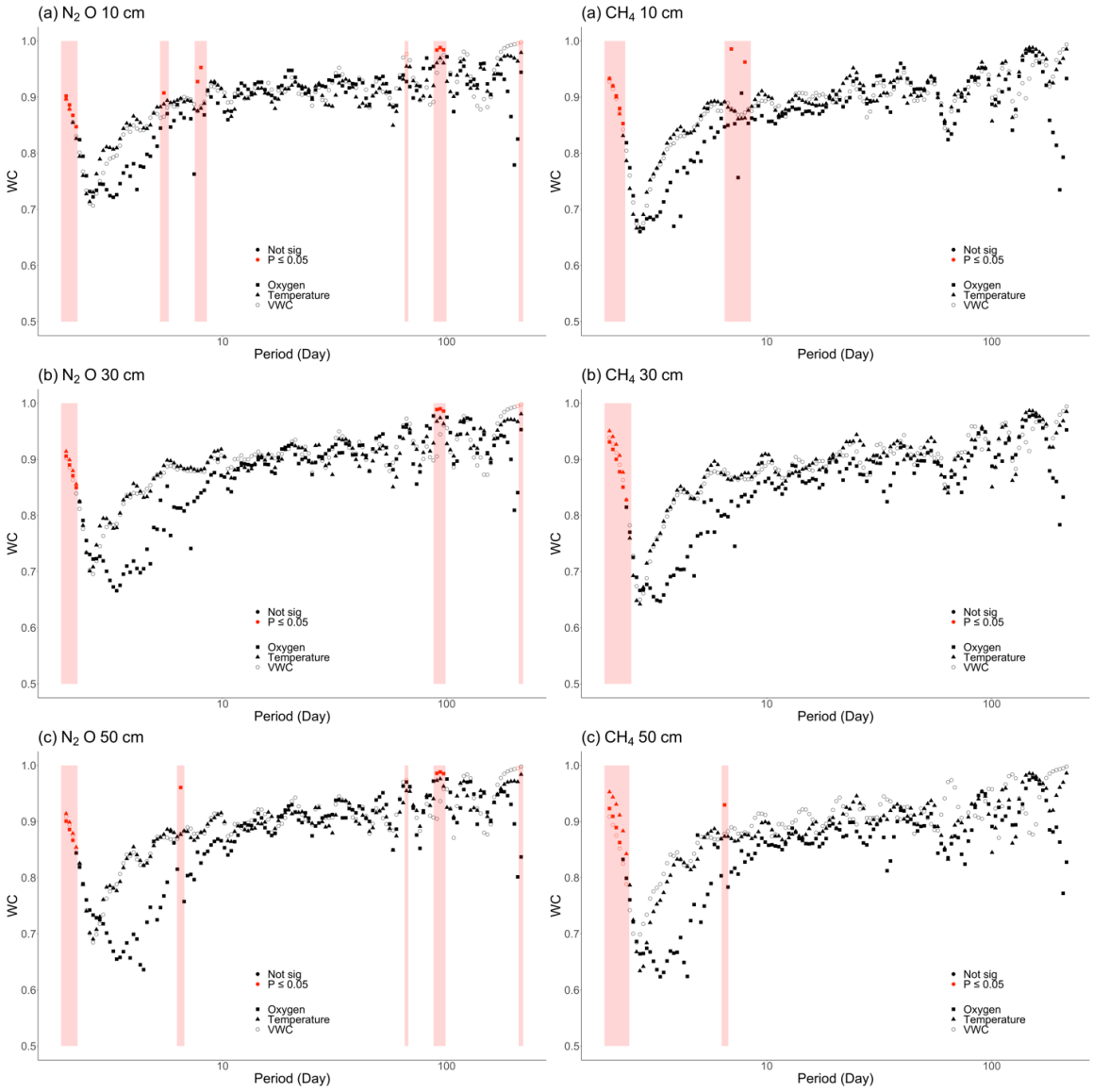

Supplemental Figure 6. Wavelet coherence (WC) for soil N_2O (g N_2O m^{-2} d^{-1}, a-c) and CH_4 (g CH_4 m^{-2} d^{-1}, d-f) fluxes with O_2 (%) concentrations (squares), soil temperature (°C, triangles), and soil moisture (%, open circles)at 10 cm (a,d), 30 cm (b,e) and 50 cm (c,f). Each point represents the average wavelet coherence across a range of periodicities (period = day). Red highlights points with significant coherence ($p < 0.05$) between soil variables and net N_2O (a-c) and CH_4 (d-f) fluxes.

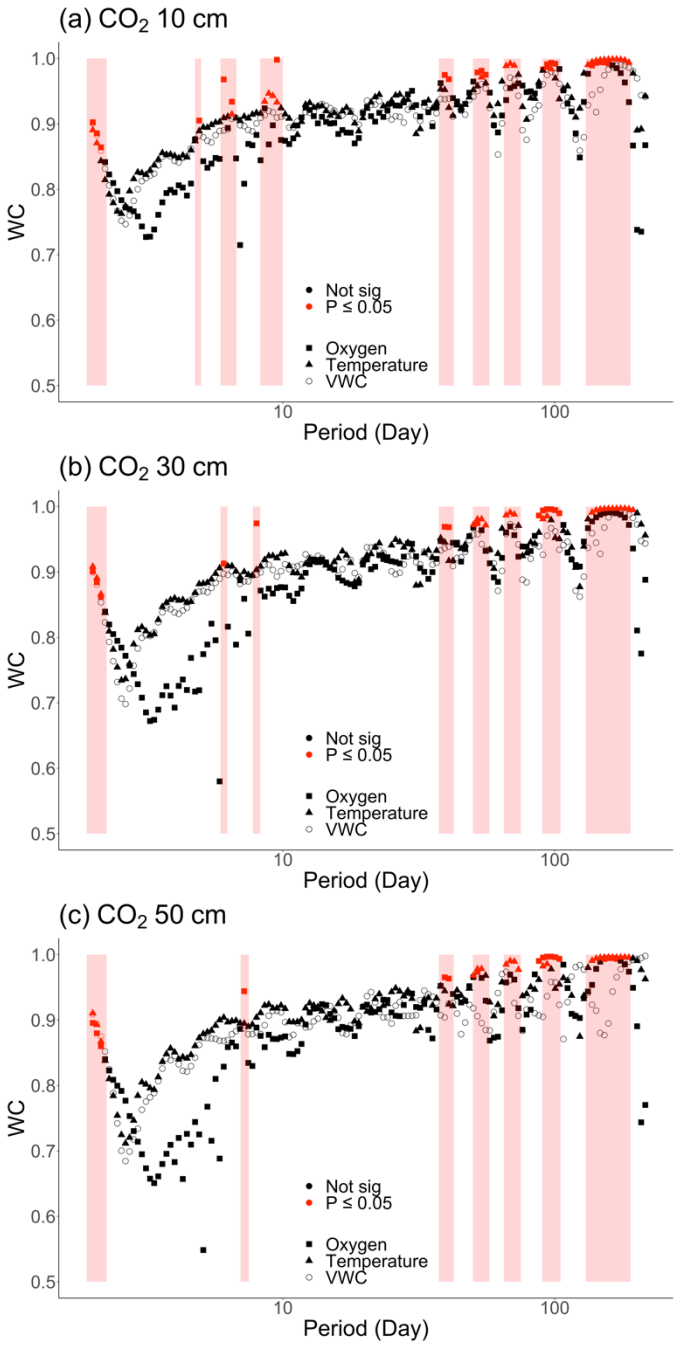

Supplemental Figure 7. Wavelet coherence (WC) for soil CO_2 (a-c) fluxes (g CO_2 m^{-2} d^{-1}) with soil O_2 (%) concentrations (squares), soil temperature (°C, triangles), and soil moisture (%, open circles) at 10 cm (a), 30 cm (b) and 50 cm (c). Each point represents the average wavelet coherence across a range of periodicities. Red highlights points with significant coherence ($p <$ 0.05) between soil variables.

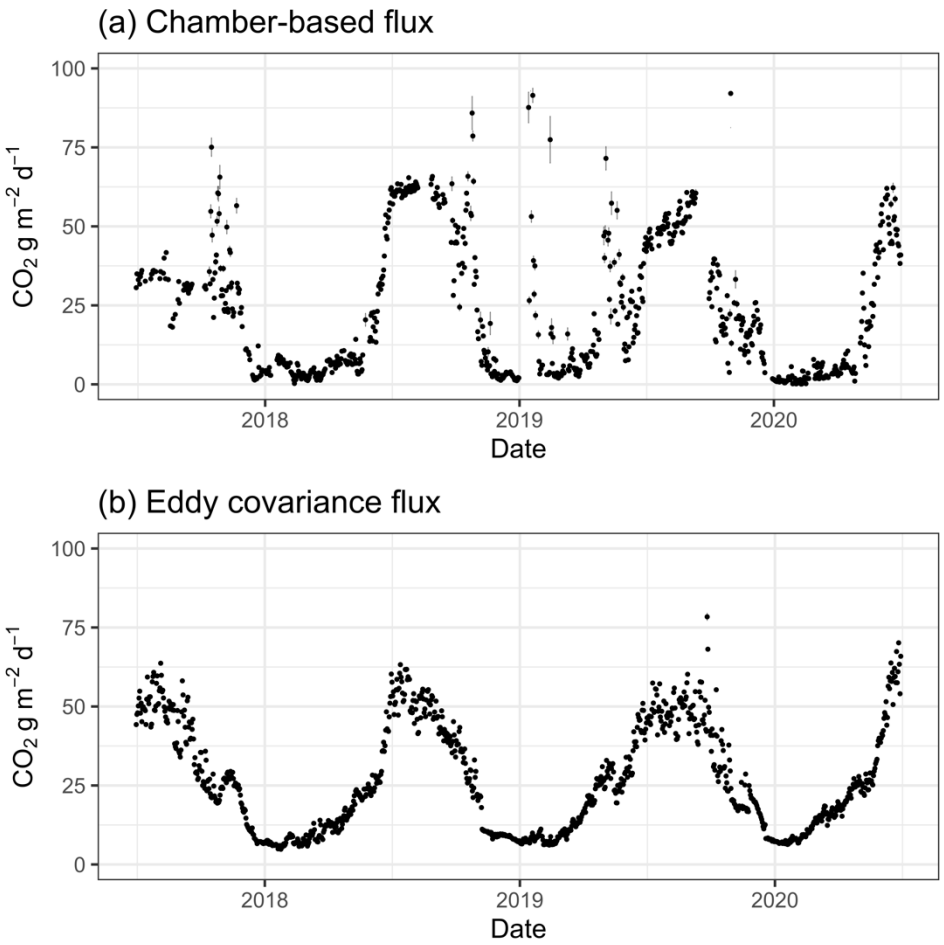

Supplemental Figure 8. Comparisons between (a) daily mean (± standard error) chamber-based soil CO_2 fluxes (g CO_2 m^{-2} d^{-1}) and (b) daily mean (± standard error) eddy covariance ecosystem respiration (g CO_2 m^{-2} d^{-1}).

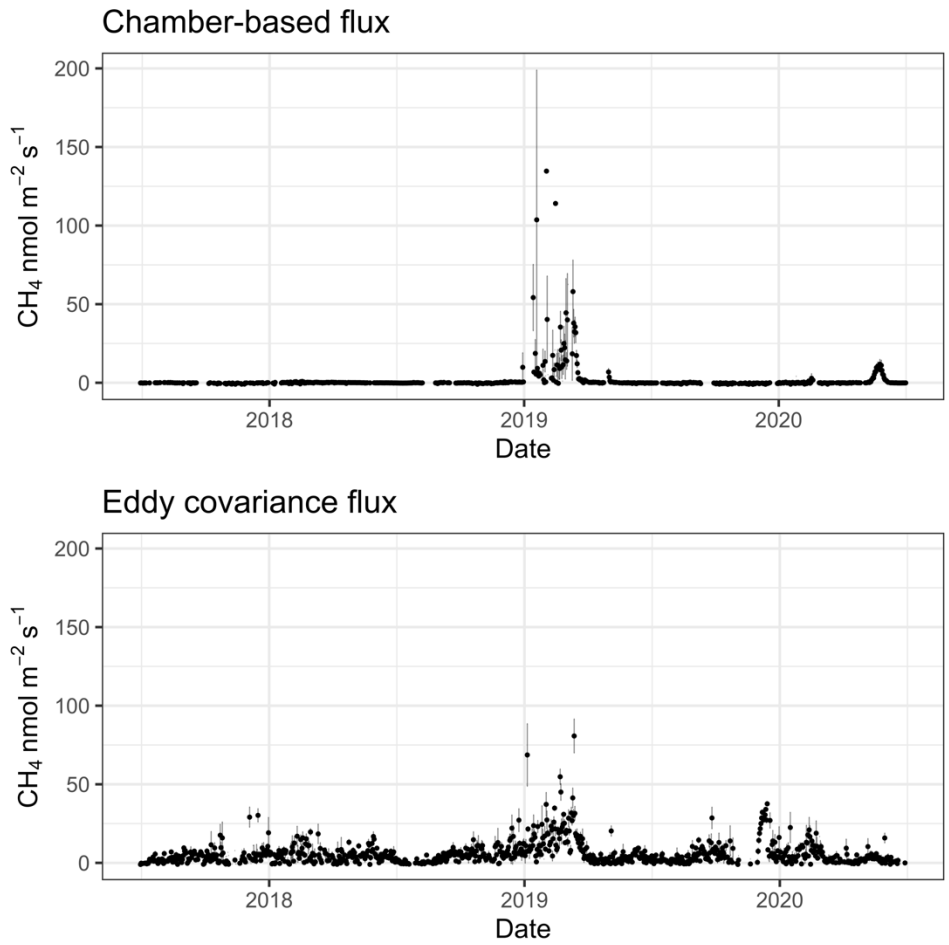

Supplemental Figure 9. Comparisons between (a) daily mean (± standard error) chamber-based soil CH_4 fluxes (g CH_4 m^{-2} d^{-1}) and (b) daily mean (± standard error) eddy covariance ecosystem respiration (g CH_4 m^{-2} d^{-1}).

Supplementary Table 5. Comparison of area- and yield-scaled emissions estimates of corn agroecosystems from previous studies.

Area-scaled emissions (Mg CO_2e ha^{-1})	Yield-scaled emissions (g CO_2e g dry $yield^{-1}$)	Citation
12.9 ± 0.7	-	Jin et al. 2014
1.78-3.43	0.27-0.56	Chai et al. 2019
2.14-2.82	0.30-0.97	Johnson et al. 2017
1.4	0.185	Linquist et al. 2012
46.67 (range 39.14-55.45)	2.88 (range 2.41-3.42)	*This study*

In **Chapter 3**, I focused on quantifying the long-term emissions of carbon dioxide (CO_2), nitrous oxide (N_2O), and methane (CH_4) from an organic-rich agricultural peatland soil. I found that most N_2O and CH_4 emissions were associated with hot moments of emission during flood irrigation events. This result was surprising as I expected to also observe significant N_2O and CH_4 emissions during the warm growing season as elevated soil temperature and moisture content at depth should stimulate both N_2O and CH_4 emissions. Using the results from **Chapter 3**, I conducted two targeted pool dilution experiments in **Chapter 4** to quantify the both the gross production and consumption pathways of N_2O and CH_4 during a winter flooding event and from drained conditions during the summer. I used a dual-isotope 13C-CH_4 and 15N-N_2O pool dilution experiment to quantify both the production and consumption pathways of N_2O and CH_4 to better understand the controls on net N_2O and CH_4 emissions I observed in **Chapter 3**.

Chapter 4. The effects of soil moisture conditions on net and gross nitrous oxide and methane fluxes in an agricultural soil

4.1 Abstract

Soil greenhouse gas emissions are the result of complex and interacting processes of production and consumption, often occurring simultaneously. Most field studies have only examined net fluxes, and thus lack information on the detailed dynamics controlling emissions in time and space. We measured continuous net greenhouse gas fluxes in a high-emitting agricultural soil to identify patterns in emission events and used a dual isotope trace gas pool dilution technique to measure simultaneous gross N_2O and CH_4 fluxes to explore potential drivers under contrasting drained and flooded soil redox conditions. Net soil N_2O fluxes were highest in surface soils shortly after soil saturation and corresponded to higher rates of gross N_2O production than when soils were drained (mean ± SE: 2.4 ± 0.7 μg N g soil^{-1} d^{-1}). Gross N_2O production was strongly correlated to soil moisture across all samples ($R^2 = 0.36$, $p < 0.001$). Gross N_2O consumption rates were higher in drained subsoils than under flooded conditions (up to 2.2 ± 1.0 μg N g soil^{-1} d^{-1}) and were correlated with nitrate (NO_3^-) concentrations ($R^2 = 0.50$-0.79, $p < 0.01$), suggesting N_2O consumption was indirectly controlled by substrate availability for denitrifiers. Net N_2O fluxes in the field were also lower during this drained period, our combined observations suggest anaerobic hotspots of consumption may be sparsely distributed at depth throughout the soil profile. This ecosystem was a net CH_4 sink during the measurement period. Gross CH_4 consumption (range: 0-5.6 μg C g soil^{-1} d^{-1}) was generally greater than gross CH_4 production (range: 0-2.8 μg C g soil^{-1} d^{-1}) during both sampling periods. Gross CH_4 production increased with soil depth, likely driven by increased soil moisture and anaerobic soil conditions. Gross CH_4 consumption was negatively correlated with soil moisture ($R^2 = 0.54$, $p < 0.001$) and positively correlated with soil pH ($R^2 = 0.70$, $p < 0.001$) in surface soils, indicating both low pH and O_2 low availability directly limit CH_4 consumption. Gross CH_4 consumption accounted for up to 24.9% of net CO_2 production (mean ± SE: 6.6% ± 3.4%) in drained soils at depth. Our results suggest that the dynamics of gross N_2O and CH_4 production in high emitting agricultural peatlands are temporally decoupled from those of gross N_2O and CH_4 consumption and are largely driven by soil moisture status with associated effects on NO_3^- and pH.

4.2 Introduction

Agricultural soils are globally significant sources of greenhouse gases (Oertel, Matschullat, Zurba, Zimmermann, & Erasmi, 2016; Smith et al., 2007) often characterized by significant hot moments of net nitrous oxide (N_2O) or methane (CH_4) emissions (Anthony & Silver, 2021; Liu, Zak, Rezanezhad, & Lennartz, 2019; Molodovskaya et al., 2012; Savage, Phillips, & Davidson, 2014; Taft, Cross, Hastings, Yeluripati, & Jones, 2019; Teh et al., 2011). Significant net N_2O and CH_4 emissions can occur following agricultural management practices that alter soil oxidation-reduction (redox) conditions, as both N_2O and CH_4 are produced and consumed in soils by microbially mediated redox-sensitive processes (Conrad, 1996b). However, the relative contribution of N_2O and CH_4 production and consumption on a gross basis and on overall fluxes is not well constrained, as most studies only periodically measure net fluxes. Measuring only net fluxes also limits our ability to infer the controls and dynamics of these processes.

Dual stable isotope (^{15}N-N_2O and ^{13}C-CH_4) pool dilution experiments measure gross production and consumption of N_2O and CH_4 by quantifying the simultaneous loss and dilution of the stable isotope labels over time (von Fischer & Hedin, 2002; Yang & Silver, 2016; Yang, Teh, & Silver, 2011). Multiple biotic and abiotic nitrogen (N) transformation processes in soils produce N_2O as an intermediate or byproduct (Firestone & Davidson, 1989) with N_2O both produced or consumed via redox-sensitive nitrification and denitrification pathways (Butterbach-Bahl, Baggs, Dannenmann, Kiese, & Zechmeister-Boltenstern, 2013). Under oxic conditions, N_2O is typically produced as a byproduct of aerobic nitrification (Zhu, Burger, Doane, & Horwath, 2013) with nitrification rates controlled by a combination of ammonium (NH_4^+) concentration, soil pH, temperature, water content, and organic carbon (C) availability (Booth, Stark, & Rastetter, 2005). Nitrous oxide can be produced as an intermediate in both nitrifier denitrification and heterotrophic denitrification under anoxic conditions where nitrate (NO_3^-) is reduced to N_2O (Firestone & Davidson, 1989). Complete denitrification under anoxic conditions consumes this intermediate N_2O by further reduction to dinitrogen (N_2); this process is likely to be sensitive to both elevated oxygen (O_2) and NO_3^-concentrations (Butterbach-Bahl et al., 2013; Morley, Baggs, Dörsch, & Bakken, 2008).

Methane can also be both produced or consumed in soils (Le Mer & Roger, 2001; Serrano-Silva, Sarria-Guzmàn, Dendooven, & Luna-Guido, 2014). Methanogenesis occurs under anoxic conditions, is often favored at a circumneutral pH, and generally increases with temperature and nutrient availability (Le Mer & Roger, 2001, Sihi, Davidson, Savage, & Liang, 2020). Methanotrophy predominantly occurs under oxic soil conditions and is thought to be controlled by O_2 and CH_4 availability (Megonigal, Hines, & Visscher, 2003); it can occur near sites of CH_4 production and quickly consume CH_4 produced (Bender & Conrad, 1994, 1995; Conrad, 2007; Kammann, Hepp, Lenhart, & Müller, 2009). Production and consumption of both N_2O and CH_4 can occur simultaneously within soils (Angle et al., 2017; Koehler et al., 2012; Sihi, Davidson, Savage, & Liang, 2020) as soil heterogeneity can produce a range of aerobic and

anaerobic conditions from the scale of microaggregates to catenas (Cardinael et al., 2017; Groffman et al., 2009; Liptzin & Silver, 2015).

Heterogeneity in the distribution of substrate availability, gas diffusivity, and microbial activity throughout a soil profile are likely to be important predictors of patterns in gross greenhouse gas production and consumption. Soil moisture content, redox conditions, and C and nutrient availability often vary with depth in soils, leading to differential patterns in C and N cycling (Jobbágy & Jackson, 2001; Krichels, DeLucia, Sanford, Chee-Sanford, & Yang, 2019; Krichels & Yang, 2019; Thorup-Kristensen et al., 2020). Changes in biogeochemistry with soil depth can impact production, consumption, and ultimate emissions of greenhouse gases. The distribution of oxic and anoxic conditions with depth likely influences the distribution and controls of N_2O and CH_4 production and consumption. Incorporating physical and biogeochemical parameters across soil depths can significantly improve predictions of soil greenhouse gas fluxes (Chatskikh, Olesen, Berntsen, Regina, & Yamulki, 2005; Feng et al., 2021; Potter, 1997; Xing, Wang, Smith, Rolston, & Yu, 2011).

Agricultural practices can also stimulate ecosystem-scale changes in substrate availability (e.g. fertilizer use and/or organic matter mineralization) and soil redox (e.g. irrigation) that can regulate gross N_2O and CH_4 fluxes (Allen, 2012; Congreves, Brown, Németh, Dunfield, & Wagner-Riddle, 2017; Petrakis, Seyfferth, Kan, Inamdar, & Vargas, 2017). Well-drained C-rich soils can facilitate nitrification and aerobic CH_4 oxidation at the soil surface, while hydrologic saturation lower in the profile can lead to increasing anaerobic soil conditions at depth (Anthony & Silver, 2021; Hatala et al., 2012; Teh et al., 2011; Theodorus et al., 2020). Flood irrigation is often deployed in agricultural soils for weed control or to create habitat for migrating waterfowl (Pellerin, Anderson, & Bergamaschi, 2014). The onset of flooding quickly alters soil redox conditions, leading to substantial N_2O emissions and a decrease in soil NO_3^- concentrations (Anthony & Silver, 2021; Kögel-Knabner et al., 2010). With extended periods of flooding agricultural soils can also be significant net CH_4 sources (Anthony & Silver, 2021; Hemes et al., 2019; Kögel-Knabner et al., 2010). The contrasting soil conditions across flooded and drained conditions and soil depths provide an excellent template to explore drivers of gross N_2O and CH_4 fluxes.

Previous research has shown iron (Fe) and aluminum (Al) minerals may be important controls on soil C accumulation and loss (Anthony & Silver, 2020; Chen, Hall, Coward, & Thompson, 2020; W. Huang, Ye, Hockaday, & Hall, 2020; Kleber et al., 2015) and Fe redox cycling may contribute to a significant portion of heterotrophic CO_2 emissions (Anthony & Silver, 2020; Hall & Silver, 2015; W. Huang et al., 2020; X. Huang et al., 2018; Yang & Liptzin, 2015). Reactive Fe and Al minerals may interact with gross N_2O and CH_4 pathways through multiple biogeochemical processes. Iron is utilized as an alternative electron acceptor in anaerobic respiration, and reduced Fe is readily oxidized in both biotic and abiotic reactions that interact with the C and N cycles (Megonigal et al., 2003; Peters & Conrad, 1996). This includes direct substrate competition with Fe reducers, Fe-induced inhibition of methanogenesis via

acetate assimilation, and Fe reduction coupled to anaerobic ammonium (NH_4^+) oxidation to NO_3^- and subsequent denitrification to N_2O (Clément, Shrestha, Ehrenfeld, & Jaffé, 2005; Megonigal et al., 2003; Peters & Conrad, 1996; Wang, Hu, Zhao, Kuzyakov, & Liu, 2016; Yang, Weber, & Silver, 2012). Iron and Al minerals can co-precipitate with organic matter under oxidized conditions (Rasmussen et al., 2018; Wiesmeier et al., 2019), protecting organic matter from decomposition. Iron or Al mineral co-precipitation also facilitates soil aggregation, which can directly limit substrate availability or generate soil anaerobic (micro)sites via O_2 diffusion limitations (Anthony & Silver, 2020; Keiluweit, Wanzek, Kleber, Nico, & Fendorf, 2017; Six & Paustian, 2014; Totsche et al., 2017). Anaerobic (micro)sites are likely hot spots for both N_2O and CH_4 production and consumption (Kravchenko et al., 2017; Sihi et al., 2020), and hot spots can represent a significant proportion of total soil emissions at an ecosystem scale (Anthony & Silver 2021; Bernhardt et al., 2017; Krichels, Sipic, & Yang, 2019; Savage et al., 2014).

The objectives of this study were to explore patterns and drivers of net and gross N_2O and CH_4 fluxes in soils under different managed moisture conditions. We used a dual isotope trace gas pool dilution technique to measure simultaneous gross N_2O and CH_4 fluxes alongside continuous, soil CO_2, CH_4, and N_2O flux measurements. Iron and Al (oxy)hydroxides were also measured to explore their potential indirect effects on N_2O and CH_4 dynamics. Previous continuous flux measurements highlight significant effects of moisture conditions on net N_2O and CH_4 emissions at this site, exhibiting substantial net N_2O emissions following soil flooding and smaller net N_2O emissions and a net CH_4 sink under drained conditions (Anthony & Silver, 2021). We hypothesized high soil moisture at depth during the drained period would sustain gross N_2O production, but gross N_2O consumption within anaerobic (micro)sites, possibly facilitated by Fe reduction and/or organo-Al complexation, would limit net N_2O emissions. We also hypothesized optimum conditions for net N_2O production would occur in surface soils shortly after flooding when NO_3^- availability was high and soil O_2 concentrations were declining. Anaerobic conditions in subsoils were expected to increase gross N_2O consumption during this period. For CH_4, we hypothesized CH_4 production in subsoils or anaerobic (micro)sites would fuel high gross CH_4 consumption rates at the surface during drained periods. Following winter flooding, we hypothesized low O_2 concentrations would limit CH_4 oxidation across all depths, leading to a decrease in the CH_4 sink or a net source of CH_4.

4.3 Methods

4.3.1 Site info

This study was located in the Sacramento-San Joaquin Delta region of California (38.11ºN, 121.5ºW). This site was a continuous conventional corn site that was irrigated via spud ditches during the growing season and was flooded after harvest to limit weed growth. The region experienced a Mediterranean climate with hot dry summers and cool wet winters, with a historical (1955-2015) mean annual temperature is 15.1 ± 6.3 °C and a yearly average rainfall of 326 ± 4 mm (Hatala et al., 2012). This was also an Ameriflux site (Ameriflux ID: US-Bi2) with

continuous eddy covariance measurements of CO_2, CH_4, and H_2O since mid-2017 (Camilo, Szutu, Baldocchi, & Hemes, 2021). Soils are classified as Histisols within the Rindge series and belong to the Euic, thermic Typic Haplosaprists taxonomic class and are characterized by deep, poorly drained marsh soils formed from decomposed plant matter (Soil Survey Staff, 2020).

Table 1. Soil carbon, nitrogen, and bulk density values (mean ± SE) across soil depths (n = 15 per depth, Anthony & Silver, 2020).

Variable	0-15 cm (± SE)	15-30 cm (± SE)	30-60 cm (± SE)
% Soil Carbon	15.2% ± 0.4%	15.9% ± 0.7%	19.5% ± 0.6%
% Soil Nitrogen	1.04% ± 0.02%	1.07% ± 0.04%	1.21% ± 0.03%
Bulk density (g cm^{-3})	0.587	0.734	0.564

4.3.2 Automated chamber fluxes and soil sensor measurements

Surface soil fluxes of N_2O, CH_4, and CO_2 were measured continuously from October 2019 through July 2020 using an automatic chamber system. This system consisted of nine opaque automated gas flux chambers (eosAC, Eosense, Nova Scotia, Canada) connected to a multiplexer (eosMX, Eosense, Nova Scotia, Canada). The multiplexer allowed for automated chamber deployment and routed gases to a cavity ring-down spectrometer (Picarro G2508, Santa Clara, CA, USA). Chambers were deployed in 10 x 10 m grid, with 5 m between each chamber. Chambers were measured over a 10-min sampling period with a 1.5-min flushing period before and after each measurement. Chambers were randomly assigned to distinct physical features (beds or furrows during growing seasons, corn stover or bare soil during fallow periods). Chamber volumes were used to calculate the minimum detectable flux (Courtois et al., 2018) with detection limits of 0.002 nmol N_2O m^{-2} s^{-1}, 0.06 nmol CO_2 m^{-2} s^{-1}, and 0.002 nmol CH_4 m^{-2} s^{-1} for 15 cm collars utilized during non-flooded conditions, and 0.004 nmol N_2O m^{-2} s^{-1}, 0.12 nmol CO_2 m^{-2} s^{-1}, and 0.004 nmol CH_4 m^{-2} s^{-1} for 35 cm collars utilized during flooded conditions. Further methodology and long-term observations from this site are described in Anthony & Silver, 2021.

4.3.3 Pool dilution study design

We quantified gross and net fluxes of CH_4 and N_2O and net CO_2 fluxes in December 2019 during peak N_2O emissions following soil flooding and again in July 2020 when soils were

drained corresponding to the period of maximum soil respiration with elevated moisture content maintained at depth. In December, seven replicate soil cores were sampled from 0-15 cm and 15-30 cm depths; the 30-60 cm depth was below the water table and thus impossible to generate a comparable set of samples from this depth. In July, seven replicate soil cores were sampled at 0-15 cm, 15-30 cm, and 30-60 cm. Incubations were established within 6 h of soil collection. Each soil sample was gently homogenized by hand and 180 g of soil was added to a 1 L mason jar that remained open until the start of flux measurements, approximately 1 h. Samples were reweighed following the lab incubations and showed minimal moisture loss (< 1%).

4.3.4 Stable isotope pool dilution and net gas flux measurements

We used a lab-based dual isotope trace gas pool dilution technique to measure rates of gross N_2O and CH_4 production and consumption in both drained and flooded soils (von Fischer & Hedin, 2002; Yang et al., 2011). To minimize gas leaks, sample jar lids were equipped with a quarter-inch stainless steel Swagelok Ultra-Torr Vacuum fitting, Restek Thermolite plus septa, and custom Viton rubber seal. After jar closure, jar headspaces were immediately injected with 10 mL of isotopically enriched spiking gas. The spiking gas consisted of 800 ppm N_2O at 4.95 atom% ^{15}N enrichment, 1200 ppm CH_4 at 4.95 atom % ^{13}C enrichment, and 0.8 ppm SF_6 (used as a conservative tracer for leakage) to achieve a ^{15}N-N_2O enrichment of 4.80 atom% and ^{13}C-CH_4 enrichment of 4.43 atom%. These values were chosen to ensure detection on the analytical instrumentation. This spiking gas injection increased the chamber headspace by 11 ppm N_2O, 17 ppm CH_4, and 10 ppb SF_6, CH_4 and N_2O concentrations were similar to previous *in-situ* soil concentrations at this site (Anthony & Silver, 2021) . We sampled 60 ml of the chamber headspace at 0, 15, 60, 120, and 180 min after spiking gas injection and replaced jar headspace with 60 ml of He after each gas sampling. We analyzed 20 ml gas samples for determination of CO_2, CH_4, N_2O, and SF_6 concentrations on a Shimadzu GC-14A gas chromatograph (Columbia, MD, USA). We also analyzed separate 20 ml samples for ^{13}C-CH_4 and ^{15}N-N_2O on an IsoPrime 100 continuous flow isotope ratio mass spectrometer interfaced with a trace gas preconcentration unit (Isoprime Ltd, Cheadle Hulme, UK) and Gilson GX271 autosampler (Middleton, WI).

Gross N_2O and CH_4 production and consumption were estimated using the pool dilution model as described by Yang et al. (2011) and von Fischer and Hedin (2002). The iterative model solves for gross production rates based on the dilution of the isotopically enriched chamber headspace of labeled N_2O or CH_4 by natural abundance N_2O or CH_4 emitted by the soil. Gross consumption rates were estimated from the empirical loss of the ^{13}C-CH_4 or ^{15}N-N_2O tracer, using the loss of the SF_6 tracer to account for physical losses such as leaks. This method may overestimate consumption by supplying substrate but is also known to underestimate gross N_2O consumption, as gross consumption is not equivalent to N_2 production as intracellular denitrification could lead to underestimates of N_2 production (Well & Butterbach-Bahl, 2013; Yang, Teh, & Silver, 2013). We assumed the isotopic composition of natural abundance N_2O was 0.3431 atom% ^{15}N and the fractionation factor associated with N_2O reduction to N_2 was 0.9924 (Yang & Silver, 2016; Yang et al., 2011). We also assumed the natural abundance CH_4

was 1.0473 atom % ^{13}C (Yang & Silver, 2016) and the fractionation factor associated with CH_4 oxidation was 0.98 (von Fischer & Hedin, 2002; Yang & Silver, 2016). Model outputs were not sensitive to the assumed values given the high isotopic enrichments utilized in this study.

4.3.5 Soil biogeochemical analyses

All subsequent analyses were performed on individual samples immediately following the pool dilution incubation. After incubation, samples were gently homogenized by hand and 15 g subsamples were extracted in 75 mL of 2M KCl for mineral N concentrations (Hart, Stark, Davidson, & Firestone, 1994). The KCl extracts were shaken at 180 rpm for one hour, filtered, and frozen until analysis on an AQ300 analyzer for NO_3^- plus nitrite (NO_2^-) and NH_4^+ (Seal Instruments, Mequon, WI).

Additional 10 g subsamples were used for gravimetric soil moisture determination, and 5 g soil subsamples were used for soil pH determination. Soil moisture was measured gravimetrically by weighing fresh soil, oven drying for 24 hours at 105 °C, and reweighing the dried soil. Soil pH was determined by creating a 1:1 soil to water solution, vortexing for 1 minute, then measuring the pH in the supernatant solution after 10 min (McLean, 1982).

4.3.6 Reactive Fe and Al pools

We utilized separate soil extractions to characterize three reactive Fe and Al pools. These indices have been mechanistically linked to microbial and geochemical interactions between Fe or Al and organic C storage and loss (see Anthony & Silver 2020, Supplementary Table 1). First, a 1.5 g soil sample was extracted with 0.5 M hydrochloric acid (HCl) for 1 h. Samples were subsequently centrifuged, decanted, and refrigerated until analysis. All 0.5 M HCl extracts were analyzed within 24 hours of extraction using a colorimetric ferrozine assay buffered with 50 mM HEMES to measure weak-acid soluble, reactive short-range order Fe(III) ($Fe(III)_{HCl}$) and soluble Fe(II) ($Fe(II)_{HCl}$) (Fredrickson et al., 1998; Viollier, Inglett, Hunter, Roychoudhury, & Van Cappellen, 2000). A second separate extraction was performed utilizing a 0.2 M sodium citrate and 0.05 M ascorbic acid (citrate-ascorbate) solution at pH 6 to provide an estimate of reducible (redox-active) short-range order Fe (Fe_{CA}) and substituted Al oxides (Al_{CA}) (Torrent, 1997). Approximately 1.5 g soil was added to 45 ml of solution and shaken for 16 h, then subsequently centrifuged, decanted, and refrigerated until analysis. A third separate chelatable Fe (Fe_{AO}) and Al (Al_{AO}) oxide (representing organo-Fe and organo-Al complexes) pool was quantified using an ammonium-oxalate extraction consisting of 0.17 M ammonium oxalate and 0.1 M oxalic acid performed in the dark at pH 3 (Loeppert & Inskeep, 1996). Approximately 0.5 g soil was added to 30 ml of solution and shaken for 2 h, then subsequently centrifuged, decanted, and refrigerated until analysis. Both citrate-ascorbate and ammonium-oxalate extractions were analyzed for Fe and Al via inductively coupled plasma optical emission spectroscopy (ICP-OES; Perkin Elmer Optima 5300 DV).

4.3.7 Statistical analyses

Statistical analyses were performed using JMP Pro 13 (SAS Institute Inc., Cary, NC). To determine differences across soil depths, data were analyzed with a two-way analysis of variance (ANOVA), in which depth and sampling period were the two main factors. These were followed by post-hoc Tukey tests using net and gross N_2O and CH_4 fluxes, net CO_2 flux, soil pH, soil moisture, $ln(NO_3^-)$, NH_4^+, Fe_{AO}, Al_{CA}, Fe_{CA}, $ln(Al_{AO})$, $Fe(II)_{HCl}$, and $Fe(III)_{HCl}$ concentrations, nested within depth values and sampling periods. Data were log-transformed when necessary to meet ANOVA assumptions. Statistical significance was determined at $p < 0.10$ level unless otherwise noted. Univariate Outlier detection was performed using the Quantile Range Outliers method, only two data outliers for gross CH_4 production and gross CH_4 consumption were detected in the same replicate. To determine the effect of outliers, means were calculated both with and without outliers. Generalized pairwise regression analyses were used to explore relationships between measured soil characteristics and gross and net CH_4 and N_2O fluxes. Values presented in the text are means ± standard errors unless otherwise noted.

4.4 Results

4.4.1 Net ecosystem greenhouse gas fluxes

Soil GHG emissions averaged 7.3 ± 1.2 g CO_2 m^{-2} d^{-1}, 4.2 ± 0.6 mg N_2O m^{-2} d^{-1} and of 0.29 ± 0.23 CH_4 mg m^{-2} d^{-1} (Figure 1). Daily mean soil respiration peaked in late June 2020 at 62.2 ± 1.5 g CO_2 m^{-2} d^{-1} with a minimum value of 0.09 ± 0.01 g CO_2 m^{-2} d^{-1} observed during soil inundation in February 2020. Maximum daily N_2O fluxes were 92.7 ± 2.5 mg N_2O m^{-2} d^{-1} in December 2019 shortly following the onset of soil flooding, and a minimum daily flux of -1.4 ± 2.5 mg N_2O m^{-2} d^{-1} was observed in October 2019 under drained conditions. Both mean net N_2O and CH_4 fluxes were significantly different across sampling dates (Figure 1, $p < 0.01$). Net mean N_2O fluxes were 8.8 ± 0.3 mg N_2O m^{-2} d^{-1} during the drained sampling date and 29.7 ± 2.5 mg N_2O m^{-2} d^{-1} during the flooded sampling date. Daily mean net N_2O sink observations (range: -0.03 to -1.4 mg N_2O m^{-2} d^{-1}) represented 17.1% (n = 44 days) of all daily mean flux values during the study period. Maximum daily CH_4 fluxes were 16.3 ± 3.1 mg CH_4 m^{-2} d^{-1} in May 2020 and occurred only after an extended period of flooded conditions. Otherwise, this system was a daily net CH_4 sink (range: -0.03 to -13.7 mg CH_4 m^{-2} d^{-1}) for 62% (n = 159 days) of the study period. Net CH_4 fluxes observed on the drained sampling date averaged -0.10 ± 0.01 mg CH_4 m^{-2} d^{-1}, while during the flooded sampling date averaged -0.81 ± 0.17 mg CH_4 m^{-2} d^{-1}.

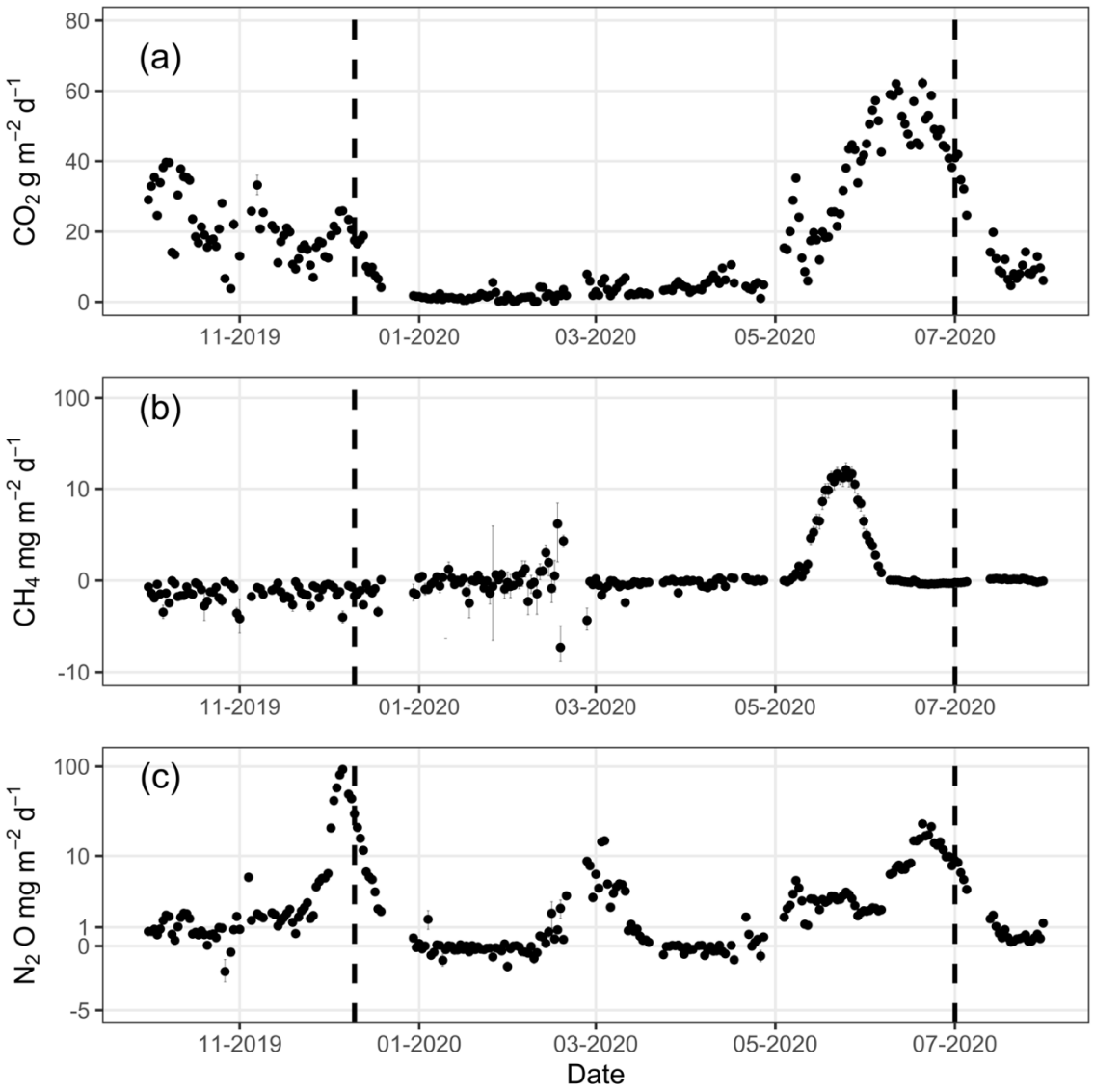

Figure 1. Daily mean greenhouse gas fluxes from October 2019 through July 2020 (± standard error) for (a) CO_2 (g CO_2 m^{-2} d^{-1}), (b) CH_4 (mg CH_4 m^{-2} d^{-1}), and (c) N_2O (mg N_2O m^{-2} d^{-1}). Black circles are daily mean flux measurements with black error bars representing daily standard error. Sampling dates for stable isotope pool dilution experiments are marked with dotted lines. Both (b) CH_4 and (c) N_2O use a pseudo-log scale to highlight net consumption and daily flux variability.

4.3.2 Gross and net N_2O fluxes

In the lab experiment, both gross N_2O production and net N_2O fluxes were significantly greater in the flooded (December) versus drained (July) soils (Figure 2a and 2c, $p < 0.05$). When soils were drained, individual gross N_2O production rates ranged from 0 µg N g $soil^{-1}$ d^{-1} at 0-15 cm to 5.2 µg N g $soil^{-1}$ d^{-1} at 30-60 cm, with the highest rates of both production and

consumption observed in the 30-60 cm samples. When soils were flooded, individual gross N_2O production rates ranged from a low of 0 µg N g soil^{-1} d^{-1} to a maximum of 8.1 µg N g soil^{-1} d^{-1}, both observed at 15-30 cm.

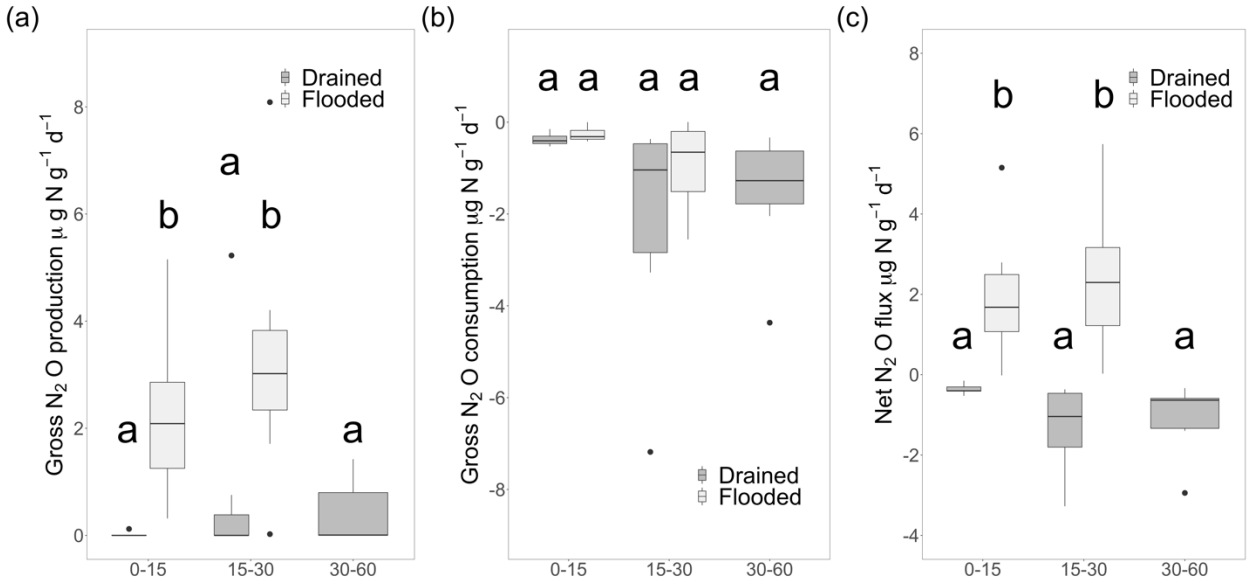

Figure 2. Boxplots of (a) gross N_2O production (µg N g^{-1} d^{-1}), (b) gross N_2O consumption (µg N g^{-1} d^{-1}), and (c) net N_2O flux (µg N g $^{-1}$ d^{-1}) across 0–15, 15–30, and 30-60 cm depths in flooded (white) and drained (gray) soils. Significant differences between soil depths and sampling dates are represented with letters at $p < 0.05$. Note the differences across y-axes.

Similar gross N_2O consumption rates were observed during both sampling periods (Figure 2b). There were no statistically significant differences in gross consumption rates across depths, although the variability of consumption rates increased at 15-30 and 30-60 cm (Figure 2b). Given the lack of observed differences in gross N_2O consumption across sampling periods, changes in gross N_2O production rates drove patterns in net N_2O fluxes (Figure 2c). Mean net N_2O fluxes were significantly greater at both depths during flooding (Figure 2c, $p < 0.01$). Average rates ranged from -1.1 ± 0.3 µg N g soil^{-1} d^{-1} at 30-60 cm during the drained period to 2.4 ± 0.7 µg N g soil^{-1} d^{-1} at 15-30 cm when flooded.

Gross N_2O consumption rates increased with gross N_2O production rates below 15 cm depth (R^2 = 0.50-0.83, $p < 0.08$, n = 35; Figure 3). In flooded surface soils, gross N_2O production was significantly greater than gross N_2O consumption in all samples, driving net N_2O emissions (Figure 2c). In drained soils, gross N_2O consumption was generally greater than gross production across all depths (Figures 2a and 2b).

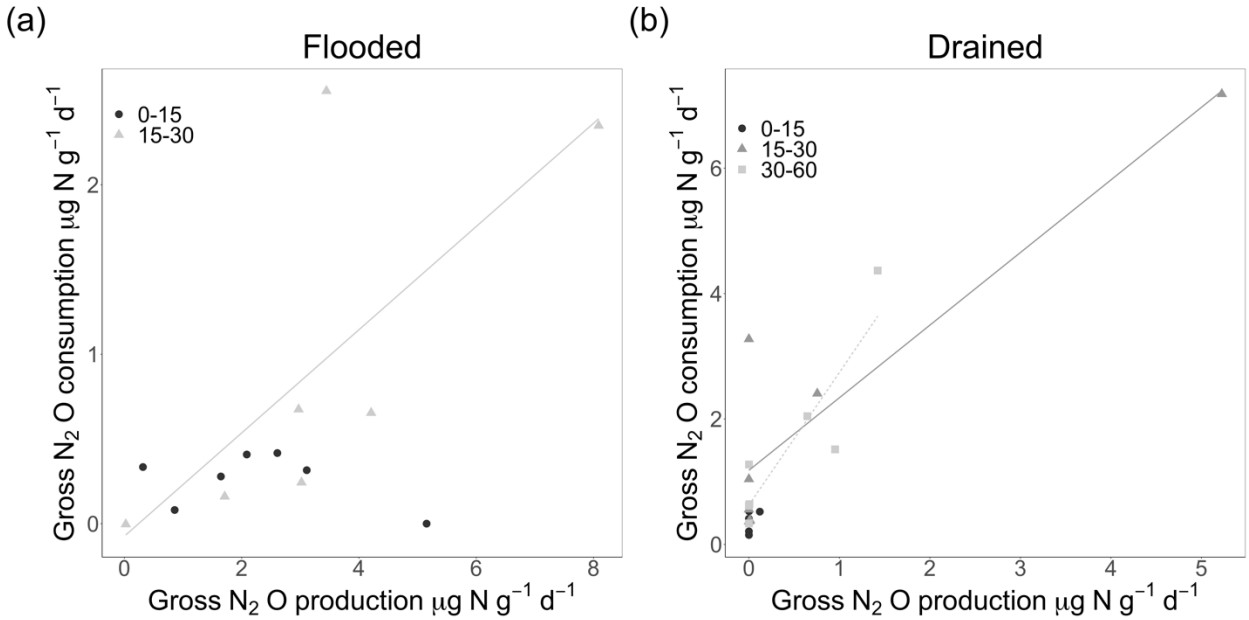

Figure 3. Linear relationships between gross N_2O production (μg N g^{-1} d^{-1}) and gross N_2O consumption (μg N g^{-1} d^{-1}) in (a) flooded and (b) drained soils across 0-15 cm (black circles), 15-30 cm (grey triangles and 30-60 cm (light grey squares). In (a), the solid line represents a linear fit for 15-30 cm soils ($R^2 = 0.50$, $p = 0.07$) In (b), the solid line represents a linear fit for 15-30 cm soils ($R^2 = 0.83$ $p < 0.01$) and the dashed line represents a linear fit for 15-30 cm soils ($R^2 = 0.80$, $p < 0.01$). Note the differences across y-axes.

The ratio of NO_3^- to CO_2 concentrations, a relationship used to calculate N_2O emissions in numerous ecosystem models (Del Grosso et al., 2000), was significantly greater in flooded soils at both 0-15 (flooded: 29.4 ± 8.5, drained: 5.5 ± 2.4) and 15-30 cm (flooded: 16.0 ± 3.3, drained: 6.0 ± 2.6, $p < 0.01$; Figure 4a) and exhibited similar trends to gross N_2O production. Median N_2O production to N_2O consumption ratios were up to four magnitudes greater in flooded versus drained surface soils ($p < 0.001$; Figure 4b).

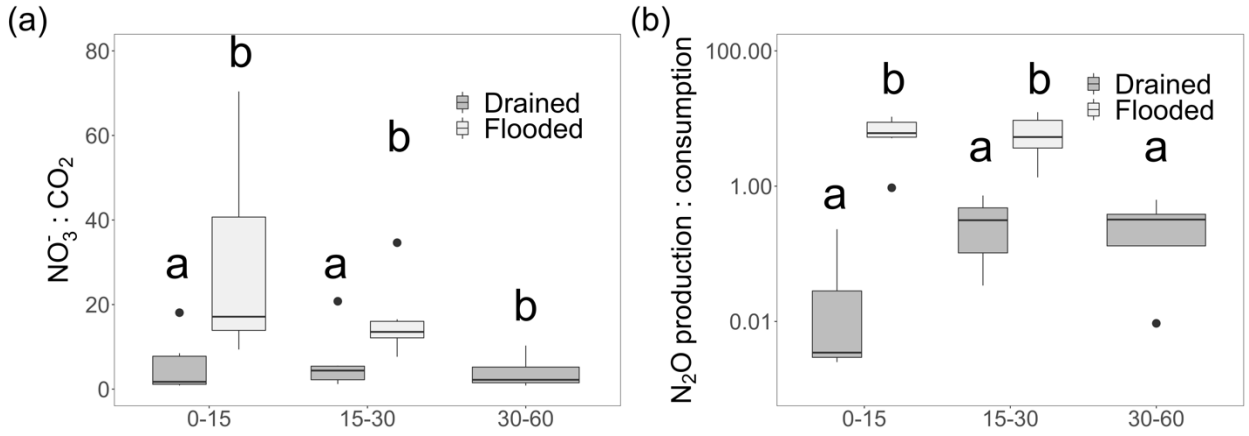

Figure 4. Boxplots of (a) NO_3^- to CO_2 ratios and (b) N_2O production: N_2O consumption ratios across 0–15, 15–30, and 30-60 cm depths in flooded (white) and drained (grey) soils. Significant differences between soil depths and sampling dates are represented with letters at $p < 0.05$.

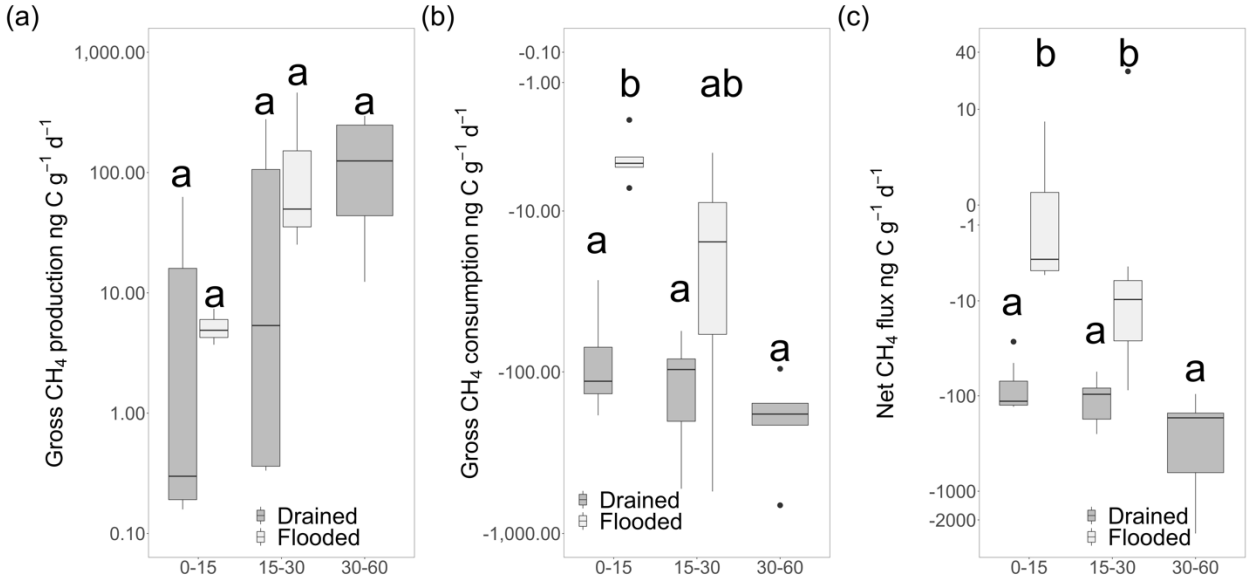

Figure 5. Boxplots of (a) gross CH_4 production (ng C g soil^{-1} d^{-1}), (c) gross CH_4 consumption (ng C g soil^{-1} d^{-1}), and (c) net CH_4 flux (ng C g soil^{-1} d^{-1}) across 0–15, 15–30, and 30-60 cm depths in flooded (white) and drained (grey) soils. Significance between soil depths. Significant differences between soil depths and sampling dates are represented with letters at $p < 0.01$. Note the differences across y-axes.

4.4.3 Gross and net CH_4 and net CO_2 fluxes

Gross CH_4 consumption rates were consistently greater than gross CH_4 production rates within seasons and depths (Figure 5). Gross CH_4 consumption rates in surface soils were significantly greater when soils were drained (drained: 108 ± 21 ng C g soil^{-1} d^{-1}, flooded: 3.5 ± 1.0 ng C g soil^{-1} d^{-1}, Figure 5b, $p < 0.001$). This increased the net CH_4 sink across depths by

approximately two orders of magnitude in July relative to December. In drained soils, CH_4 consumption rates were not statistically different across soil depths but were always greater than CH_4 production rates. Gross CH_4 production in drained soils was also not statistically different across depths. When soils were flooded**,** both maximum CH_4 production and consumption rates significantly increased with depth, and net fluxes were close to zero. Under flooded conditions, the individual outlier observations (15-30 cm) increased gross mean CH_4 production by 383% and gross mean CH_4 consumption by 361%, respectively.

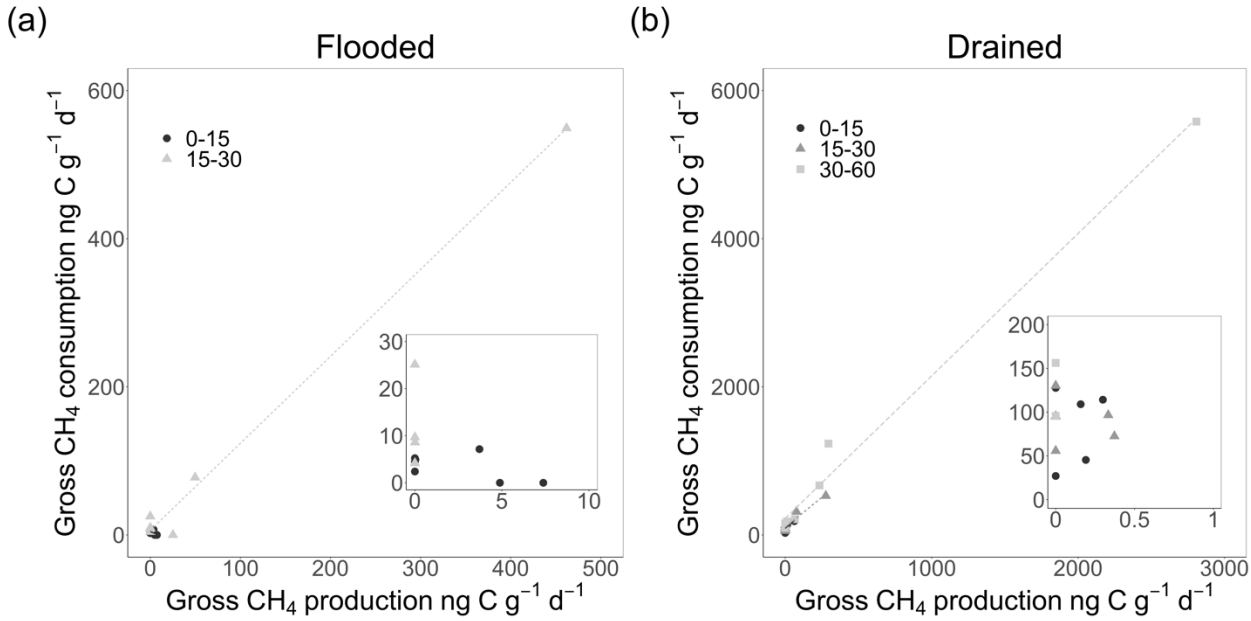

Figure 6. Log-linear relationships of gross CH_4 production (ng C g^{-1} d^{-1}) and gross CH_4 consumption (ng C g^{-1} d^{-1}) rates from with (a) flooded and (b) drained soils across 0–15 cm (black circles), 15-30 cm (grey triangles), and 30-60 cm (light grey squares). In (a), linear fits are represented by a dashed line for 15-30cm soils ($R^2 = 0.99$, $p = 0.08$). In (b), linear fits are represented by the solid line for 0-15 cm soils ($R^2 = 0.50$, $p = 0.08$), a dashed line for 15-30 cm soils ($R^2 = 0.93$, $p < 0.001$) and a long-dashed light grey line for 30-60 cm soils ($R^2 = 0.99$, $p < 0.001$).

Overall, gross CH_4 consumption was positively correlated with gross CH_4 production (Figure 6, $R^2 = 0.33$-0.99, $p < 0.05$, n = 35). Removing the largest production and consumption replicates from both datasets did not statistically impact this relationship under drained conditions ($p < 0.001$) but did reduce the significance under flooded conditions ($p = 0.08$). Gross CH_4 production rates were not significantly correlated to any soil characteristics measured, and periods of zero gross production represented 33% and 43% of samples from drained and flooded sample periods, respectively. Net CO_2 fluxes were not statistically different across depths or sampling periods (Figure 6a). The fraction of net CO_2 flux produced from CH_4 consumption, calculated by dividing gross CH_4 consumption rates by net CO_2 flux, varied significantly across sampling periods in 0-15 cm soils (Figure 7b, $p < 0.01$) but no significant differences were

observed at 15-30 cm. Gross CH_4 consumption contributed to a mean (± standard error) of 6.6 ± 3.4% of net CO_2 production in drained soils 30-60 cm with a maximum observation of 24.9%.

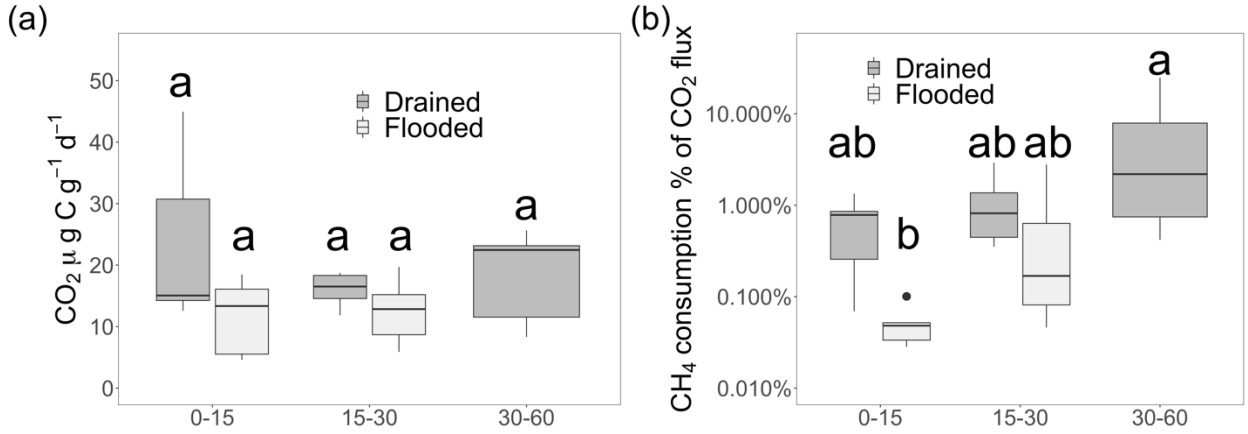

Figure 7. Boxplots of (a) net CO_2 flux (µg C g soil^{-1} d^{-1}) and (b) CH_4 consumption percent of CO_2 flux across 0–15, 15–30, and 30-60 cm depths in flooded (grey) and drained (white) soils. Significant differences between soil depths and sampling dates are represented with letters at $p <$ 0.01

4.4.4 Soil characteristics

Soil moisture ranged from 23.2 ± 0.6 % in surface drained soils to 47.0 ± 1.0% for the 15-13 cm depth flooded soils (Table 2) and differed significantly between sampling periods ($p <$ 0.001). Soil moisture was also significantly different across depths within both drained ($p <$ 0.001) and flooded ($p = 0.05$) sampling periods. Soil pH was significantly higher in drained versus flooded soils at both depths (Table 2, $p < 0.001$). The highest mean pH value was observed at 15-30 cm in drained soils and the lowest values were at 15-30 cm in flooded soils. Soil NH_4^+ ranged from 2.3 µg N g soil^{-1} at 0-15 cm in flooded conditions to 14.4 µg N g soil^{-1} at 15-30 cm in drained conditions (Table 2). Soil NH_4^+ concentrations were significantly higher in surface soils when drained compared to flooded soils but there were not significant differences in soils at 15-30 cm at depth (Table 2, $p = 0.001$-0.02). Soil NO_3^- concentrations were significantly greater in flooded soils at 0-15 cm ($p <0.001$). Soil NO_3^- concentrations at 15-30 cm were not statistically different given the large variation observed in drained soils, ranging from 18.6 to 227 µg N g soil^{-1}.

Both Al_{CA} and Al_{AO} were significantly higher in drained soils at all depths (Table 2, $p <$ 0.001). Al_{CA}, which represents a reactive, poorly crystalline Al pool, was highest in the 30-60 cm soil when drained ($p = 0.01$) and at 15-30 cm when flooded ($p < 0.01$). No statistically significant differences were observed in Al_{AO} (reactive organo-Al complexes) concentrations across depths.

Table 2. Comparison of soil characteristics across soil depths and sampling periods (mean ± SE). Letters indicate significant differences between depth and sampling periods ($p < 0.02$).

Variable	Depth (cm)	Drained (± SE)	Flooded (± SE)
Soil Moisture (%)	**0-15**	23.2 ± 0.6 c	42.1 ± 2.0 a
	15-30	28.2 ± 0.6 c	47.0 ± 1.0 a
	30-60	34.2 ± 0.1 b	-
pH	**0-15**	6.05 ± 0.06 a	5.62 ± 0.03 b
	15-30	6.30 ± 0.08 a	5.6 ± 0.04 b
	30-60	6.16 ± 0.05 a	-
Al_{AO} (mg g $soil^{-1}$)	**0-15**	2.7 ± 0.1 a	0.6 ± 0.1 b
	15-30	3.0 ± 0.3 a	0.9 ± 0.1 b
	30-60	3.2 ± 0.1 a	-
Al_{CA} (mg g $soil^{-1}$)	**0-15**	1.7 ± 0.1 a	0.8 ± 0.1 c
	15-30	1.6 ± 0.1 a	1.2 ± 0.1 ac
	30-60	2.3 ± 0.3 b	-
NO_3^- (µg N g $soil^{-1}$)	**0-15**	85 ± 28 a bc	239 ± 30 a
	15-30	101 ± 47 bc	172 ± 18 ab
	30-60	51 ± 12 c	-
NH_4^+ (µg N g $soil^{-1}$)	**0-15**	6.6 ± 1.1 a	3.6 ± 0.5 b
	15-30	7.5 ± 1.9 ab	4.9 ± 0.5 ab
	30-60	4.7 ± 0.5 ab	-

Soil $Fe(III)_{HCl}$ concentrations were significantly lower in drained soils at both 0-15 and 15-30 cm (Table 3, 0-15 cm: $p = 0.02$, 15-30 cm: $p = 0.01$). Soil Fe_{CA} concentrations, representing a reactive, poorly crystalline Fe pool, did not differ significantly across depths or sampling periods. In contrast Fe_{AO}, representative of organo-Fe complexes, exhibited significantly greater concentrations across all depths in drained soils ($p < 0.001$). Drained soils exhibited the highest mean concentrations of both Fe_{CA} and Fe_{AO}, with 11.2 ± 1.3 mg g^{-1} Fe_{CA} at 15-30 cm and 8.3 ± 0.9 mg g^{-1} Fe_{AO} at 30-60 cm, respectively.

Table 3. Comparison of reactive Fe pools across soil depths and sampling periods (mean ± SE). Letters indicate significant differences between sampling periods ($p < 0.02$).

Variable	Depth (cm)	Drained (± SE)	Flooded (± SE)
% Fe(II)	0-15	8.9 ± 1.0 ab	5.6 ± 0.1 b
	15-30	12.1 ± 2.1 a	5.7 ± 0.1 b
	30-60	11.4 ± 1.7 a	-
$Fe(II)_{HCl}$ (mg g $soil^{-1}$)	0-15	0.55 ± 0.03 ab	0.48 ± 0.04 b
	15-30	0.59 ± 0.04 ab	0.56 ± 0.04 ab
	30-60	0.74 ± 0.07 a	-
$Fe(III)_{HCl}$ (mg g $soil^{-1}$)	0-15	5.9 ± 0.5 bc	8.2 ± 0.8 ab
	15-30	4.9 ± 0.8 c	9.1 ± 0.5 a
	30-60	6.1 ± 0.5 bc	-
Fe_{CA} (mg g $soil^{-1}$)	0-15	7.0 ± 0.5 a	6.5 ± 0.6 a
	15-30	7.2 ± 0.4 a	7.6 ± 0.8 a
	30-60	8.3 ± 0.9 a	-
Fe_{AO} (mg g $soil^{-1}$)	0-15	8.6 ± 0.2 a	4.6 ± 0.4 b
	15-30	11.1 ± 1.3 a	5.5 ± 0.5 b
	30-60	10.4 ± 0.4 a	

4.4.5 Relationships with gross N_2O and CH_4 fluxes

Gross N_2O consumption in subsurface soils was significantly positively correlated with NO_3^- concentrations when soils were drained (Figure 8a, $p < 0.01$). Gross N_2O production in the flooded soils was positively correlated to both soil moisture (0-15cm: $R^2 = 0.40$, 15-30 cm: $R^2 = 0.35$, Figure 8b) and soil pH (0-15cm: $R^2 = 0.40$, 15-30 cm: $R^2 = 0.35$, Figure 8c). Gross N_2O production was also correlated to soil moisture across all samples ($R^2 = 0.36$, $p < 0.01$). Gross CH_4 consumption rates were significantly negatively correlated to soil moisture ($R^2 = 0.54$, $p < 0.001$) and positively related to soil pH ($R^2 = 0.70$, $p < 0.001$) at 0-15 cm across sampling periods (Figure 9). Observed relationships were strongest in surface soils, with weaker relationships observed with increasing soil depth.

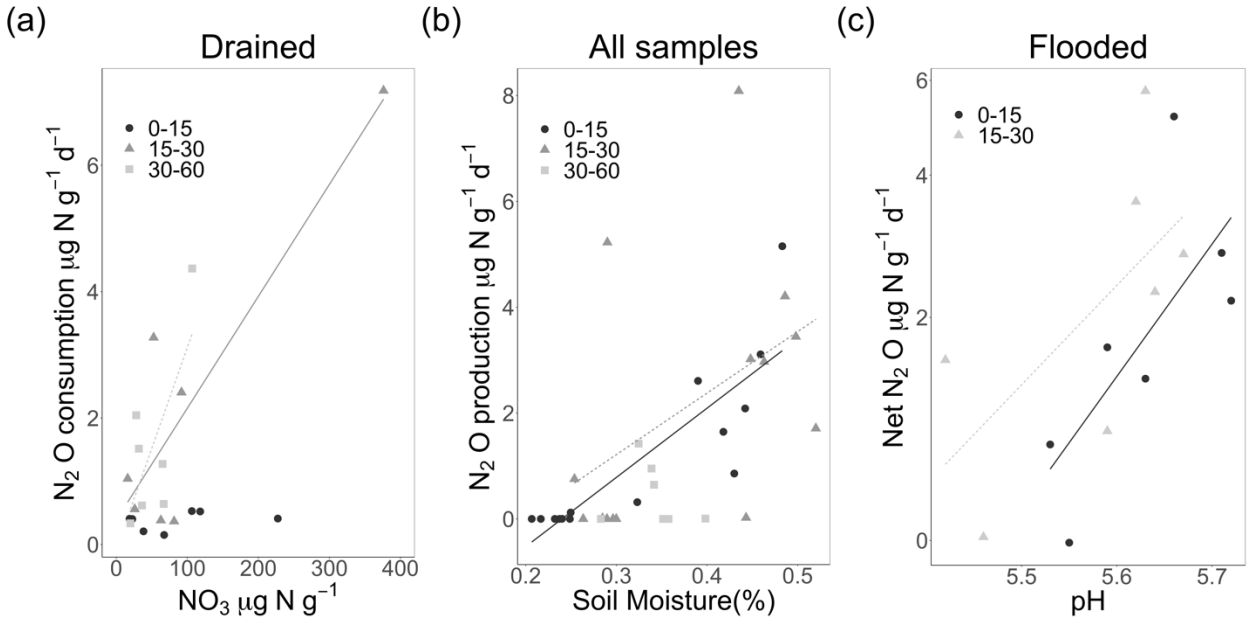

Figure 8. Linear relationships between (a) summer drained NO_3^- (μg N g^{-1} d^{-1}) and gross N_2O consumption (μg N g^{-1} d^{-1}) (15-30 cm: $R^2 = 0.79$, 30-60 cm: $R^2 = 0.50$, $p < 0.01$), (b) measurements of soil moisture (%) vs gross N_2O production across all samples (μg N g^{-1} d^{-1}) (0-15 cm: $R^2 = 0.74$, 15-30 cm: $R^2 = 0.22$, $p < 0.01$) and (c) winter flooded soil pH and net N_2O flux (μg N g^{-1} d^{-1}) (0-15cm: $R^2 = 0.40$, 15-30 cm: $R^2 = 0.35$, $p < 0.01$). Black circles and solid lines represent 0-15 cm, grey triangles and dashed lines represent 15-30 cm, and grey squares and long-dashed lines represent 30-60 cm.

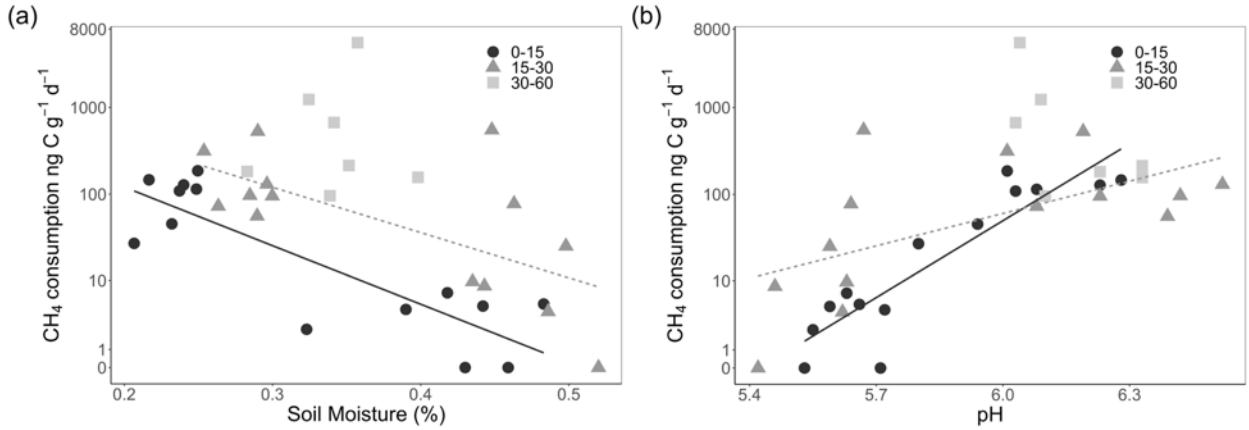

Figure 9. Log-linear relationships of gross CH_4 consumption (ng C g^{-1} d^{-1}) rates from all samples with (a) soil moisture and (b) soil pH across 0–15 cm (black circles)), 15-30 cm (grey triangles). In (a), linear fits are represented by the solid line for 0-15 cm soils ($R^2 = 0.88$, $p < 0.001$) and a dashed line for 15-30cm soils ($R^2 = 0.25$, $p = 0.08$). In (b), linear fits are represented by the solid line for 0-15 cm soils ($R^2 = 0.64$, $p < 0.001$) and a dashed line for 15-30cm soils ($R^2 = 0.32$, $p < 0.05$).

4.5 Discussion

4.5.1 Nitrous oxide dynamics

Increased soil moisture associated with flooding and associated changes in soil O_2 availability (Anthony & Silver, 2021) substantially increased surface net N_2O fluxes and gross N_2O production in the subsoil relative to drained conditions, partially confirming our hypothesis. This increase was likely driven by denitrification stimulated by both elevated NO_3^- concentrations from aerobic nitrification prior to winter flooding and decreased soil O_2 concentrations at the onset of soil wetting (Anthony & Silver, 2021). Gross N_2O consumption was positively correlated with gross production at depth in flooded soils, suggesting more complete denitrification at depth as soils experienced increasingly anaerobic soil conditions. Continuous flux measurements during flooded conditions show this system was a net N_2O sink followed an extended period of anaerobic conditions suggesting the occurrence of extracellular N_2O consumption (Schlesinger, 2013). However, N_2O consumption was not correlated with gross N_2O production in the flooded surface soils. The high NO_3^- concentrations observed may have led to a dominance of incomplete denitrification to N_2O as opposed to higher rates of N_2 production (Firestone & Davidson, 1989). Ratios of N_2O production to N_2O consumption under flooded soil conditions further support that NO_3^- and O_2 concentrations likely regulate soil redox state in surface soils, generating conditions unfavorable to complete denitrification (Firestone & Davidson, 1989).

We observed low rates of both gross N_2O production and gross N_2O consumption in drained surface (0-15 cm) soils, driven by lower soil moisture that likely increases O_2 diffusion (Anthony & Silver, 2021). In drained soils both N_2O production and consumption rates increased with soil depth, although gross production rates were not significantly correlated to any measured soil characteristics. In periodically flooded agricultural soils, Fe redox cycling has been shown to drive microtopographic variations in N_2O emissions (Krichels, Sipic, et al., 2019). Therefore it was surprising we observed no relationships between gross N_2O fluxes and reactive Fe pools given and the numerous potential interactions between Fe and N pathways (Clément et al., 2005; Krichels, Sipic, & Yang, 2019; Megonigal et al., 2004; Peters & Conrad, 1996; Wang et al., 2016 Yang, Weber, & Silver, 2012). The elevated C and NO_3^- observed likely maintained an active denitrifier community with microbially-mediated denitrification driving N_2O production, overriding any potential influence of Fe-mediated chemodenitrification.

4.5.2 Methane dynamics

Soils sampled during the drained period were a significant net CH_4 sink, with net fluxes regulated by gross CH_4 consumption evidenced by strong positive correlations between gross CH_4 production and consumption. Gross CH_4 production and consumption both increased with depth, suggesting CH_4 consumption is likely coupled to nearby sources of CH_4 production. During drainage, CH_4 consumption contributed up to 25% of the CO_2 produced in subsoils and

may be a significant pathway of net C loss even in these high emitting soils. We also observed that both gross and net CH_4 consumption were negatively correlated with increasing soil moisture and increasing soil acidity. Higher pH and lower O_2 availability are known limit methanotrophic activity (Conrad, 2007; Hütsch, Webster, & Powlson, 1994). While pH generally increases with decreasing soil redox (Peters & Conrad, 1996) soil pH values in the flooded soils were lower than in the drained soils, likely driven by organic acid deprotonation via increased organic matter mineralization in oxidized C-rich soils (Anthony & Silver, 2021; Fageria & Nascente, 2014). Gross CH_4 consumption was negatively correlated with increasing soil moisture, suggesting O_2 diffusion limitations with elevated soil moisture limited aerobic methanotrophic activity (Anthony & Silver, 2021; Tiedje, Sexstone, Parkin, & Revsbech, 1984). This increase in anaerobic conditions with soil depth was also associated with increasing gross CH_4 production as increases in soil moisture further limited O_2 diffusion into subsoils. There were no consistent trends between gross CH_4 fluxes and soil mineralogical indices, suggesting bulk soil redox conditions as the main control on gross CH_4 flux.

4.6 Conclusion

Our study found the magnitude and distribution of gross N_2O and CH_4 production and consumption in an agricultural peatland soil varied with depth and flooding management. Variation in soil moisture content and its likely effect on redox and substrate availability were key drivers of gross N_2O and CH_4 fluxes. Soil NO_3^- concentrations and soil moisture content drove gross N_2O production, suggesting denitrification as the main pathway mediating N_2O fluxes. Gross CH_4 consumption was always greater than gross CH_4 production and both increased with soil depth, suggesting CH_4 availability strongly influenced CH_4 consumption and CH_4 consumption generally regulated net CH_4 flux. Both elevated soil moisture and decreasing pH were associated with decreased CH_4 consumption rates in flooded soils, like directly affecting CH_4 consumption. The effects of soil depth on soil diffusion limitations and substrate availability also contributed to the trends observed, suggesting more reducing conditions at depth limit net N_2O flux during flooded conditions but increase CH_4 consumption under drained conditions. Our results further our understanding on how gross production and consumption pathways mediate net soil greenhouse fluxes and soil flooding stimulates N_2O emissions through increases in gross N_2O production while decreasing net CH_4 uptake through decreases in gross consumption. Further research is needed to explore the importance of organo-Al complexation in generating anaerobic hotspots of microbial activity and the importance of hot spots on gross N_2O and CH_4 fluxes, as well as exploring the relevance of gross CH_4 consumption during hot moments of net CH_4 flux.

4.7 Acknowledgments

We appreciate assistance from Heather Dang, Tibisay Peréz, Wendy Yang, Brian Yudkin, and Summer Ahmed. This work was supported by a Contract by the California Department of Water Resources (award 4600011240). We thank the California Department of

Water Resources and the Metropolitan Water District of Southern California for research site access. T. L. Anthony was supported by the California Sea Grant Delta Science Fellowship. This material is based upon work supported by the Delta Stewardship Council Delta Science Program under Grant No. 5298 and California Sea Grant College Program Project R/SF-89. The contents of this material do not necessarily reflect the views and policies of the Delta Stewardship Council or California Sea Grant, nor does mention of trade names or commercial products constitute endorsement or recommendation for use. McIntire Stennis grant CA- B-ECO-7673-MS to W. L. Silver partially supported this work. W. L. Silver was also supported by funds from Breakthrough Strategies & Solutions, and the V. Kann Rasmussen, Oak Creek, Jewish Community, Northern Trust, and Trisons Foundations.

4.8 References

Allen, L. H. (2012). Greenhouse gas fluxes of drained organic and flooded mineral agricultural soils in the United States. *Managing Agricultural Greenhouse Gases*, (3), 221–238. https://doi.org/10.1016/B978-0-12-386897-8.00013-9

Angle, J. C., Morin, T. H., Solden, L. M., Narrowe, A. B., Smith, G. J., Borton, M. A., … Wrighton, K. C. (2017). Methanogenesis in oxygenated soils is a substantial fraction of wetland methane emissions. *Nature Communications*, *8*(1), 1567. https://doi.org/10.1038/s41467-017-01753-4

Anthony, T. L., & Silver, W. L. (2020). Mineralogical associations with soil carbon in managed wetland soils. *Global Change Biology*, (March), 1–13. https://doi.org/10.1111/gcb.15309

Anthony, T. L., & Silver, W. L. (2021). Hot moments drive extreme nitrous oxide and methane emissions from agricultural peatlands. *Global Change Biology*, *n/a*(n/a). https://doi.org/https://doi.org/10.1111/gcb.15802

Bender, M., & Conrad, R. (1994). Methane oxidation activity in various soils and freshwater sediments: Occurrence, characteristics, vertical profiles, and distribution on grain size fractions. *Journal of Geophysical Research*, *99*(D8), 16531. https://doi.org/10.1029/94JD00266

Bender, M., & Conrad, R. (1995). Effect of Ch4 Concentrations and Soil Conditions on the Induction of Ch4 Oxidation Activity. *Soil Biology and Biochemistry*, *27*(12), 1517–1527.

Bernhardt, E. S., Blaszczak, J. R., Ficken, C. D., Fork, M. L., Kaiser, K. E., & Seybold, E. C. (2017). Control Points in Ecosystems: Moving Beyond the Hot Spot Hot Moment Concept. *Ecosystems*, *20*(4), 665–682. https://doi.org/10.1007/s10021-016-0103-y

Booth, M. S., Stark, J. M., & Rastetter, E. (2005). Controls on nitrogen cycling in terrestrial ecosystems: A synthetic analysis of literature data. *Ecological Monographs*, *75*(2), 139–157. https://doi.org/10.1890/04-0988

Butterbach-Bahl, K., Baggs, E. M., Dannenmann, M., Kiese, R., & Zechmeister-Boltenstern, S. (2013). Nitrous oxide emissions from soils: how well do we understand the processes and their controls? *Philosophical Transactions of the Royal Society of London. Series B, Biological Sciences*, *368*(1621), 20130122.

https://doi.org/10.1098/rstb.2013.0122
Camilo, R.-S., Szutu, D., Baldocchi, D., & Hemes, K. (2021). AmeriFlux US-Bi2 Bouldin Island corn. United States. https://doi.org/10.17190/AMF/1419513
Cardinael, R., Guenet, B., Chevallier, T., Dupraz, C., Cozzi, T., & Chenu, C. (2017). Additional SOC storage in a long-term agroforestry system is explained by high organic inputs – An overview combining experimental and modeling approaches. *Biogeosciences Discussions*, (April). https://doi.org/10.5194/bg-2017-125
Chatskikh, D., Olesen, J. E., Berntsen, J., Regina, K., & Yamulki, S. (2005). Simulation of effects of soils, climate and management on N2O emission from grasslands. *Biogeochemistry*, *76*(3), 395–419. https://doi.org/10.1007/s10533-005-6996-8
Chen, C., Hall, S. J., Coward, E., & Thompson, A. (2020). Iron-mediated organic matter decomposition in humid soils can counteract protection. *Nature Communications*, *11*(1), 2255. https://doi.org/10.1038/s41467-020-16071-5
Clément, J. C., Shrestha, J., Ehrenfeld, J. G., & Jaffé, P. R. (2005). Ammonium oxidation coupled to dissimilatory reduction of iron under anaerobic conditions in wetland soils. *Soil Biology and Biochemistry*, *37*(12), 2323–2328. https://doi.org/10.1016/j.soilbio.2005.03.027
Congreves, K. A., Brown, S. E., Németh, D. D., Dunfield, K. E., & Wagner-Riddle, C. (2017). Differences in field-scale N2O flux linked to crop residue removal under two tillage systems in cold climates. *GCB Bioenergy*, *9*(4), 666–680. https://doi.org/10.1111/gcbb.12354
Conrad, R. (1996a). Soil Microorganisms as Controllers of Atmospheric Trace Gases (H2 , CO, CH4, OCS, N2O, and NO), *60*(4), 609–640.
Conrad, R. (1996b, December). *Soil microorganisms as controllers of atmospheric trace gases (H2, CO, CH4, OCS, N2O, and NO)*. *Microbiological Reviews*. Retrieved from http://mmbr.asm.org/content/60/4/609.abstract
Conrad, R. (2007). Microbial Ecology of Methanogens and Methanotrophs. *Advances in Agronomy*, *96*(07), 1–63. https://doi.org/10.1016/S0065-2113(07)96005-8
Del Grosso, S. J., Parton, W. J., Mosier, a R., Ojima, D. S., Kulmala, a E., & Phongpan, S. (2000). General model for N2O and N2 gas emissions from soils when comparing observed and gas emission rates from irrigated field soils used for model testing NO2. *Global Biogeochemical Cycles*, *14*(4), 1045–1060.
Fageria, N. K., & Nascente, A. S. (2014). *Management of soil acidity of South American soils for sustainable crop production*. *Advances in Agronomy* (Vol. 128). Elsevier. https://doi.org/10.1016/B978-0-12-802139-2.00006-8
Feng, J., Yang, T., Li, F., Zhou, X., Xu, C., & Fang, F. (2021). Impact of tillage on the spatial distribution of CH4 and N2O in the soil profile of late rice fields. *Soil and Tillage Research*, *211*(3), 105029. https://doi.org/10.1016/j.still.2021.105029
Firestone, M. K., & Davidson, E. A. (1989). Microbiologial Basis of NO and N2O production and consumption in soil. *Exchange of Trace Gases between Terrestrial Ecosystems and the Atmosphere*, (November), 7–21. https://doi.org/10.1017/CBO9781107415324.004
Fredrickson, J. K., Zachara, J. M., Kennedy, D. W., Dong, H., Onstott, T. C., Hinman, N. W., & Li, S. M. (1998). Biogenic iron mineralization accompanying the

dissimilatory reduction of hydrous ferric oxide by a groundwater bacterium. *Geochimica et Cosmochimica Acta*, *62*(19–20), 3239–3257. https://doi.org/10.1016/S0016-7037(98)00243-9

Groffman, P. M., Butterbach-Bahl, K., Fulweiler, R. W., Gold, A. J., Morse, J. L., Stander, E. K., … Vidon, P. (2009). Challenges to incorporating spatially and temporally explicit phenomena (hotspots and hot moments) in denitrification models. *Biogeochemistry*, *93*(1–2), 49–77. https://doi.org/10.1007/s10533-008-9277-5

Hall, S. J., & Silver, W. L. (2015). Reducing conditions, reactive metals, and their interactions can explain spatial patterns of surface soil carbon in a humid tropical forest. *Biogeochemistry*, *125*(2), 149–165. https://doi.org/10.1007/s10533-015-0120-5

Hart, S. C., Stark, J. M., Davidson, E. A., & Firestone, M. K. (1994). Nitrogen Mineralization, Immobilization, and Nitrification. In R. W. Weaver, J. S. Angle, & P. S. Bottomley (Eds.), *Methods of Soil Analysis, Part 2. Microbial and Biochemical Properties* (pp. 985–1018). Madison, WI: Soil Science Society of America.

Hatala, J. A., Detto, M., Sonnentag, O., Deverel, S. J., Verfaillie, J., & Baldocchi, D. D. (2012). Greenhouse gas (CO2, CH4, H2O) fluxes from drained and flooded agricultural peatlands in the Sacramento-San Joaquin Delta. *Agriculture, Ecosystems and Environment*, *150*, 1–18. https://doi.org/10.1016/j.agee.2012.01.009

Hemes, K. S., Chamberlain, S. D., Eichelmann, E., Anthony, T., Valach, A., Kasak, K., … Baldocchi, D. D. (2019). Assessing the carbon and climate benefit of restoring degraded agricultural peat soils to managed wetlands. *Agricultural and Forest Meteorology*, *268*, 202–214. https://doi.org/10.1016/j.agrformet.2019.01.017

Huang, W., Ye, C., Hockaday, W. C., & Hall, S. J. (2020). Trade-offs in soil carbon protection mechanisms under aerobic and anaerobic conditions. *Global Change Biology*, (March), 3726–3737. https://doi.org/10.1111/gcb.15100

Huang, X., Tang, H., Kang, W., Yu, G., Ran, W., Hong, J., & Shen, Q. (2018). Redox interface-associated organo-mineral interactions: A mechanism for C sequestration under a rice-wheat cropping system. *Soil Biology and Biochemistry*, *120*, 12–23. https://doi.org/10.1016/j.soilbio.2018.01.031

Hütsch, B. W., Webster, C. P., & Powlson, D. S. (1994). Methane oxidation in soil as affected by land use, soil pH and N fertilization. *Soil Biology and Biochemistry*, *26*(12), 1613–1622. https://doi.org/10.1016/0038-0717(94)90313-1

Jobbágy, E. G., & Jackson, R. B. (2001). The distribution of soil nutrients with depth: Global patterns and the imprint of plants. *Biogeochemistry*, *53*(1), 51–77. https://doi.org/10.1023/A:1010760720215

Kammann, C., Hepp, S., Lenhart, K., & Müller, C. (2009). Stimulation of methane consumption by endogenous CH4 production in aerobic grassland soil. *Soil Biology and Biochemistry*, *41*(3), 622–629. https://doi.org/10.1016/J.SOILBIO.2008.12.025

Keiluweit, M., Wanzek, T., Kleber, M., Nico, P., & Fendorf, S. E. (2017). Anaerobic

Microsites have an Unaccounted Role in Soil Carbon Stabilization. *Nature Communications*, *8*(1771), 1–8. https://doi.org/10.1038/s41467-017-01406-6
Kleber, M., Eusterhues, K., Keiluweit, M., Mikutta, C., Mikutta, R., & Nico, P. S. (2015). *Mineral-Organic Associations: Formation, Properties, and Relevance in Soil Environments*. *Advances in Agronomy* (Vol. 130). Elsevier Ltd. https://doi.org/10.1016/bs.agron.2014.10.005
Koehler, B., Corre, M. D., Steger, K., Well, R., Zehe, E., Sueta, J. P., & Veldkamp, E. (2012). An in-depth look into a tropical lowland forest soil: Nitrogen-addition effects on the contents of N2O, CO2 and CH4 and N2O isotopic signatures down to 2-m depth. *Biogeochemistry*, *111*(1–3), 695–713. https://doi.org/10.1007/s10533-012-9711-6
Kögel-Knabner, I., Amelung, W., Cao, Z., Fiedler, S., Frenzel, P., Jahn, R., … Schloter, M. (2010). Biogeochemistry of paddy soils. *Geoderma*, *157*(1–2), 1–14. https://doi.org/10.1016/j.geoderma.2010.03.009
Kravchenko, A. N., Toosi, E. R., Guber, A. K., Ostrom, N. E., Yu, J., Azeem, K., … Robertson, G. P. (2017). Hotspots of soil N2O emission enhanced through water absorption by plant residue. *Nature Geoscience*, (June). https://doi.org/10.1038/ngeo2963
Krichels, A. H., DeLucia, E. H., Sanford, R., Chee-Sanford, J., & Yang, W. H. (2019). Historical soil drainage mediates the response of soil greenhouse gas emissions to intense precipitation events. *Biogeochemistry*, *142*(3), 425–442. https://doi.org/10.1007/s10533-019-00544-x
Krichels, A. H., Sipic, E., & Yang, W. H. (2019). Iron redox reactions can drive microtopographic variation in upland soil carbon dioxide and nitrous oxide emissions. *Soil Systems*, *3*(3), 1–16. https://doi.org/10.3390/soilsystems3030060
Krichels, A. H., & Yang, W. H. (2019). Dynamic Controls on Field-Scale Soil Nitrous Oxide Hot Spots and Hot Moments Across a Microtopographic Gradient. *Journal of Geophysical Research: Biogeosciences*, *124*(11), 3618–3634. https://doi.org/10.1029/2019JG005224
Le Mer, J., & Roger, P. (2001). Production, oxidation, emission and consumption of methane by soils: A review. *European Journal of Soil Biology*, *37*(1), 25–50. https://doi.org/10.1016/S1164-5563(01)01067-6
Liptzin, D., & Silver, W. L. (2015). Spatial patterns in oxygen and redox sensitive biogeochemistry in tropical forest soils. *Ecosphere*, *6*(November), 1–14. https://doi.org/10.1890/ES14-00309.1
Liu, H., Zak, D., Rezanezhad, F., & Lennartz, B. (2019). Soil degradation determines release of nitrous oxide and dissolved organic carbon from peatlands. *Environmental Research Letters*, *14*(9), 094009. https://doi.org/10.1088/1748-9326/ab3947
Loeppert, R. H., & Inskeep, W. P. (1996). *Methods of Soil Analysis. Part 3. Chemical Methods*.
McLean, E. O. (1982). Soil pH and Lime Requirement. In *Page, A.L., Ed., Methods of Soil Analysis. Part 2. Chemical and Microbiological Properties, American Society of Agronomy, Soil Science Society of America, Madison,* (pp. 199–224).
Megonigal, J. P., Hines, M. E., & Visscher, P. T. (2003). Anaerobic Metabolism:

Linkages to Trace Gases and Aerobic Processes. In *Treatise on Geochemistry* (pp. 317–424). Elsevier. https://doi.org/10.1016/B0-08-043751-6/08132-9
Molodovskaya, M., Singurindy, O., Richards, B. K., Warland, J., Johnson, M. S., & Steenhuis, T. S. (2012). Temporal Variability of Nitrous Oxide from Fertilized Croplands: Hot Moment Analysis. *Soil Science Society of America Journal*, *76*(5), 1728. https://doi.org/10.2136/sssaj2012.0039
Morley, N., Baggs, E. M., Dörsch, P., & Bakken, L. (2008). Production of NO, N2O and N2 by extracted soil bacteria, regulation by NO2- and O2 concentrations. *FEMS Microbiology Ecology*, *65*(1), 102–112. https://doi.org/10.1111/j.1574-6941.2008.00495.x
Oertel, C., Matschullat, J., Zurba, K., Zimmermann, F., & Erasmi, S. (2016). Greenhouse gas emissions from soils - A review. *Chemie Der Erde - Geochemistry*, *76*(3), 327–352. https://doi.org/10.1016/j.chemer.2016.04.002
Pellerin, B., Anderson, F. E., & Bergamaschi, B. (2014). *Assessing the role of winter flooding on baseline greenhouse gas fluxes from corn fields in the Sacramento-San Joaquin Bay Delta*. *California Energy Commission*.
Peters, V., & Conrad, R. (1996). Sequential reduction processes and initiation of CH4 production upon flooding of oxic upland soils. *Soil Biology and Biochemistry*, *28*(3), 371–382, doi:10.1016/0038-0717(95)00146-8. https://doi.org/10.1016/0038-0717(95)00146-8
Petrakis, S., Seyfferth, A., Kan, J., Inamdar, S., & Vargas, R. (2017). Influence of experimental extreme water pulses on greenhouse gas emissions from soils. *Biogeochemistry*. https://doi.org/10.1007/s10533-017-0320-2
Potter, C. S. (1997). An ecosystem simulation model for methane production and emission from wetlands. *Global Biogeochemical Cycles*, *11*(4), 495–506. https://doi.org/10.1029/97GB02302
Rasmussen, C., Heckman, K., Wieder, W. R., Keiluweit, M., Lawrence, C. R., Berhe, A. A., … Wagai, R. (2018). Beyond clay: towards an improved set of variables for predicting soil organic matter content. *Biogeochemistry*. https://doi.org/10.1007/s10533-018-0424-3
Savage, K., Phillips, R., & Davidson, E. (2014). High temporal frequency measurements of greenhouse gas emissions from soils. *Biogeosciences*, *11*(10), 2709–2720. https://doi.org/10.5194/bg-11-2709-2014
Schlesinger, W. H. (2013). An estimate of the global sink for nitrous oxide in soils. *Global Change Biology*, *19*(10), 2929–2931. https://doi.org/10.1111/gcb.12239
Serrano-Silva, N., Sarria-Guzmàn, Y., Dendooven, L., & Luna-Guido, M. (2014). Methanogenesis and Methanotrophy in Soil: A Review. *Pedosphere*, *24*(3), 291–307. https://doi.org/10.1016/S1002-0160(14)60016-3
Sihi, D., Davidson, E. A., Savage, K. E., & Liang, D. (2020). Simultaneous numerical representation of soil microsite production and consumption of carbon dioxide, methane, and nitrous oxide using probability distribution functions. *Global Change Biology*, *26*(1), 200–218. https://doi.org/10.1111/gcb.14855
Six, J., & Paustian, K. (2014). Aggregate-associated soil organic matter as an ecosystem property and a measurement tool. *Soil Biology and Biochemistry*, *68*, A4–A9. https://doi.org/10.1016/j.soilbio.2013.06.014

Smith, P., Cai, Z., Gwary, D., Janzen, H., Kumar, P., McCarl, B., … Sirotenko, O. (2007). Agriculture In Climate Change 2007: Mitigation. *Cambridge University Press*, (4), 1–44. https://doi.org/10.2753/JES1097-203X330403

Soil Survey Staff. (2020). Natural Resources Conservation Service, United States Department of Agriculture. Official Soil Series Descriptions. Available online. Accessed [June/08/2020].

Taft, H. E., Cross, P. A., Hastings, A., Yeluripati, J., & Jones, D. L. (2019). Estimating greenhouse gases emissions from horticultural peat soils using a DNDC modelling approach. *Journal of Environmental Management*, *233*(January), 681–694. https://doi.org/10.1016/j.jenvman.2018.11.113

Teh, Y. A., Silver, W. L., Sonnentag, O., Detto, M., Kelly, M., & Baldocchi, D. D. (2011). Large Greenhouse Gas Emissions from a Temperate Peatland Pasture. *Ecosystems*, *14*(2), 311–325. https://doi.org/10.1007/s10021-011-9411-4

Theodorus, S., Weideveld, J., Liu, W., Berg, M. Van Den, Peter, L., Lamers, M., & Fritz, C. (2020). Sub-soil irrigation does not lower greenhouse gas emission from drained peat meadows, (July). https://doi.org/doi.org/10.5194/bg-2020-230

Thorup-Kristensen, K., Halberg, N., Nicolaisen, M., Olesen, J. E., Crews, T. E., Hinsinger, P., … Dresbøll, D. B. (2020). Digging Deeper for Agricultural Resources, the Value of Deep Rooting. *Trends in Plant Science*, *25*(4), 406–417. https://doi.org/10.1016/j.tplants.2019.12.007

Tiedje, J. M., Sexstone, A. J., Parkin, T. B., & Revsbech, N. P. (1984). Anaerobic processes in soil. *Plant and Soil*, *76*(1–3), 197–212. https://doi.org/10.1007/BF02205580

Torrent, I. R. J. (1997). Citrate-Ascorbate as a Highly Selective Extractant for Poorly Crystalline Iron Oxides. *Soil Science Society of America Journal*, *61*, 1647–1654. https://doi.org/10.2136/sssaj1997.03615995006100060015x

Totsche, K. U., Amelung, W., Gerzabek, M. H., Guggenberger, G., Klumpp, E., Knief, C., … Kögel-Knabner, I. (2017). Microaggregates in soils. *Journal of Plant Nutrition and Soil Science*, 104–136. https://doi.org/10.1002/jpln.201600451

Viollier, E., Inglett, P. W., Hunter, K., Roychoudhury, A. N., & Van Cappellen, P. (2000). The ferrozine method revisited: Fe(II)/Fe(III) determination in natural waters. *Applied Geochemistry*, *15*(6), 785–790. https://doi.org/10.1016/S0883-2927(99)00097-9

von Fischer, J. C., & Hedin, L. O. (2002). Separating methane production and consumption with a field-based isotope pool dilution technique. *Global Biogeochemical Cycles*, *16*(3). https://doi.org/10.1029/2001GB001448

Wang, M., Hu, R., Zhao, J., Kuzyakov, Y., & Liu, S. (2016). Iron oxidation affects nitrous oxide emissions via donating electrons to denitrification in paddy soils. *Geoderma*, *271*, 173–180. https://doi.org/10.1016/j.geoderma.2016.02.022

Well, R., & Butterbach-Bahl, K. (2013). Comments on "A test of a field-based 15N-nitrous oxide pool dilution technique to measure gross N2O production in soil" by Yang et al. (2011), Global Change Biology, 17, 3577-3588. *Global Change Biology*, *19*(1), 133–135. https://doi.org/10.1111/gcb.12005

Wiesmeier, M., Urbanski, L., Hobley, E., Lang, B., von Lützow, M., Marin-Spiotta, E., … Kögel-Knabner, I. (2019). Soil organic carbon storage as a key function of

soils - A review of drivers and indicators at various scales. *Geoderma*, *333*(July 2018), 149–162. https://doi.org/10.1016/j.geoderma.2018.07.026
Xing, H., Wang, E., Smith, C. J., Rolston, D., & Yu, Q. (2011). Modelling nitrous oxide and carbon dioxide emission from soil in an incubation experiment. *Geoderma*, *167–168*(3), 328–339. https://doi.org/10.1016/j.geoderma.2011.07.003
Yang, W. H., & Liptzin, D. (2015). High potential for iron reduction in upland soils. *Ecology*, *96*(7), 2015–2020. https://doi.org/10.1890/14-2097.1
Yang, W. H., & Silver, W. L. (2016). Net soil-atmosphere fluxes mask patterns in gross production and consumption of nitrous oxide and methane in a managed ecosystem. *Biogeosciences*, *13*(5), 1705–1715. https://doi.org/10.5194/bg-13-1705-2016
Yang, W. H., Teh, Y. A., & Silver, W. L. (2011). A test of a field-based 15N-nitrous oxide pool dilution technique to measure gross N2O production in soil. *Global Change Biology*, *17*(12), 3577–3588. https://doi.org/10.1111/j.1365-2486.2011.02481.x
Yang, W. H., Teh, Y. A., & Silver, W. L. (2013). Measuring gross N2O production in soil: A reply to Well and Butterbach-Bahl. *Global Change Biology*, *19*(4), 985–987. https://doi.org/10.1111/gcb.12097
Yang, W. H., Weber, K. A., & Silver, W. L. (2012). Nitrogen loss from soil through anaerobic ammonium oxidation coupled to iron reduction. https://doi.org/10.1038/ngeo1530
Zhu, X., Burger, M., Doane, T. A., & Horwath, W. R. (2013). Ammonia oxidation pathways and nitrifier denitrification are significant sources of N2O and NO under low oxygen availability. *Proceedings of the National Academy of Sciences of the United States of America*, *110*(16), 6328–6333. https://doi.org/10.1073/pnas.1219993110

4.9 Appendix

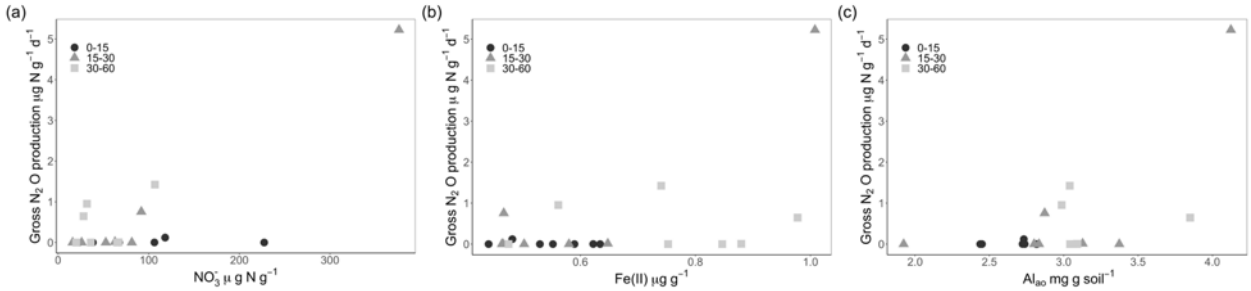

Supplemental Figure 1. Relationships between (a) NO_3^- (μg N g^{-1} d^{-1}) and gross N_2O production (μg N g^{-1} d^{-1}) (b) measurements of Fe (II) (μg g^{-1}) and gross N_2O production (μg N g^{-1} d^{-1}) and (c) organo-Al complexes (Al_{AO} mg g $soil^{-1}$) and gross N_2O production (μg N g^{-1} d^{-1}). Black circles lines represent 0-15 cm, grey triangles represent 15-30 cm, and grey squares and lines represent 30-60 cm.

In **Chapters 3 and 4** I quantified total soil carbon dioxide (CO_2), nitrous oxide (N_2O), and methane (CH_4) emissions and further explored their controls in an organic-rich agricultural peatland soil. We found that organic-rich agricultural peatland soils were significant sources of both N_2O and CH_4, and targeted analyses further confirmed that flood irrigation was the dominant control on both N_2O and CH_4 emissions. However, the controls on greenhouse gas emissions may differ between organic-rich and mineral-rich agricultural peatlands. **In Chapter 5**, I quantified total soil CO_2, N_2O, and CH_4 emissions from a mineral-rich alfalfa peatland ecosystem. I build on **Chapters 3 and 4** by conducting similar analyses in this mineral-rich soil ecosystem to further explore the controls on greenhouse emissions in agricultural soils. Additionally, quantifying total ecosystem greenhouse gas budgets from a mineral-rich alfalfa ecosystem helped directly compare agricultural peatland emissions across soil types and land uses. This comparison is needed to appropriately prioritize wetland restoration projects that maximally reduce greenhouse emissions.

Chapter 5. Continuous, long-term soil greenhouse gas measurements from flood-irrigated alfalfa

5.1 Abstract

Agriculture is a significant source of carbon dioxide (CO_2) and methane (CH_4) and is the dominant source of anthropogenic nitrous oxide (N_2O) emissions. Changes in agricultural land management practices that reduce overall greenhouse gas (GHG) emissions have been suggested to help mitigate climate change, but a better understanding of the timing, magnitude, and drivers of GHG fluxes is needed. Alfalfa agroecosystems may be significant sources of N_2O given their ability to increase N inputs through symbiotic N_2 fixation and frequent irrigation events that create conditions for hot moments of N_2O production. However, few studies have explored long-term N_2O emissions and their associated drivers in alfalfa ecosystems. We collected over 108,000 CO_2, CH_4 and N_2O soil-atmosphere flux measurements over four years using cavity ring-down spectroscopy from a conventional alfalfa field in California, USA. This ecosystem was a consistent source of N_2O (annual mean: 624.4 ± 27.8 mg N_2O m^{-2} yr^{-1}, range: 263.6. ± 5.6 to 901.9 ± 74.5 mg N_2O m^{-2} yr^{-1}) and a small net sink of CH_4 (annual mean: -53.5 ± 2.5 mg CH_4 m^{-2} yr^{-1}, range: -78.2 ± 8.8 to -31.6 ± 2.5 mg CH_4 m^{-2} yr^{-1}). Soil CO_2 fluxes averaged 4925.9 ± 13.5 g CO_2 m^{-2} yr^{-1} and were greater than other alfalfa ecosystem estimates, likely driven by elevated temperatures and plant productivity throughout the growing season. Hot moments of N_2O flux represented only 0.2% to 1.1% of annual measurements but were 31.6% to 56.8% of the annual flux. We found that both the magnitude and the contribution of N_2O hot moments to annual emissions decreased over time. Normalized difference vegetation index (NDVI), soil temperature, moisture, and O_2 were all significantly correlated with soil CO_2, N_2O, and CH_4 fluxes, although associations varied across both soil depth and timescales. Our results suggest that flood-irrigated alfalfa is a significant source of agricultural N_2O emissions, and that plant productivity and soil moisture effects on O_2 availability may modulate the net GHG budget of alfalfa agroecosystems.

5.2 Introduction

The agricultural sector is a significant source of anthropogenic greenhouse gas (GHG) emissions of carbon dioxide (CO_2) and methane (CH_4) and is the dominant source of anthropogenic nitrous oxide (N_2O) (Oertel, Matschullat, Zurba, Zimmermann, & Erasmi, 2016; Smith et al., 2007; U.S Energy Information Administration, 2011). Alfalfa (*Medicago Sativa* L.) is the most widely grown perennial forage legume worldwide and is the largest crop by acreage in the Western United States (Ottman et al., 2013; Yang et al., 2008). Alfalfa is traditionally used as dairy cattle feed and growth in alfalfa acreage is largely driven by increasing global feed demand for dairy and other livestock production (Q. Wang, Hansen, & Xu, 2013).

Alfalfa has been suggested as a more climate-friendly feedstock than corn given its potential to increase soil C sequestration as a deep-rooting, perennial plant (Alberti et al., 2010). Alfalfa can also fix atmospheric dinitrogen (N_2) thus decreasing the need for inorganic nitrogen fertilizers. Long-term continuous flux measurements of CO_2 and CH_4 suggest that agricultural alfalfa systems can be net GHG sinks (Alberti et al., 2010; Hemes et al., 2019), but few long-term datasets exist for N_2O flux measurements from continuous alfalfa (Burger, Haden, Chen, Six, & Horwath, 2016; Burton, Bergstrom, Covert, Wagner-Riddle, & Beauchamp, 1997; Savage, Phillips, & Davidson, 2014; Wagner-Riddle, Thurtell, Kidd, Beauchamp, & Sweetman, 1997). Given alfalfa's increasing agricultural demand, continuous long-term GHG measurements with N_2O are needed to appropriately quantify total GHG budgets of alfalfa systems.

Alfalfa agroecosystems can be sources of N_2O to the atmosphere (Burger et al., 2016; Del Grosso et al., 2006) given their ability to increase N inputs through symbiotic N_2 fixation (Peterson & Russelle, 1991). Increased N inputs could stimulate both nitrification and denitrification, N transformation pathways that produce N_2O (Vinet & Zhedanov, 2010). Alfalfa typically has a high water demand (Jia et al., 2009), and is often irrigated throughout the growing season to maintain productivity. Irrigation events can create short periods of anaerobiosis (Tiedje, Sexstone, Parkin, & Revsbech, 1984), and when combined with elevated soil N inputs could create ideal conditions for hot moments of N_2O production (Butterbach-Bahl, Baggs, Dannenmann, Kiese, & Zechmeister-Boltenstern, 2013; Davidson, Keller, Erickson, Verchot, & Veldkamp, 2000). Previous short-term (<1 y) studies using periodic manual flux measurements identified irrigation events as a potential driver of N_2O production in alfalfa (Burger et al., 2016; J. Ning et al., 2020). However, short-term chamber measurements may miss or significantly underestimate the role of hot moments in annual N_2O fluxes (Anthony and Silver 2021).

Nitrous oxide fluxes are expected to increase with stand age in alfalfa, driven by increasing organic matter inputs from more developed root systems (Burger et al., 2016). However, irrigation frequency is likely to decrease over time in more established systems, particularly in systems supported by subsurface irrigation or a shallow water table (Kandelous et al., 2012; Noory, Liaghat, Chaichi, & Parsinejad, 2009; Shouse, Ayars, & Šimůnek, 2011).

Therefore, decreasing irrigation events with stand age may instead lower the occurrence and magnitude of N_2O emission events (Orchard & Cook, 1983).

Alfalfa is generally thought to be a net sink of CH_4 (Alberti et al., 2010; Hemes et al., 2019; Serrano-Silva, Sarria-Guzmàn, Dendooven, & Luna-Guido, 2014). Subsurface drip irrigation can also facilitate increased CH_4 uptake relative to flood irrigation (Meng et al., 2020; G. Wang et al., 2016). However, extended periods of soil inundation from flood irrigation or significant rainfall can create anaerobic conditions favorable for methanogenesis and net CH_4 emission (Estop-Aragones, Knorr, & Blodau, 2013). A better understanding of the role of soil moisture dynamics on net GHG fluxes is needed to determine the potential of alfalfa agriculture as a driver of climate change or climate change mitigation.

Here, we explored the patterns and drivers of soil-atmosphere fluxes of CO_2, CH_4 and N_2O in a conventional alfalfa field in California, USA. We used continuous cavity ring-down spectroscopy to collect over 108,000 N_2O, CH_4, and CO_2 flux measurements over four years to investigate the global warming potential of alfalfa ecosystems. Soil oxygen (O_2), moisture, and temperature sensors were installed in the soil profile and a yearlong soil mineral nitrogen (N) and soil pH sampling campaign were conducted in parallel to determine controls on net soil GHG fluxes. We hypothesized that elevated nitrate (NO_3^-) concentrations and flood irrigation during the growing season would stimulate hot moments of N_2O emission. For CH_4, we hypothesized that hot moments of CH_4 emissions would only occur following sustained periods of high soil moisture and low O_2 availability following heavy irrigation events or significant winter rainfall.

5.3 Methods

5.3.1 Site information

The study was conducted in the Sacramento-San Joaquin Delta region of California, USA (38.11ºN, 121.5ºW). Alfalfa and corn are the dominant agricultural land use in the region. The site was in conventional perennial alfalfa (> 5 years) that was periodically flood irrigated during the growing season. The climate was Mediterranean with hot dry summers and cool wet winters. The region's historical mean annual temperature was 15.1 ± 6.3 °C and a mean annual rainfall averaging 326 ± 4 mm (Hatala et al., 2012). Site year rainfall data was collected from a nearby (< 1 km) eddy covariance site (Camilo, Szutu, Baldocchi, & Hemes, 2021). Daily 3 m resolution normalized difference vegetation index (NDVI) was collected from Planet Labs satellite imagery (Houborg & McCabe, 2016; PlanetTeam, 2021) and subsampled in MATLAB (MathWorks, Natick, MA, USA) to only represent the field of interest.

Ryde is the major soil series found under alfalfa in the region and is widespread across the Sacramento San Joaquin-Delta and along the central coast of California (Soil Survey Staff, 2020). Ryde soils belong to the fine-loamy, mixed, superactive, thermic Cumulic Endoaquolls taxonomic class and are very deep, poorly drained soils formed in alluvium from mixed rock sources and decomposed vegetative matter (Soil Survey Staff, 2020). Total soil C concentrations

(mean ± standard error) were 5.26% ± 0.02% at 0-15 cm, 5.00% ± 0.15% at 15-30 cm, and 1.99% ± 0.09% at 30-60 cm (Anthony and Silver, 2020). Total soil N concentrations were 0.38% ± 0.003% at 0-15 cm, 0.35% ± 0.01% at 15-30 cm, and 0.16% ± 0.01% at 30-60 cm (Anthony and Silver, 2020).

5.3.2 Automated chamber measurements

Surface fluxes of N_2O, CH_4, and CO_2 were measured continuously from January 2017 to February 2021 using an automated chamber system. The system consisted of nine opaque, automated gas flux chambers (eosAC, Eosense, Nova Scotia, Canada) connected to a multiplexer (eosMX, Eosense, Nova Scotia, Canada). The multiplexer allowed for dynamically signaled chamber deployment and routed gases to a cavity ring-down spectrometer (Picarro G2508, Santa Clara, CA, USA). Chambers were measured sequentially over a 10 min sampling period with a 1.5 min flushing period before and after each measurement.

Chambers were deployed in a 10 x 10 m grid, with each chamber 5 m apart. Due to periodic flooding events, extended 15 cm soil collars were utilized to maintain measurement collection and ensure chambers were not inundated. When installed, chambers were randomly assigned to either plant rows (n = 5) or inter-plant areas of bare soil (n = 4). The extended 15 cm collars also allowed for the incorporation of plants inside closed chambers and raised chambers above the maximum water table height during flood irrigation. Chambers remained in their original positions throughout the field campaign, except for short periods (< 3 days) during field management activities (e.g., harvest, winter grazing). Plants within chambers were minimally trimmed as needed between harvests if plants inhibited chamber closure.

To determine chamber volume, chamber collar heights were measured weekly and interpolated between measurements to account for changes in chamber height over time. Chamber volumes were also used to calculate the minimum detectable flux of 0.002 nmol N_2O m^{-2} s^{-1}, 0.06 nmol CO_2 m^{-2} s^{-1}, and 0.002 nmol CH_4 m^{-2} s^{-1} (Nickerson, 2016). The minimum detectable fluxes reported here are conservative estimates, as the actual chamber volume was always smaller than the maximum theoretical volume used to calculate these values.

Flux calculations and analyses were first performed using Eosense eosAnalyze-AC v. 3.7.7 software, then data quality assessment and control were subsequently performed in R (RStudio, v.1.1.4633, O'Connell, Ruan, & Silver, 2018). Fluxes were removed from the final dataset if they were associated with erroneous spectrometer cavity temperature or pressure readings or if any gas concentrations were negative, corresponding to instrument malfunction. Fluxes were also removed if the chamber deployment period was less than 9 min or greater than 11 min, indicative of chamber malfunction. Data filtering removed 2.1% of flux measurement periods, generating a final dataset of 108,638 simultaneous flux measurements of CO_2, N_2O, and CH_4. Following data filtering, all statistical analyses were performed using JMP Pro 15 (SAS Institute Inc., Cary, NC). Differences in site year, hourly, and seasonal mean flux values were

analyzed with one-way ANOVAs followed by post-hoc Tukey tests. Values reported in the text are means ± standard errors unless otherwise noted.

5.3.3 Quantifying hot moments of N_2O emission

Following data filtering, the quantity and magnitude of hot moment measurements were determined to identify hot moments of N_2O emission and their impact on annual flux estimates. We defined hot moments as flux measurements with values greater than four standard deviations from the mean (Anthony & Silver, 2021), as statistically 99.9% of the population should fall within four standard deviations of the mean. Yearly mean flux values were then calculated for only hot moment fluxes, the entire flux dataset, and the flux dataset with hot moment observations removed to determine the impact of outlier fluxes on annual GHG emissions. Given our large and continuous dataset, we could also compare mean fluxes with and without high flux events (Benhadi-Marín, 2018, Anthony and Silver 2021) to better quantify the importance of hot moments.

5.3.4 Weekly soil measurements

Weekly soil samples (0-15 cm depth, n = 10/week) were collected from April 2018 to May 2019. Soil samples were analyzed for gravimetric soil moisture, soil pH, and 2M potassium chloride (KCl) extractable nitrate (NO_3^-) plus nitrite (NO_2^-) and ammonium (NH_4^+). For KCl extracts, we utilized a 5:1 ratio of 2 M KCl volume to oven dry equivalent (ODE) soil that were shaken for 1 hour and subsequently filtered with Whatman Grade 1 filter paper (Hart, Stark, Davidson, & Firestone, 1994). The KCl extracts were then analyzed colorimetrically for NH_4^+ and NO_3^- using an AQ300 analyzer (Seal Instruments, Mequon, WI). Soil moisture was determined gravimetrically by drying 10 g of field-fresh soil to a constant weight at 105 $^\circ$C. Soil pH was measured in a slurry of 10 g of field-fresh soil in 10 mL of distilled deionized water (McLean, 1982).

5.3.5 Soil sensor measurements

Two replicate sets of soil sensors were installed from September 2018-February 2021 at depths of 10 cm, 30 cm, and 50 cm. This included SO-110 oxygen (O_2) and soil temperature sensors (Apogee Instruments, Logan, UT) and CS616 moisture sensors (Campbell Scientific, Logan, UT) connected to a CR1000 datalogger (Campbell Scientific, Logan, UT) storing data at 15 min intervals. Sensors remained installed throughout the year. Erroneous data corresponding to sensor malfunction were removed from the dataset, which included 1.7% (n = 1,234) of soil moisture measurements and 3.4% (n = 2,472) of soil O_2 measurements. In total, there were 73 of 839 days missing during the soil sensor measurement period.

5.3.6 Weekly soil depth gas samples

Two replicate soil gas samples for CO_2, CH_4, and N_2O were taken approximately weekly at 10 cm, 30 cm, and 50 cm depths from September 2018 to December 2019. Instrument grade stainless steel 1/8" tubing (Restek, Bellefonte, PA) was installed in parallel to the soil sensors above, with approximately 15 cm of tubing with multiple sampling holes parallel to the soil surface. Sampling septa (Restek, Bellefonte, PA) were installed in 1/8" Swagelok union (Swagelok, Solon, OH) permanently connected to the stainless steel tubing. Septa were changed monthly. Gas samples were collected weekly with 30 ml BD syringes after first clearing the tubing dead volume. Short periods of soil inundation following extensive rainfall (March-April 2019) made it impossible to collect gas samples from some depths. Samples were stored over-pressurized with thick septa (Geomicrobial Technologies, Oechelata, OK) in 20 ml glass vials until manual sample injection analysis on a Shimadzu GC-34 (Shimadzu Corp., Tokyo, Japan). Generalized pairwise regression analyses were used to explore the relationships between measured soil atmosphere CO_2, CH_4, and N_2O concentrations across depths and surface soil CO_2, CH_4, and N_2O fluxes.

5.3.7 Wavelet coherence analysis

Wavelet coherence analysis was used to identify interactions between GHG fluxes, NDVI, and the soil variables measured (Liu, 1994; Wood, Detto, & Silver, 2013, Anthony and Silver 2021). Wavelet coherence measures the cross-correlation between time series and allowed us to explore relationships between GHG fluxes and potential controls of NDVI, O_2, moisture, and temperature at daily, monthly, and annual timescales. Wavelet coherence is derived from two time series as a function of decomposed frequency (Wave.xy) and the wavelet power spectrum (Power.x, Power.y) of each individual time series (Rösch & Schmidbauer, 2018):

$$Coherence = \frac{|Wave.xy|^2}{Power.x \cdot Power.y} \quad (1)$$

A more detailed description of the approach and calculations can be found in Rösch & Schmidbauer (2018) and Wood et al., (2013). Missing data were replaced with zeroes to compute an unbiased estimator of the wavelet variance for gappy time series (Mondal & Percival, 2010; Wood et al., 2013). Statistical significance (p-value) was computed using 1000 Monte Carlo simulations. All wavelet decomposition and coherence calculations were conducted using the WaveletComp 1.1 R package (Rösch & Schmidbauer, 2018).

5.4 Results

5.4.1 Greenhouse gas fluxes

Mean annual soil CO_2 flux rates were 4925.9 ± 13.5 g CO_2 m^{-2} y^{-1} and exhibited significant interannual variability with the lowest rates observed in year 4 (Table 1, $p < 0.001$). The soils were a consistent source of N_2O and consistent net sink of CH_4 on an annual scale. Annual mean soil N_2O emissions were 624.4 ± 27.8 mg N_2O m^{-2} y^{-1} and were highest in site

years 2 and 3 (Table 1, $p < 0.001$) and lowest in site year 4 ($p < 0.001$). Annual mean soil CH_4 emissions were -53.5 ± 2.5 mg CH_4 m^{-2} y^{-1}; the net CH_4 sink was significantly greater in site year 4 than all other years (Table 1, $p < 0.001$).

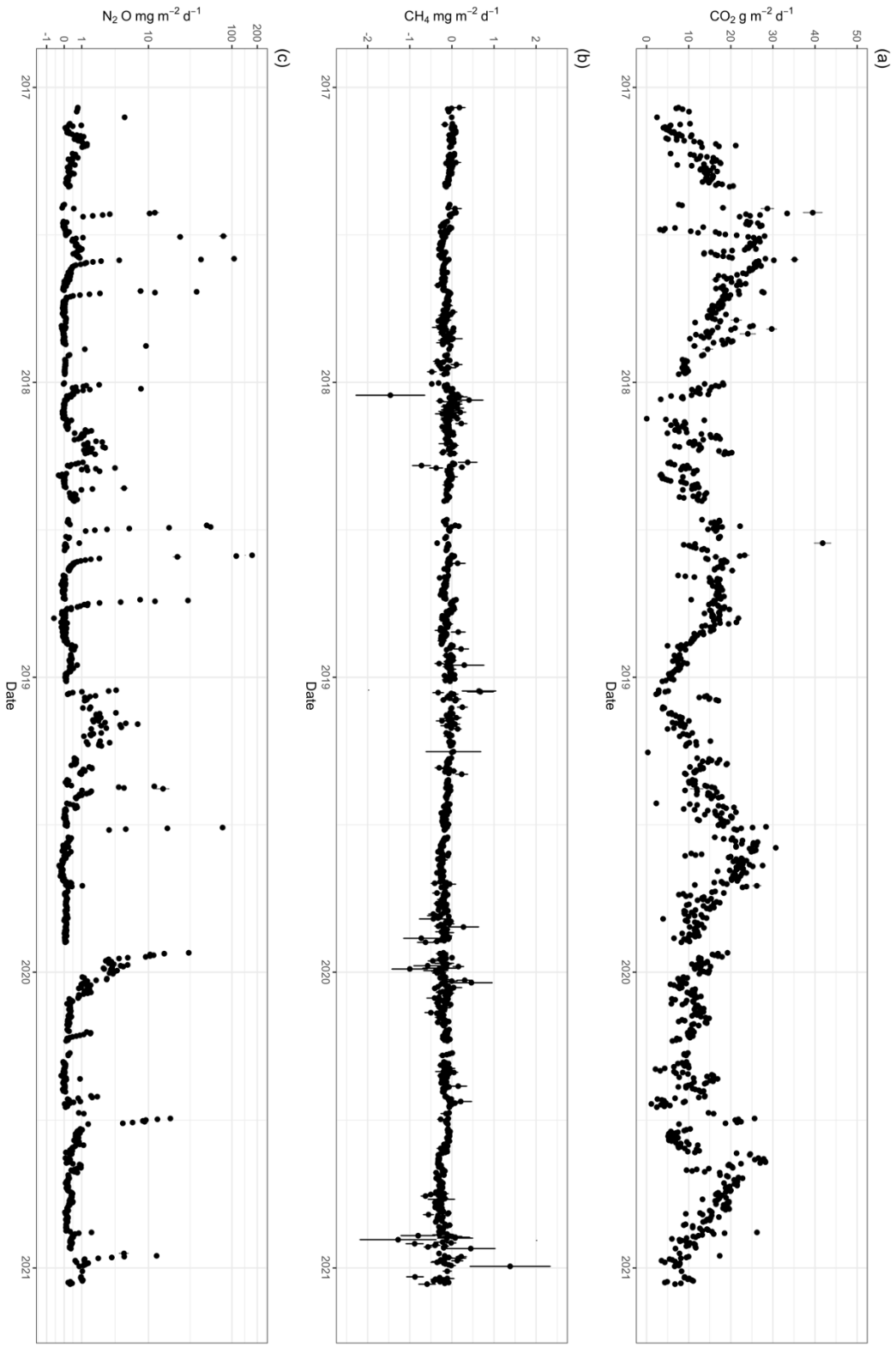

Figure 1. Daily mean fluxes (± standard error) for (a) CO_2 (g CO_2 m^{-2} d^{-1}), (b) CH_4 (mg CH_4 m^{-2} d^{-1}), and (c) N_2O (mg N_2O m^{-2} d^{-1})**.** Black circles represent daily mean flux measurements.

Soil CO_2 fluxes exhibited similar seasonal and diel trends to mean air temperature (Figures 2a, 2b, and 5), with emissions significantly higher during the summer and the lowest daily mean CO_2 fluxes observed during the winter (Figure 2b, $p < 0.001$). Diel trends in soil CH_4 fluxes were much more variable and were not significantly associated with any measured soil variable (Figure 2d). The largest negative CH_4 fluxes and largest variability observed occurred between 1600-2100 hours during the fall; the largest sinks were observed between 900-1200 hours during other seasons. Spring and winter CH_4 fluxes were significantly less negative than in summer and fall (Figure 2d, $p < 0.001$). We observed no significant effects of plant or bare soil sampling groups on overall CO_2, CH_4, or N_2O emissions.

Table 1. Mean (± standard error) annual CO_2, CH_4, and N_2O fluxes, annual mean 0-50 cm soil moisture, and total annual rainfall by site year (e.g January 27th to January 26th). *Site year 2 soil moisture values includes 5 out of 12 months. Letters denote significant differences between annual values ($p < 0.01$).

Site Year	Mean CO_2 flux (g CO_2 m^{-2} y^{-1})	Mean CH_4 flux (mg CH_4 m^{-2} y^{-1})	Mean N_2O flux (mg N_2O m^{-2} y^{-1})	Annual Soil Moisture (%)	Annual Rainfall (mm y^{-1})	Annual NDVI
1 (2017-2018)	5869.5 ± 31.4 a	-44.0 ± 2.2 ab	610.5 ± 68.1 a	-	444 a	-
2 (2018-2019)	4135.0 ± 25.4 b	-31.6 ± 2.5 a	901.9 ± 74.5 b	47.8 ± 7.8 b*	356 ab	0.76 ± 0.01 a
3 (2019-2020)	5217.3 ± 23.9 c	-60.6 ± 2.8 b	777.1 ± 52.0 ab	35.3 ± 17.1 a	447 a	0.71 ± 0.01 b
4 (2020-2021)	4565.2 ± 26.5 d	-78.2 ± 8.8 c	263.6. ± 5.6 c	24.3 ± 4.3 c	176 b	0.64 ± 0.01 c
All years	4925.9 ± 13.5	-53.5 ± 2.5	624.4 ± 27.8	31.5 ± 14	331 ± 64	0.70 ± 0.01

Soil N_2O fluxes were significantly greater in the summer and lowest in the fall (Figure 2c, $p < 0.001$). Summer hourly mean fluxes were at least an order of magnitude greater than all other seasons. In the summer, the only significant hourly differences observed were between the lowest N_2O fluxes at approximately 900 hours and the largest N_2O fluxes at 1800 hours ($p = 0.06$). The peak at 1800 hours may represent the onset of irrigation events that typically began in the late afternoon and lasted approximately 24 hours.

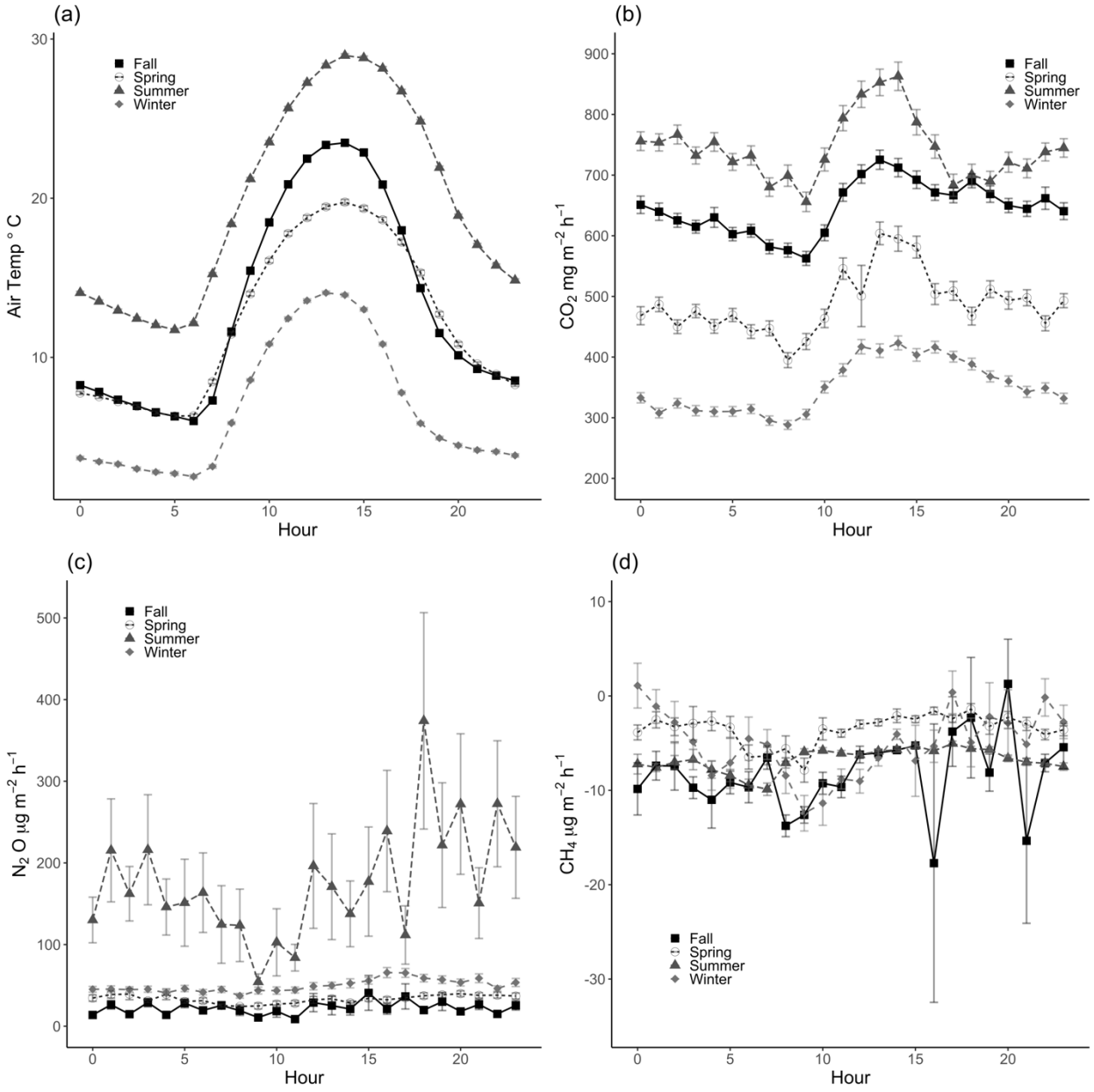

Figure 2. Hourly mean (± SE) (a) air temperature (ºC), (b) CO_2 fluxes (mg m^{-2} h^{-1}), (c) CH_4 fluxes (µg m^{-2} h^{-1}), and (d) N_2O fluxes (µg m^{-2} h^{-1}), grouped by season (Fall = squares, Spring = open circles, Summer = triangles, and Winter = diamonds) over the entire measurement period.

5.4.2 Soil biogeochemistry and greenhouse gas fluxes

Weekly soil pH values from April 2018-April 2019 averaged 5.82 ± 0.01, with weekly means ranging from 5.26 ± 0.03 in early October 2018 to 6.31 ± 0.04 in late March 2019. Soil NO_3^- concentrations averaged 4.9 ± 1.3 µg NO_3^- g $soil^{-1}$ and weekly variation in soil NO_3^- values was not associated with increased N_2O emissions (Figure 3b). Weekly soil NH_4^+ concentrations averaged 11.5 ± 0.8 µg NH_4^+ g $soil^{-1}$ and were not significantly associated with soil fluxes

(Figure 4b). Annual rainfall averaged 330.8 ± 63.5 and ranged from a max of 444 mm y^{-1} in site year 3 to a minimum of 176 mm y^{-1} in site year 4 (Table 1, $p < 0.01$). Annual soil moisture values (0-50 cm) were highest in year 2, significantly decreasing in years 3 and 4 (Table , 1$p <$ 0.001).

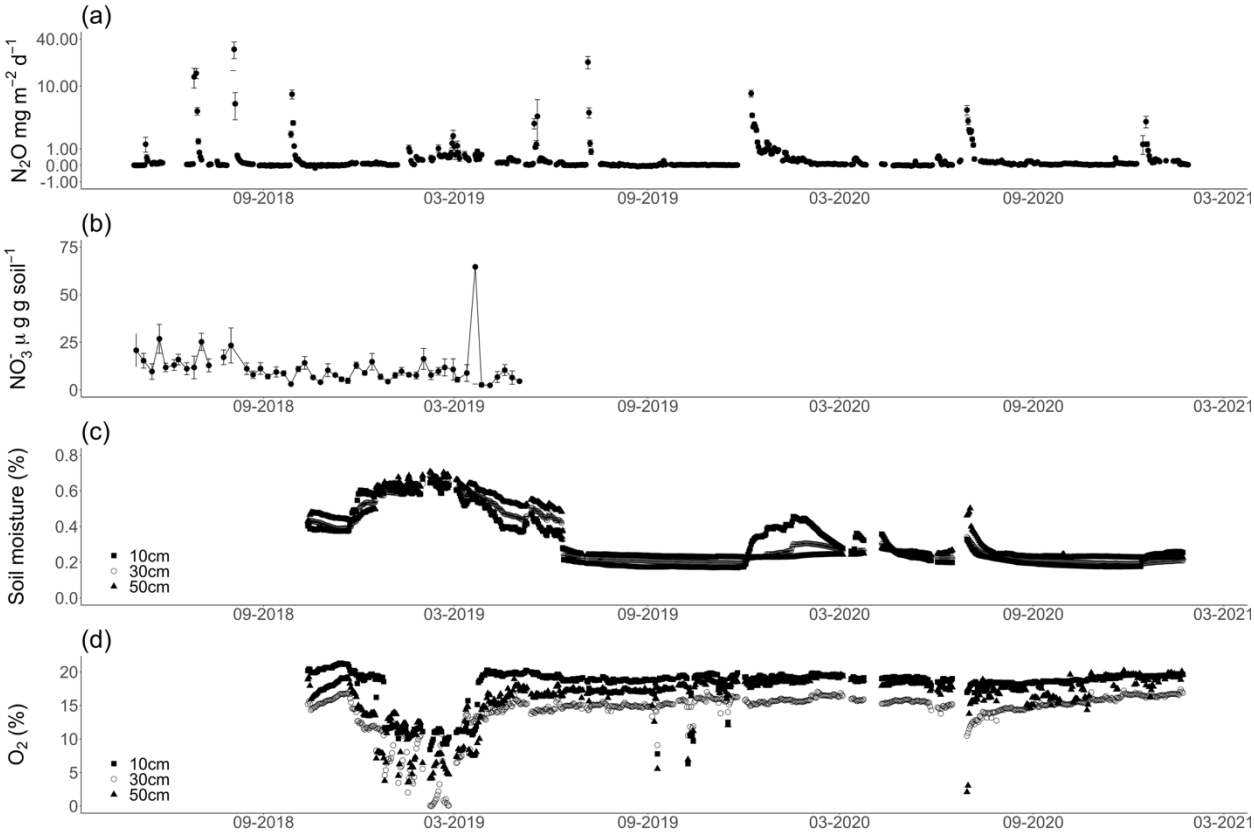

Figure 3. Daily mean (± SE) (a) N_2O fluxes, (b) soil NO_3^-, (c) soil moisture and (d) soil O_2 over the soil sensor measurement period. Soil NO_3^- measurements (0-10 cm depth) were conducted weekly from May 2018-May 2019. For (c) soil O_2 and (d) soil moisture, depth values are labeled as squares (10 cm), open circles (30 cm), and triangles (50 cm).

We explored the importance of high flux events of soil N_2O emissions by defining hot moments as individual flux measurements more than four standard deviations from the annual mean (Table 2). Hot moment N_2O fluxes represented only 0.2 % to 1.1% of annual measurements but represented 31.6% to 56.8% of the annual flux. The magnitude of hot moment events decreased with stand age, and the contribution of hot moments to the annual flux also decreased over time (Figure 1c, Table 2, $p < 0.001$).

Periods of decreased O_2 concentrations across soil depths did not consistently correspond to hot moments of N_2O emission, although daily mean N_2O emissions did increase by an order of magnitude during extended suboxic periods in February and March 2019 (Figure 3d). Increases in N_2O emissions occurred following significant increases in soil moisture at depth (Figure 3a

and 3c), with increases in moisture driven by seasonal rainfall inputs or irrigation events. Short-term (< 24 hour) irrigation events did not always increase soil moisture at depths of 10 cm or greater (Figure 3d). This suggests limited downward percolation and increases in N_2O flux following irrigation events likely occurred from increased N_2O production in surface soils (< 10 cm). Wavelet coherence analysis suggested temporal patterns in soil moisture, soil temperature, and bulk soil O_2 concentrations across all depths were significantly related to patterns in net N_2O fluxes on a daily timescale (Figure S1, $p < 0.05$). At weekly and monthly timescales, N_2O fluxes were predominantly associated with soil temperature and moisture at 10 and 30 cm depths (Figure S1, $p < 0.05$).

Table 2. Mean (± standard error) annual N_2O fluxes by site year, number of measurements, number of hot moment measurements, hot moment mean (± standard error) N_2O fluxes, mean N_2O fluxes (± standard error) without hot moments included, and contribution of hot moments to total mean flux. Hot moments were calculated separately for each year and in aggregate for the total dataset (All years).

Site Year	Annual mean (mg N_2O m^{-2} y^{-1})	Flux (n)	Hot moment flux (n)	Hot moment mean (mg N_2O m^{-2} d^{-1})	Hot moments removed mean (mg N_2O m^{-2} y^{-1})	Hot moments % of total flux
1 (2017-2018)	610.5 ± 68.1	25,252	48	496.1 ± 66.8	263.4 ± 9.9	+56.8%
2 (2018-2019)	901.9 ± 74.5	25,169	74	456.6 ± 43.0	402.4 ± 13.7	+55.3%
3 (2019-2020)	777.1 ± 52.0	26,261	55	363.1 ± 46.2	485.7 ± 10.4	+37.5%
4 (2020-2021)	263.6. ± 5.6	25,336	273	19.8 ± 0.7	180.39 ± 2.6	+31.6%
All years	624.4 ± 27.8	103,013	201	401.1 ± 26.9	346.9 ± 4.7	+44.4%

Periods of CH_4 uptake were highest in the late summer, occurring when soils were the driest throughout the soil profile (Figure 4a and 4c). Lower soil moisture across the soil profile generally corresponded to higher rates of CH_4 uptake, also corresponding to an increased annual uptake with stand age except for site year 2 (Table 1). Wavelet coherence analysis of net CH_4 fluxes exhibited significant coherence with soil moisture at 50 cm on a daily and weekly scale, and soil moisture at 10 cm at weekly and monthly timescales (Figure S2, $p < 0.05$). Wavelet coherence analysis also suggested that O_2 concentrations at 10 cm were significantly associated with CH_4 emissions at daily timescales and at 50 cm at monthly and seasonal timescales (Figure S2, $p < 0.05$). Soil temperature had significant coherence with CH_4 fluxes on daily, weekly, monthly, and seasonal timescales across depths, except at 10 cm depths on a daily timescale (Figure S2, $p < 0.05$).

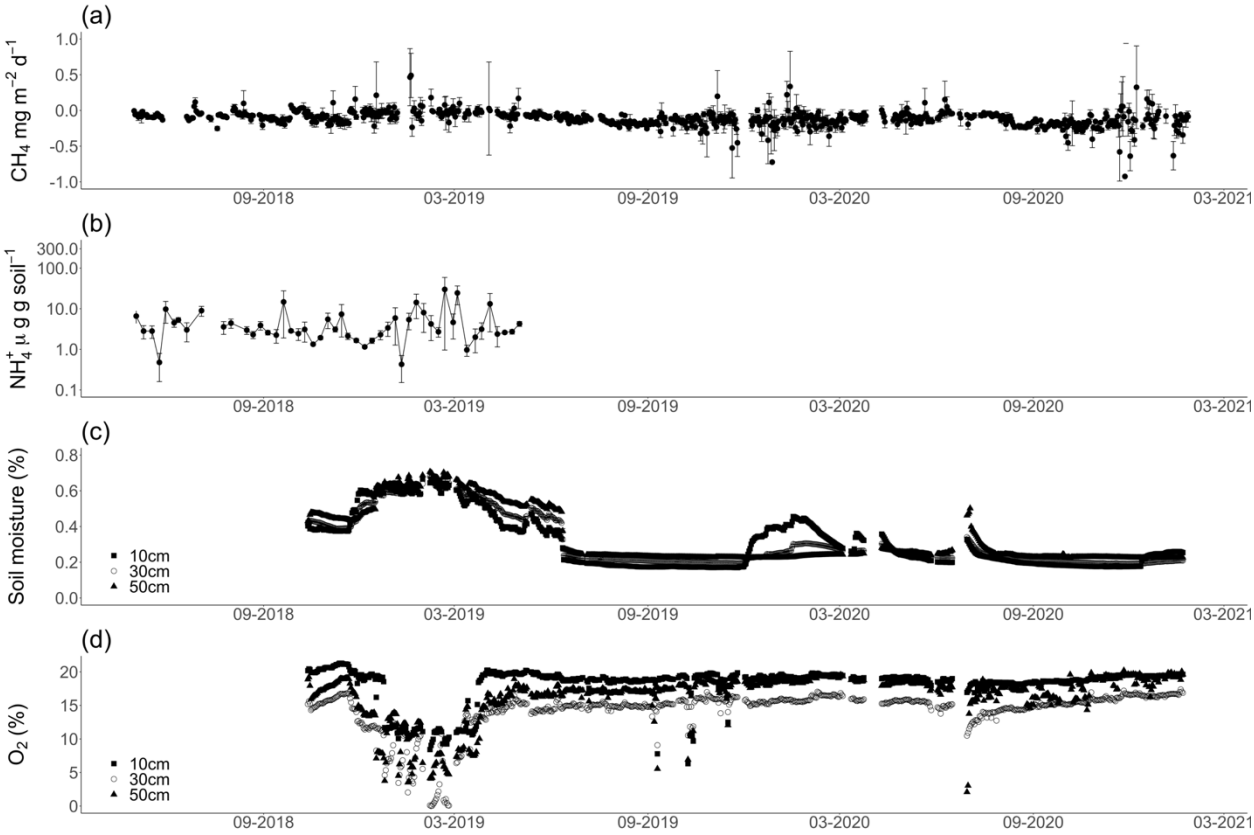

Figure 4. Daily mean (± SE) (a) CH_4 fluxes, (b) soil NH_4^+ concentrations, (c) soil moisture and (d) soil O_2 concentrations over the soil sensor measurement period. Soil NH_4^+ measurements (0-10 cm depth) were conducted weekly from May 2018-May 2019. For (c) soil O_2 and (d) soil moisture, depth values are labeled as squares (10 cm), open circles (30 cm), and triangles (50 cm).

As plants were present within chamber collars in a subset of the deployed flux chambers, chamber CO_2 fluxes were representative of total plant and soil respiration. Generally, CO_2 fluxes closely followed seasonal patterns in soil temperature, with similar trends in soil temperature observed across depths (Figures 5a and 5b). Alfalfa can be harvested up to seven times per year, where the majority of plant biomass is removed above the soil surface (Baldocchi et al., 2020; Hemes et al., 2019). Cuttings corresponded to significant reductions in mean daily respiration values throughout the summer, although respiration values typically recovered within 5-7 days (Figures 5a).

Wavelet coherence analysis of CO_2 fluxes suggested that daily scale fluxes were significantly associated with soil moisture and soil O_2 at 10 cm depth and were associated with soil moisture and temperature at 30 and 50 cm depths (Figure S3, $p < 0.05$). CO_2 fluxes were predominantly associated with soil temperature across all depths at weekly, monthly, and seasonal timescales (Figure S3, $p < 0.05$). At longer timescales, significant coherence with soil O_2 was only observed at monthly timescales across all depths and seasonal scales at 10 cm

depths (Figure S3, $p < 0.05$). Soil moisture at 10 cm was significantly associated with CO_2 fluxes at weekly timescales and at 10 and 30 cm on seasonal timescales (Figure S3, $p < 0.05$).

5.4.3 Plant phenology and greenhouse gas fluxes

We observed significant differences in NDVI following alfalfa cutting events (Figure 5c) and annual mean NDVI decreased significantly across the measurement period (Table 1, $p < 0.001$). Wavelet coherence analysis suggested that CO_2 fluxes were only significantly associated with NDVI at approximately biweekly and seasonal timescales. (Figure S4a, $p < 0.05$). Similar relationships were observed between NDVI and soil CH_4 fluxes, but also included significant coherence at the biannual scale (Figure S4b, $p < 0.05$). Only N_2O was significant associated with NDVI at a daily scale, but also exhibited significant coherence at monthly, seasonal, and biannual timescales (Figure S4c, $p < 0.05$).

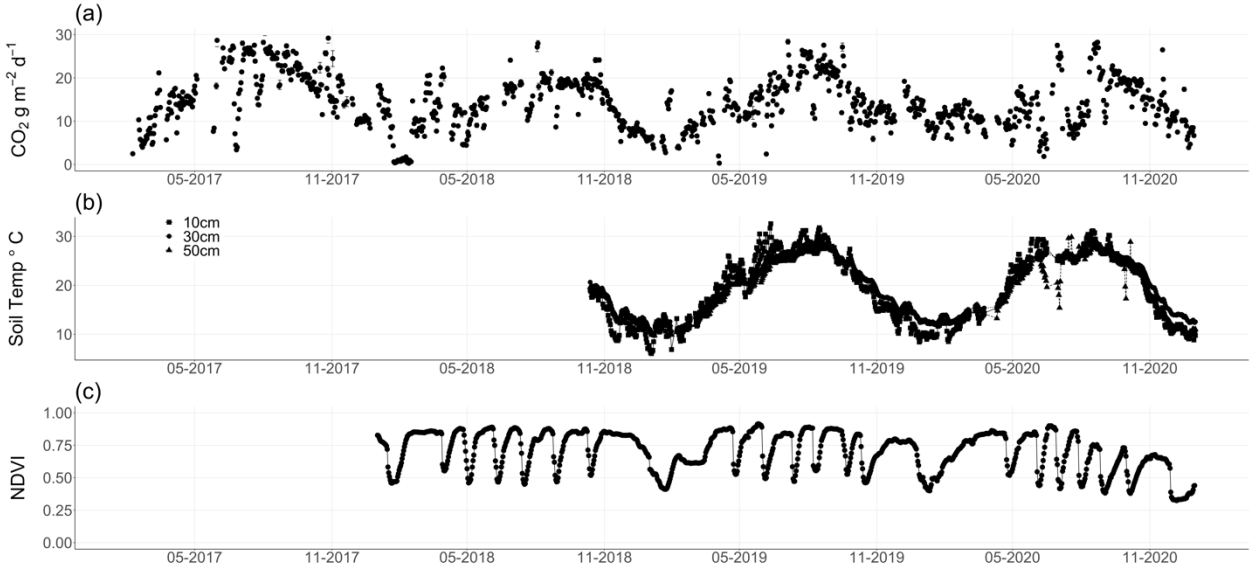

Figure 5. Daily mean (± SE) (a) CO_2 fluxes (b) soil temperature (ºC), and daily normalized difference vegetation index (NDVI). For (b) soil temperature, (c) soil O_2, and (d) soil moisture, depth values are labeled as squares (10 cm), open circles (30 cm), and triangles (50 cm).

5.4.4 Depth trends in soil greenhouse gas concentrations

Measurements of soil gas concentrations indicated significant temporal variability in soil CO_2 concentrations and high N_2O and CH_4 concentration events within the soil environment (Figure 6a-6c). Measurements of soil atmospheric CO_2 concentrations were generally high (> 10,000 ppm) throughout the year, particularly at depth (30-50 cm). Soil CO_2 concentration decreased significantly following rainfall events in March-April 2019. Rainfall during this period generated extended soil waterlogging that reduced soil O_2 concentrations (Figure 4d and 6a). However, soil CO_2 concentrations exhibited no statistical relationships with soil CO_2 fluxes.

The peak in soil atmosphere N_2O concentrations corresponded to the onset of soil inundation following substantial rainfall, which led to a significant increase in soil moisture and significant decrease in soil O_2 across soil depths (Figure 2c and 2d). The observed peak in soil CH_4 concentrations occurred near the end of this soil saturation event. The peaks in soil N_2O and CH_4 did not correspond to significant hot moments of net soil N_2O and CH_4 emissions, although soils were a consistent N_2O source and an occasional small daily source of CH_4 (Figure 1b and 1c). Daily mean soil N_2O fluxes were positively correlated with soil atmospheric N_2O concentrations across soil depths (10 cm $R^2 = 0.60$, $p < 0.001$, 30 cm $R^2 = 0.53$, $p < 0.001$, 50 cm $R^2 = 0.45$, $p < 0.001$; Figure 7). No significant relationships were observed between soil CO_2 and CH_4 concentrations and net CO_2 and CH_4 fluxes (Figures S5 and S6).

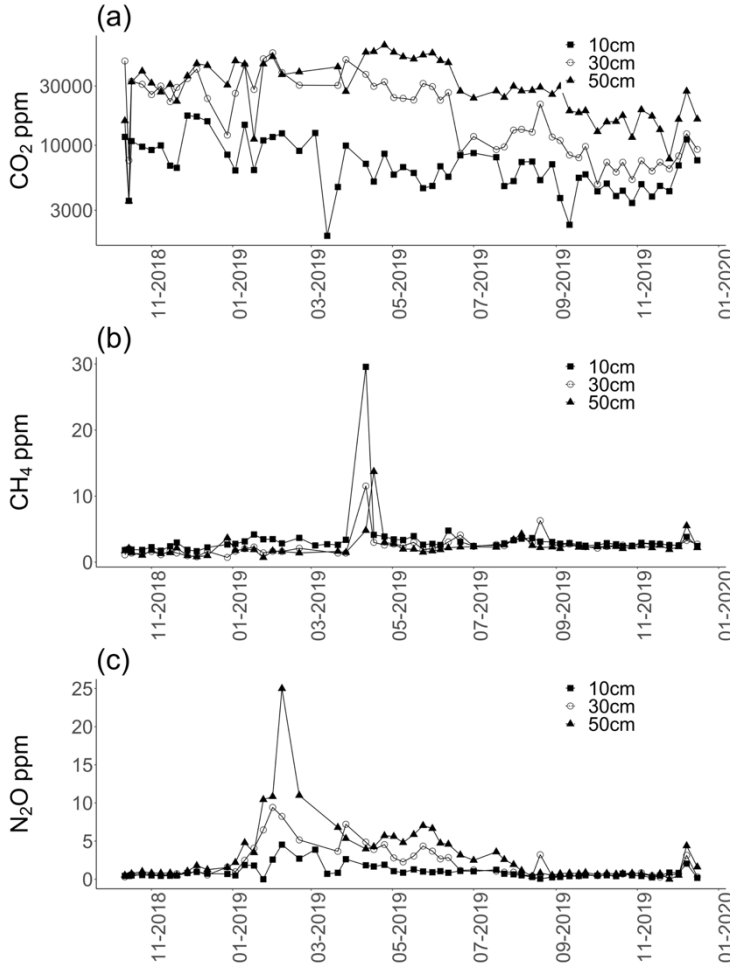

Figure 6. Daily mean (± SE) (a) depth CO_2 concentrations, (b) depth CH_4 concentrations, and (c) depth N_2O concentrations. Depth values are labeled as squares (10 cm), open circles (30 cm), and triangles (50 cm).

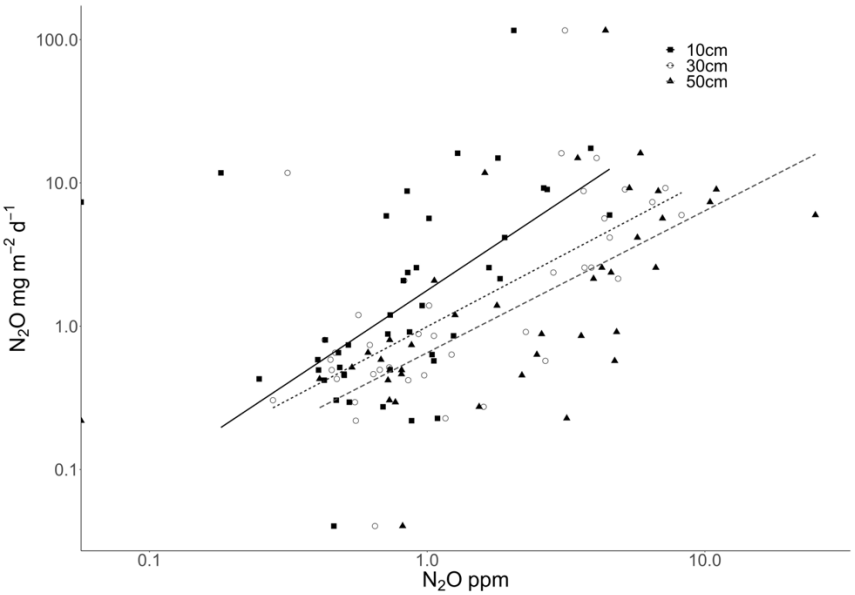

Figure 7. Linear correlations of daily mean soil N_2O fluxes (mg m^{-2} d^{-1}) and soil atmosphere N_2O concentrations (ppmv) across soil depths (10 cm: squares, 30 cm: open circles, and 50 cm: triangles) with daily mean soil N_2O flux in mg m^{-2} d^{-1} (10 cm: $R^2 = 0.60$, $p < 0.001$, 30 cm: $R^2 = 0.53$, $p < 0.001$, 50 cm: $R^2 = 0.45$, $p < 0.001$).

5.5 Discussion

5.5.1 Soil N_2O emissions

Annual mean N_2O fluxes were 599.4 ± 26.8 mg N_2O m^{-2} yr^{-1} (range: 247.0 ± 5.7 to 803.4 ± 66.94 mg N_2O m^{-2} yr^{-1}) and were significantly greater than other alfalfa N_2O flux estimates (Malhi, Lemke, & Schoenau, 2010; Rochette et al., 2004; Wagner-Riddle et al., 1997) but comparable to similar temperate, flood-irrigated alfalfa ecosystems (Burger et al., 2016). Inter- and intra-annual variability in N_2O fluxes were largely driven by differences in the magnitude and frequency of hot moments of N_2O production. Soil NO_3^- and NH_4^+ concentrations were not directly correlated to hot moments of net N_2O production, partially rejecting our hypothesis. This suggests that N availability was unlikely to limit N_2O emissions in this ecosystem.

This large, continuous dataset allowed us to quantify the dynamics of N_2O hot moments and their impact on total N_2O emissions. While hot moments represented only 0.2-1.1% of annual N_2O measurements they contributed up to 57% of total N_2O emissions. We observed a decrease in the magnitude of N_2O hot moments over time, corresponding to a decreased contribution of hot moments to overall emissions with increasing stand age. The observed decrease in the magnitude of hot moments of N_2O flux over time may be partially explained by increased alfalfa taproot development with stand age. A more developed alfalfa taproot system can maintain access to a deep-water table to support plant water demands, reducing drought stress (Moran et al., 1994; Tang et al., 2013) and thus reduce the need for irrigation events that

may stimulate hot moments of N_2O flux. However, the decrease in the magnitude of N_2O hot moments did not consistently correspond to decreases in annual emissions. This may be partially due to increases in N_2O emissions associated with the accumulation and mineralization of organic matter in soils (Burger et al., 2016), although we observed no significant relationships between N_2O flux and stand age.

However, we observed significant wavelet coherence between N_2O fluxes and NDVI across daily, monthly, seasonal, and biannual timescales. The observed combination of annual decreases in both NDVI and N_2O emissions suggests a decrease in net primary productivity (Houborg & McCabe, 2016; T. Ning, Liu, Lin, & Song, 2015) may directly decrease N_2O emissions. Alfalfa releases a small proportion of its symbiotically fixed N_2 as NH_4^+ to the soil environment (Brophy & Heichel, 1989; Burity, Ta, Faris, & Coulman, 1989; Thilakarathna, McElroy, Chapagain, Papadopoulos, & Raizada, 2016) and decreases in plant activity may also decrease N release via this pathway. While no relationships were observed between soil NH_4^+ concentrations and N_2O emissions during our one-year weekly soil sampling campaign, this observed coherence between NDVI and N_2O emissions suggests this plant-derived NH_4^+ may regulate non-hot moment N_2O emissions via nitrification on a daily timescale. This may also suggest plant cuttings alter the rate of N release, with alfalfa reallocating N to new plant growth immediately after cutting but increasing root N exudates throughout the growing period.

Wavelet coherence analysis and seasonal and diel trends in soil N_2O fluxes also highlighted the importance of soil moisture changes from irrigation or rainfall events, partially confirming our hypothesis. Hourly mean N_2O fluxes during dry summer periods, when most irrigation events occurred, were consistently greater than all other seasons. Hourly mean N_2O fluxes peaked at 1800 hours, shortly following the onset of overnight irrigation events. Surprisingly, short periods of irrigation did not always correspond to increased soil moisture at depths below 10 cm and did not consistently influence soil O_2 concentrations. This would suggest that the majority of N_2O production during hot moments occurred near the soil surface. However, daily mean N_2O fluxes were strongly correlated with weekly measurements of soil atmosphere N_2O concentrations across sampled depths down to 50 cm. Wavelet coherence analysis further suggested short-term increases in N_2O emissions were stimulated by changes in soil moisture and O_2 concentrations in surface soils, but temperature and moisture were the predominant controls at longer timescales. Our combined observations suggest hot moments of N_2O production occurred following rapid increases in moisture and decreases in soil O_2 in warm surface soils, with lower winter soil temperatures limiting net N_2O emissions. Low-magnitude, consistent N_2O fluxes appeared to be regulated by plant activity, soil moisture, and soil temperature with ear continuous N_2O production potentially facilitated by continuously anaerobic (micro)sites distributed throughout the soil profile (Sihi, Davidson, Savage, & Liang, 2020). While hot moments of production drove a significant portion of annual N_2O emissions, persistent anaerobic (micro)sites likely contributed to the consistent net N_2O emissions observed.

5.5.2 Soil CH_4 emissions

This ecosystem was a net CH_4 sink to the atmosphere (annual mean: -53.5 ± 2.5 mg CH_4 m^{-2} yr^{-1}, range: -78.2 ± 8.8 to -31.6 ± 2.5 mg CH_4 m^{-2} yr^{-1}). Sinks measured here were larger than other alfalfa ecosystem estimates using different approaches or shorter sampling periods (Hemes et al., 2019; J. Ning et al., 2020; Savage et al., 2014). Except for site year 2, net CH_4 consumption increased with stand age. The significant coherence observed between CH_4 fluxes and temperature across depths and timescales suggest temperature was the strongest control on net CH_4 consumption. Wavelet coherence analyses further highlight the observed relationship between decreases in soil moisture and increases in net CH_4 consumption, as decreases in soil moisture increases diffusivity (Min et al., 2020; Von Fischer, Butters, Duchateau, Thelwell, & Siller, 2009) and likely increased O_2 availability.

However, decreases in bulk soil O_2 concentrations did not drive significant increases in net CH_4 production or decreases in the CH_4 sink, rejecting our hypothesis. Instead, only extended periods of soil anaerobiosis may stimulate net CH_4 production (Anthony & Silver, 2021; Conrad, 1996), and this was not observed during the 4-year measurement period. We did observe a substantial increase in soil CH_4 concentrations shortly following the largest decrease in soil O_2 concentrations in March-April 2019. Elevated soil moisture may have limited gas diffusion with methanotrophic consumption near the soil surface potentially regulating net CH_4 efflux during this period (Bender & Conrad, 1994; Kammann, Hepp, Lenhart, & Müller, 2009). We also observed significant variability in hourly mean diel CH_4 fluxes, but this variability was not significantly correlated with any measured soil characteristics.

5.5.3 Soil CO_2 emissions

Soil CO_2 fluxes, which here represent combined soil and plant respiration due to the presence of plants within opaque soil chambers, averaged 4925.9 ± 13.5 g CO_2 m^{-2} yr^{-1}. Ecosystem respiration rates were greater than other alfalfa ecosystems (Alberti et al., 2010), likely driven by a combination of high plant productivity and warm temperatures throughout the growing season. Surprisingly, CO_2 fluxes were not significantly associated with NDVI on a daily scale, although significant coherence between CO_2 fluxes and NDVI on longer timescales highlight the importance of plant cuttings and phenology on regulating CO_2 flux (Baldocchi et al., 2020). Soil temperature across depths was significantly associated with respiration rates across timescales, suggesting that cooler temperatures during non-growing seasons were the primary control on the metabolic activity of both plants and soil microbes. However, significant coherence with soil moisture and O_2 also suggest short-term increases in moisture content and associated decreases in O_2 availability throughout the year were important controls on soil respiration rates.

5.6 Conclusion

Here we present one of the largest, longest, and most comprehensive soil CO_2, N_2O, and CH_4 flux datasets from irrigated alfalfa. Our findings highlight the interacting and contrasting effects of plant phenology, soil moisture, temperature, and O_2 availability on CO_2, CH_4, and N_2O fluxes from agricultural alfalfa. We found that NDVI, soil temperature, moisture, and O_2 were significant drivers of soil CO_2, N_2O, and CH_4 fluxes, although relationships varied across both depth and timescales. Additionally, hot moments of soil N_2O emissions accounted for a significant portion of the annual N_2O fluxes from irrigated alfalfa. N_2O fluxes were also significantly correlated with soil N_2O concentrations across the soil profile, suggesting N_2O produced within persistent or common anaerobic (micro)sites throughout the profile regulated non-hot moment soil N_2O emissions. Relationships between NDVI and N_2O suggest plant N inputs on a daily timescale may be an important source of sustained non-hot moment N_2O emissions. Together our results suggest that hot moments of N_2O emissions from changes in soil moisture associated with water management practices or future climate change could have important effects on the overall GHG budgets of alfalfa agroecosystems.

5.7 Acknowledgments

We appreciate assistance, data availability, and feedback from Heather Dang, Tibisay Peréz, Dennis Baldocchi, Joseph Verfaillie, and numerous other members of both the Silver Lab and the Berkeley Biometeorology Lab at University of California, Berkeley. We thank Christine O'Connell for the initial code development for data filtering. This work was supported by a Contract by the California Department of Water Resources (award 4600011240). We thank the California Department of Water Resources and the Metropolitan Water District of Southern California for research site access. T. L. Anthony was supported by the California Sea Grant Delta Science Fellowship. This material is based upon work supported by the Delta Stewardship Council Delta Science Program under Grant No. 5298 and California Sea Grant College Program Project R/SF-89. The contents of this material do not necessarily reflect the views and policies of the Delta Stewardship Council or California Sea Grant, nor does mention of trade names or commercial products constitute endorsement or recommendation for use. McIntire Stennis grant CA- B-ECO-7673-MS to W. L. Silver partially supported this work. W. L. Silver was also supported by funds from Breakthrough Strategies & Solutions, and the V. Kann Rasmussen, Oak Creek, Jewish Community, Northern Trust, and Trisons Foundations.

5.8 References

Alberti, G., Vedove, G. D., Zuliani, M., Peressotti, A., Castaldi, S., & Zerbi, G. (2010). Changes in CO2 emissions after crop conversion from continuous maize to alfalfa. *Agriculture, Ecosystems and Environment*, *136*(1–2), 139–147. https://doi.org/10.1016/j.agee.2009.12.012

Anthony, T. L., & Silver, W. L. (2021). Hot moments drive extreme nitrous oxide and

methane emissions from agricultural peatlands. *Global Change Biology*, *n/a*(n/a). https://doi.org/https://doi.org/10.1111/gcb.15802

Baldocchi, D. D., Ryu, Y., Dechant, B., Eichelmann, E., Hemes, K., Ma, S., … Berry, J. A. (2020). Outgoing Near-Infrared Radiation From Vegetation Scales With Canopy Photosynthesis Across a Spectrum of Function, Structure, Physiological Capacity, and Weather. *Journal of Geophysical Research: Biogeosciences*, *125*(7). https://doi.org/10.1029/2019JG005534

Bender, M., & Conrad, R. (1994). Methane oxidation activity in various soils and freshwater sediments: Occurrence, characteristics, vertical profiles, and distribution on grain size fractions. *Journal of Geophysical Research*, *99*(D8), 16531. https://doi.org/10.1029/94JD00266

Benhadi-Marín, J. (2018). A conceptual framework to deal with outliers in ecology. *Biodiversity and Conservation*, *27*(12), 3295–3300. https://doi.org/10.1007/s10531-018-1602-2

Brophy, L. S., & Heichel, G. H. (1989). Nitrogen release from roots of alfalfa and soybean grown in sand culture. *Plant and Soil*, *116*(1), 77–84. https://doi.org/10.1007/BF02327259

Burger, M., Haden, V. R., Chen, H., Six, J., & Horwath, W. R. (2016). Stand age affects emissions of N2O in flood-irrigated alfalfa: a comparison of field measurements, DNDC model simulations and IPCC Tier 1 estimates. *Nutrient Cycling in Agroecosystems*, *106*(3), 335–345. https://doi.org/10.1007/s10705-016-9808-8

Burity, H. A., Ta, T. C., Faris, M. A., & Coulman, B. E. (1989). Estimation of nitrogen fixation and transfer from alfalfa to associated grasses in mixed swards under field conditions. *Plant and Soil*, *114*(2), 249–255. https://doi.org/10.1007/BF02220805

Burton, D. L., Bergstrom, D. W., Covert, J. A., Wagner-Riddle, C., & Beauchamp, E. G. (1997). Three methods to estimate N2O fluxes as impacted by agricultural management. *Canadian Journal of Soil Science*, *77*(2), 125–134. https://doi.org/10.4141/S96-102

Butterbach-Bahl, K., Baggs, E. M., Dannenmann, M., Kiese, R., & Zechmeister-Boltenstern, S. (2013). Nitrous oxide emissions from soils: how well do we understand the processes and their controls? *Philosophical Transactions of the Royal Society of London. Series B, Biological Sciences*, *368*(1621), 20130122. https://doi.org/10.1098/rstb.2013.0122

Camilo, R.-S., Szutu, D., Baldocchi, D., & Hemes, K. (2021). AmeriFlux US-Bi2 Bouldin Island corn. United States. https://doi.org/10.17190/AMF/1419513

Conrad, R. (1996, December). *Soil microorganisms as controllers of atmospheric trace gases (H2, CO, CH4, OCS, N2O, and NO)*. *Microbiological Reviews*. Retrieved from http://mmbr.asm.org/content/60/4/609.abstract

Davidson, E. a., Keller, M., Erickson, H. E., Verchot, L. V., & Veldkamp, E. (2000). Testing a Conceptual Model of Soil Emissions of Nitrous and Nitric Oxides. *BioScience*, *50*(8), 667. https://doi.org/10.1641/0006-3568(2000)050[0667:TACMOS]2.0.CO;2

Del Grosso, S. J., Parton, W. J., Mosier, A. R., Walsh, M. K., Ojima, D. S., & Thornton, P. E. (2006). DAYCENT National-Scale Simulations of Nitrous Oxide Emissions from Cropped Soils in the United States. *Journal of Environment Quality*, *35*(4), 1451. https://doi.org/10.2134/jeq2005.0160

Estop-Aragones, C., Knorr, K. H., & Blodau, C. (2013). Belowground in situ redox dynamics and methanogenesis recovery in a degraded fen during dry-wet cycles and flooding. *Biogeosciences*, *10*(1), 421–436. https://doi.org/10.5194/bg-10-421-2013

Hart, S. C., Stark, J. M., Davidson, E. A., & Firestone, M. K. (1994). Nitrogen Mineralization, Immobilization, and Nitrification. In R. W. Weaver, J. S. Angle, & P. S. Bottomley (Eds.), *Methods of Soil Analysis, Part 2. Microbial and Biochemical Properties* (pp. 985–1018). Madison, WI: Soil Science Society of America.

Hatala, J. A., Detto, M., Sonnentag, O., Deverel, S. J., Verfaillie, J., & Baldocchi, D. D. (2012). Greenhouse gas (CO2, CH4, H2O) fluxes from drained and flooded agricultural peatlands in the Sacramento-San Joaquin Delta. *Agriculture, Ecosystems and Environment*, *150*, 1–18. https://doi.org/10.1016/j.agee.2012.01.009

Hemes, K. S., Chamberlain, S. D., Eichelmann, E., Anthony, T., Valach, A., Kasak, K., … Baldocchi, D. D. (2019). Assessing the carbon and climate benefit of restoring degraded agricultural peat soils to managed wetlands. *Agricultural and Forest Meteorology*, *268*, 202–214. https://doi.org/10.1016/j.agrformet.2019.01.017

Houborg, R., & McCabe, M. F. (2016). High-Resolution NDVI from planet's constellation of earth observing nano-satellites: A new data source for precision agriculture. *Remote Sensing*, *8*(9). https://doi.org/10.3390/rs8090768

Jia, Y., Li, F. M., Zhang, Z. hua, Wang, X. L., Guo, R., & Siddique, K. H. M. (2009). Productivity and water use of alfalfa and subsequent crops in the semiarid Loess Plateau with different stand ages of alfalfa and crop sequences. *Field Crops Research*, *114*(1), 58–65. https://doi.org/10.1016/j.fcr.2009.07.004

Kammann, C., Hepp, S., Lenhart, K., & Müller, C. (2009). Stimulation of methane consumption by endogenous CH4 production in aerobic grassland soil. *Soil Biology and Biochemistry*, *41*(3), 622–629. https://doi.org/10.1016/J.SOILBIO.2008.12.025

Kandelous, M. M., Kamai, T., Vrugt, J. A., Šimůnek, J., Hanson, B., & Hopmans, J. W. (2012). Evaluation of subsurface drip irrigation design and management parameters for alfalfa. *Agricultural Water Management*, *109*, 81–93. https://doi.org/10.1016/j.agwat.2012.02.009

Liu, P. C. (1994). Wavelet Spectrum Analysis and Ocean Wind Waves. In E. Foufoula-Georgiou & P. B. T.-W. A. and I. A. Kumar (Eds.), *Wavelets in Geophysics* (Vol. 4, pp. 151–166). Academic Press. https://doi.org/https://doi.org/10.1016/B978-0-08-052087-2.50012-8

Malhi, S. S., Lemke, R., & Schoenau, J. J. (2010). Influence of time and method of alfalfa stand termination on yield, seed quality, N uptake, soil properties and

greenhouse gas emissions under different N fertility regimes. *Nutrient Cycling in Agroecosystems*, *86*(1), 17–38. https://doi.org/10.1007/s10705-009-9271-x

McLean, E. O. (1982). Soil pH and Lime Requirement. In *Page, A.L., Ed., Methods of Soil Analysis. Part 2. Chemical and Microbiological Properties, American Society of Agronomy, Soil Science Society of America, Madison,* (pp. 199–224).

Meng, C., Wang, F., Yang, K., Shock, C. C., Engel, B. A., Zhang, Y., … Gu, X. (2020). Small wetted proportion of drip irrigation and non-mulched treatment with manure application enhanced methane uptake in upland field. *Agricultural and Forest Meteorology*, *281*, 107821. https://doi.org/https://doi.org/10.1016/j.agrformet.2019.107821

Min, K., Berhe, A. A., Khoi, C. M., van Asperen, H., Gillabel, J., & Six, J. (2020). Differential effects of wetting and drying on soil CO2 concentration and flux in near-surface vs. deep soil layers. *Biogeochemistry*, *7*. https://doi.org/10.1007/s10533-020-00658-7

Mondal, D., & Percival, D. B. (2010). Wavelet variance analysis for gappy time series. *Annals of the Institute of Statistical Mathematics*, *62*(5), 943–966. https://doi.org/10.1007/s10463-008-0195-z

Moran, J. F., Becana, M., Iturbe-Ormaetxe, I., Frechilla, S., Klucas, R. V., & Aparicio-Tejo, P. (1994). Drought induces oxidative stress in pea plants. *Planta*, *194*(3), 346–352. https://doi.org/10.1007/BF00197534

Nickerson, N. (2016). Evaluating gas emission measurements using Minimum Detectable Flux (MDF). *White Paper*, (March).

Ning, J., He, X. Z., Hou, F., Lou, S., Chen, X., Chang, S., … Zhu, W. (2020). Optimizing alfalfa productivity and persistence versus greenhouse gases fluxes in a continental arid region. *PeerJ*, *2020*(3), 1–19. https://doi.org/10.7717/peerj.8738

Ning, T., Liu, W., Lin, W., & Song, X. (2015). NDVI Variation and Its Responses to Climate Change on the Northern Loess Plateau of China from 1998 to 2012. *Advances in Meteorology*, *2015*. https://doi.org/10.1155/2015/725427

Noory, H., Liaghat, A. M., Chaichi, M. R., & Parsinejad, M. (2009). Effects of water table management on soil salinity and alfalfa yield in a semi-arid climate. *Irrigation Science*, *27*(5), 401–407. https://doi.org/10.1007/s00271-009-0155-2

O'Connell, C. S., Ruan, L., & Silver, W. L. (2018). Drought drives rapid shifts in tropical rainforest soil biogeochemistry and greenhouse gas emissions. *Nature Communications*, *9*(1), 1348. https://doi.org/10.1038/s41467-018-03352-3

Oertel, C., Matschullat, J., Zurba, K., Zimmermann, F., & Erasmi, S. (2016). Greenhouse gas emissions from soils - A review. *Chemie Der Erde - Geochemistry*, *76*(3), 327–352. https://doi.org/10.1016/j.chemer.2016.04.002

Orchard, V. A., & Cook, F. J. (1983). Relationship Between Soil Respiration and Soil Moisture. *Soil Biology and Biochemistry*, *15*(4), 447–453.

Ottman, M., Putnam, D., Barlow, V., Brummer, J., Bohle, M., Davison, J., … Norberg, S. (2013). Long term trends and the future of the alfalfa and forage industry. *Proceedings, 2013 Western Alfalfa & Forage Symposium, Reno, NV, 11-13, December, 2013. UC Cooperative Extension, Plant Sciences Department,*

University of California, Davis, CA 95616., 11–13. Retrieved from http://www.pnas.org/lookup/doi/10.1073/pnas.1707322114
Peterson, T. A., & Russelle, M. P. (1991). Alfalfa and the nitrogen cycle in the Corn Belt. *Journal of Soil and Water Conservation*, *46*(3), 229 LP – 235. Retrieved from http://www.jswconline.org/content/46/3/229.abstract
PlanetTeam. (2021). Planet Application Program Interface: In Space for Life on Earth.
Rochette, P., Angers, D. A., Bélanger, G., Chantigny, M. H., Prévost, D., & Lévesque, G. (2004). Emissions of N 2 O from Alfalfa and Soybean Crops in Eastern Canada . *Soil Science Society of America Journal*, *68*(2), 493–506. https://doi.org/10.2136/sssaj2004.4930
Rösch, A., & Schmidbauer, H. (2018). WaveletComp: Computational Wavelet Analysis. R package version 1.1., 1–38. Retrieved from http://www.hs-stat.com/projects/WaveletComp/WaveletComp_guided_tour.pdf%0Ahttps://cran.r-project.org/package=WaveletComp
Savage, K., Phillips, R., & Davidson, E. (2014). High temporal frequency measurements of greenhouse gas emissions from soils. *Biogeosciences*, *11*(10), 2709–2720. https://doi.org/10.5194/bg-11-2709-2014
Serrano-Silva, N., Sarria-Guzmàn, Y., Dendooven, L., & Luna-Guido, M. (2014). Methanogenesis and Methanotrophy in Soil: A Review. *Pedosphere*, *24*(3), 291–307. https://doi.org/10.1016/S1002-0160(14)60016-3
Shouse, P. J., Ayars, J. E., & ŠimŮnek, J. (2011). Simulating root water uptake from a shallow saline groundwater resource. *Agricultural Water Management*, *98*(5), 784–790. https://doi.org/10.1016/j.agwat.2010.08.016
Sihi, D., Davidson, E. A., Savage, K. E., & Liang, D. (2020). Simultaneous numerical representation of soil microsite production and consumption of carbon dioxide, methane, and nitrous oxide using probability distribution functions. *Global Change Biology*, *26*(1), 200–218. https://doi.org/10.1111/gcb.14855
Smith, P., Cai, Z., Gwary, D., Janzen, H., Kumar, P., McCarl, B., … Sirotenko, O. (2007). Agriculture In Climate Change 2007: Mitigation. *Cambridge University Press*, (4), 1–44. https://doi.org/10.2753/JES1097-203X330403
Soil Survey Staff. (2020). Natural Resources Conservation Service, United States Department of Agriculture. Official Soil Series Descriptions. Available online. Accessed [June/08/2020].
Tang, L., Cai, H., Ji, W., Luo, X., Wang, Z., Wu, J., … Bai, X. (2013). Overexpression of GsZFP1 enhances salt and drought tolerance in transgenic alfalfa (Medicago sativa L.). *Plant Physiology and Biochemistry*, *71*, 22–30. https://doi.org/10.1016/j.plaphy.2013.06.024
Thilakarathna, M. S., McElroy, M. S., Chapagain, T., Papadopoulos, Y. A., & Raizada, M. N. (2016). Belowground nitrogen transfer from legumes to non-legumes under managed herbaceous cropping systems. A review. *Agronomy for Sustainable Development*, *36*(4). https://doi.org/10.1007/s13593-016-0396-4
Tiedje, J. M., Sexstone, A. J., Parkin, T. B., & Revsbech, N. P. (1984). Anaerobic processes in soil. *Plant and Soil*, *76*(1–3), 197–212. https://doi.org/10.1007/BF02205580

U.S Energy Information Administration. (2011). Emissions of Greenhouse Gases in the United States 2009. *U.S Department of Energy, Washington, DC.*, (March). Retrieved from https://www.eia.gov/environment/emissions/ghg_report/pdf/0573%282009%29.pdf

Vinet, L., & Zhedanov, A. (2010). A "missing" family of classical orthogonal polynomials. *Exchange of Trace Gases between Terrestrial Ecosystems and the Atmosphere*, (January 1989), 7–21. https://doi.org/10.1088/1751-8113/44/8/085201

Von Fischer, J. C., Butters, G., Duchateau, P. C., Thelwell, R. J., & Siller, R. (2009). In situ measures of methanotroph activity in upland soils: A reactiondiffusion model and field observation of water stress. *Journal of Geophysical Research: Biogeosciences*, *114*(1), 1–12. https://doi.org/10.1029/2008JG000731

Wagner-Riddle, C., Thurtell, G. W., Kidd, G. K., Beauchamp, E. G., & Sweetman, R. (1997). Estimates of nitrous oxide emissions from agricultural fields over 28 months. *Canadian Journal of Soil Science*, *77*(2), 135–144. https://doi.org/10.4141/S96-103

Wang, G., Liang, Y., Zhang, Q., Jha, S. K., Gao, Y., Shen, X., … Duan, A. (2016). Mitigated CH4 and N2O emissions and improved irrigation water use efficiency in winter wheat field with surface drip irrigation in the North China Plain. *Agricultural Water Management*, *163*, 403–407. https://doi.org/10.1016/j.agwat.2015.10.012

Wang, Q., Hansen, J., & Xu, F. (2013). China's emerging dairy markets and potential impacts on U.S. alfalfa and dairy product exports. *Climate Change 2013 - The Physical Science Basis*, *53*(9), 1–30. Retrieved from https://www.cambridge.org/core/product/identifier/CBO9781107415324A009/type/book_part

Wood, T. E., Detto, M., & Silver, W. L. (2013). Sensitivity of soil respiration to variability in soil moisture and temperature in a humid tropical forest. *PLoS ONE*, *8*(12). https://doi.org/10.1371/journal.pone.0080965

Yang, S., Gao, M., Xu, C., Gao, J., Deshpande, S., Lin, S., … Zhu, H. (2008). Alfalfa benefits from Medicago truncatula: The RCT1 gene from M. truncatula confers broad-spectrum resistance to anthracnose in alfalfa. *Proceedings of the National Academy of Sciences of the United States of America*, *105*(34), 12164–12169. https://doi.org/10.1073/pnas.0802518105

5.9 Appendix

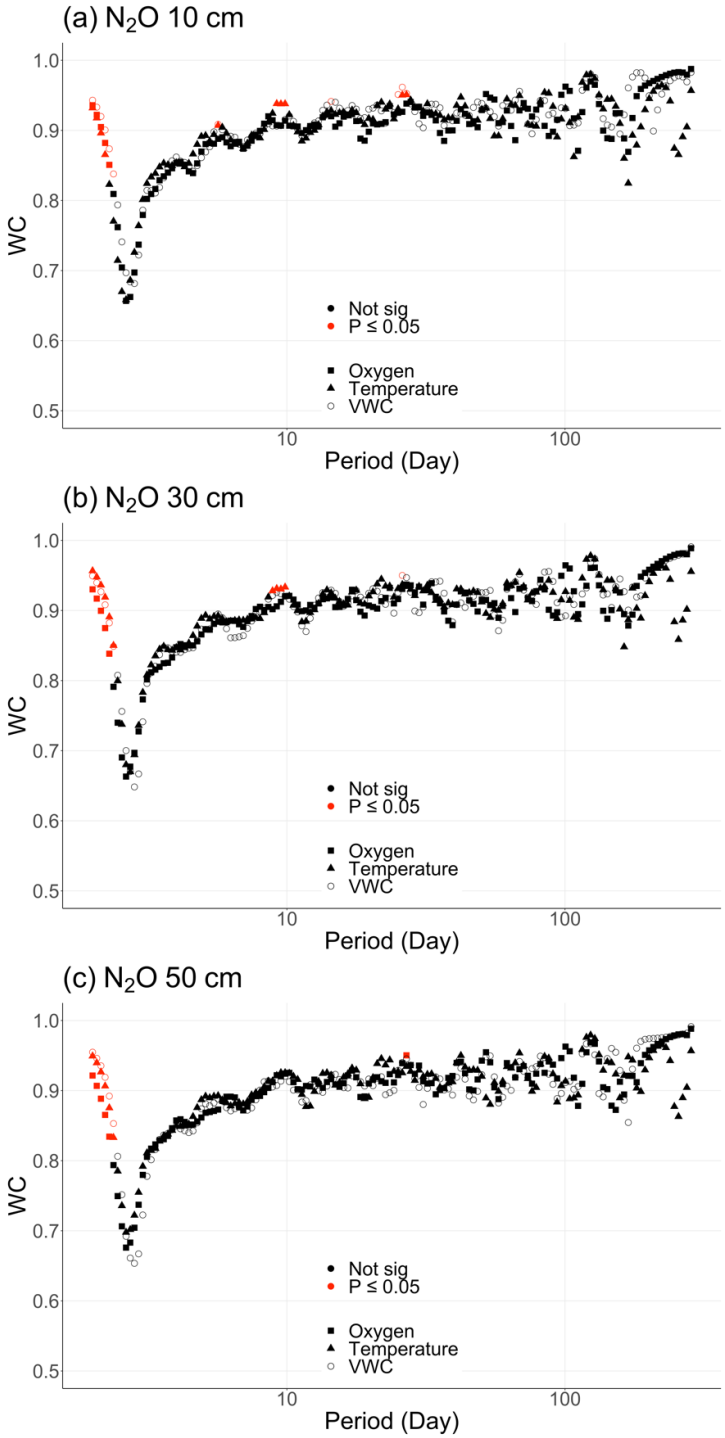

Figure S1. Wavelet coherence (WC) for soil N_2O fluxes with O_2 (%) concentrations (squares), soil temperature (°C, triangles), and soil moisture (%, open circles) at 10 cm (a), 30 cm (b) and 50 cm (c). Each point represents the average wavelet coherence across a range of periodicities (period = day). Red highlights indicate significant coherence ($p < 0.05$).

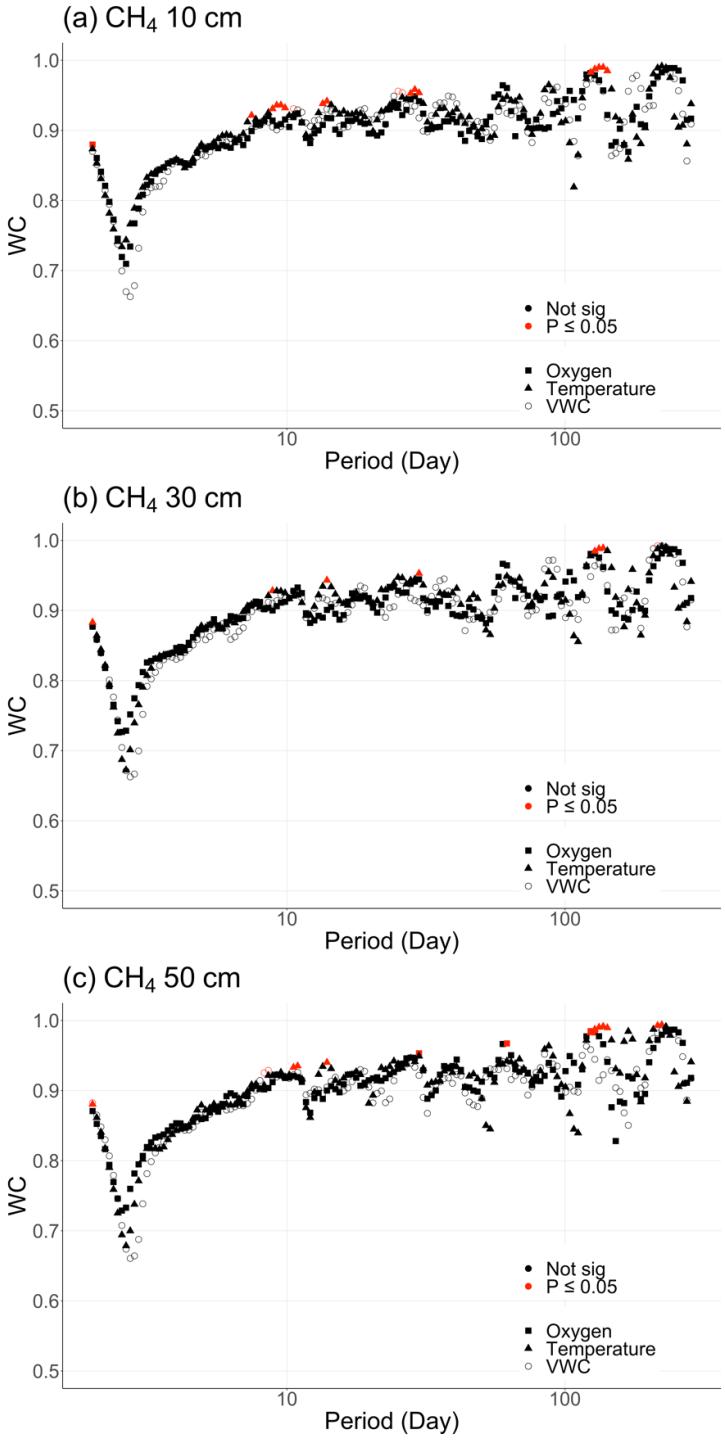

Figure S2. Wavelet coherence (WC) for soil CH_4 fluxes with O_2 (%) concentrations (squares), soil temperature (°C, triangles), and soil moisture (%, open circles) at 10 cm (a), 30 cm (b) and 50 cm (c). Each point represents the average wavelet coherence across a range of periodicities (period = day). Red highlights indicate significant coherence ($p < 0.05$).

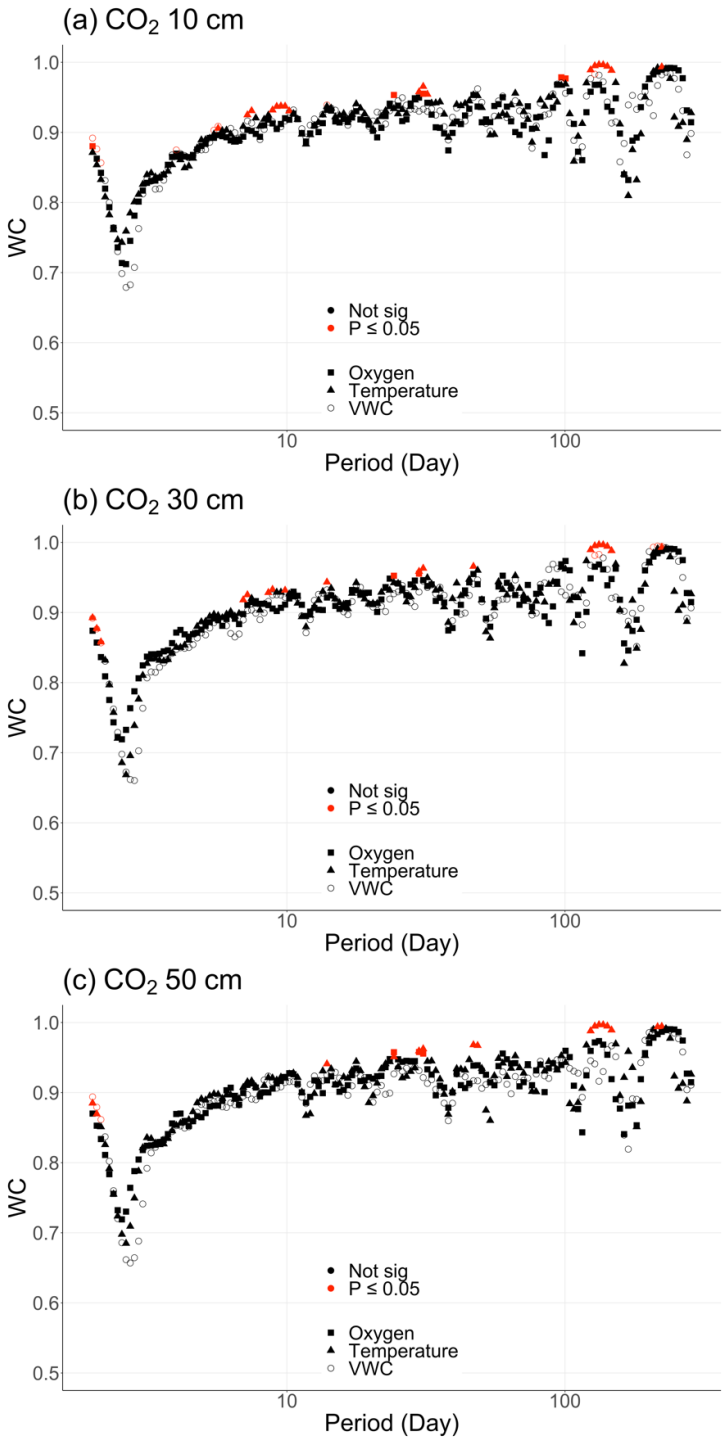

Figure S3. Wavelet coherence (WC) for soil CO_2 fluxes with O_2 (%) concentrations (squares), soil temperature (°C, triangles), and soil moisture (%, open circles) at 10 cm (a), 30 cm (b) and 50 cm (c). Each point represents the average wavelet coherence across a range of periodicities (period = day). Red highlights indicate significant coherence ($p < 0.05$).

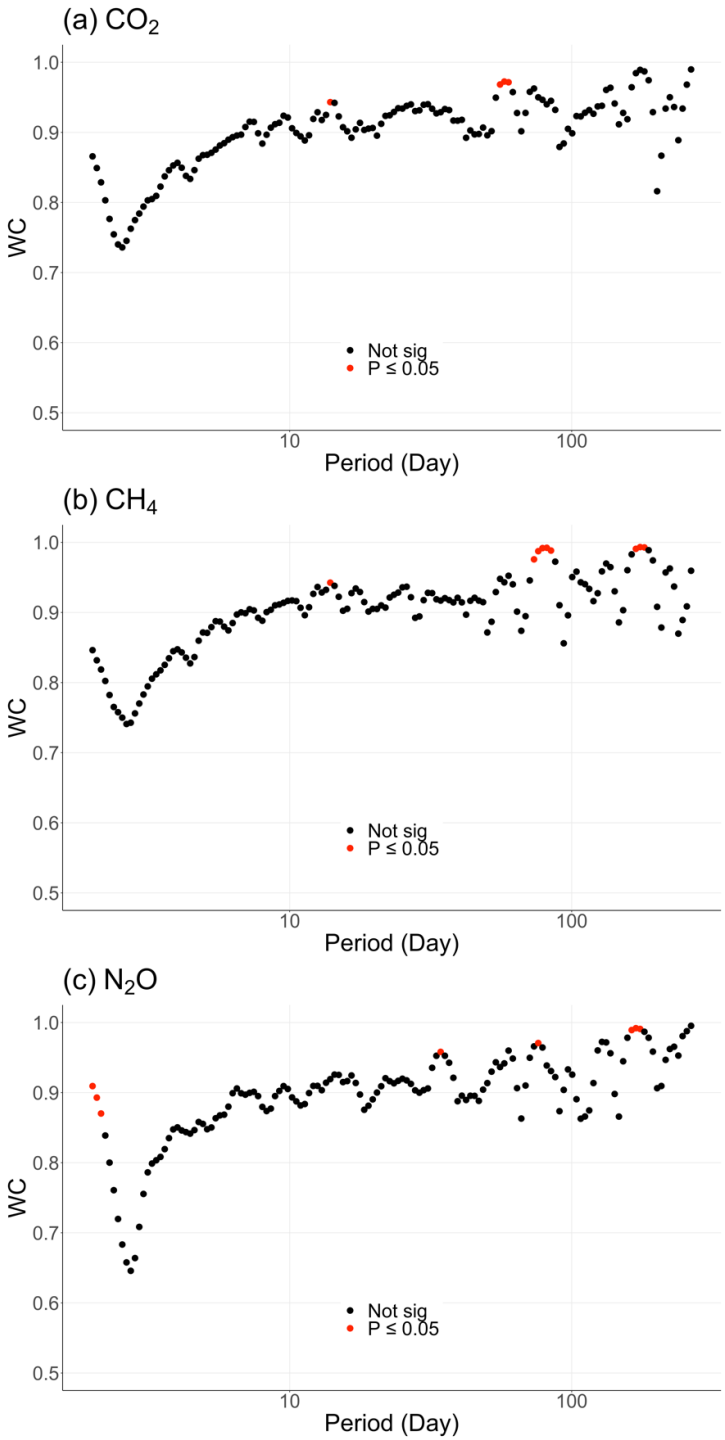

Figure S4. Wavelet coherence (WC) for (a) soil N_2O, (b) CH_4, and (c) CO_2 fluxes with normalized difference vegetation index (NDVI). Each point represents the average wavelet coherence across a range of periodicities (period = day). Red highlights indicate significant coherence ($p < 0.05$).

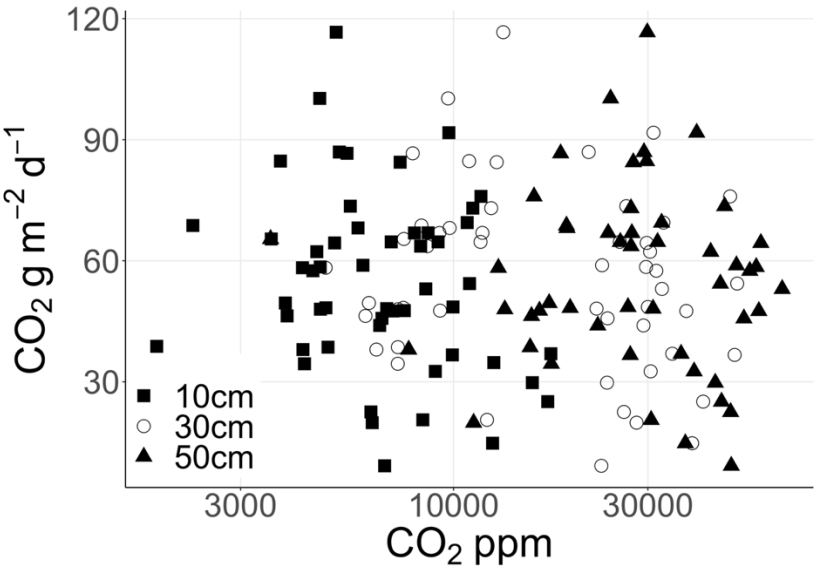

Figure S4. Relationships between daily mean soil CO_2 flux (g m^{-2} d^{-1}) and soil atmosphere CO_2 concentrations (ppmv) across soil depths (10 cm: squares, 30 cm: open circles, and 50 cm: triangles).

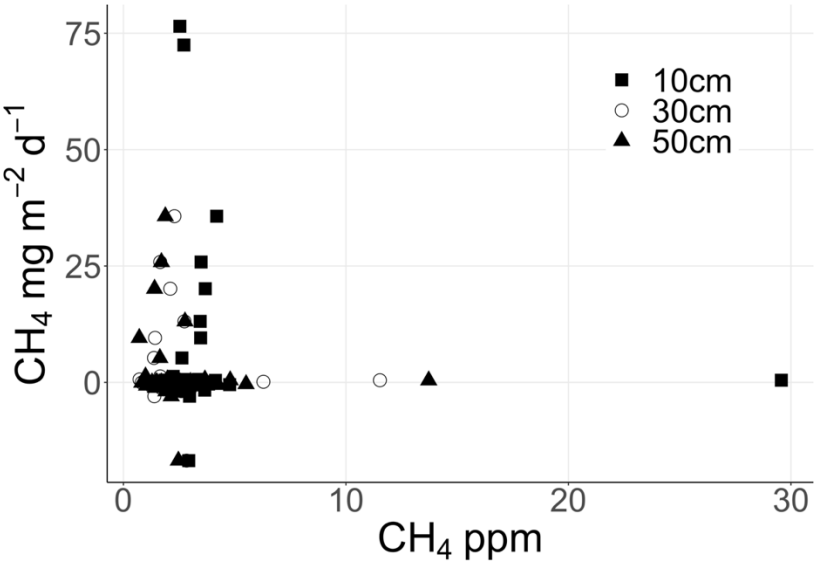

Figure S5. Relationships between daily mean soil CH_4 flux (mg m^{-2} d^{-1}) and soil atmosphere CH_4 concentrations (ppmv) across soil depths (10 cm: squares, 30 cm: open circles, and 50 cm: triangles).

Chapter 6. Conclusions

Agricultural peatlands emit 10% of global greenhouse gas emissions from land use, but the temporal dynamics and controls are poorly understood. Restoration of agricultural peatlands to wetlands represents a potential pathway to reduce greenhouse gas emissions and sequester carbon (C) from the atmosphere, but the mechanisms controlling soil C accumulation in restored wetlands are poorly understood. My dissertation further explored both the dynamics and controls of these greenhouse emissions and how residual soil minerals may impact potential soil C sequestration.

My dissertation first explored how residual soil minerals affect soil C accumulation in both drained and restored wetland soils, highlighting that reactive iron (Fe) and aluminum (Al) minerals may have contrasting controls on wetland soil C storage and loss. Using some of the longest continuous measurements of soil carbon dioxide, methane, and nitrous oxide (N_2O) flux measurements my dissertation also explored the temporal dynamics of soil greenhouse gas emissions from two agricultural peatland soil types and dominant land uses to further explore how land management may drive heterogeneity in agricultural peatland emissions. Using three years of continuous flux measurements I found seasonally flooded, organic-rich maize ecosystems are extreme greenhouse gas sources. Importantly up to 35% of these carbon dioxide (CO_2)-equivalent emissions were from N_2O alone, and roughly half of N_2O emissions occurred only 1% of the time. By using continuous soil sensors and a yearlong soil sampling campaign, I found that a combination of soil moisture, oxygen concentrations, and nitrate (NO_3^-) content drove patterns in N_2O emissions. Using long-term measurements, I used targeted stable isotope pool dilution measurements to further explore the production and consumption pathways of N_2O and methane (CH_4) from this drained peatland ecosystem. Gross N_2O production was strongly correlated to soil moisture while gross N_2O consumption was correlated with NO_3^- concentrations, suggesting N_2O consumption was indirectly controlled by substrate availability for denitrifiers. Combined with a decline in net N_2O fluxes observed under drained soil conditions, this suggests anaerobic hotspots may maintain areas of N_2O consumption sparsely distributed throughout the soil. In contrast, gross CH_4 production increased with soil depth, likely driven by both increased soil moisture and anaerobic soil conditions. Gross CH_4 consumption was negatively correlated with soil moisture and positively correlated with soil pH in surface soils, indicating both low pH and O_2 availability directly limit CH_4 consumption. Our results suggest that gross N_2O and CH_4 production were temporally decoupled from gross N_2O and CH_4 consumption and were driven by soil moisture and its associated effects on NO_3^- and pH. I also took long-term soil greenhouse gas measurements from a mineral-rich alfalfa ecosystem, which represents the other dominant land use for agricultural peatlands. Importantly this work highlighted similar controls on hot moments of N_2O emissions, with only 0.2% to 1.1% of annual measurements contributing to 31.6% to 56.8% of annual N_2O fluxes although mineral-rich soils in alfalfa ecosystems were smaller overall greenhouse gas sources.

Overall, my combined observations further our understanding of agricultural peatland soil greenhouse gas emissions and the importance of continuous measurements to decipher their biogeochemical controls. My dissertation highlights that management practices, predominantly flood irrigation length and timing, are an important control on hot moments of soil greenhouse gas emissions. It also highlights that organic-rich agricultural peatland soils emit significant amounts of N_2O during via short-term hot moments of emission, while mineral-rich soils exhibit similar but lower magnitude hot moments and lower overall emissions. The findings from my dissertation suggest that restoring organic-rich agricultural peatlands low in reactive Fe content are needed to minimize future agricultural peatland greenhouse gas emissions and maximizing future soil C sequestration. My dissertation results suggest that changes to irrigation practices may dramatically reduce greenhouse gas emissions from agricultural peatlands, and wetland restoration efforts should focus on organic-rich soils with low reactive Fe content to maximize soil C sequestration.